

**SPARSE DIRECTION-OF-ARRIVAL ESTIMATION WITH  
CONSTRAINED ANTENNA ARRAYS**

BY  
**SALEH AHMED YASLAM ALAWSH**

A Dissertation Presented to the  
DEANSHIP OF GRADUATE STUDIES

**KING FAHD UNIVERSITY OF PETROLEUM & MINERALS**

DHAHRAN, SAUDI ARABIA

1963 ١٣٨٣  
In Partial Fulfillment of the  
Requirements for the Degree of

**DOCTOR OF PHILOSOPHY**  
In

**ELECTRICAL ENGINEERING**

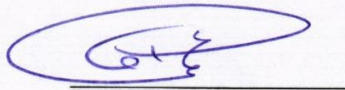
**April 2018**

KING FAHD UNIVERSITY OF PETROLEUM & MINERALS


DHAHRAN- 31261, SAUDI ARABIA

**DEANSHIP OF GRADUATE STUDIES**

This thesis, written by **Saleh Ahmed Yaslam Alawsh** under the direction of his thesis advisor and approved by his thesis committee, has been presented and accepted by the Dean of Graduate Studies, in partial fulfillment of the requirements for the degree of **DOCTOR OF PHILOSOPHY IN ELECTRICAL ENGINEERING**.



Dr. Ali A. Alshaikhi  
Department Chairman

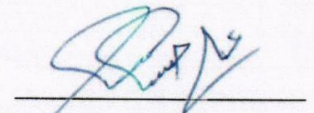


Dr. Salam A. Zummo  
Dean of Graduate Studies

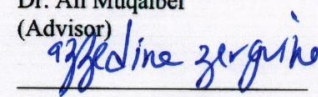


8/8/17

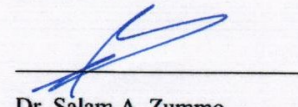
Date



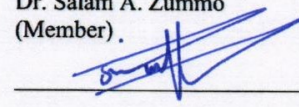
Dr. Ali Muqaibel  
(Advisor)



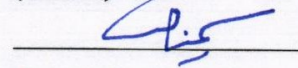
Dr. Azzedine Zerguine  
(Member)



Dr. Salam A. Zummo  
(Member)



Dr. Mohammad S. Sharawi  
(Member)



Dr. Samir N. Al-Ghadhban  
(Member)

© SALEH AHMED YASLAM ALAWSH

2018

*Dedicated to my*

*Parents*

*Brothers*

*Sisters*

*Wife and Children*

*Relatives*

*Friends Everywhere*

## ACKNOWLEDGMENTS

First and foremost thanks to Allah for giving me strength, patience, and ability to accomplish this research.

My deep acknowledgement for my parents who spent their life prays and asks Allah to help me during my study.

I would like to express my thankful for my advisor Dr. Ali Hussein Muqaibel for his guidance and support during my dissertation. I appreciate his incredible patience, his continued guidance, and encouragement all through my graduate studies. It is my luck to work with Dr. Muqaibel during my Master and PhD programs. I have got excellent background in measurements, antenna arrays, communications, and signal processing. During my research with Dr. Muqaibel, I have increased my knowledge in the area of interest. Actually, no words can express my appreciation for my advisor.

I would like to give special acknowledgment to the King Fahd University of Petroleum & Minerals, Hadhramout University for Science & Technology and Hadhramout Establishment for Human Development for supporting my graduate studies.

I would like to acknowledge the Deanship of Scientific Research (DSR) at King Fahd University of Petroleum and Minerals (KFUPM) for funding and supporting this work.

I would like to extend my appreciation to my committee members Professor Azzedine Zerguine, Professor Salam A. Zummo, Professor Mohammad S. Sharawi, and Dr. Samir Al-Ghadhban for their suggestions and valuable comments that definitely enrich the dissertation.

Special thanks to my brothers (Fahmi, Anies, and Waleed), sisters, wife, and children for being there whenever I needed them. Many thanks to all my relatives who keep on touch all the time in order not to feel being lonely outside my country. Distinct thanks to our neighbors staying here in the Kingdom. I really appreciate their welcome all the time and being like my family or even more.

No words could satisfy my thanks for Engineer Abdullah Ahmed Bugshan for his continuous encouragement and support. During my study, I always find him wherever needed. He used to give us most of his valuable time to set with us and solve problems if any.

Exceptional thanks to my colleagues, Dr. Abdi Talib, Dr. Mohammed Tamim, and Mr. Ali AlBeladi. Many thanks to Mr. Ahmed Oweis, Mr. Saeed Alamoudi, Mohammed Aldhaheeri, Mr. Omar Al Khazragi, Mohammed Yafeai, and Abdulmalik Almazrua for their valuable help . I would also like to acknowledge all my friends everywhere especially at KFUPM campus who share with me my happiness and life.

Saleh Ahmed Yaslam Alawsh

# TABLE OF CONTENTS

ACKNOWLEDGMENTS .....	III
TABLE OF CONTENTS.....	V
LIST OF TABLES.....	XI
LIST OF FIGURES.....	XII
LIST OF ABBREVIATIONS.....	XVII
LIST OF SYMBOLS .....	XIX
LIST OF NOTATIONS AND OPERATIONS.....	XXIV
ABSTRACT .....	XXV
ملخص الرسالة .....	XXIX
CHAPTER 1 INTRODUCTION.....	1
1.1 Overview .....	1
1.2 Research Contributions .....	2
1.3 Motivation .....	4

<b>1.4 Problem Statement .....</b>	<b>5</b>
<b>1.5 Objectives.....</b>	<b>6</b>
<b>1.6 Thesis Organization .....</b>	<b>7</b>
 <b>CHAPTER 2 TECHNICAL BACKGROUND.....</b>	 <b>8</b>
<b>2.1 Introduction .....</b>	<b>8</b>
<b>2.2 Algorithms for DOA Estimation: A Review .....</b>	<b>9</b>
<b>2.3 System Model.....</b>	<b>11</b>
<b>2.4 Technical Background.....</b>	<b>13</b>
2.4.1 Source Localization through DOA .....	13
2.4.2 Antenna and Array Configurations .....	15
2.4.3 Overview of Basic DOA Estimation Algorithms.....	16
2.4.4 Performance Metrics .....	22
<b>2.5 Chapter Summary.....</b>	<b>24</b>
 <b>CHAPTER 3 DOA ESTIMATION WITH PRACTICAL ANTENNA ARRAYS .....</b>	 <b>25</b>
<b>3.1 Practical Limitations .....</b>	<b>25</b>
<b>3.2 Evaluation and Comparison.....</b>	<b>28</b>
3.2.1 Comparison for DOA Estimation Algorithms .....	29
3.2.2 Results for Localizing a Single Source .....	31
3.2.3 Results for Localizing Multiple Sources .....	38
3.2.4 Source Location Dependency .....	45



3.2.5 Processing Time .....	48
<b>3.3 Chapter Summary.....</b>	<b>50</b>
 <b>CHAPTER 4 EXPERIMENTAL DOA ESTIMATION USING SPARSE ARRAYS IN REALISTIC CHANNELS.....</b>	 <b>52</b>
 <b>4.1 DOA Estimation with Moving Coprime Array Configuration .....</b>	 <b>53</b>
4.1.1 Introduction.....	53
4.1.2 Signal Model with Moving Coprime Array.....	55
4.1.3 Latency (Waiting Time) .....	63
4.1.4 Experimental Setup and Discussion of Results .....	65
4.1.5 Concluding Remarks .....	70
 <b>4.2 Sparse DOA Estimation Based on Software-Defined Radio Platform .....</b>	 <b>71</b>
4.2.1 Introduction.....	71
4.2.2 System Model .....	74
4.2.3 Experimental Setup .....	76
4.2.4 Results and Discussion.....	81
4.2.5 Concluding Remarks .....	84
 <b>4.3 Prototyping Coprime Arrays with Directive Radiation Pattern.....</b>	 <b>85</b>
4.3.1 Introduction.....	85
4.3.2 DOA Signal Model with Directive Antennas .....	88
4.3.3 Array Configuration .....	89
4.3.4 Gain and Phase Responses .....	90
4.3.5 Simulation and Results Based on Simulated Arrays .....	94
4.3.6 Simulation and Results Based on Fabricated Arrays.....	103
4.3.7 Concluding Remarks .....	106

<b>CHAPTER 5 GENERALIZED MULTI-LEVEL PRIME ARRAYS FOR SPARSE SAMPLING .....</b>	<b>108</b>
<b>5.1 Introduction .....</b>	<b>108</b>
<b>5.2 System Model.....</b>	<b>113</b>
5.2.1 Multi-Level Prime Array (MLPA) .....	113
5.2.2 Special Cases of MLPA Configurations .....	115
<b>5.3 The Difference Coarray Prospective in MLPA.....</b>	<b>118</b>
<b>5.4 MLPA Design Alternatives .....</b>	<b>120</b>
5.4.1 Selecting the Number of Sensors .....	121
5.4.2 The Ordered Inter-Element Spacing .....	123
<b>5.5 The Optimum MLPA Configurations .....</b>	<b>128</b>
<b>5.6 An Upper Bound of the Achievable DOFs of the 3LPA.....</b>	<b>129</b>
5.6.1 An Upper Bound of DOFs for the 3LPA Config.A.....	133
5.6.2 An Upper Bound of DOFs for the 3LPA Config.B.....	137
<b>5.7 Results and Analysis .....</b>	<b>138</b>
5.7.1 MLPAs with Minimum Number of Sensors.....	138
5.7.2 Array Configurations.....	139
5.7.3 The Number of Lags versus the Number of Sensors.....	148
5.7.4 Optimum Arrays .....	151
5.7.5 Number of Unit Spacings .....	156
5.7.6 Upper Bound of the DOFs of 3LPA.....	157
<b>5.8 Chapter Summary.....</b>	<b>159</b>

## **CHAPTER 6 SPARSE DOA ESTIMATION BASED ON MULTI-LEVEL PRIME ARRAY WITH COMPRESSION..... 161**

<b>6.1 Introduction .....</b>	<b>161</b>
<b>6.2 System Model.....</b>	<b>166</b>
6.2.1 Multi-Level Prime Array (MLPA) .....	166
6.2.2 DOA Signal Model .....	167
<b>6.3 Multi-Level Prime Array With Compressed Subarray (MLPAC) .....</b>	<b>169</b>
<b>6.4 Simulation and Results .....</b>	<b>175</b>
6.4.1 Impact of Compression on the DOFs .....	175
6.4.2 Statistical Error Analysis.....	176
<b>6.5 Chapter Summary.....</b>	<b>183</b>

## **CHAPTER 7 DOA ESTIMATION WITH TWO DIMENSIONAL MLPA ARRAY CONFIGURATION ..... 185**

<b>7.1 Introduction .....</b>	<b>185</b>
<b>7.2 System Model.....</b>	<b>189</b>
7.2.1 Proposed Array .....	189
7.2.2 2D-DOA Estimation .....	191
<b>7.3 2D-DOA Estimation via Sparse Representation.....</b>	<b>193</b>
<b>7.4 Simulation and Results .....</b>	<b>195</b>
7.4.1 Difference Coarray in 2D.....	196
7.4.2 Impact of Compression in 2D.....	198

7.4.3 Statistical Error Analysis.....	199
<b>7.5 Chapter Summary.....</b>	<b>200</b>
 <b>CHAPTER 8 CONCLUSIONS AND FUTURE WORK.....</b>	 <b>201</b>
8.1 Summary of Findings .....	201
8.2 Suggestions for Future Work .....	204
 <b>BIBLIOGRAPHY .....</b>	 <b>206</b>
 <b>PUBLICATIONS FROM THE DISSERTATION.....</b>	 <b>219</b>
 <b>VITAE.....</b>	 <b>222</b>

## LIST OF TABLES

Table 4-1: NI-USRP 2950R specifications.....	75
Table 5-1: Main steps to select the number of sensors in each subarray .....	123
Table 5-2: Main steps to decide on the inter-element spacing and select the best MLPA configuration .....	126
Table 5-3: 3LPA Config.A and Config.B characteristics .....	130
Table 5-4: MLPA configurations using the minimum possible number of sensors .....	140
Table 5-5: Comparison between array's characteristics for $N = 10$ .....	142
Table 5-6: 3LPA characteristics for $N = 12$ .....	143
Table 5-7: 4LPA characteristics for $N = 16$ .....	146
Table 5-8: 3LPA versus 4LPA characteristics for $N = 20$ .....	148
Table 5-9: Design alternatives for 4LPA .....	153
Table 5-10: Design alternatives for 5LPA .....	155
Table 5-11: Design alternatives for 6LPA .....	155
Table 6-1: The ordered inter-element spacing for different MLPA levels .....	167
Table 6-2: Comparison between array's characteristics for $N = 10$ .....	174
Table 6-3: 3LPA and 3LPAC characteristics for $N = 12$ .....	174
Table 6-4: 4LPA and 4LPAC characteristics for $N = 14$ .....	174

# LIST OF FIGURES

Figure 2-1: System model for source localization .....	12
Figure 2-2: Main topics of the study .....	14
Figure 2-3: DOA versus antenna locations .....	14
Figure 2-4: Main steps of $l_1$ -SVD algorithm .....	21
Figure 3-1: Spatial spectra for uncorrelated and correlated sources with DOAs of $63^\circ$ , $73^\circ$ and $N = 8$ .....	29
Figure 3-2: RMSE versus SNR for different $N$ and $K = 1$ .....	31
Figure 3-3: RMSE versus $d/\lambda$ for $N = 2, 4, 8$ , SNR = 20 dB, and $K = 1$ .....	33
Figure 3-4: 3dB beamwidth versus $d/\lambda$ for different $N$ , SNR = 20 dB, and $K = 1$ .....	34
Figure 3-5: 3dB and 6dB beamwidth versus SNR for different $N$ , and $K = 1$ .....	35
Figure 3-6: RMSE versus $T$ for different $N$ when SNR = 20 dB and $K = 1$ .....	36
Figure 3-7: 3dB beamwidth as function of $T$ for different $N$ when $K = 1$ .....	37
Figure 3-8: RMSE versus SNR for different $N$ and $K = 2$ .....	39
Figure 3-9: RMSE versus $d/\lambda$ for two sources and different $N$ .....	40
Figure 3-10: Probability of source resolvability versus $T$ with SNR = 10 dB (dashed lines), SNR = 20 dB (solid lines) and $N = 4, 8$ .....	41
Figure 3-11: Bias in localizing two sources versus angular separation with SNR = 10 dB (solid lines), 20 dB (dotted lines), $N = 8$ , and $K = 2$ .....	43
Figure 3-12: Probability of source resolvability versus SNR: upper subplots $N = 4$ (solid lines), $N = 8$ (dashed lines), and lower subplots: $\theta = [60^\circ, 80^\circ]$ (solid lines), $\theta = [60^\circ, 100^\circ]$ (dashed lines) .....	44

Figure 3-13: RMSE in degree versus source location and the number of elements with SNR = 0 dB.....	46
Figure 3-14: PRR versus source location and the number of elements with SNR = 0 dB.....	47
Figure 3-15: Beamwidth in degree versus source location and the number of elements with SNR = 0 dB.....	48
Figure 3-16: Average processing time versus the number of elements .....	49
Figure 4-1: Coprime array structure and the corresponding difference coarray.....	57
Figure 4-2: System model for DOA estimation.....	58
Figure 4-3: Latency versus the total number of antenna elements .....	64
Figure 4-4: Moving coprime array and scene layout .....	66
Figure 4-5: Measurements setup.....	67
Figure 4-6: Normalized spectrum versus frequency and estimated DOA using Lasso algorithm for moving coprime array .....	69
Figure 4-7: Normalized spectrum versus frequency and estimated DOA using MUSIC algorithm for a ULA .....	70
Figure 4-8: NI-USRP 2950R module .....	76
Figure 4-9: The whole system installed on a rack .....	77
Figure 4-10: DOA estimation setup.....	78
Figure 4-11: The received signals before and after phase calibration .....	80
Figure 4-12: The phase of the received signals when the transmitter at zero degree .....	81
Figure 4-13: The normalized spectrum using different algorithms .....	82

Figure 4-14: Estimated angles versus actual angles based on ULA and coprime array for a single transmitter .....	84
Figure 4-15: Characteristics and layout of coprime array of patch elements .....	91
Figure 4-16: Gain and phase responses for a printed coprime array with monopole and patch elements .....	92
Figure 4-17: Gain and phase responses for printed ULAs of monopole elements .....	93
Figure 4-18: Gain and phase responses for printed ULAs of patch elements .....	94
Figure 4-19: Normalized spectra using Lasso versus DOA in noise free environment for coprime array with isotropic and directive antennas.....	97
Figure 4-20: RMSE versus SNR when $\theta \sim [-40^\circ, 40^\circ]$ using Lasso algorithm for (a) isotropic and (b) directed antenna .....	98
Figure 4-21: RMSE versus SNR for different source distributions (a) $\theta \sim [-40^\circ, 40^\circ]$ and (b) $\theta \sim [-50^\circ, 50^\circ]$ based on different algorithms with $\delta = 11$ .....	99
Figure 4-22: RMSE versus number of samples for different source arrivals based on different algorithms with $\delta = 11$ .....	101
Figure 4-23: RMSE versus SNR when $\theta \sim [-50^\circ, 50^\circ]$ using (a) MUSIC and (b) Lasso algorithms with isotropic and directive antennas for different unit inter-element spacing, $K = 4$ sources, and $\delta = 11$ .....	102
Figure 4-24: RMSE versus SNR of coprime array of monopole and patch elements for different source distributions using Lasso and MUSIC algorithms with $\delta = 11$ .....	104
Figure 4-25: Experimental setup with 5-element ULA using patch antenna elements ..	105



Figure 4-26: Estimated DOA versus the actual angle using six different printed arrays with monopole and patch antenna elements.....	106
Figure 5-1: The MLPA configuration.....	115
Figure 5-2: MLPAs with $N = 10$ sensors.....	116
Figure 5-3: Difference coarray of the 3LPA configuration using $m = [2,3,7]$ and $\mathcal{S} = [M_2, M_3, M_1]d$ .....	119
Figure 5-4: MLPA characteristics: (a) Number of pairwise coprime integer vectors versus $N$ , (b) Number of inter-element spacing versus $N_p$ .....	127
Figure 5-5: The difference coarray of 3LPA configurations and PA configurations .....	142
Figure 5-6: 3LPAs with $N = 12$ sensors (ii)-(iii) using $m_1 = [3,4,7]$ and (iv)-(v) using $m_2 = [2,5,7]$ .....	144
Figure 5-7: 4LPAs with $N = 16$ sensors using $m = [3,4,5,7]$ .....	146
Figure 5-8: MLPA features including 3LPA, 4LPA, 5LPA, and 6LPA versus the number of sensors.....	150
Figure 5-9: The optimal inter-element spacing versus $N$ for 3LPA.....	152
Figure 5-10: The optimal inter-element spacing versus $N$ for 4LPA.....	153
Figure 5-11: The optimal inter-element spacing versus $N$ for 5LPA.....	154
Figure 5-12: The optimal inter-element spacing versus $N$ for 6LPA.....	156
Figure 5-13: Number of unit spacings versus the total number of elements .....	157
Figure 5-14: The upper bounds of the achievable DOFs for 3LPA Config.A and Config.B .....	159
Figure 6-1: The 3LPA and 3LPAC configurations and the corresponding weight .....	172

Figure 6-2: Spatial spectra estimated using MUSIC (upper subplots) and CS (lower subplots) algorithms for PA (column 2), PAC15 (column 2), and PAC23 (column 3) Config.A using $N = 10$ and with $K = 16$ .....	176
Figure 6-3: RMSE versus SNR for (a)-(b) 3LPA and 3LPAC (c)-(d) PA and PAC with $K = 12$ sources, and $N = 10$ . MUSIC (dotted lines) and CS (solid lines)....	180
Figure 6-4: RMSE as a function of the SNR for 3LPA and 3LPAC with $K = 15$ sources and $N = 12$ elements. MUSIC (dotted lines) and CS (solid lines).....	181
Figure 6-5: RMSE versus number of samples for the 3LPA Config.A and its compressed versions with $K = 12$ sources, SNR = 0 dB, and $N = 10$ elements. MUSIC (dotted lines) and CS (solid lines) .....	182
Figure 6-6: RMSE versus different window size for the 3LPA Config.A and its compressed versions with $K = 12$ sources, SNR = 0 dB, and $N = 10$ elements. MUSIC (dotted lines) and CS (solid lines) .....	183
Figure 7-1: Parallel MLPA configurations for 2D-DOA estimation .....	190
Figure 7-2: The difference coarray of (a) Ref. [138], [139], (b) Ref. [140], [141], (c)-(d) 2D-3LPA and its difference coarray (e)-(f) 2D-3LPAC22 and its difference coarray .....	197
Figure 7-3: 2D-DOA estimation based on 2D-3LPA and 2D-3LPAC22 using CS with $K = 26$ sources in noise free and $N = 24$ elements .....	198
Figure 7-4: RMSE versus SNR based on 2D-3LPA and 2D-3LPAC22 using CS with $K = 16$ , $\delta = 3$ , and $N = 24$ .....	200

## LIST OF ABBREVIATIONS

Abbreviation	Stand for
1D	One dimensional
2D	Two dimensional
3LPA	Three-level prime array
4LPA	Four-level prime array
5LPA	Five-level prime array
6LPA	Six-level prime array
AMSDL	Antennas and Microwave Structure Design Laboratory
BPDN	Basis pursuit de-noising
CACIS	Coprime array with compressed inter-element spacing
CS	Compressive sensing
DF	Direction finding
DOA	Direction of arrival
DOD	Direction of departure
DOFs	Degrees-of-freedom
ESPRIT	Estimation of signal parameter via rotational invariance techniques
EVD	Eigen value decomposition
HFSS	High frequency structure simulator
GCD	Greatest common divisor
LabVIEW	Laboratory virtual instrument engineering workbench
MIMO	Multiple-input-multiple-output
MLPA	Multi-level prime array
MLPAC	Multi-level prime array with compressed subarray
MRA	Minimum redundancy array

Abbreviation	Stand for
MUSIC	Multiple signal classification
MVDR	Minimum variance distortionless response
NI	National instruments
NMRA	Nested MRA
VNA	Vector network analyzer
PCI	Peripheral component interconnect
PRR	Peak-to-ripple ratio
PXI	eXtensions for instrumentation
RF	radio frequency
RMSE	Root mean square error
Rx	Receiver
SFCW	Stepped frequency continuous wave
SDR	Software-defined radio
SNR	Signal-to-noise ratio
SVD	Singular value decomposition
TDOA	Time difference of arrival
TOA	Time of arrival
TRL	Telecommunication research lab
Tx	Transmitter
UCA	Uniform circular arrays
ULA	Uniform linear array
URA	Uniform rectangular arrays
USRP	Universal software radio peripheral
UWB	Ultra-wideband

## LIST OF SYMBOLS

Symbol	Indication
$A$	Amplitude of the estimated spectrum
$\mathbf{A}(\theta)$	Steering matrix
$\mathbf{A}_s$	A matrix constructed with rows of specific permutations of $\mathbf{m}_{n_s}$
$\mathbf{A}_d(\theta)$	Steering matrix of directive antenna elements
$\tilde{\mathbf{A}}$	Extended steering matrix
$\tilde{\mathbf{A}}^{(l)}$	Steering matrix (2D case)
$\tilde{\mathbf{A}}_z$	A sensing matrix constructed using all possible angles (2D case)
$\mathbf{A}_a$	A matrix with rows having $N_p$ pairwise coprime integers
$\mathbf{a}(\theta)$	Steering vector
$\mathbf{A}^{(l)}$	Steering matrix (2D case)
$\mathbf{a}^{(l)}(\alpha_i)$	Steering vector (2D case)
$\alpha_i$	Angle between the $i^{th}$ source and the $y$ -axis
$\alpha_i^g$	Discretized angle at the $i^{th}$ grid point
$\mathbf{B}$	A matrix constructed by appending a vector to the extended matrix, $[\tilde{\mathbf{A}}, \tilde{\mathbf{I}}]$
$\tilde{\mathbf{B}}$	The corresponding matrix of $\mathbf{B}$ for real data, $\tilde{\mathbf{B}} = [\text{real}(\mathbf{B})^T, \text{imag}(\mathbf{B})^T]^T$
$\tilde{\mathbf{B}}^g$	A sensing matrix constructed using all possible DOA
$\mathbf{b}$	A vector that contains signal power of all $K$ sources, $\mathbf{b} = [\sigma_1^2, \sigma_2^2, \dots, \sigma_K^2]^T$ , and scaled by $e^{-j\pi \cos(\beta_i)}$ (2D case)
$\beta_i$	Angle between the $i^{th}$ source and the $x$ -axis
$\mathbb{C}_p$	A set of the virtual sensors within the difference coarray
$C_{\text{MLPA}}$	Number of possible ordered inter-element spacing for an MLPA
$c$	Compression factor in MLPAC
$\epsilon$	A user specified bound for $l_0$ -norm

Symbol	Indication
$\eta_c, \eta_{c^-}$	Number of unique lags in $\mathbb{L}_c$ and $\mathbb{L}_c^-$ , respectively
$\eta_p$	Total number of unique lags in $\mathbb{L}_p$
$\eta_l$	Number of unique integers in $\mathbb{L}_l$
$D$	Dimension or aperture size of the array
$D^{(l)}$	Aperture size (2D case)
$d$	Unit inter-element spacing
$f_c$	Carrier frequency
$\mathbf{G}(\boldsymbol{\theta})$	Complex gain matrix of all antenna elements
$\mathbf{g}_i(\boldsymbol{\theta})$	Complex gain vector of the $i^{th}$ antenna element
$g_i(\theta_i)$	Complex gain of the $i^{th}$ antenna element form the $i^{th}$ angle
$\mathbf{I}$	Identity matrix
$\tilde{\mathbf{I}}$	A vector constructed by vectorizing $\mathbf{I}$
$\tilde{\mathbf{I}}_1$	A vector of length $l_{cg} \times 1$ with “1” at the $(l_x + 1)^{th}$
$K$	Number of sources to be estimated
$k_i$	A counter of integer numbers $0 \leq k_i \leq M_i - 1$
$\mathbf{L}$	A matrix contains the Eigen values of $\mathbf{Y}$ after applying SVD
$I_{iter}$	Total number of Monte Carlo trails
$\mathbb{L}_c, \mathbb{L}_c^-$	Positions of the cross-differences and their mirrors of the MLPA
$\mathbb{L}_{cij}, \mathbb{L}_{cij}^-$	A subset of $\mathbb{L}_c$ , constructed by taking all differences between $\mathbb{P}_i$ and $\mathbb{P}_j$ , $\forall j > i$ , and its negative mirror position
$\mathbb{L}_l$	A set which account for the intersection between $\mathbb{L}_{cij}, \mathbb{L}_{cij}^-, \forall i, i$
$\mathbb{L}_s, \mathbb{L}_s^-$	Positions of the self-differences and their mirrors of the MLPA
$\mathbb{L}_p$	A set of unique integers within the difference coarray
$l_c, l_s$	An entry that belong to $\mathbb{L}_c$ and $\mathbb{L}_s$ , respectively
$-l_c, -l_s$	An entry that belong to $\mathbb{L}_c^-$ and $\mathbb{L}_s^-$ , respectively

Symbol	Indication
$l_{ug}$	Number of unique lags in the difference coarray
$l_{cg}$	Number of consecutive lags in the difference coarray
$\lambda$	Wavelength
$\lambda_g$	Regularized parameter
$\mathbf{m}$	A vector that contains $N_p$ pairwise coprime integers
$\mathbf{m}^{(l)}$	A vector that contains $N_p$ pairwise coprime integers (2D case)
$M_i$	Number of elements in the $i^{th}$ subarray
$\mathbf{M}$	A matrix that contains $N_s$ rows of all possible pairwise coprime vectors
$\mathbf{m}_{n_s}$	The $n_s^{th}$ row of $\mathbf{M}$
$N$	Total number of receive antenna elements or sensors
$N_c$	Number of MLPA configurations for a specific $N$ and $N_p$
$N_p$	Number of subarrays or array level
$N_s$	Number of pairwise coprime vectors valid to construct an MLPA
$\mathbf{N}_{SV}$	White Gaussian noise matrix after applying SVD
$N_\theta$	Number of possible angles within the sampling grid of $\theta$
$N_\alpha$	Number of possible angles within the sampling grid of $\alpha$
$\mathbf{n}(t)$	White Gaussian noise vector
$\mathbf{n}^{SV}$	White Gaussian noise vector after applying SVD
$P(\theta)$	Total averaged output power out of an array as a function of $\theta$
$P(\mathbf{w})$	Total averaged output power out of an array as a function of $\mathbf{w}$
$\mathbb{P}$	A set of element locations within the array
$\mathbb{P}_i$	A subset of element locations within the $i^{th}$ subarray
$\mathbf{p}$	Positions of the elements within the array
$p_m$	Position of the $m^{th}$ antenna element

Symbol	Indication
$\mathbf{q}$	Eigenvector associated with $N - K$ smallest eigenvalues
$\mathbf{R}_{SS}$	Covariance matrix of the transmitted signals
$\mathbf{R}_{YY}$	Covariance matrix of the received data
$\mathbf{R}_{Y^{(2)}Y^{(1)}}$	Covariance matrix of the received data in 2D
$\mathbf{R}_{zz}^{SS}$	Spatially smoothed matrix
$\mathbf{r}$	A vector generated by appending the noise variance to $\mathbf{b}$
$\mathbf{r}^g$	Sparse vector over the discretized grid search
$\hat{\mathbf{r}}^g$	Estimated sparse vector using Lasso over the discretized grid search
$\mathbf{S}$	Transmitted signals matrix
$\mathbf{S}_{SV}$	Transmitted signals matrix (sparse) after applying SVD (sparse)
$\mathbf{s}^{SV}$	Transmitted signal vector after applying SVD
$\tilde{\mathbf{s}}^{(l_2)}$	$l_2$ -norm to find the sparse variable
$s(t)$	Transmitted signal
$\sigma_i^2$	Signal power of the $i^{th}$ source
$\sigma_n^2$	Noise variance
$\mathbf{\Sigma}$	Diagonal matrix contains the Eigen values of $\mathbf{R}_{zz}^{SS}$ after applying EVD
$\mathcal{S}$	Ordered inter-element spacing vector of all subarrays
$\mathcal{S}_i$	Inter-element spacing of the $i^{th}$ subarray normalized by $d$
$\mathcal{S}^{(l)}$	Ordered inter-element spacing vector of all subarrays (2D case)
$\mathcal{S}_i^{(l)}$	Inter-element spacing of the $i^{th}$ subarray normalized by $d$ (2D case)
$T$	Number of samples or snapshots
$\Delta\theta$	Absolute value of the difference between the DOAs for two sources
$\theta_i$	DOA of the $i^{th}$ source
$\theta_i^g$	Discretized DOA at the $i^{th}$ grid point



Symbol	Indication
$\hat{\boldsymbol{\theta}}$	Estimated DOA
$\theta_{3dB}$	3dB beamwidth
$\theta_{6dB}$	6dB beamwidth
$\mathbf{U}_s$	Signal subspace
$\mathbf{u}$	An arbitrary vector belong to $\mathbb{P}$
$\mathbf{V}_n$	Noise subspace
$\mathbf{v}$	An arbitrary vector belong to $\mathbb{P}$
$v_\Delta$	Number of unit spacings
$\mathbf{w}$	Weight vector
$w$	Weight function
$\mathbf{Y}$	Received measurement matrix
$\mathbf{Y}^{(l)}$	Received measurement matrix (2D case)
$\mathbf{Y}_{SV}$	Received measurement matrix after applying SVD
$\mathbf{y}^{SV}(k)$	Received measurement vector after applying SVD
$\mathbf{y}(t)$	Received measurement vector
$\mathbf{y}^{(l)}(t)$	Received measurement vector (2D case)
$y_d(t)$	Weighted received signal
$\mathbf{z}$	A complex vector resulting from vectorizing the covariance matrix
$\mathbf{z}_1$	A vector extracted from $\mathbf{z}$ based on the consecutive lags
$\tilde{\mathbf{z}}$	The real vector of $\mathbf{z}$ which constructed as $\tilde{\mathbf{z}} = [\text{real}(\mathbf{z})^T, \text{imag}(\mathbf{z})^T]^T$

## LIST OF NOTATIONS AND OPERATIONS

Notation	Denote
Lower-case	Vectors
Upper-case	Matrices
$E(.)$	Statistical expectation operator
$\text{diag}(x)$	A diagonal matrix that uses the elements of $x$ as its diagonal elements
$\otimes$	Kronecker product
$I_N$	Identity matrix of size $N \times N$
$(.)^*$	Complex conjugation of a matrix or vector
$(.)^T$	Transpose of a matrix or vector
$(.)^H$	Conjugate transpose of a matrix or vector
$\text{vec}(.)$	Vectorizing a matrix into a vector by column-wise
$\ \cdot\ _2,  \cdot _1$	Euclidean $l_2$ and $l_1$ Norms
$ \cdot $	Cardinality operation
$\mathbb{Z}^+$	Set of positive integers
$\text{Re}(.)$ and $\text{Im}(.)$	Real and imaginary parts of complex element
$C(n, k) = \binom{n}{k}$	Combination of
$P(n, k)$	Permutations
$n!$	Factorial operation: $n(n - 1)(n - 2) \dots \times 2 \times 1$
$\cup$	Union operation on sets
$\cap$	Intersection operation on sets
$\subseteq$	A subset of or equal to

## **ABSTRACT**

Full Name : [Saleh Ahmed Yaslam Alawsh]

Thesis Title : [Sparse Direction-of-Arrival Estimation with Constrained Antenna Arrays]

Major Field : [Electrical Engineering]

Date of Degree : [April 2018]

A set of antenna/sensor elements arranged in a certain geometry is called an antenna/sensor array. One application of antenna arrays is to estimate the direction of arrival (DOA) of signals emitted from certain sources. DOA estimation has many applications in beam steering to improve signal reception and interference suppression. Generally, the received signal is corrupted by different impairments as it propagates through the communication channel. These impairments include noise, multipath, narrowband/wideband interference, etc. Therefore, a robust technique is needed to estimate the DOA of the received signal. Multiple signal classification (MUSIC) and estimation of signal parameter via rotational invariance techniques (ESPRIT) are among the main used estimation techniques. Compressive sensing (CS) was also proposed for DOA estimation due to its ability to work with reduced data. In general, the number of sources to be estimated is small. Therefore, sparse reconstruction can be exploited to work with reduced data sets and hence shorter processing time.

Hardware implementation of DOA techniques in handheld wireless devices has two main constraints. First, limited number of antennas and second, limited inter-element spacing.

DOA estimation with constrained arrays calls for extra processing and/or efficient array configurations. Very close antenna elements suffer from mutual coupling effect.

The problem of DOA estimation with constrained number of elements and limited inter-element spacing antenna arrays is examined. The main objective is to strike an optimal balance between complexity and accuracy. Different performance measures have been discussed and evaluated. A comparison between important DOA estimation algorithms is presented including: beamforming, Capon, MUSIC, and first-norm singular value decomposition ( $l_1$ -SVD). Experimental setups were also built using moving coprime arrays and based on software-defined radio (SDR) in realistic channel environments. The moving array uses only one antenna element which moves along the array axis to cover all pre-specified locations. The complexity in terms of the number of antennas and receivers is reduced and the mutual coupling effect is eliminated. Prototyped antenna arrays were also evaluated experimentally to study the effect of antenna directionality on the accuracy of DOA estimation. Moreover, the radiation patterns of the designed arrays were extracted using high frequency structure simulator (HFSS) and were augmented in the sparse reconstruction framework. Based on the simulation and experimental evaluation, several requirements have been identified which calls for novel array configurations. Based on the moving coprime array, very narrow beamwidth is realized using Lasso algorithm compared with that based on a uniform linear array using MUSIC algorithm even if the number of elements is doubled. With the SDR platform using one source, we have proved that the beamwidth at the estimated angle using Lasso algorithm is significantly sharper than those produced by MUSIC and Capon. The results also show that the maximum errors in noise free environment for estimating a source among the assumed four sources with isotropic

and directive antennas are  $0.5^\circ$  and  $2.5^\circ$ , respectively using the simulated coprime array with patch elements. For the prototyped antenna arrays, the coprime array with patch elements realizes the best performance. The 4-element uniform linear array with monopole elements has got the largest error that is around  $15^\circ$ .

This dissertation proposes a multi-level prime array (MLPA) configuration for sparse sampling that can further increase the degrees-of-freedom (DOFs). The proposed array uses multiple uniform linear subarrays where the number of sensors in the subarrays are pairwise coprime integers. The inter-element spacing between the sensors is formulated as a scaled multiple of half-wavelength where the subarrays share only their first element. For a given number of sensors, the proposed array has smaller aperture and achieves more unique and consecutive lags compared with coprime arrays. The proposed configuration has limited holes in the difference coarray. The analytical expressions of both the difference coarray and the aperture size are derived. Different MLPA configurations can be constructed for fixed number of antennas and the one that maximizes the DOFs is exploited. We have found that MLPAs can achieve higher DOFs compared with coprime arrays provided that the number of elements is large enough. Under equal aperture size and comparable DOFs with that of nested arrays, the proposed MLPA results in less mutual coupling effects. The number of consecutive lags is further increased by properly compressing the inter-element spacing of one subarray under a fixed number of antennas and without changing the aperture size. The resultant array, MLPA with compressed subarray (MLPAC), can have a hole-free difference coarray as in nested array case. Sparse reconstruction and MUSIC algorithms are utilized based on the difference coarray. The MLPAC can estimate larger number of sources using both MUSIC and sparse

reconstruction algorithms. At 0 dB signal-to-noise ratio (SNR) and ten antenna elements, the root mean square error (RMSE) based on an MLPAC with three subarrays is larger than that based on nested array by around  $0.05^\circ$  and  $2^\circ$  to  $2.6^\circ$  using CS and MUSIC algorithms, respectively.

Finally, modified configuration with two parallel MLPAs is extended for two dimensions (2D-DOA) estimation. We have shown that the proposed configuration can realize the same performance as the 2D-nested array by increasing the SNR by only 1 dB.

Simulation and experimental results confirm the derived conclusions and demonstrate the superiority of the proposed configurations in DOA estimation especially for constrained aperture size.

## ملخص الرسالة

الاسم الكامل: صالح أحمد يسلم العوش

عنوان الرسالة: تقدير زاوية وصول الإشارة باستخدام مصفوفة الهوائي المقيدة

التخصص: هندسة كهربائية

تاريخ الدرجة العلمية: إبريل 2018م

تسمى مجموعة من عناصر الهوائي/المستشعر مرتبة في هندسة معينة صفيف الهوائي/المستشعر. أحد تطبيقات مصفوفات الهوائي هو تقدير اتجاه زاوية الوصول (DOA) للإشارات المنبعثة من بعض المصادر. يتضمن تقييم زاوية الوصول العديد من التطبيقات في توجيه الحزمة لتحسين استقبال الإشارات وإزالة التداخل. بشكل عام ، تتعطل الإشارة المستقبلية من خلال عدة عوامل مختلفة أثناء انتشارها عبر قناة الاتصال. وتشمل هذه العيوب الضوضاء ، وتعدد مسارات انتشار الموجة ، وتداخل النطاق الضيق / النطاق العريض ، وما إلى ذلك. لذلك ، هناك حاجة إلى تقنية قوية لتقدير زاوية الوصول للإشارة المستقبلية. يعتبر تصنيف الإشارات المتعددة (MUSIC) وتقدير معلمة الإشارة عبر تقنيات الثبات الدوراني (ESPRIT) من بين تقنيات التقدير الرئيسية المستخدمة. كما تم اقتراح الاستشعار عن طريق الضغط (CS) لتقدير زاوية الوصول بسبب قدرتها على العمل مع انخفاض البيانات. بشكل عام ، عدد المصادر التي سيتم تقديرها قليل جداً. لذلك ، يمكن استغلال إعادة البناء المتفرقة للعمل مع مجموعات بيانات مخفضة وبالتالي وقت معالجة أقصر.

تطبيق الأجهزة في تقنية تحديد زاوية الوصول في الأجهزة اللاسلكية المحمولة لديها اثنين من القيود الرئيسية. أولاً ، عدد محدود من الهوائيات والثاني ، تباعد محدود بين الهوائيات. يتطلب تقدير زاوية الوصول مع صفائف مقيدة معالجة إضافية و/أو تكوينات صفيف فعالة. عندما تكون عناصر الهوائي متقاربة جداً فإنها تعاني من تأثير اقتران المتبادل.

يتم فحص مشكلة تقدير زاوية الوصول مع عدد مقيد من العناصر ومصفوفات هوائيات التباعد بين العناصر المحدودة. الهدف الرئيسي هو تحقيق توازن مثالي بين التعقيد والدقة. وقد تم مناقشة وتقييم مقاييس الأداء المختلفة. يتم تقديم مقارنة بين خوارزميات تقدير زاوية الوصول الهامة بما في ذلك: تكوين الشعاع (beamforming) ، أدنى تباين استجابة التشويش (Capon) ، تصنيف الإشارات المتعددة (MUSIC) ، وتحلل القيمة المفردة من المستوى الأول ( $l_1$ -SVD). كما تم بناء الاعدادات التجريبية باستخدام مصفوفات ال coprime المتحركة والاعتماد على الراديو المحدد بالبرمجيات (SDR) أثناء وجود مصادر مختلفة

كتعدد الانتشار التي تؤثر على الإشارة في قناة الاتصال. تستخدم المجموعة المتحركة عنصر هوائي واحدًا يتحرك على طول محور الصفيف لتغطية جميع المواقع المحددة مسبقًا. يتم تقليل التعقيد من حيث عدد الهوائيات وأجهزة الاستقبال ويتم التخلص من تأثير الاقتران المتبادل. كما تم صُممت مجموعات من صفيف الهوائي بشكل نمطي وتم فحصها بشكل تجريبي لدراسة تأثير اتجاهية الهوائي على دقة تقدير زاوية الوصول. وعلاوة على ذلك، تم استخراج أنماط الإشعاع من هذه المصفوفات المُصنعة باستخدام هيكل محاكي الترددات العالية (HFSS) وتجربتها في إطار إعادة الإعمار المتناثر. استنادًا إلى المحاكاة والتقييم التجريبي، تم تحديد العديد من المتطلبات التي تستدعي تكوين صفيف جديد. بناءً على مجموعة coprime المتحركة، تم الحصول على عرض حزمة ضيق جدًا باستخدام خوارزمية Lasso مقارنة مع تلك القائمة على صفيف خطي منتظم باستخدام خوارزمية يعتبر تصنيف الإشارات المتعددة (MUSIC) حتى إذا تضاعف عدد العناصر. باستخدام منصة الراديو المحدد بالبرمجيات (SDR) وعند وجود مصدر واحد، أثبتنا أن عرض الحزمة عند الزاوية المقدرة باستخدام خوارزمية Lasso أكثر وضوحًا من تلك التي تنتجها MUSIC و Capon. تظهر النتائج أيضًا أن الحد الأقصى للأخطاء في بيئة خالية من الضوضاء لتقدير مصدر واحد بين المصادر الأربعة المفترضة باستخدام هوائيات متماثلة (isotropic) و هوائيات موجهة (directive) هي  $0.5^\circ$  و  $2.5^\circ$ ، على التوالي باستخدام مصفوفة coprime المحاكاة مع عناصر التصحيح (patch). بالنسبة لمصفوفات الهوائي التي تم تصميمها، فإن مصفوفة coprime مع عناصر التصحيح (patch) تحقق أفضل أداء. لقد حصلت المجموعة الخطية المنتظمة المكونة من 4 عناصر مع العناصر أحادية القطب (monopole) على أكبر خطأ وهو تقريبًا  $15^\circ$ .

تقترح هذه الأطروحة تشكيل صفيف هوائي متعدد المستويات (MLPA) لأخذ العينات المتناثر الذي يمكن أن يزيد من درجة الحرية أو التغيير (DOFs). تستخدم الصفيف المقترح عدة مجموعات فرعية خطية موحدة حيث يكون عدد أجهزة الاستشعار في الطبقة الفرعية عبارة عن أعداد صحيحة أولية لا يوجد بينها عوامل مشتركة. تمت صياغة التباعد بين عناصر المستشعرات كمضاعف لنصف طول الموجة حيث تتشارك المجموعات الفرعية العنصر الأول فقط. بالنسبة لعدد معين من أجهزة الاستشعار، فإن الصفيف المقترح يتطلب أبعاد ومساحة أصغر ويعطي مواقع فريدة مختلفة ومتوالية بدون انقطاع أو ثغرات فيما بينها مقارنة بالمصفوفات المكونة من رقمين أوليين (coprime). التكوين المقترح يحتوي على ثغرات محدودة في فوراق مواقع عناصر مصفوفة الهوائي (difference coarray). تمت صياغة التعبيرات الرياضية لفوراق مواقع عناصر مصفوفة الهوائي والابعاد المطلوبة لتشكيل المصفوفة. يمكن إنشاء تكوينات MLPA مختلفة من أجل عدد ثابت من الهوائيات واستغلال المصفوفة التي



تزيد من درجة التعبير (DOFs). لقد وجدنا أن MLPAs يمكن تحقيق أعلى DOFs مقارنة مع صفائف coprime شريطة أن يكون عدد العناصر كبير بما فيه الكفاية. تحت حجم الفتحة المتساوية وقيم DOFs المقارنة مع صفائف متداخلة (nested arrays)، ينتج عن MLPA المقترح تأثيرات اقتران أقل. يتم زيادة عدد الفترات المتتالية عند اخذ الفوارق بين مواقع عناصر الهوائي بشكل أكبر عن طريق ضغط التباعد بين العناصر لواحدة من المجموعات الفرعية بشكل صحيح مع عدم تغيير عدد الهوائيات وبدون تغيير حجم المصفوفة. الصفيف الناتج يسمى صفيف هوائي متعدد المستويات المضغوط (MLPAC) الذي يمكن أن تكون الفوارق بين مواقع عناصره متوالية و خالية من أي ثغرات كما هو الحال في حالة المصفوفة المتداخلة (nested arrays). يتم استخدام خوارزميات إعادة البناء المتناثر و تصنيف الإشارات المتعددة استنادًا إلى الفوارق بين مواقع عناصر الهوائي. يمكن لصفيف الهوائي متعدد المستويات المضغوط تقدير عدد أكبر من الزوايا باستخدام كلا الخوارزميتين. عندما تكون نسبة الإشارة إلى الضوضاء (SNR) تساوي 0 ديسيبل وعند استخدام عشرة عناصر من الهوائي، يكون جذر متوسط مربع الخطأ (RMSE) الناتج عن استخدام MLPAC ذو الثلاثة مستويات أكبر من ذلك الناتج عند استخدام صفيف متداخل بحوالي  $0.05^0$  و  $2^0$  إلى  $2.6^0$  باستخدام خوارزميات الضغط (CS) و تصنيف الإشارات المتعددة (MUSIC)، على التوالي.

وأخيرًا، تم اقتراح مصفوفة هوائي أخرى باستخدام وحدتي الهوائي المتعدد المستويات بشكل متوازيين لتقدير زاويتين للوصول (2D-DOA). لقد أظهرنا أن مصفوفة الهوائي المقترحة يمكن أن تحقق نفس الأداء مثل الصفيف المتداخل (2D-nested array) ثنائي الأبعاد بزيادة النسبة SNR بمقدار 1 ديسيبل فقط.

تؤكد نتائج المحاكاة والنتائج التجريبية الاستنتاجات المشتقة التي توصلنا لها وتظهر تفوق التكوينات المقترحة في تقدير زاوية الوصول خاصة بالنسبة بالنسبة للصفائف ذات الحجم المقيّد.

## CHAPTER 1 INTRODUCTION

### 1.1 Overview

There are numerous methods for determining the location of a signal emitter using diverse types of direction finding (DF) techniques. One of the most widely used techniques is the direction of arrival (DOA) technique that estimates the angle from which the signal arrives. Another DF technique is the direction of departure (DOD) which is defined as the angle at which the signal is emitted from the transmitter. Two more techniques used for localization are: time of arrival (TOA) and time difference of arrival (TDOA), with the difference that TOA is defined as the time required for the transmitted signal to reach the receiver, whereas TDOA measures the difference of propagation delays to different receivers.

An antenna array consists of a set of antennas or sensors that are arranged in a certain geometry such as linear, circular, coprime, nested, etc. The main objective of the antenna array in our context is to find the direction of the sources that emit their signals on the array. The accuracy of estimation depends on the measurements at the outputs of these antenna elements and the given array geometry as well as the characteristics of the propagation medium.

Generally, the received signal is corrupted by different impairments as it propagates through the communication channel. These impairments include noise, multipath, narrowband/wideband interference, etc. Therefore, a robust technique is needed to estimate the DOA of the received signal. In practical mobile applications, DOA estimation is

restricted by the small size of the devices. Thus, the practical implementation of DOA algorithm in handheld wireless devices has two main limitations. First, limited number of antennas and second, limited inter-element spacing between these antennas.

The remaining sections of this chapter are as follows. In Section 1.2, research contributions are listed. Section 7 is dedicated to motivate the research problem followed by specific problem statement in Section 1.4. The main objectives of this research are enumerated in Section 1.5. The outlines of the dissertation are presented in Section 1.6.

## **1.2 Research Contributions**

In this dissertation, the following contributions have been achieved:

1. We have studied the problem of DOA estimation in the presence of two main limitations namely, limited number of antenna elements and limited inter-element spacing via simulation.
2. A moving coprime array configuration is proposed and implemented for DOA estimation under sparse reconstruction framework. The proposed array uses only one antenna element. The antenna moves along the array axis to cover certain locations specified by the conventional coprime array. The proposed system has reduced complexity and eliminates the mutual coupling effect.
3. A software-defined radio (SDR) platform is implemented for sparse DOA estimation based on sparse array configurations. With an SDR, the system becomes flexible, simple, practical, reconfigurable, and can be experimentally-tested.
4. We have evaluated sparse DOA estimation for directive coprime arrays. The complex radiation patterns are extracted using an electromagnetic simulator and

then incorporated in the DOA estimation. In addition, printed array configurations with monopole and patch elements are assessed and experimentally tested to study the impact of antenna directivity on the accuracy.

5. A generalized multi-level prime array (MLPA) configuration is proposed for sparse sampling that can increase the degrees-of-freedom (DOFs). The proposed array uses multiple uniform linear subarrays where the number of sensors in the subarrays are pairwise coprime integers. For a given number of sensors, the proposed array has smaller aperture and achieves more unique and consecutive lags compared with coprime arrays. The proposed configuration has limited holes in the difference coarray. The analytical expressions of both the difference coarray and the aperture size are derived.
6. We have proposed a sparse DOA estimation based on MLPA configuration. In MLPA, the number of consecutive lags can be increased by properly compressing the inter-element spacing of one subarray by integer multiple of half wavelength under a fixed number of antennas and without changing the aperture size. The resultant array, MLPA with compressed subarray (MLPAC), can have a hole-free difference coarray as in nested array case. Sparse reconstruction algorithm is utilized based on the difference coarray. The MLPAC can estimate larger number of sources using both multiple signal classification (MUSIC) and sparse reconstruction algorithms.
7. We have extend MLPA configuration for two dimensions (2D) 2D-DOA estimation. The array has a closed form expression for the antenna locations and

few holes appear in the difference coarray. The difference coarray was improved using an optimized MLPACs instead of the MLPAs.

### 1.3 Motivation

DOA estimation has many applications in beam-steering for improving signal reception, interference suppression and target tracking. Basically, if a receiver knows the DOA of a certain transmitter, more energy can be collected by steering the array towards that specific angle. Similarly, the receiver can avoid reception from certain interference by directing its array away from that source. Consequently, this will enhance the signal-to-noise ratio (SNR) at the receiver side as well as reduce the bit error rate during the decoding process for any communication system.

The problem of the DOA estimation becomes more challenging in case of practical circumstances. Employing more antennas for sure will enhance the receiver capability for DOA estimation. Moreover, the inter-element spacing between the antennas is restricted as well by the available physical size in mobile handsets. Definitely, the size of current mobile handsets affect both issues. Most of the previous works have tested the performance using simulations. Only few papers did experimental studies. In addition, very few publications considered the practical limitations in the design of their arrays.

In general, the number of sources needed to be estimated is very few. In other words, the scene of interest in which we are searching in contains only limited number of sources. Therefore, compressive sensing (CS) and sparse representation can be formulated in order to work with reduced data sets. In addition, the processing time can be further decreased. Thus, complexity reduction is one of the most important issues in our study.

## 1.4 Problem Statement

Future handsets are very light and have small size. With such restrictions, there will be a difficulty to design an efficient receiver with DOA capability. The reason is that we have to use only few receive antenna elements in addition to limited inter-element spacing in between. Hence the problem addressed by this dissertation can be stated as follows:

*Propose an array configuration and novel sparse DOA estimation technique, which works under limited number of elements and limited inter-element spacing.*

This dissertation aims to find a promising solution for DOA estimation in future handsets. As such, we discuss two practical issues; limited number of antennas and limited spacing in between. In addition, the performance is investigated for different number of antenna elements, using different performance criteria. Under a given dimension restriction, different inter-element spacing is examined to optimize the DOA estimation. To make the analysis more general, the ratio between the unit inter-element spacing and wavelength is considered. Extensive simulations are conducted to study and inspect the effect of this ratio on the system performance based on some performance.

Moreover, extensive analysis is performed to study the effect of other parameters in the presence of both restrictions. In addition, extensive investigation is accomplished to validate the effectiveness of the proposed configurations. This shall include the number of sources to be estimated and the number of samples or snapshots, and others.

## 1.5 Objectives

For successful consideration of the problem stated above, a full comparative understanding of sparse DOA estimation algorithms is needed. We investigate the estimation problem under practical limitations and compare the performance of candidate algorithms. Based on this understanding, a novel antenna array is adopted and the signal processing part is optimized. The main objectives of this research can be further detailed as follows:

1. Study the problem of DOA estimation based on **reduced data sparse frame work**.
2. Optimize the performance of different DOA estimation algorithms under two **practical limitations**:
  - a. Limited number of antennas
  - b. Limited spacing
3. Evaluate the system performance under **realistic channel environment**.
4. **Build a prototype array** with antenna distribution optimized for sparse DOA estimation.
5. **Design a novel array configuration** that requires small aperture size and can improve the DOFs.
6. **Design an array configuration** with **two-dimensional DOA** capability using **coprime** array extensions.

Objectives 1, 2, and 5 are accomplished using MATLAB®. Experimental setups augment MATLAB® simulation to achieve objectives 3 and 4. To achieve objective 4, raw material and resources were utilized.

## 1.6 Thesis Organization

This dissertation consists of seven chapters. Each chapter in this dissertation presents the details of the work done, including literature review, signal model, analysis towards certain objectives. The rest of the dissertation is structured as follows. CHAPTER 1 discusses the introduction and motivation for the dissertation with problem statement and the main objectives. CHAPTER 2 presents a technical background and literature review for DOA estimation algorithms. CHAPTER 3 provides a review on DOA estimation with focus on practical limitations. Then, some preliminary results when there is a constrain on the physical size of the handsets. Other review is also distributed within the related chapters. In CHAPTER 4, the effect of different channel impairments on the performance of DOA estimation is investigated based on experimental results. 0 proposes a novel array configuration that generalizes the coprime array structure. In CHAPTER 6, the proposed configuration in 0 is further optimized in order to increase the degrees-of-freedom (DOFs). In addition, sparse DOA estimation based on the two novel configurations is proposed. CHAPTER 7 proposes a new configuration for two dimensions DOA estimation. CHAPTER 8 concludes the dissertation, summarize all results and findings of all chapters, and gives recommendations for future work.



## CHAPTER 2 TECHNICAL BACKGROUND

Measuring or estimating the DOA is one of the most common approaches to find the location of sources. This is useful in many applications ranging from wireless communications, such as sonar, navigation, radar, radio astronomy [1], to localization of illegal repeaters [2]. In these applications, the target to be located does not have to be an active target, as it can be a passive target that reflects the signal produced by the DOA estimation system. Some systems can estimate the location of a single target while others can estimate more. Different configurations have been developed, and each has its own advantages and disadvantages. For a given array, the received signals are processed to estimate the DOA. Choosing a proper DOA estimation algorithm is crucial to get the best result for the desired application. This chapter mainly reviews the most widely used DOA estimation algorithms. Other reviews are distributed within the related chapters. Moreover, we briefly discuss and review the basic ideas of these algorithms. In addition, the performance measures used to assess the problem of DOA estimation are defined.

### 2.1 Introduction

The problem of DOA estimation has attracted many researchers due to its important applications. Researchers have developed and proposed different algorithms for DOA estimation. Beamforming, Capon, and subspace-based techniques are among the main used DOA estimation techniques. Sparse reconstruction algorithms are also used since they can work with reduced data sets.

The rest of the chapter is organized as follows. Section 2.2 provides a review on the most widely used DOA estimation algorithms. The system model is presented in Section 2.3. Section 2.4 reviews some technical backgrounds. This includes source localization, antennas, array configurations, DOA estimation algorithms, and some performance metrics.

## **2.2 Algorithms for DOA Estimation: A Review**

Wideband source localization using beamforming was considered in [3], [4], [5]. DOA estimation using Capon algorithm was originally developed in [6]. Based on time reversal for multiple-input-multiple-output (MIMO) radars, Capon algorithm or what is called minimum variance distortionless response (MVDR) was introduced in [7].

A variety of multiple signal classification (MUSIC) algorithms have been widely studied in MIMO radar systems for target localization [8], [9] as well as for source localization [10]–[13]. The sources maybe located in the far-field or in the near-field. Sometimes both far-field and near-field narrowband sources exist [11], [12], [14]. A second order statistics based on MUSIC algorithm has been applied efficiently to estimate DOAs [12]. As an extension to [12], the authors in [14] estimated the DOAs and the power of the far-field sources first. Then these components are removed from the signal subspace. Finally, a near-field reconstruction is employed. This approach is more efficient than [12] since it enhances the reconstruction accuracy and realizes a significant classification of the signal types. The proposed approaches in [12], [14], [15] are not complicated since they do not need a multidimensional search or higher order statistics.

The problem of DOA estimation has been resolved using estimation of signal parameter via rotational invariance techniques (ESPRIT) algorithm [16]–[19]. MUSIC and ESPRIT subspace-based algorithms were suggested to localize sources in [16]. The reconstruction of the DOA was accomplished through two successive one-dimensional searches. Target localization has been investigated based on ESPRIT algorithm in [17]–[19] and auto-pairing of direction of departure (DOD) and DOA [18]. The authors in [17] modified the ESPRIT algorithm to use the SVD instead of using the Eigen value decomposition (EVD) to estimate the signal subspace. As a result, the performance was enhanced in the presence of interference. Compared with ESPRIT algorithm, the error was reduced by around  $1.2^\circ$  at SNR = 0 dB in the presence of two interfering signals [17].

Different approaches were developed for DOA estimation based on CS [20]–[24] since the received signal from the unknown sources is sparse in some domains. DOA estimation based on MUSIC and Capon always uses linear arrays sampled at Nyquist rate with inter-element spacing less than or equal to half-wavelength. Both algorithms need a computation of the covariance matrix. This is not the case using CS which can work at sub-Nyquist sampling rates [20]. Statistical and probabilistic approaches known as Bayesian approaches based on CS can be also applied for DOA estimation. They use the signal distribution to tackle the DOA estimation problem. In [21], the authors used sparse Bayesian learning when the number of the unknown sources is greater than the number of measurements. Reference [22] estimated the DOA by solving a set of Basis Pursuit De-Noising (BPDN) problems. In addition, grid position refinement was used to reduce the complexity of the BPDN problem. In [24], antennas with known and different sparse array geometries were used successfully for localization.

Narrowband source localization in terms of DOA estimation using the first-norm singular value decomposition ( $l_1$ -SVD) algorithm was investigated in [25]–[27]. All  $l_1$ -SVD algorithms use CS first, so they can be considered also as CS based algorithms. In [25],  $l_1$ -SVD was proposed for multiple time or frequency samples such that sharp estimate and super-resolution is achieved. The results show that only the  $l_1$ -SVD algorithm can resolve two uncorrelated sources separated by  $5^\circ$  at 0 dB SNR compared with beamforming, Capon, and MUSIC algorithms [25]. The  $l_1$ -SVD algorithm has also the ability to estimate highly correlated sources which is not the case with beamforming, Capon, and MUSIC algorithms. Reference [27] suggested a modified  $l_1$ -SVD algorithm which can improve the performance in the presence of an interference. The interference is filtered first and then the DOA is recovered where the noise power is estimated and incorporated to solve an optimization problem. Based on the a modified  $l_1$ -SVD algorithm, the RMSE for estimating a single source close to an interference was reduced by around  $0.7^\circ$  [27].

### 2.3 System Model

Assume  $K$  narrowband unknown active sources and located in the far-field transmit signals  $s_k(t)$  for  $k = 1, \dots, K$  with  $\theta_k$  as the DOA with respect to the array axis, see Figure 2-1. A uniform linear array (ULA) is considered for the time being. The receiver has  $N$  omnidirectional antennas located along the  $x$ -axis where  $d$  represents the inter-element spacing between any two antennas. The received corrupted measurements,  $\mathbf{y}(t) = [y_1(t_1), y_2(t_2), \dots, y_N(t_T)]^T$  where  $[\cdot]^T$  indicates the transpose operation, with additive white Gaussian noise,  $\mathbf{n}(t)$ , at the array output can be expressed as:

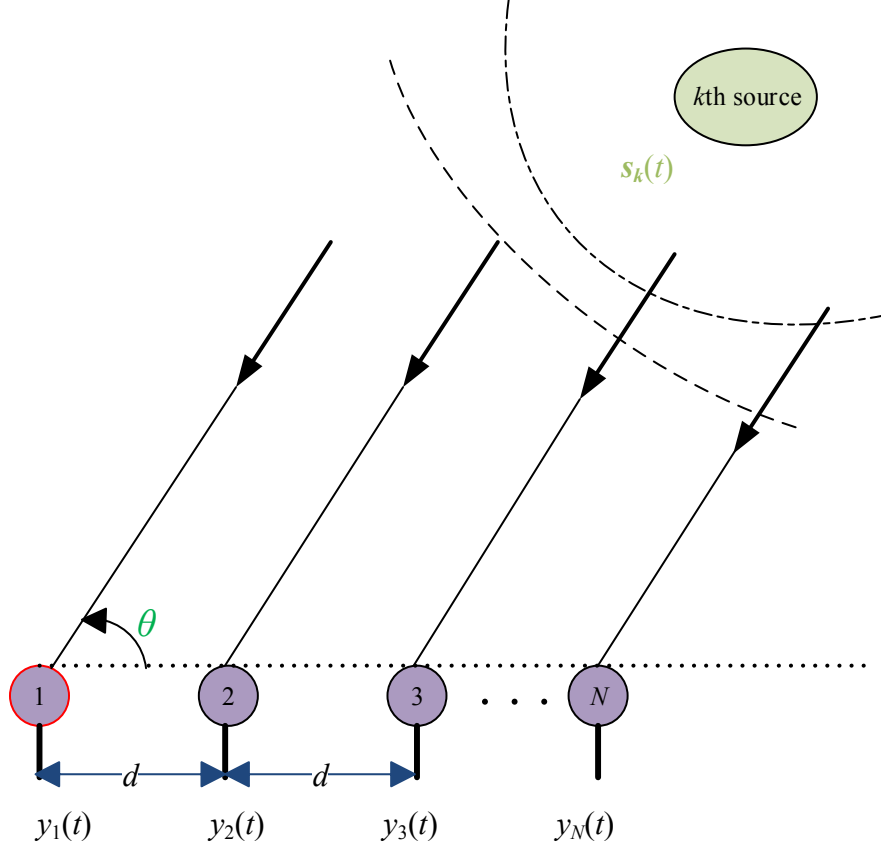


Figure 2-1: System model for source localization

$$\mathbf{y}(t) = \mathbf{A}(\boldsymbol{\theta})\mathbf{s}(t) + \mathbf{n}(t), t \in \{t_1, t_2, \dots, t_T\} \quad (2-1)$$

where  $\mathbf{A}(\boldsymbol{\theta}) = [\mathbf{a}(\theta_1), \dots, \mathbf{a}(\theta_K)]$  is the steering matrix with steering vector  $\mathbf{a}(\theta_k) = \left[ 1, e^{\frac{j2\pi d \cos(\theta_k)}{\lambda}}, \dots, e^{\frac{j2\pi d(N-1) \cos(\theta_k)}{\lambda}} \right]^T$  and  $\lambda, T$  are the signal wavelength and the number of samples or snapshots respectively. The unknown DOAs are represented by  $\boldsymbol{\theta} = [\theta_1, \theta_1, \dots, \theta_K]^T$  and  $\mathbf{s}(t) = [s_1(t), \dots, s_K(t)]^T$  is the transmitted narrowband signals from the unknown sources. Given  $\mathbf{y}(t)$  and the array geometry, we have to find  $\hat{\boldsymbol{\theta}}$ , which is an estimate of  $\boldsymbol{\theta}$  and the number of active sources,  $K$ .

Let  $\mathbf{p} = [p_1, p_2, \dots, p_N]^T$  denote the positions of the elements within the array. The position of the  $n^{th}$  antenna element is located at  $p_n = nd$  with  $n = 0, 1, \dots, N - 1$  and  $d \leq \lambda/2$  to avoid the grating lobe. The above model can be extended for two dimension DOA estimation.

## 2.4 Technical Background

This research covers the intersection of three main topics which are MIMO systems, DOA and CS as depicted in Figure 2-2. The following subsections provide the reader with the needed background.

### 2.4.1 Source Localization through DOA

DOA estimation and localization involves two different tracks: active source localization and passive source localization. This research focuses on active sources that emit power. The sources maybe located in the far-field, near-field or mix of both fields. In this study, the unknown sources are located in the far-field, thus DOA is assumed to be the same for each source across the array. Sources at distance greater than  $\frac{2D^2}{\lambda}$  are considered to be in the far-field [28] where  $D$  represents the aperture size of the array. Figure 2-3 shows a verification of the different source's fields. This is an example for illustrations in which the corresponding DOA (in degrees) is plotted relative to each receive element in meter. The sources are assumed at  $\boldsymbol{\theta} = [160, 100, 30]^o$  with respect to the first antenna element located at zero meter. The ranges in the three subplots are adjusted at random such that different scenarios can be illustrated.

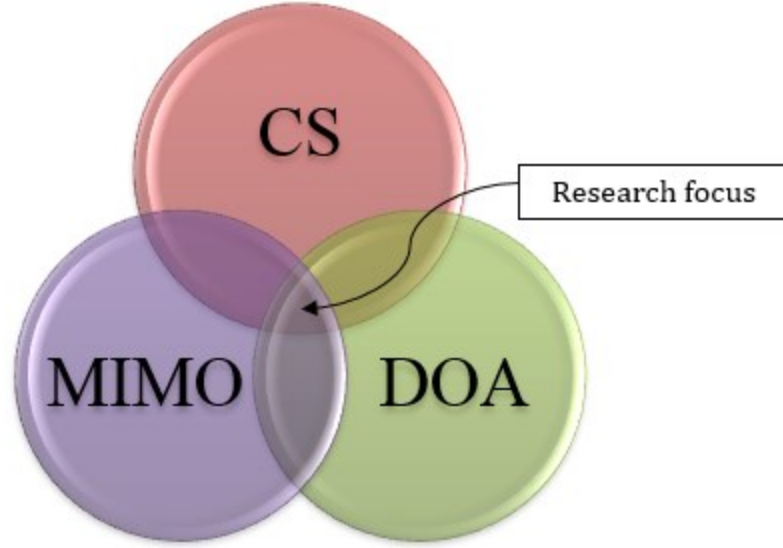
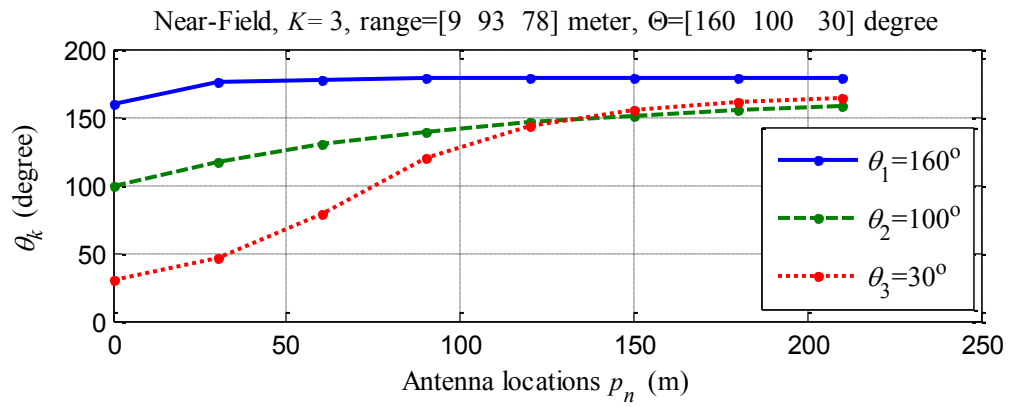
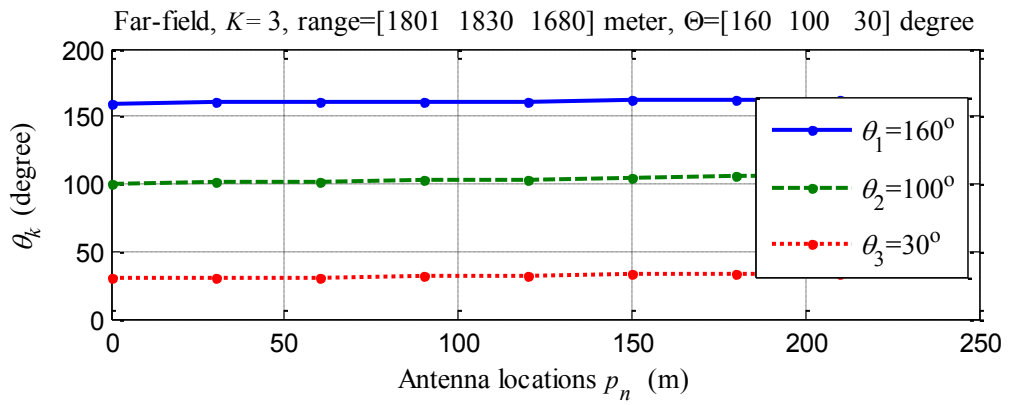


Figure 2-2: Main topics of the study



(a) Near-field



(b) Far-field

Figure 2-3: DOA versus antenna locations

For the near-field case the range of the active sources are assumed at [9,93,78] meter. The variation across the array elements of the DOA is very evident, see Figure 2-3(a). For the far-field, Figure 2-3(b) shows insignificant variations of the angles if the sources are assumed at [1801,1830,1680] meter. The mix-field scenario is a combination of the two cases.

### 2.4.2 Antenna and Array Configurations

A set of antenna/sensor elements arranged in a certain geometry is called an antenna/sensor array. There are many applications for antenna arrays, however DOA estimation is our focus. This could be achieved by relying on: the array geometry, the characteristics of the medium and the received measurements.

#### *A. Antennas*

Antennas are available in different types such as dipole, monopole, and patch like among others. The pattern of an antenna is a plot of the received energy at different directions. The pattern is not distributed uniformly in all directions, and thus antennas have different degrees of directivity. This directivity affects the ability of the antenna in receiving the incoming waves, and thus the performance varies with direction. In our work, we start by assuming isotropic antenna. Later on, directive antenna shall be utilized.

#### *B. Array Geometry*

An antenna array at the transmitter or the receiver can be organized or designed in different configurations. Many array configurations were investigated in the literature for DOA estimation. These include ULA [29], nonuniform linear array [30], uniform circular array (UCA) [31], uniform rectangular array (URA) [32], uniform rectangular frame array [32],



coprime array [33], nested array [34], arbitrary arrays [35], random array [20], and others. Each one of these arrays has its own advantages and limitations.

Antenna arrays can enhance the directivity, in return enhancing the SNR as well as providing the system some control over the maximum radiation power. Thus the beam of the array can be steered towards certain directions and thus enhance its DOA capability [36].

### 2.4.3 Overview of Basic DOA Estimation Algorithms

Normally, the number of sources needed to be estimated is very few. In other words, the scene of interest in which we are searching on contains only limited number of sources. Therefore, CS and sparse representation can be formulated in order to work with reduced data sets and thus decreased processing time. Therefore, complexity reduction is one of the most important issues in our study. There are lots of DOA estimation algorithms in the literature. This overview focuses on the most important and widely used ones, namely: beamforming, Capon, MUSIC, and  $l_1$ -SVD. All  $l_1$ -SVD algorithms use CS first, so they can be considered also as CS based algorithms.

#### *A. Beamforming Algorithm*

The idea here is to direct the array in a certain direction at a time and measure the output power. Maximum output power will be received whenever the “steered” direction matches with DOA of a signal. A weight vector  $\mathbf{w}$  is used to linearly combine the received signal by the sensors to form a single output,  $y_d(t)$ , as [28], [37]:

$$y_d(t) = \mathbf{w}^H \mathbf{y}(t) \quad (2-2)$$

where  $[\cdot]^H$  represents the conjugate transpose (Hermitian) operation. Thus, the total averaged output power,  $P(\mathbf{w})$ , of an array over  $T$  samples can be written as [37]:

$$P(\mathbf{w}) = \frac{1}{T} \sum_{n=1}^T |y_d(t_n)|^2 = \frac{1}{T} \sum_{i=1}^T \mathbf{w}^H \mathbf{y}(t_i) \mathbf{y}^H(t_i) \mathbf{w} = \mathbf{w}^H \mathbf{R}_{yy} \mathbf{w} \quad (2-3)$$

where  $\mathbf{R}_{yy} = \frac{1}{T} \sum_{i=1}^T \mathbf{y}(t_i) \mathbf{y}^H(t_i)$  is the estimated covariance matrix of the received signal.

In beamforming algorithm, the weight vector is equal to the steering vector defined in the system model, i.e.  $\mathbf{w} = \mathbf{a}(\theta)$  where  $\theta$  represents an arbitrary look angle (search angle). If this angle coincides with an angle coming from any source, the spectrum will have a peak at this angle. Essentially, the weight vector is normalized such as:

$$\mathbf{w} = \frac{\mathbf{a}^H(\theta)}{\sqrt{\mathbf{a}^H(\theta) \mathbf{a}(\theta)}} \quad (2-4)$$

Therefore, the output power as a function of the DOA becomes:

$$P(\theta) = \frac{\mathbf{a}^H(\theta) \mathbf{R}_{yy} \mathbf{a}(\theta)}{\mathbf{a}^H(\theta) \mathbf{a}(\theta)} \quad (2-5)$$

The weight vector matches the angles of the incoming signal to produce a peak but attenuate the output power for signals not coming from the angles of the incoming signals.

### *B. Capon Algorithm*

When there is more than one signal present, the array output power contains signal contributions from the desired and undesired angle(s). Capon algorithm overcomes this by forming a beam in the look direction and simultaneously nulls in other directions to reject

other signals. It minimizes the power in all directions and keeps it one in the look direction, as [7], [28], [38], [39]:

$$\min P(\mathbf{w}) \text{ subject to } \mathbf{w}^H \mathbf{a}(\theta) = 1 \quad (2-6)$$

The weight vector is given by:

$$\mathbf{w} = \frac{\mathbf{R}_{yy}^{-1} \mathbf{a}^H(\theta)}{\mathbf{a}^H(\theta) \mathbf{R}_{yy}^{-1} \mathbf{a}(\theta)} \quad (2-7)$$

The output power spectrum becomes:

$$P(\theta) = \frac{1}{\mathbf{a}^H(\theta) \mathbf{R}_{yy}^{-1} \mathbf{a}(\theta)} \quad (2-8)$$

Therefore, the  $K$  largest peaks of  $P(\theta)$  correspond to DOAs of the estimated sources. The inversion of the estimated covariance matrix should exist.

### *C. MUSIC Algorithm*

There are variety of MUSIC algorithms proposed in the literature. The original one relies on the characteristics of the correlation matrix of the received signal,  $\mathbf{R}_{yy}$ . The eigenvectors that span the space of  $\mathbf{R}_{yy}$  can be divided into the signal subspace,  $\mathbf{a}(\theta)$ , and the noise subspace,  $\mathbf{V}_n$ , which are orthogonal. The steering vectors correspond to the signal subspace. The signal/noise subspace is spanned by the eigenvectors that correspond to the larger/smaller eigenvalues of the correlation matrix.

Following the derivation presented in the system model above, we can write the correlation matrix of the received data [28], [37], [38] as follows:

$$\mathbf{R}_{yy} = \mathbf{A}(\boldsymbol{\theta})\mathbf{R}_{ss}\mathbf{A}^H(\boldsymbol{\theta}) + \sigma_n^2\mathbf{I}_N \quad (2-9)$$

where  $\mathbf{R}_{ss} = E[\mathbf{s}(t)\mathbf{s}^H(t)]$  is the covariance matrix of the transmitted signals,  $\mathbf{I}_N$  and  $\sigma_n^2$  are the identity matrix, and the noise variance, respectively. The eigenvector,  $\mathbf{q}_i$ , associated with  $(N - K)$  smallest eigenvalues, related to the eigenvalue,  $\lambda_i$ , fulfils the following relation:

$$(\mathbf{R}_{yy} - \lambda_i\mathbf{I}_N)\mathbf{q}_i = 0, i = K + 1, \dots, N \quad (2-10)$$

This can be further expanded as in [28] because the two subspaces are orthogonal:

$$\mathbf{A}^H\mathbf{q}_i = 0, \text{ or } \{\mathbf{a}(\theta_1), \dots, \mathbf{a}(\theta_K)\} \perp \{\mathbf{q}_{K+1}, \dots, \mathbf{q}_N\} \quad (2-11)$$

The noise subspace is constructed by the eigenvectors associated with the smallest eigenvalues, as:

$$\mathbf{V}_n = [\mathbf{q}_{K+1}, \dots, \mathbf{q}_N] \quad (2-12)$$

When the arbitrary angle equals the DOA of an incoming signal that is  $\theta = \theta_k$  for  $k = 1, 2, \dots, K$ , the steering vectors,  $\mathbf{a}^H(\theta)$ , are orthogonal to the noise subspace, i.e.

$$\mathbf{a}^H(\theta)\mathbf{V}_n\mathbf{V}_n^H\mathbf{a}(\theta) = 0 \quad (2-13)$$

Thus, the output power as a function of DOA can be expressed as [28], [37], [38]:

$$P(\theta) = \frac{1}{\mathbf{a}^H(\theta)\mathbf{V}_n\mathbf{V}_n^H\mathbf{a}(\theta)} \quad (2-14)$$

Hence the  $K$  largest peaks of  $P(\theta)$  correspond to DOAs of the unknown sources.

#### *D. First-Norm ( $l_1$ ) Singular Value Decomposition (SVD) Algorithm*

The  $l_1$ -SVD algorithm is based on the SVD as well as CS. First, the data matrix is decomposed into the signal and noise subspaces. Then, we preserve the signal subspace and model the problem with lower dimensions through multiple-sample sparse estimation. Since the received corrupted measurements depend on the actual locations which are not known, it is a challenging task to estimate the DOA [25], [27].

To exploit the concept of sparsity and then apply CS to find  $\hat{\boldsymbol{\theta}}$ , let  $\{\theta_1^g, \theta_2^g, \dots, \theta_{N_\theta}^g\}$  be a set that represents a sampling grid for all possible source locations where  $\theta_i^g$  is the  $i^{th}$  sampled angle and  $N_\theta \gg K$  is the total number of the sampling grid. Therefore, the steering matrix  $\mathbf{A} = [\mathbf{a}(\tilde{\theta}_1), \dots, \mathbf{a}(\tilde{\theta}_{N_\theta})]$  of size  $N \times N_\theta$  is independent of the actual locations. We can reformulate the problem and express it in a matrix format as [25]:

$$\mathbf{Y} = \mathbf{AS} + \mathbf{N} \quad (2-15)$$

where  $\mathbf{Y} = [\mathbf{y}(t_1), \dots, \mathbf{y}(t_T)]$  and  $\mathbf{N} = [\mathbf{n}(t_1), \dots, \mathbf{n}(t_T)]$  are matrices of size  $N \times T$ . The  $K$  transmitted signals are arranged to be the rows of the matrix  $\mathbf{S}$  of size  $N_\theta \times T$ . The  $n^{th}$  row equals  $s_k(t)$  if source  $k$  comes from  $\tilde{\theta}_n$  for  $k = 1, 2, \dots, K$  and zeros otherwise. Thus one can apply CS to find  $\hat{\boldsymbol{\theta}}$ . Henceforth, the matrix  $\mathbf{S}$  is sparse in the spatial domain because it has only  $K$  nonzero rows. Therefore, once  $\mathbf{S}$  is found,  $\hat{\boldsymbol{\theta}}$  correspond to the peaks in  $\mathbf{S}$  [25], [27].

Figure 2-4 illustrates the main steps to be accomplished in the  $l_1$ -SVD algorithm. First, the SVD is computed on  $\mathbf{Y}$  and we keep a reduced dimension  $\mathbf{Y}_{SV} = \mathbf{U}_s \mathbf{L} \mathbf{D}_K = \mathbf{Y} \mathbf{V}_n \mathbf{D}_K$  of size  $N \times K$  that contains most of the signal energy. The matrices  $\mathbf{U}_s$  and  $\mathbf{V}_s$  represent the

subspaces of the signal and noise, respectively. The matrix  $\mathbf{L}$  contains the eigenvalues and  $\mathbf{D}_K = [\mathbf{I}_K \mathbf{0}']$ , where  $\mathbf{0}$  is  $K \times (T - K)$  matrix of zeros. Similar reduction in dimension is done to get  $\mathbf{S}_{SV}$  and  $\mathbf{N}_{SV}$  from  $\mathbf{S}$  and  $\mathbf{N}$ , respectively [25].

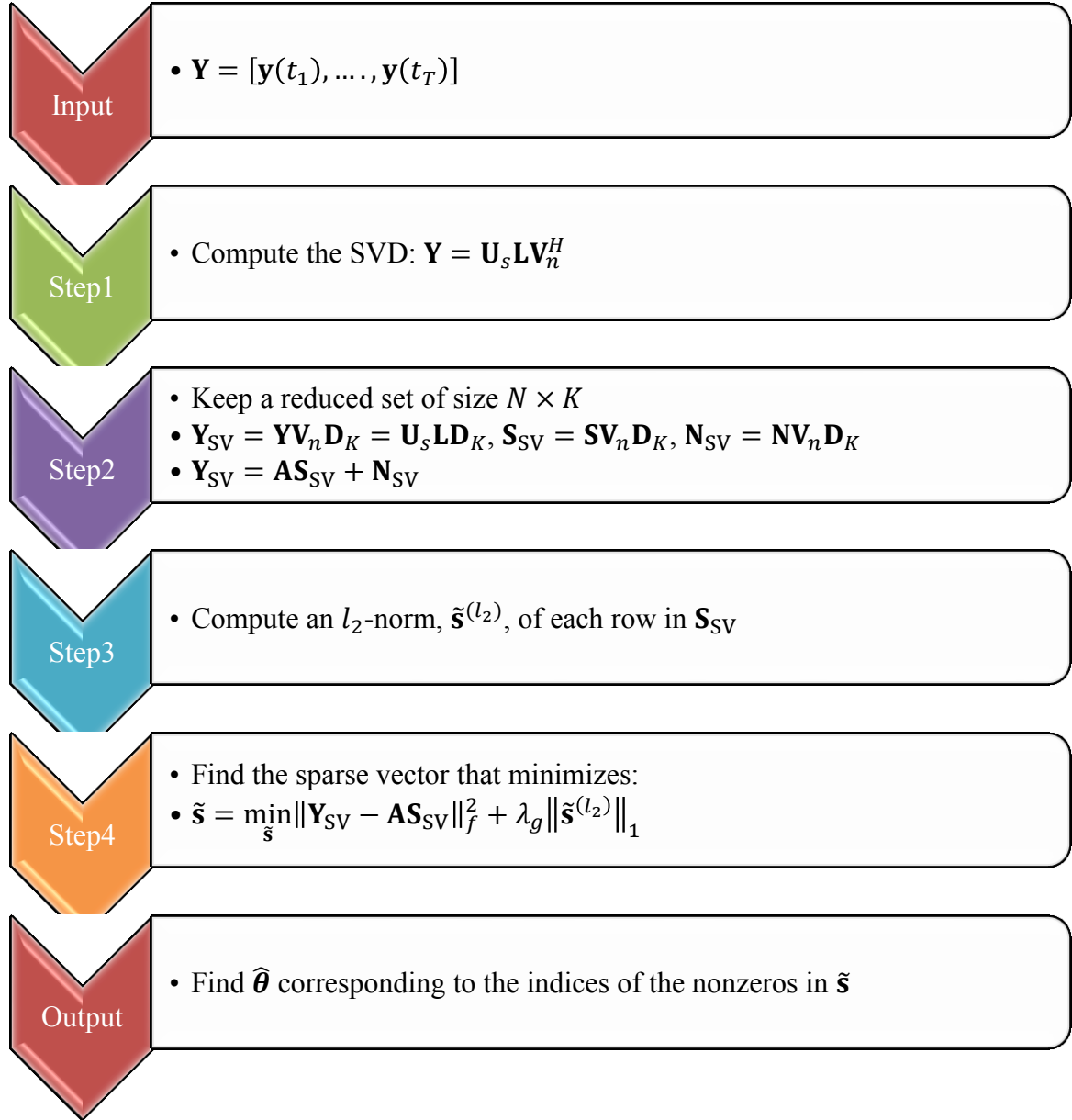


Figure 2-4: Main steps of  $l_1$ -SVD algorithm

The matrix  $\mathbf{S}_{SV}$  is sparse in the spatial domain (column wise), hence the problem can be expressed as multiple-sample sparse estimation, given by:  $\mathbf{y}^{SV}(k) = \mathbf{A}\mathbf{s}^{SV}(k) + \mathbf{n}^{SV}(k), k = 1, 2, \dots, K$  where  $\mathbf{y}^{SV}(k)$ ,  $\mathbf{n}^{SV}(k)$ , and  $\mathbf{s}^{SV}(k)$  are the  $k^{th}$  columns of  $\mathbf{Y}_{SV}$ ,  $\mathbf{N}_{SV}$ , and  $\mathbf{S}_{SV}$ , respectively. In matrix format, we can write the problem as:  $\mathbf{Y}_{SV} = \mathbf{A}\mathbf{S}_{SV} + \mathbf{N}_{SV}$ . Finally, we can solve an optimization problem (step 4) based on the  $l_2$ -norm,  $\tilde{\mathbf{s}}^{(l_2)}$ , of each row in  $\mathbf{S}_{SV}$  in order to find the sparse variable  $\|\tilde{\mathbf{s}}^{(l_2)}\|_1 = \sum_{i=1}^{N_\theta} \sqrt{\sum_{k=1}^K \left(s_i^{SV}(k)\right)^2}$ . The later is equivalent to the  $l_1$ -norm of the computed  $l_2$ -norm and  $\lambda_g$  is the regularization parameter. The term  $\|\mathbf{Y}_{SV} - \mathbf{A}\mathbf{S}_{SV}\|_f^2 = \|\text{vec}(\mathbf{Y}_{SV} - \mathbf{A}\mathbf{S}_{SV})\|_2^2$  is the Frobenius norm [25]. The estimated DOA  $\hat{\boldsymbol{\theta}}$  corresponds to the indices of the nonzero entries of  $\tilde{\mathbf{s}}$ .

#### 2.4.4 Performance Metrics

There are many performance metrics that have been used to assess the DOA estimation algorithms. The root mean square error (RMSE) is one of the very important measures. In addition, the beamwidth, bias, probability of source resolvability, and the peak-to-ripple ratio (PRR) [40], [41] have been also used in the literature.

##### A. Root Mean Squared Error (RMSE)

One of the most widely performance metrics used in the literature to assess the DOA estimation is the RMSE. The RMSE of the estimated DOA is defined as [33]:

$$\text{RMSE} = \sqrt{\frac{\sum_{j=1}^{I_{iter}} \sum_{i=1}^K \left(\theta_i - \hat{\theta}_i(j)\right)^2}{I_{iter}K}} \quad (2-16)$$

where  $\hat{\theta}_i(j)$  is the estimate DOA of  $\theta_i$  at the  $j^{th}$  Monte Carlo trial,  $j = 1, 2, \dots, I_{iter}$  with  $I_{iter}$  being the number of Monte Carlo trials and  $K$  is the number of sources to be localized.

### B. Beamwidth

The beamwidth is a good performance measure which reflects the resolution of the utilized DOA estimation algorithm. Narrow beamwidth indicates a good resolution and vice-versa. The 3dB beamwidth ( $\theta_{3dB}$ ), and 6dB beamwidth ( $\theta_{6dB}$ ) are used.

### C. Bias

The bias can be defined as the difference between the actual location of a source and its estimated location [25], [42]. Reference [37] defines the bias as the absolute value of the difference between the actual and the estimated locations. In this research, we use the first definition when calculating the bias. The bias of the  $i^{th}$  source can be expressed as:

$$Bias_i = \frac{1}{I_{iter}} \sum_{j=1}^{I_{iter}} (\theta_i - \hat{\theta}_i(j)) \quad (2-17)$$

### D. Sources Resolvability

The probability of source resolvability is calculated based on the following definition. Two sources are resolvable if the absolute value of the difference between the estimated and actual locations for each one is less than or equal to the absolute value of the difference between their actual locations divided by two [3], [43]. Mathematically, this can be expressed as:

$$|\theta_i - \hat{\theta}_i| \leq \frac{\Delta\theta}{2} \quad (2-18)$$



where  $\Delta\theta = |\theta_2 - \theta_1|$  and  $\theta_i$  and  $\hat{\theta}_i$  are the actual and the estimated DOAs of two sources for  $i = 1, 2$ , respectively.

#### *E. The Peak-to-Ripple Ratio (PRR)*

The peak-to-ripple ratio (PRR) is defined as the ratio between the square of the amplitude at the estimated DOA angle to the sum of the squares of all amplitudes at other angles in the spectrum [40], [41]:

$$\text{PRR} = \frac{A_j^2}{\sum_{i=1, i \neq j}^{N_\theta} A_i^2} \quad (2-19)$$

where  $A_j$  is the amplitude at the DOA estimate at the source location for  $j = 1, \dots, K$ .

## 2.5 Chapter Summary

In this chapter, a literature review for the most widely used DOA algorithms was presented. Then the general model for DOA estimation was demonstrated with some technical backgrounds including array configurations, DOA algorithms, and the most important performance measures of DOA estimation.

## CHAPTER 3 DOA ESTIMATION WITH PRACTICAL ANTENNA ARRAYS

Future handsets are characterized by their small size which limit the number of antennas and the inter-element spacing in between. This chapter mainly focuses on DOA estimation based on CS algorithm with practical limitations. The main objective is to strike an optimal balance between complexity and accuracy. A comparison between important DOA estimation algorithms is presented including: beamforming, Capon, MUSIC, and  $l_1$ -SVD.

The practical implementation of DOA techniques in handheld wireless devices is limited by the number of antennas and the inter-element spacing between them. A robust DOA estimation technique is needed to overcome the different impairments in the communication channel. The following provides a review on DOA estimation with practical antenna arrays followed by some preliminary results in the presence of practical limitations to understand the topic.

### 3.1 Practical Limitations

The inter-element spacing between the antennas is restricted by the available physical size in mobile handsets. Very close antenna elements suffer from the mutual coupling effect. While, the grating lobe problem appears if the inter-element spacing between those elements increases beyond half-wavelength. Under the given dimension restriction, researchers examined different inter-element spacing to optimize the DOA estimation. The authors in [23] investigated different CS-based algorithms for source localization. The

minimum adjacent antenna separations was evaluated by exploiting the antenna size as a constraint. The authors in [44] suggested antenna spacing of  $0.1\lambda$  with  $\lambda$  being the signal wavelength. Although the estimation was significantly enhanced, impedance matching was suggested to avoid the degradation with such close spacing [44]. Other researchers examined different configurations for distributing the antennas within the array based on a restriction on the minimum distance between elements [45]. It has been shown that the capability of the random array enhances if a constraint on the minimum separation between sensors is used [45].

The size of the handsets also put a limit on the number of antennas. Employing more antennas improves the system performance. Though, mutual coupling problems arise in dense arrays [46], [47]. More antennas also need large storage and increase the measurement and processing time. Considering the physical limitations in MIMO systems for small antennas is among several tasks of a sub-working group within the European Association of Antennas and Propagation (EurAAP) on “Small Antennas” [48]. Limited number of publications in DOA estimation problem considered the practical limitations which is the main scope of this dissertation. The authors in [49] used only two antennas for DOA estimation. The system utilized MUSIC algorithm and only one radio frequency (RF) was used to reduce the complexity. A switch was used to change from one element to the other and to take the measurement in a very precise operation. The error in [49] was around  $10^\circ$  at 5 dB and 20 dB SNR for line-of-sight and non-line-of-sight conditions, respectively. In [50], preprocessing the received signal and performing data reduction was used to work with two receive antenna elements. The maximum likelihood estimator was approximated to generalized least squares estimator.

Developing a receiver with DOA estimation capability is restricted by the physical size of the handsets. Thus, we discuss two practical issues; limited number of antennas and limited inter-element spacing in between. Based on the literature review, very few publications considered the practical limitations in the design of their arrays. To the best of our knowledge, no one has used CS under such limitation to handle the problem of DOA estimation. The performance is investigated for different number of antenna elements, using different performance criteria. The number of antennas that we evaluate is two and four (2 and 4-element MIMO). The case of eight elements is also examined for comparison. Under a given dimension restriction, different antenna arrangements are examined to optimize the DOA estimation. To make the analysis more general, the ratio between the inter-element spacing and the wavelength is considered. Extensive simulations are conducted to study and inspect the effect of this ratio on the system performance. In addition, other parameters are also investigated like the RMSE, beamwidth, bias, and probability of source resolvability. It is shown that MUSIC and Capon methods performs well at high SNR when the sources are not highly correlated. Whereas,  $l_1$ -SVD does not require high SNR and can detect strongly correlated sources. When considering two antennas with practical antenna spacing limitations, simulation shows that the RMSE of the estimated DOAs is the same for all algorithms in the presence of one unknown source. Simulation concludes that working with a ratio between the wavelength and the unit inter-element spacing of 3 realizes the smallest RMSEs and beamwidth. The  $l_1$ -SVD algorithm is recommended due to the narrow beamwidth and high resolution.

### 3.2 Evaluation and Comparison

In this section we present some results for DOA estimation using different algorithms and parameters. The effects of the most important parameters presented in the system model are investigated; including the number of the receive antenna elements, inter-element spacing, number of sources, number of samples and the source separation. The results are based on MATLAB® simulations. In the coming chapters, the results will be augmented by experimental data.

The sources are assumed to be located in the far-field with discrete uniform DOA angle distribution,  $\theta_k \sim U[0^\circ, 180^\circ]$ . A ULA is considered with  $N$  sensors spaced by  $d = \lambda/2$  and the number of samples is  $T = 200$  samples. The search grid is uniform with  $1^\circ$  step size and  $N_\theta = 181$ . All these parameters are fixed unless stated otherwise. The two practical limitations are adjusted to be:  $N = 2$  and  $d = \lambda/2$ . The solution of the sparse vector based  $l_1$ -SVD algorithm was conducted using CVX toolbox [51] in MATLAB®. To remove the location dependence on the accuracy of the estimation, the actual angle for each source was randomly changed in every run. All performance measures are calculated based on  $I_{iter} = 500$  independent runs and then averaged.

It is worth to mention that the  $l_1$ -SVD exploits the sparsity and the SVD in the estimation process. Thus, it works with further reduced data compared with other algorithms considered in this reserach. The processed data using  $l_1$ -SVD algorithm is reduced from  $N \times T$  into  $N \times K$ . This huge amount of reduction is realized because  $T \gg K$  with  $T = 200$  samples and  $K = 1$  or  $2$  sources.

## 3.2.1 Comparison for DOA Estimation Algorithms

This subsection compares the previous algorithms discussed in Section 2.4.3 in terms of their ability to resolve closely spaced correlated or uncorrelated sources. The number of sources is  $K = 2$  and a total of  $N = 8$  isotropic antenna elements are assumed. The resolution of the aforementioned algorithms in terms of the beamwidth at the estimated locations is investigated.

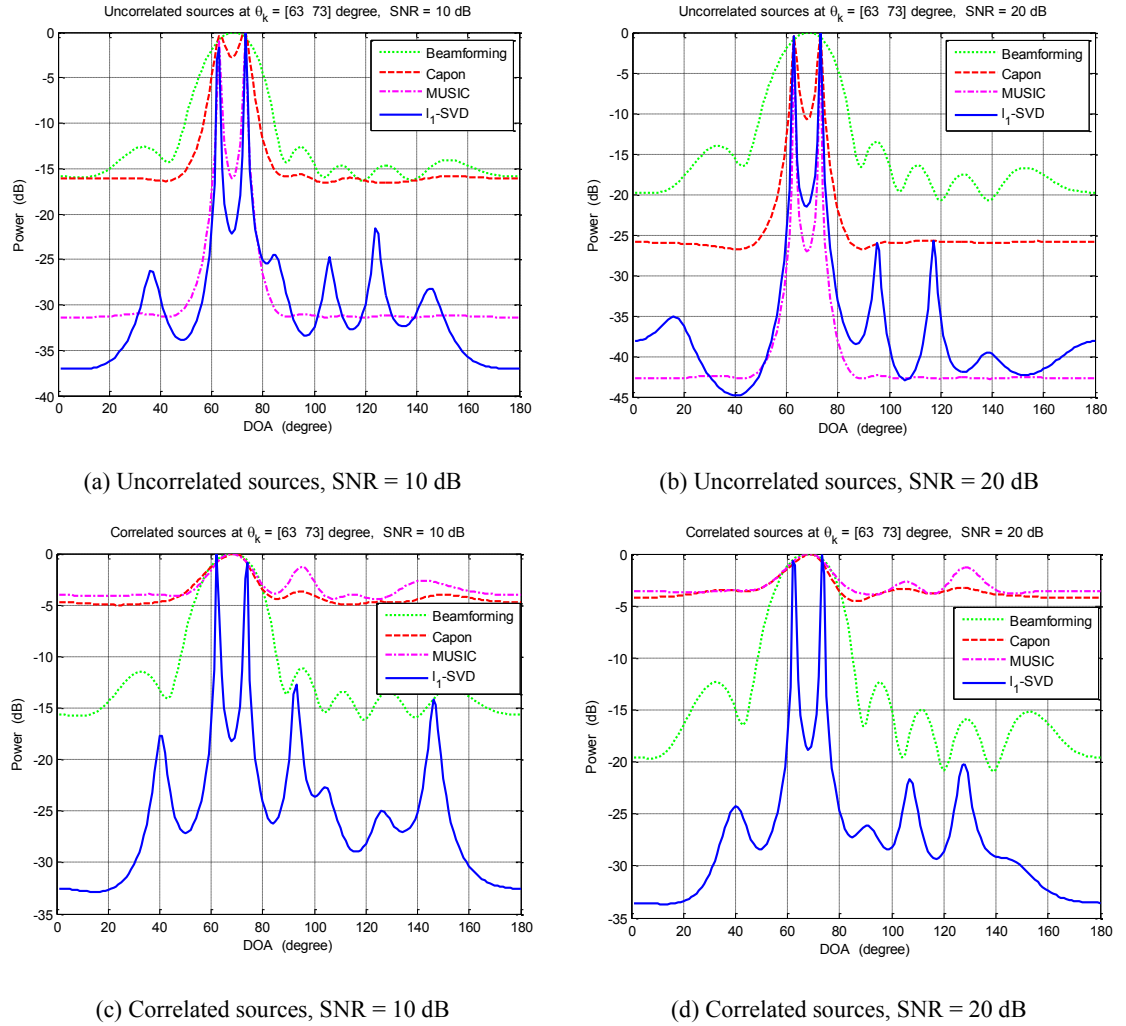


**Figure 3-1:** Spatial spectra for uncorrelated and correlated sources with DOAs of 63°, 73° and  $N = 8$

Figure 3-1 shows the normalized power spectrum in dB versus the estimated DOA using beamforming, Capon, MUSIC and  $l_1$ -SVD algorithms. The SNR is 10 and 20 dB in the upper, lower subplots, respectively. Two sources are assumed at 63 and 73 degree. The sources in Figure 3-1 (a) and (b) are uncorrelated while they are correlated in Figure 3-1 (c) and (d). Apart from beamforming, all algorithms can resolve the two uncorrelated sources with SNR = 10 dB as Figure 3-1 (a) depicts. The ability of Capon and MUSIC algorithms to resolve the sources is enhanced when the SNR = 20 dB, see Figure 3-1 (b). The resolution of the  $l_1$ -SVD algorithm is better than MUSIC algorithm, though MUSIC is better in terms of reducing the side lobes. Beamforming algorithm merges the two uncorrelated sources even at large SNR with larger side lobes compared to other algorithms. In case of correlated sources, only  $l_1$ -SVD algorithm resolves the two sources with much smaller side lobes compared with others as Figure 3-1 (c) and (d) depict.

The accurate estimation for the DOA is not the only way for assessment. The estimated locations exhibit different beamwidths (sharpness) which is referred to as resolution. Figure 3-1 indicates that the narrowest beamwidth at the estimated locations is achieved using  $l_1$ -SVD algorithm at SNR = 10 dB. MUSIC and Capon algorithms have comparable beamwidth whereas a very wide beam was realized using the beamforming algorithm. Although the beamforming algorithm can estimate the DOA, the beamwidth at the estimated angle is very wide and consequently the resolution is very poor. Additionally, the side lobes have very high levels. MUSIC and Capon algorithms need to have a high SNR as well as the sources should not be highly correlated. Whereas,  $l_1$ -SVD does not need high SNR and can detect a strongly correlated sources. Unlike  $l_1$ -SVD, MUSIC and Capon algorithms require sufficient number of samples [25].

### 3.2.2 Results for Localizing a Single Source

In this part, the objective is to estimate the DOA for a single source, i.e.  $K = 1$ . Extensive simulations were conducted to evaluate the statistical measures.

#### A. Impact of the Signal-to-Noise Ratio

Herein, the impact of the SNR on the system performance is studied. We plot the RMSE versus the SNR for each algorithm under different number of receiver antenna elements as shown in Figure 3-2. The RMSE decrease as  $N$  increases for all algorithms. Though, the RMSE is almost the same when the SNR greater than 20 dB. For fixed  $N$ , the RMSE is approximately the same for all algorithms since only a single source needs to be localized.

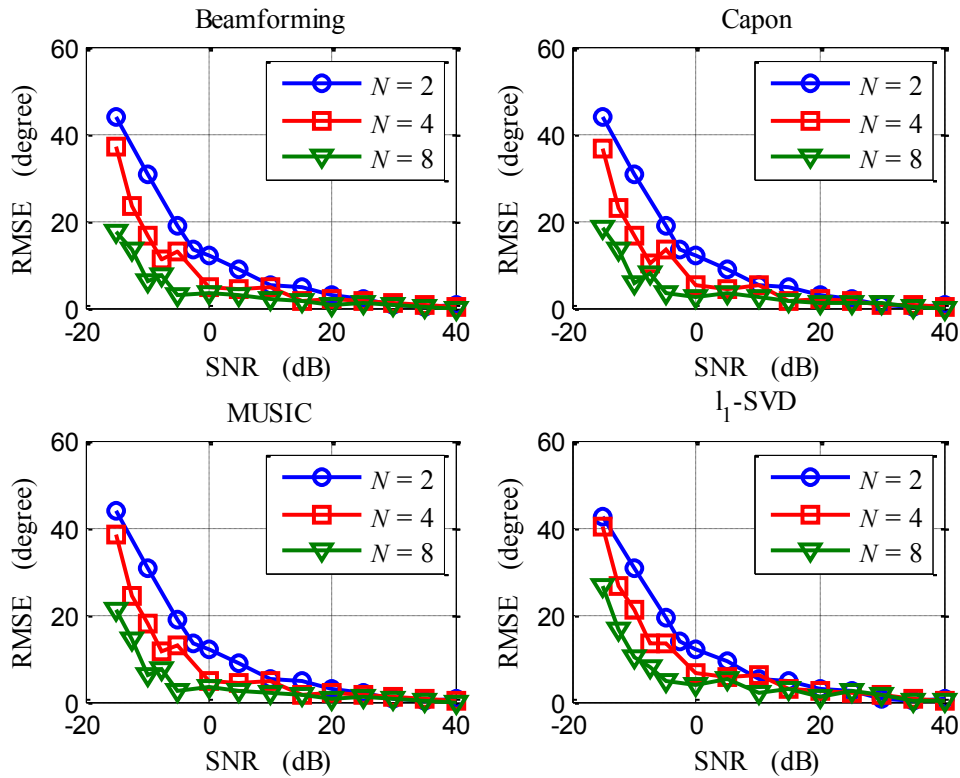


**Figure 3-2:** RMSE versus SNR for different  $N$  and  $K = 1$



### *B. Impact of the Inter-Element Spacing*

To study the impact of inter-element spacing, we investigate some cases which are involved in practical scenarios. To make the analysis general, the ratio between the element spacing and wavelength  $\frac{d}{\lambda} = \frac{1}{8}, \frac{1}{6}, \frac{1}{4}, \frac{1}{3}, \frac{1}{2}, \frac{2}{3}, 1, \frac{4}{3}$  and 2 are considered.

The RMSE for different values of  $N$  are shown in Figure 3-3 as a function of  $d/\lambda$  with  $\text{SNR} = 20$  dB. In each subplot, all algorithms are compared for fixed  $N$ . If  $d/\lambda > 1/2$ , there will be two solutions for the estimated direction which creates ambiguity. This is called spatial aliasing where in addition to the main lobe of the actual direction, other lobes appear in the estimated spectrum; grating lobe effect. There are some oscillations in the RMSE for  $d/\lambda > 1/2$  because the ambiguity increases. The peaks of the actual location and the ambiguities most probably have different magnitude. Therefore, if we pick an ambiguous peak, error will occur. As more antenna elements are employed, left to right subplots, the RMSE is reduced. The  $l_1$ -SVD is the algorithm that is most affected by the increase in  $d/\lambda$ . Regardless of  $N$ , all algorithms achieve the minimum RMSE when  $d/\lambda = 1/3$ . Consequently working at this ratio is preferred and recommended.

The RMSE degrades dramatically when  $d/\lambda$  is small using  $l_1$ -SVD algorithm. This can be figured out as: almost all antennas have the same measurements since they are very close to each other. In addition, the dominant factor for this degradation, especially for  $N = 8$ , is the data reduction from  $N \times T$  to  $N \times K$ .

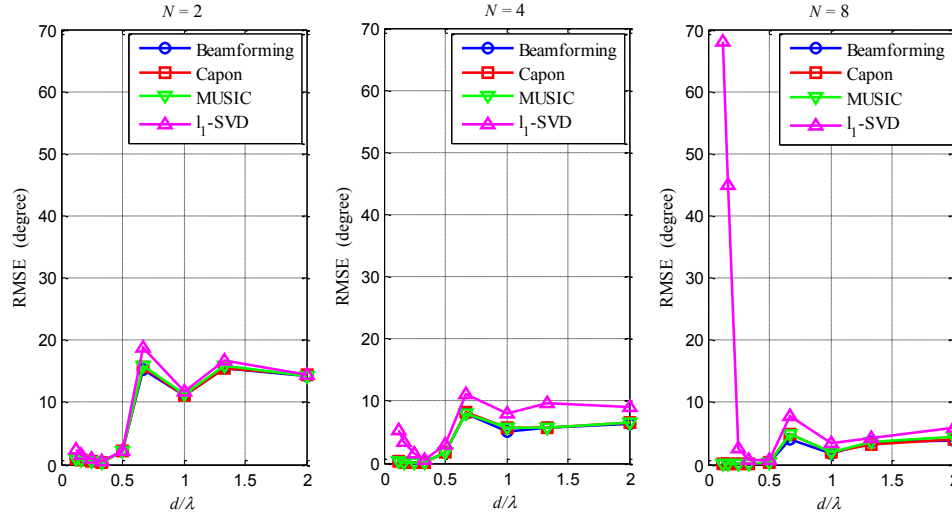


**Figure 3-3:** RMSE versus  $d/\lambda$  for  $N = 2, 4, 8$ , SNR = 20 dB, and  $K = 1$

Figure 3-4 depicts the  $\theta_{3dB}$  as function of  $\frac{d}{\lambda}$  for different  $M$ , SNR = 20 dB and  $K = 1$ . In beamforming and capon algorithms, different values of  $N$  give significant performance differences. While MUSIC and  $l_1$ -SVD algorithms are not very sensitive to changing  $N$ . Decreasing  $\frac{d}{\lambda}$  results in wider  $\theta_{3dB}$  because of the field coupling effect in both beamforming and Capon algorithms. Although, decreasing  $\frac{d}{\lambda}$  does not cause large degradation in the resolution. MUSIC and  $l_1$ -SVD achieve beams less than  $1^\circ$ , and  $0.2^\circ$ , for  $N = 4$  and  $8$  respectively. When  $d/\lambda > 1/2$ , the ambiguity increases however the beams get narrower. The ambiguity problem is pronounced in terms of RMSE as in Figure 3-3. Multiple peaks appear in the power spectrum at different angles and we calculated only the  $\theta_{3dB}$  of the maximum peak.

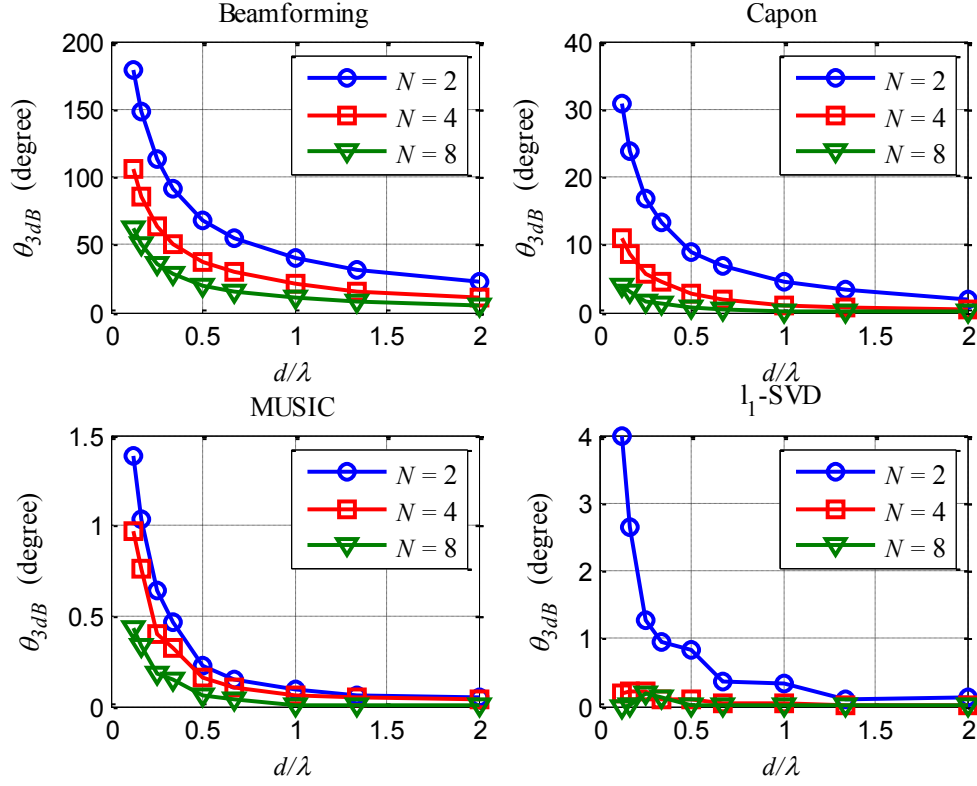


Figure 3-4: 3dB beamwidth versus  $d/\lambda$  for different  $N$ , SNR = 20 dB, and  $K = 1$

### C. Impact of the Number of Receive Antenna Elements

The effect of  $M$  versus the SNR based on the RMSE was investigated in Part A. Figure 3-5 shows the  $\theta_{3dB}$  and  $\theta_{6dB}$  as function of SNR for different  $M$ . The  $\theta_{6dB}$  is presented for completeness and comparison purposes. At low SNR, beamforming and capon beams cover the entire range of  $N_\theta$  i.e.  $180^\circ$ . There is no improvement in the beamforming performances as the SNR increases above 5 dB. While for Capon, the beams get narrower as SNR increases. MUSIC is much better than beamforming and Capon even at low SNR. Much narrower beams are achieved using  $l_1$ -SVD except for  $N = 2$ . At this limit of the receive antenna elements, the beams are around  $55^\circ$ ,  $30^\circ$  at SNR =  $-15$  dB for the  $\theta_{3dB}$  and  $\theta_{6dB}$ , respectively.

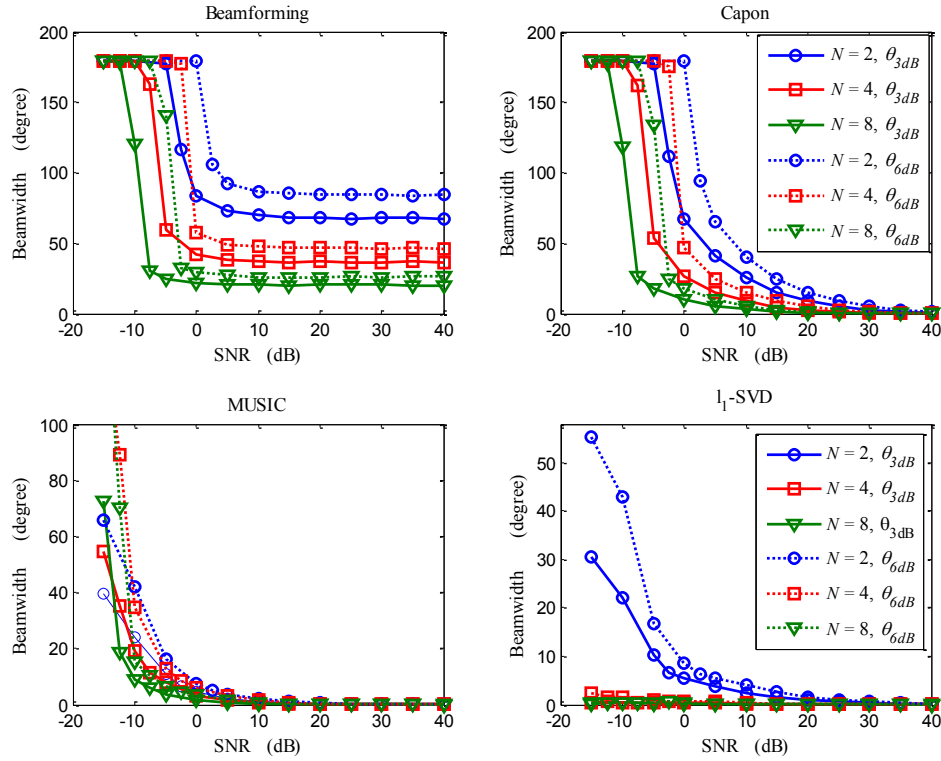


Figure 3-5: 3dB and 6dB beamwidth versus SNR for different  $N$ , and  $K = 1$

For SNR above 5 dB, the difference between the  $\theta_{3dB}$  and  $\theta_{6dB}$  is more than  $15^\circ$  using beamforming with  $N = 2$ , and it reduces from around  $24^\circ$  to almost  $0^\circ$  at SNR = 30 dB using Capon. On the other hand, these differences are further reduced as  $N$  increases and they reach to approximately  $0^\circ$  using  $l_1$ -SVD with  $M = 8$  at SNR =  $-15$  dB.

#### D. Impact of the Number of Samples

There are many algorithms which depend on the correlation matrix of the received signal. Since we do not have the statistics, the covariance matrix is estimated using  $T$  samples. Therefore, the number of samples affects the performance. Figure 3-6 shows the RMSE for  $T = 1, 20, 50, 100, 150$  and 200 samples with SNR = 20 dB using different values of  $N$ .

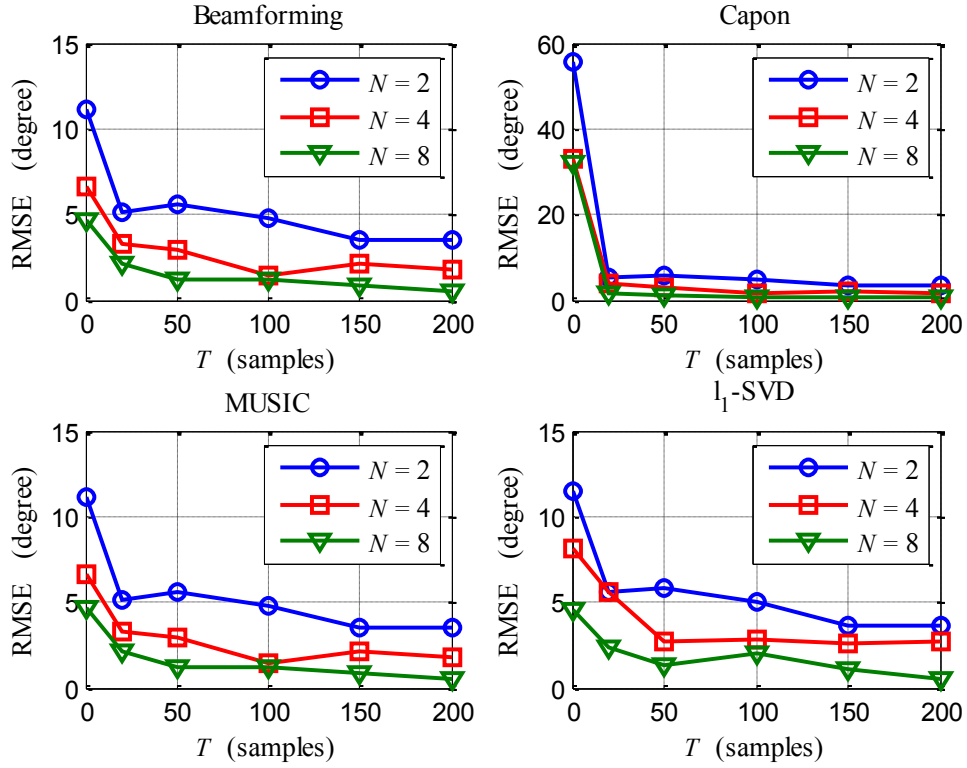


Figure 3-6: RMSE versus  $T$  for different  $N$  when SNR = 20 dB and  $K = 1$

Using one data sample yields comparable RMSE for beamforming, MUSIC and  $l_1$ -SVD algorithms for all  $N$  since we have only one source. Though, the RMSE based on Capon algorithm is large compared with others using one sample. In general, increasing  $T$  reduces the RMSE for all algorithms since a better estimation for the correlation matrix is achieved.

Figure 3-7 shows the  $\theta_{3dB}$  as a function of  $T$  with SNR = 20 dB using different  $N$ . Using one data sample yields very large beams for beamforming and Capon algorithms for all  $N$ . However, this is not the case for MUSIC and  $l_1$ -SVD algorithms with one sample. The resolution using beamforming algorithm is low since the  $\theta_{3dB}$  is more than  $20^\circ$  for all  $T$  and  $N$ . Simulation as well shows that the  $\theta_{3dB}$  is a weak or a negligible function of  $T$  based on beamforming. The same observation is made for Capon algorithm for  $T \geq 20$  samples.

MUSIC and  $l_1$ -SVD algorithms are affected more by increasing  $T$ . The smallest beams are attained with  $l_1$ -SVD with only one sample and  $N = 4, 8$ , therefore, this algorithm has super resolution (very narrow beamwidth). Nevertheless, in the limited case i.e.  $N = 2$ , MUSIC algorithm has relatively lower  $\theta_{3dB}$  by around  $1.5^\circ$  compared with  $l_1$ -SVD algorithm using one sample.

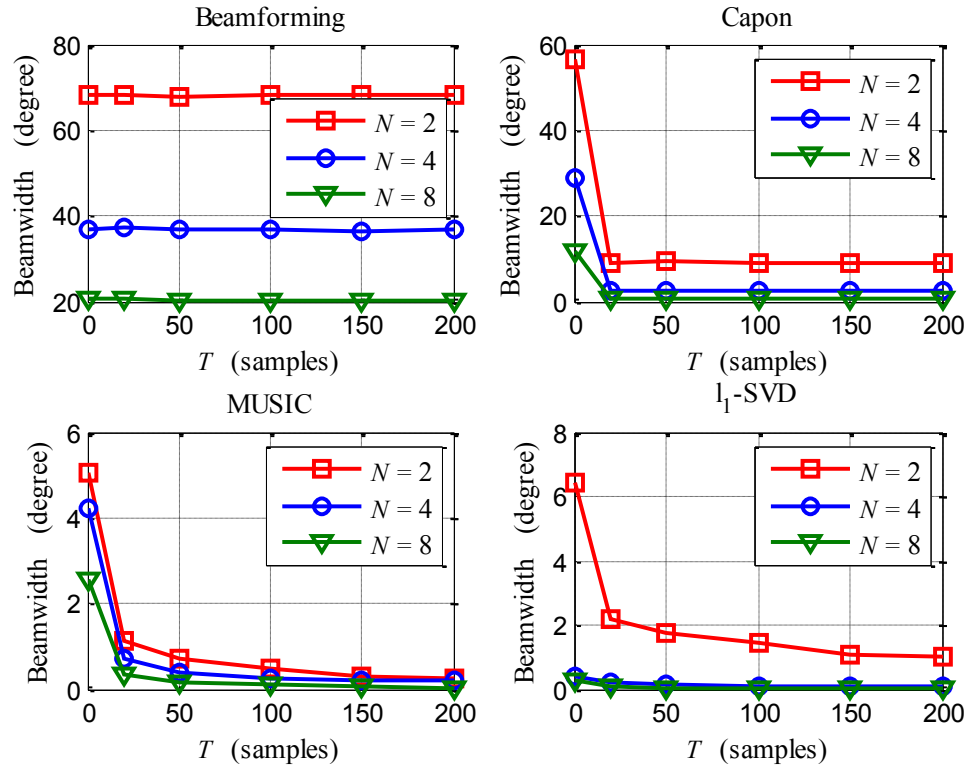


Figure 3-7: 3dB beamwidth as function of  $T$  for different  $N$  when  $K = 1$

### 3.2.3 Results for Localizing Multiple Sources

The system performance in the presence of multiple sources for DOA estimation is considered in this part. Some simulation results are presented.

#### *A. Impact of the Signal-to-Noise Ratio*

From now on, we assume that we have two unknown source locations i.e.  $K = 2$ . Figure 3-8 displays the RMSE versus SNR for different  $N$ . We can notice that the RMSE is very large with  $N = 2$  based on all algorithms and even with SNR = 40 dB. The RMSE using MUSIC algorithm when  $N = 2$  is larger than others because  $K = N$ . The extracted noise subspace from the correlation matrix should have  $\mathbf{V}_n = [\mathbf{q}_{K+1}, \dots, \mathbf{q}_N]$  as discussed in Section 2.4.3-C, though the size of the correlation matrix is  $2 \times 2$ . Consequently, the noise subspace becomes an empty matrix and degradation occurs. Therefore, two antenna elements are not enough to estimate the locations of two sources.

Apart from beamforming algorithm, using more antenna elements improve the performance significantly. Increasing the SNR reduces the RMSE as well, though this improvement is negligible beyond SNR = 20 dB using  $l_1$ -SVD algorithm. After this SNR, simulation proves that Capon and MUSIC algorithms realize quite better RMSE.

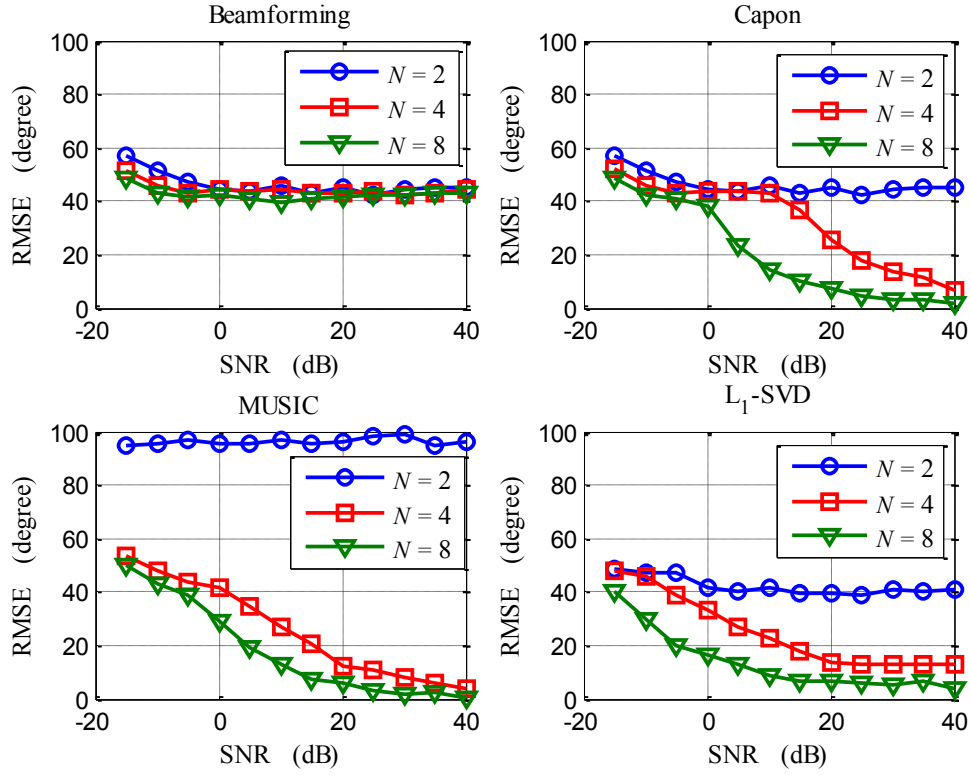


Figure 3-8: RMSE versus SNR for different  $N$  and  $K = 2$

### B. Impact of the Ratio between the Inter-Element Spacing and Wavelength

As we did in Figure 3-3 but here  $K = 2$ , the RMSE is plotted versus  $\frac{d}{\lambda} = \frac{1}{8}, \frac{1}{6}, \frac{1}{4}, \frac{1}{3}, \frac{1}{2}, \frac{2}{3}, 1, \frac{4}{3}$  and 2 with SNR = 20 dB is plotted in Figure 3-9. The RMSE for MUSIC and  $l_1$ -SVD algorithms decreases as  $d/\lambda < 1/2$  since the mutual effect reduces. On the other hand, the RMSE increases when  $d/\lambda > 1/2$  because the ambiguity increases due to the grating lobes. The same observation was made as in Figure 3-3 regarding the minimum RMSE at  $d/\lambda = 1/3$  but only for MUSIC and  $l_1$ -SVD algorithms with  $N = 4, 8$  and Capon algorithm only  $N = 8$ . The reason behind this is the presence of multiple sources which is not the case in Figure 3-3. Although, the system performance has got almost the same trend.



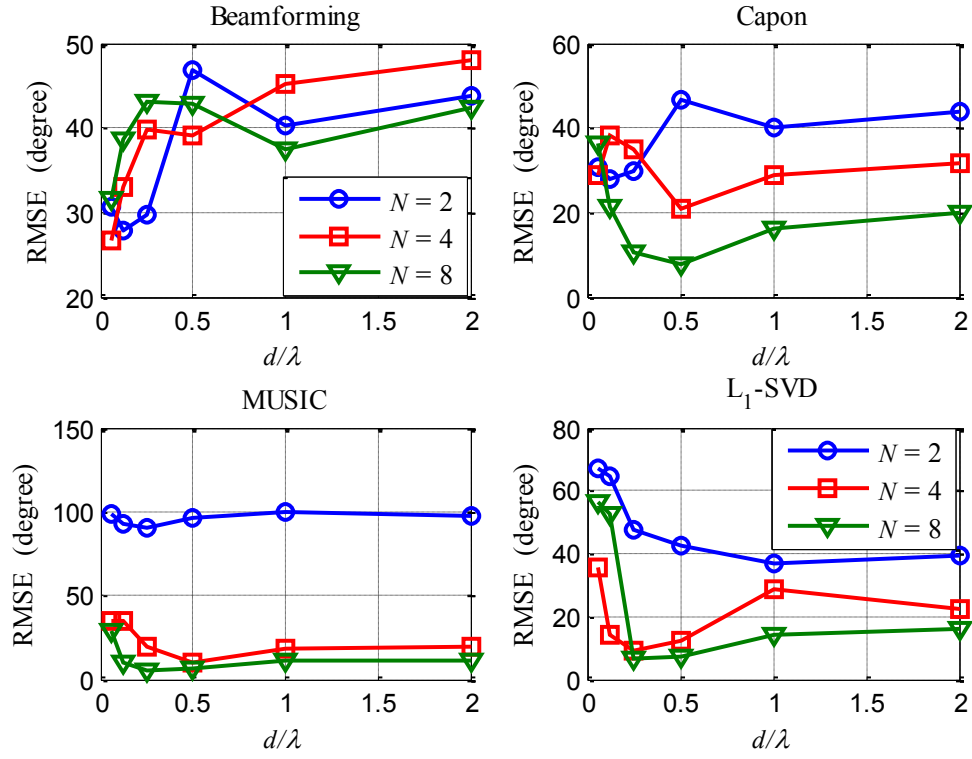
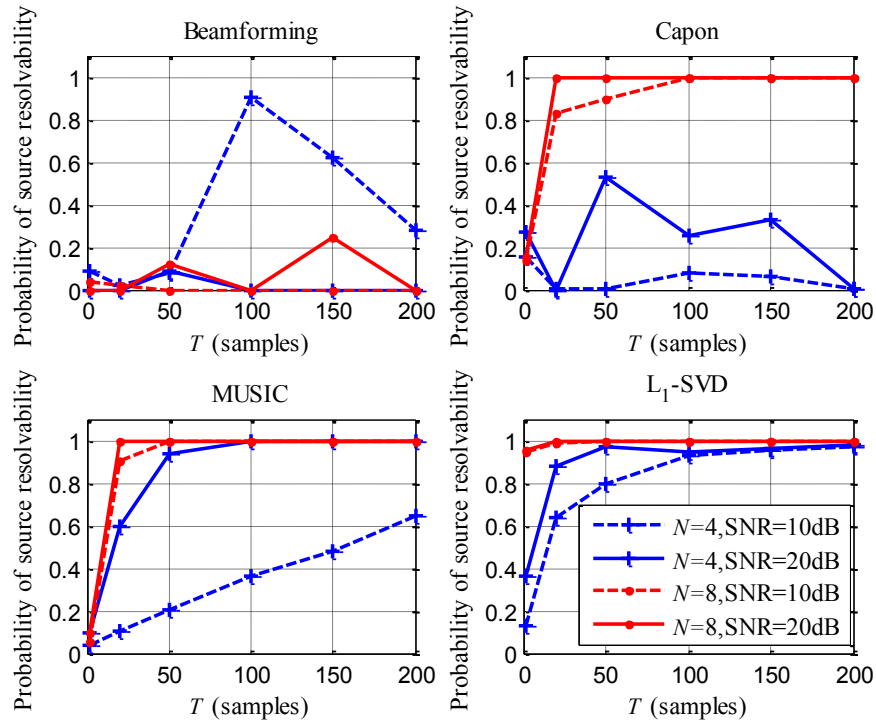
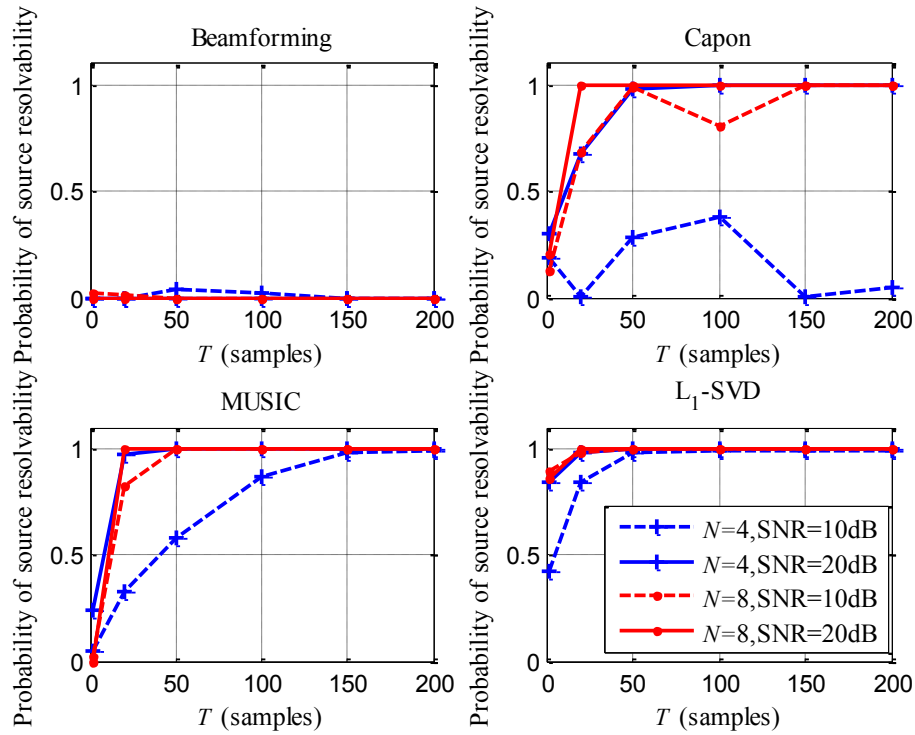


Figure 3-9: RMSE versus  $d/\lambda$  for two sources and different  $N$

### C. Impact of the Number of Samples

The effect of the number of samples can be evaluated using the probability of detection or the probability of source resolvability. The two sources are adjusted to be located at  $\theta = [60^\circ, 80^\circ]$ ,  $\theta = [60^\circ, 100^\circ]$  as shown in Figure 3-10 (a) and (b) respectively, using  $N = 4, 8$  and the SNR = 10, 20 dB. The probability of source resolvability is plotted against  $T = 2, 20, 50, 100, 150$  and 200 samples.

(a)  $\theta = [60^\circ, 80^\circ]$ (b)  $\theta = [60^\circ, 100^\circ]$ 

**Figure 3-10:** Probability of source resolvability versus  $T$  with SNR = 10 dB (dashed lines), SNR = 20 dB (solid lines) and  $N = 4, 8$

Generally speaking, the probability of detection enhances when the sources are separated by 40 degrees compared with that of 20 degrees. Apart from  $l_1$ -SVD algorithm, using only two samples is not enough to achieve a good probability of detection. However, using  $l_1$ -SVD the probabilities with only two samples are much greater than all other algorithms, see Figure 3-10 (a) and (b). The probability of detection reaches around 0.958 as shown in Figure 3-10 (b) with  $N = 8$  and SNR = 10, 20 dB using  $l_1$ -SVD. The same probability is achieved using  $N = 4$  and SNR = 20 dB. When the sources are separated by 20 degrees, the probabilities achieved with  $l_1$ -SVD are quite smaller. Figure 3-10 (b) shows also that MUSIC,  $l_1$ -SVD algorithms need 150, 50 samples to achieve around 100% probability of detection because MUSIC algorithm relies on the correlation matrix of the received data. Thus, increasing the number of samples leads to better estimate for the correlation matrix. Capon algorithm needs large SNR and large number of samples in order to resolve the two sources perfectly. Beamforming algorithm has the worst performance among all algorithms.

#### *D. Impact of the Separation between the Sources*

In this part, the first source is fixed at 42 degree while the second one is changing. The bias is analyzed as a function of the angular separation between the two sources. For the case when the SNR = 10 dB (solid lines), 20 dB (dotted lines) with  $N = 8$  shown in Figure 3-11, we observe some bias for low separations. Though this bias vanishes when the SNR = 10 dB at around 16, 14 and 12 degrees for Capon, MUSIC and  $l_1$ -SVD algorithms, respectively. On the other hand, the bias increases with separations using beamforming algorithm since it is search based algorithm and it has a very wide beamwidth. Apart from beamforming algorithm, when the SNR increases to 20 dB all biases decrease.

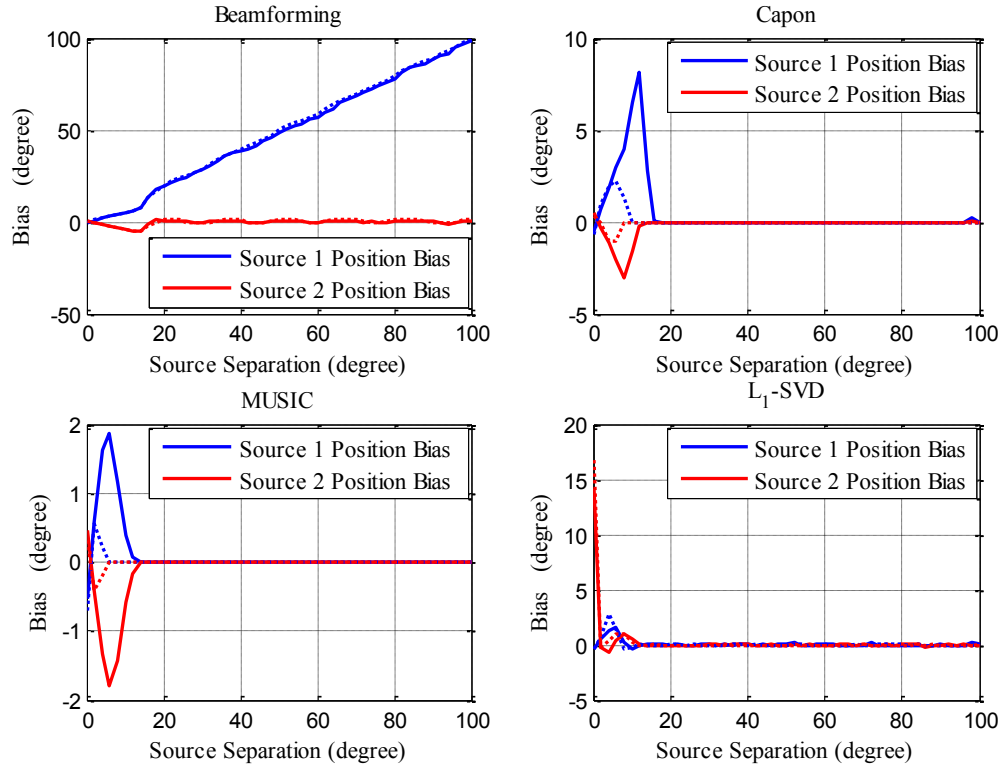


**Figure 3-11:** Bias in localizing two sources versus angular separation with SNR = 10 dB (solid lines), 20 dB (dotted lines),  $N = 8$ , and  $K = 2$

The probability of source resolvability is another criterion used to assess the performance of the DOA estimation. This metric gives an indication on how certain DOA algorithm is capable to resolve two sources. The two sources in the first upper subplots of Figure 3-12 are adjusted to be located at  $\theta = [60^\circ, 80^\circ]$  and we compare  $N = 4$  (solid lines) and  $N = 8$  (dashed lines). All subplots have the same legend and markers. A probability of 1 is achieved using  $l_1$ -SVD at low SNR compared with other algorithms. In order to realize probability of detection greater than 0.8, around 7.5 and 10 dB are required using MUSIC and Capon algorithms, respectively, using eight receive antenna elements. Moreover, we have almost the same trend using four receive antenna elements. Beamforming algorithm cannot resolve the two sources.

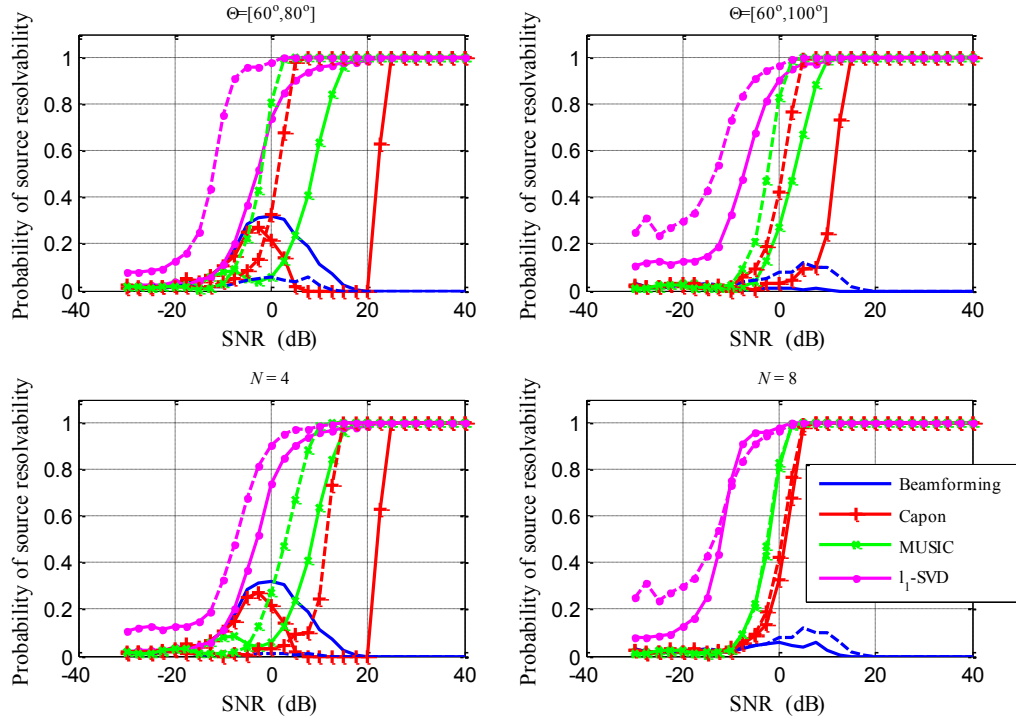


**Figure 3-12:** Probability of source resolvability versus SNR: upper subplots  $N = 4$  (solid lines),  $N = 8$  (dashed lines), and lower subplots:  $\theta = [60^\circ, 80^\circ]$  (solid lines),  $\theta = [60^\circ, 100^\circ]$  (dashed lines)

The two sources in the second upper subplots of Figure 3-12 are adjusted to be located at  $\theta = [60^\circ, 100^\circ]$  and we compare  $N = 4$  (solid lines) and  $N = 8$  (dashed lines). Again beamforming algorithm merges the two sources and cannot resolve them. Similarly,  $l_1$ -SVD is better than MUSIC and Capon algorithms. Comparing the two cases with  $N = 4$  and  $N = 8$ , the differences between them are not as before (smaller) because the sources now are separated by 40 degrees.

How much improvement one can achieve if the sources are separated by 20 or 40 degrees for the same number of receive antenna elements? The lower subplots provide the answer to this question. For  $N = 4$  in the third subplot, sources separated by 20 degree (solid lines) need around 5, 7.5 and 10 dB more compared with those separated by 40 degree (dashed lines) in order to be fully resolved using  $l_1$ -SVD, MUSIC and Capon algorithms,

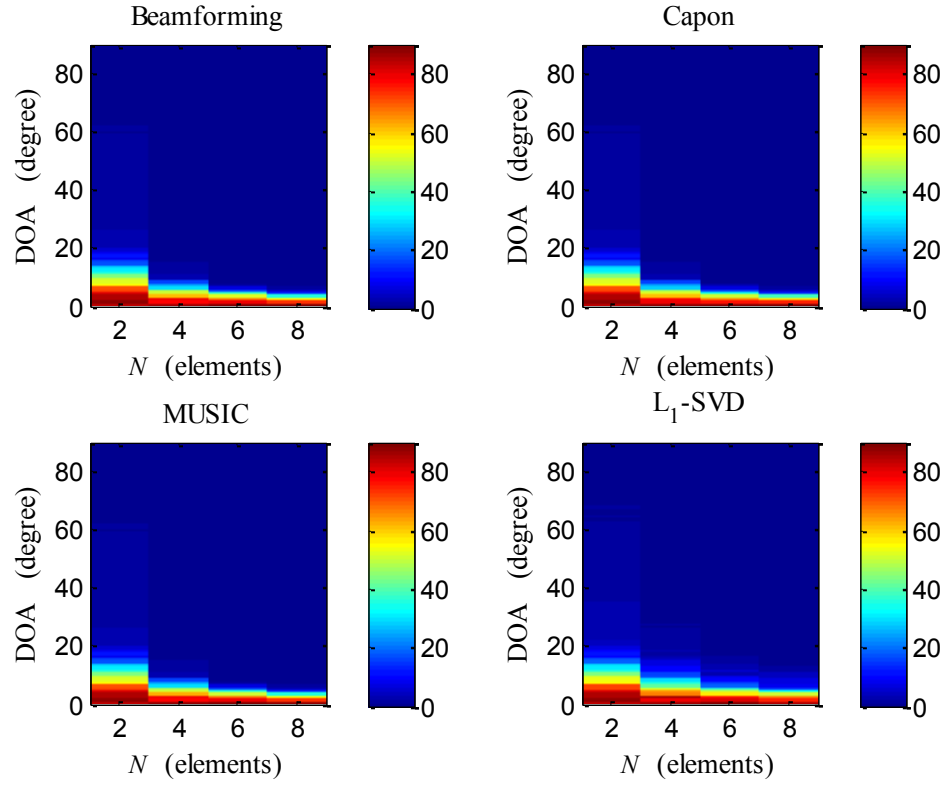
respectively. When  $N = 8$ , the performances are almost the same for all algorithms as shown in the fourth subplot of Figure 3-12.

#### 3.2.4 Source Location Dependency

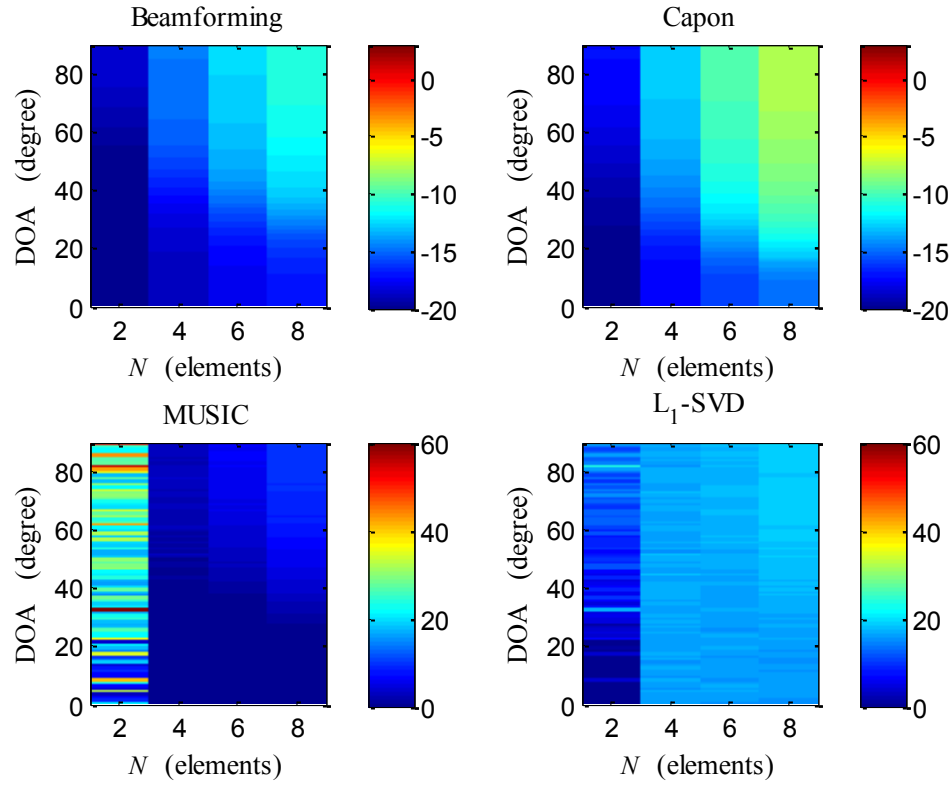
The effect of the source location (DOA) on the performance measures is evaluated. In this subsection, a single source is assumed to be located at all possible angles using ULA and with  $\text{SNR} = 0$  dB. The RMSE, PRR, and 3dB beamwidth are used to assess the performance. All performance measures are plotted versus the number of antenna elements in the  $x$ -axis and the DOA in the  $y$ -axis, respectively. Our range of interest is as before  $[0^\circ, 180^\circ]$ . We show only the results from  $[0^\circ, 90^\circ]$  and the results of the remaining angles are symmetric.

Figure 3-13 demonstrates that almost all algorithms realize similar RMSE and behavior where the RMSE increase as the source location moves toward zero degree and vice versa. The RMSE also decreases as  $N$  increases.

The PRR is also used to assess the location dependency. As the PRR increases means that the side lobes are so small compared with those at the estimated angles. Consequently, better resolution is realized. The PRR with all algorithms enhances as the DOA moves to the middle of the range of interest and as we increase the number of antenna elements as Figure 3-14 depicts. The smallest PRR is realized with beamforming algorithm then that with Capon algorithm. Since MUSIC algorithm assumes certain data model (orthogonality) and according to (2-14), large spikes occurs at the candidate source locations compared with the remaining angles in the estimated spectrum. This is why the PRR with MUSIC algorithm is larger than others. Since the  $l_1$ -SVD algorithm has high resolution, large PRR is achieved.



**Figure 3-13:** RMSE in degree versus source location and the number of elements with SNR = 0 dB



**Figure 3-14:** PRR versus source location and the number of elements with SNR = 0 dB

The beamwidth is less affected by the location of the source as Figure 3-15 shows. Very wide beamwidth is achieved with beamforming algorithm followed by Capon algorithm. Super resolution and very narrow beamwidth is realized with  $l_1$ -SVD algorithm.



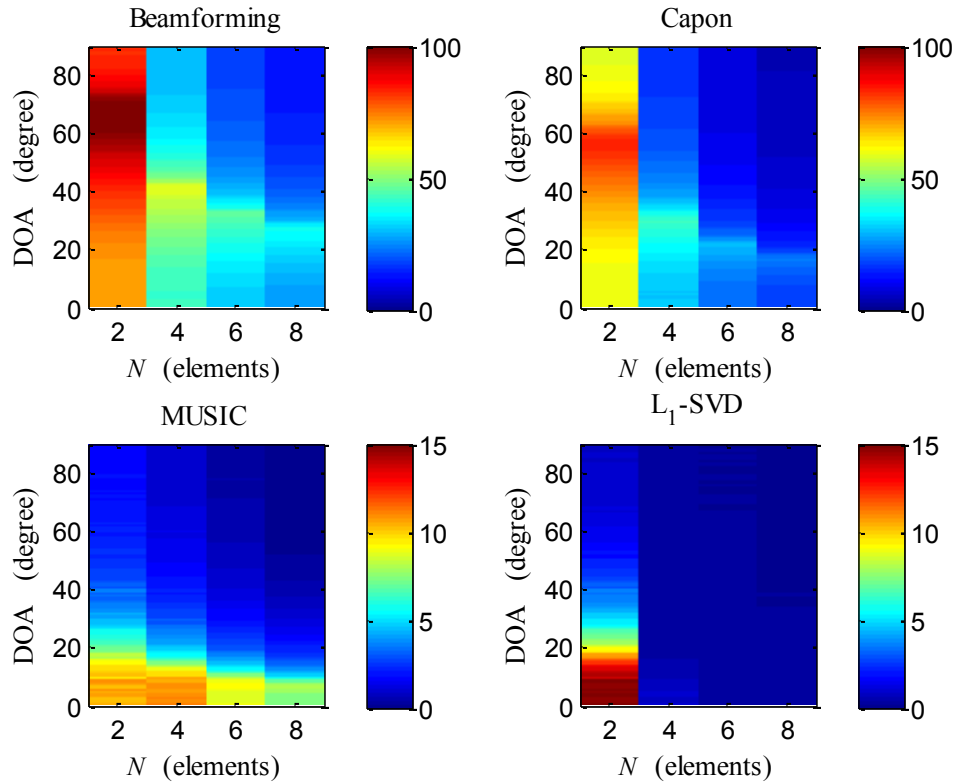


**Figure 3-15:** Beamwidth in degree versus source location and the number of elements with SNR = 0 dB

### 3.2.5 Processing Time

Figure 3-16 demonstrates the processing time required for DOA estimation's scenario presented in Section 3.2.4 versus the number of antenna elements. The results were averaged over 500 runs. The time was calculated using a “tic” and “toc” commands in MATLAB, which installed on a PC with an Intel i5 processor running at 3.3 GHz.

MUSIC algorithm performs EVD to find the DOA and it requires the smallest processing time as shown in Figure 3-16. Beamforming algorithm is the simplest computationally algorithm among the remaining ones according to (2-3). Capon algorithm on the other hand executes matrix inversion operation to find the DOA. Therefore, it requires larger processing time compared with MUSIC and beamforming algorithms. Since the  $l_1$ -SVD

algorithm performs SVD first then solves an optimization problem to find the DOA, the processing time for this algorithm is so larger than others. In addition, we use CVX toolbox to conduct the  $l_1$ -SVD algorithm in our simulation. This also adds extra processing time since this toolbox is a general-purpose one designed to solve much wider variety of problems.

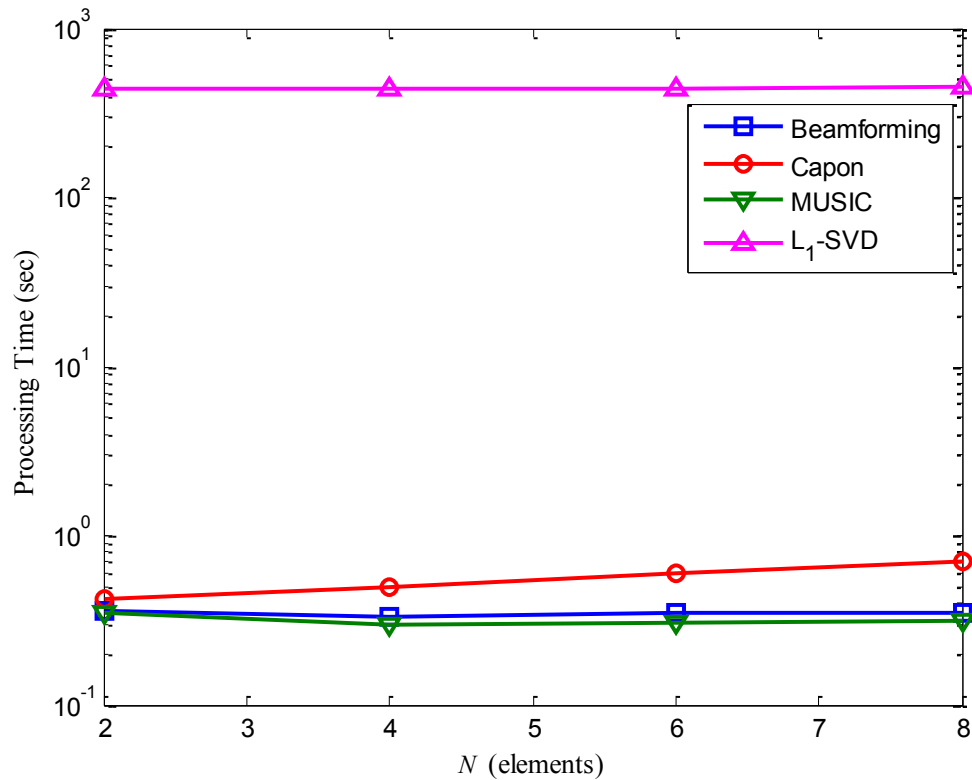


**Figure 3-16:** Average processing time versus the number of elements

### 3.3 Chapter Summary

In this chapter, we presented a comparative study on sparse DOA estimation with practical antenna arrays. Two practical issues were discussed namely: limited number of antenna elements and limited inter-element spacing in between. Different performance measures have been used in the evaluation process. This includes the RMSE, beamwidth, bias and the sources resolvability. The  $N = 2$  of a ULA case can represent a 2-element MIMO antenna system in current wireless terminals. Other higher order cases such as  $N = 4, 8$  of the ULA can represent MIMO antennas on larger devices (tablets, laptops, etc.) or at access points. We have discussed the basic ideas for different algorithms namely: beamforming, Capon, MUSIC,  $l_1$ -SVD and compare their performances. Both Capon and MUSIC algorithms depend on the correlation matrix. The former requires matrix inversion, since the inversion of the correlation matrix appears in the denominator of the output power. On the other hand, MUSIC algorithm depends on the orthogonality between the noise and the signal subspaces where a prior knowledge of the number of sources to be localized is needed. MUSIC algorithm offers an improved resolution capability (narrower peaks) compared to beamforming and Capon. However, those two algorithms are more robust than MUSIC as they do not assume any specific model for the data. All algorithms have been examined for practical cases where we have limited number of antennas and limited antenna spacing. It was shown that the RMSE for all algorithms is the same using only two antenna elements with limited spacing in between. Working with  $d/\lambda = 1/3$  realizes the smallest RMSE with  $\text{SNR} = 20$  dB. Accordingly, working at this ratio is preferred and recommended. The  $l_1$ -SVD algorithm attains super-resolution since the beamwidth at the

estimated angle is very narrow. It also utilizes both sparsity and SVD concepts. Thus, it can work with a reduced data set and the processing time is reduced dramatically.

In addition to the physical size, other factors also deteriorate the performance of DOA estimation including antenna directivity, antenna radiation pattern, multipath, noise, interference, etc. In the following chapter, the performance of DOA estimation in realistic channels is investigated based on experimental results. Moreover, the impact of antenna directionality is considered as well.

## **CHAPTER 4 EXPERIMENTAL DOA ESTIMATION USING SPARSE ARRAYS IN REALISTIC CHANNELS**

Many factors affect the performance of DOA estimation, including the physical size of the handset, antenna type, noise, multipath, and interference. The performance is severely affected in practical circumstances. Signal strength, received phase, false sources (due to multipath), and the steering matrix are all affected in realistic environments.

Sparse arrays such as coprime arrays [52] can estimate the DOA of large number of sources greater than the number of antennas. Coprime arrays are a good candidate when a half-wavelength inter-element is infeasible due to the large antenna size and in the presence of mutual coupling effect. Coprime arrays were proposed with ideal isotropic antennas. In practice, antennas have different gain and phase which are function of the DOA.

In this chapter, the performance of coprime arrays is experimentally evaluated in realistic channel environments. This chapter is divided into three main sections. Section 4.1 examines a moving coprime array for DOA estimation under sparse reconstruction framework. Section 4.2 uses software-defined radio (SDR) to implement a DOA-estimation system and tests its performance. In Section 4.3, the performance is evaluated when the effect of antenna directivity and antenna radiation patterns are incorporated. The constructed systems in Section 4.1 and Section 4.2 are tested successfully in the laboratory with dense multipath environment. The results show that CS produces sharper beams compared with other algorithms. We have also shown that the complexity and the mutual

coupling effect are reduced using a moving coprime array. The impact of antenna directivity is observed as well which we discuss in details in the third section. We have found that the radiation pattern has a direct impact on the estimation accuracy. Due to the radiation pattern, it is difficult to estimate any source of an angle outside the main beam of the directional antenna even in noise free circumstances.

## **4.1 DOA Estimation with Moving Coprime Array Configuration**

### **4.1.1 Introduction**

In this section, a moving coprime array configuration is implemented for DOA estimation under a sparse reconstruction framework. The examined array uses only one receive antenna element. The antenna moves along the array axis to cover certain locations specified by the conventional coprime array. A stepped frequency continuous wave (SFCW) signal over ultra-wideband (UWB) is used. A microcontroller is used to control the movement and the data acquisition from the vector network analyzer to the computer. Two main advantages arise out of this approach. First, the complexity in terms of the total number of antenna elements and receivers needed to implement the array is reduced. Second, the mutual coupling effect is eliminated since only one antenna is present at a time. On the other hand, there is a waiting time to collect the measurements. In addition, power consumption and mechanical control issues have to be addressed. Experimental results in real scenarios were conducted to validate the sparse configuration. It is shown that coprime sampling is superior to uniform sampling with the same number of elements. The impact of the antenna directivity is highlighted.

Two ULAs with  $M_1$  and  $M_2$  antenna elements spaced by  $M_2$  and  $M_1$  units respectively are used to construct the conventional coprime array where  $M_1$  and  $M_2$  are coprime integers and the unit inter-element spacing is half-wavelength [52]. Coprime arrays has the ability to resolve  $\mathcal{O}(M_1 M_2)$  sources using  $M_1 + M_2 - 1$  elements [52], [53], [54], [55]. The optimal coprime pair is the one that has values of  $M_1$  and  $M_2$  as close as possible [56], [57].

A technique to increase the degrees-of-freedom (DOFs) was proposed based on a moving coprime array in [58]. Based on narrowband estimation scheme, the redundant lags in the difference coarray were considered to reduce the complexity for wideband DOA estimation [59]. The work presented some experimental results with  $M_1 = 2, M_2 = 5$  coprime microphone array system [59]. A frequency band of 5 kHz to 10 kHz giving a minimum wavelength of  $\lambda_{min} = 3.4$  cm was considered [59]. The performance was enhanced as the unit inter-element spacing increases beyond  $\lambda_{min}/2$  since the aperture size has enlarged. However, it was degraded when the unit inter-element spacing becomes greater than  $\lambda_{max}/2$  due to the aliasing problems. The error was reduced from  $0.1^\circ$  with spacing of  $\lambda_{min}/2$  to around  $0.03^\circ$  with  $1.6\lambda_{min}/2$  spacing at 0 dB SNR [59].

Most of the previous works have examined the performance using simulations. Only few papers did experimental studies. Few researchers considered the case of a moving coprime array in DOA estimation as in [58] and in imaging such as these in [60], [61], [62]. To the best of the authors' knowledge, no one has used a moving coprime array for DOA estimation under the sparse reconstruction framework.

The suggested moving coprime array in this section is equivalent to the conventional coprime but one antenna element is active at a time. While the data acquisition time is

longer, the complexity is reduced and mutual coupling effects are eliminated. Experimental results using only a single snapshot were performed to evaluate the suggested configuration. Performance comparison of the proposed work against that of a ULA is considered with very limited number of antenna array elements.

The rest of the section is organized as follows. The signal model is presented in Section 4.1.2 in which the coprime array and the utilized moving coprime array are discussed. The waiting time required by the suggested approach is discussed in Section 4.1.3. Experimental results are discussed in Section 4.1.4 and Section 4.1.5 summarizes this section.

#### 4.1.2 Signal Model with Moving Coprime Array

After recalling the structure of the coprime array, the suggested moving coprime array is presented followed by the far-field based DOA estimation model.

##### *A. Coprime Array*

Coprime arrays can be constructed using two linear subarrays. One subarray has  $M_2$  elements spaced by  $M_1$  units and the other has  $M_1$  elements spaced by  $M_2$  units. The two numbers,  $M_1$  and  $M_2$ , are selected to be coprime integers and  $M_1 < M_2$ . The unit inter-element spacing is  $d = \lambda/2$ . The elements of this array [33], [52] are located at:

$$\mathbb{P} = \{M_1 n d | 0 \leq n \leq M_2 - 1\} \cup \{M_2 m d | 0 \leq m \leq M_1 - 1\} \quad (4-1)$$

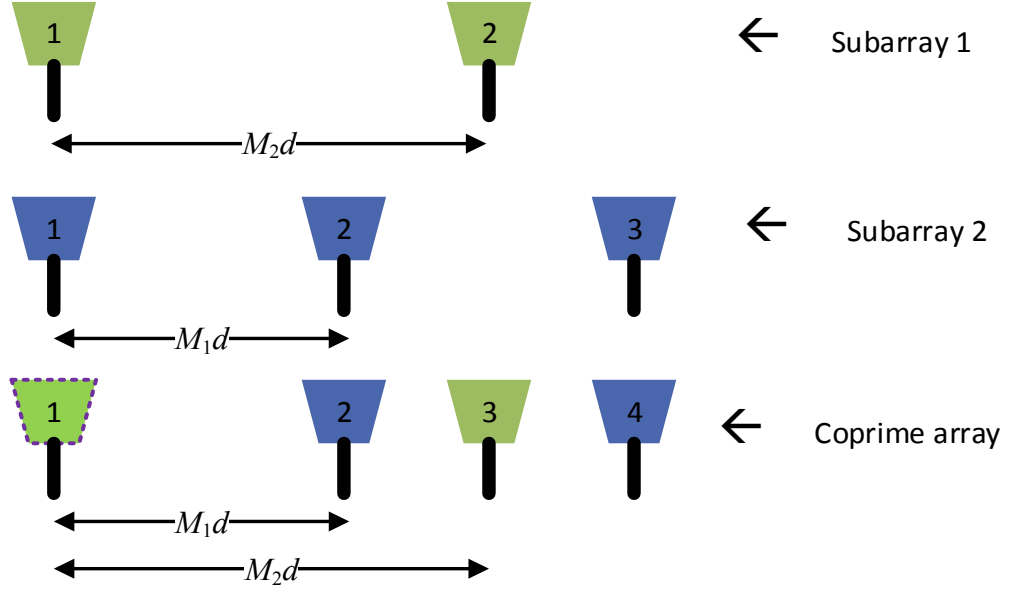
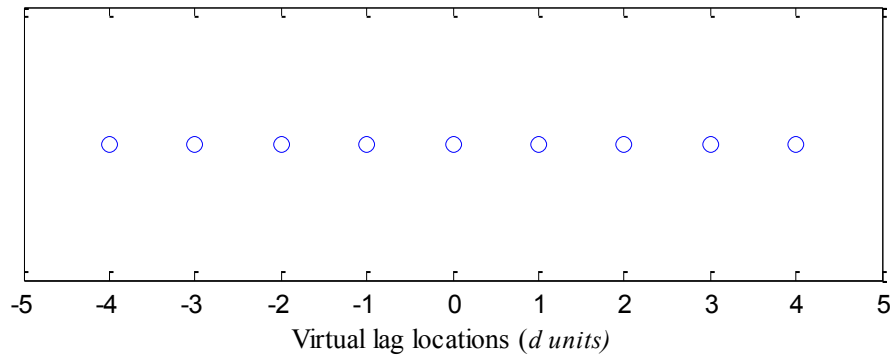
The two ULA subarrays share the first element, hence the total number of elements becomes  $N = M_1 + M_2 - 1$ . Moreover, the aperture size,  $D$ , of the array is  $D = (M_2 - 1)M_1 d$ . Coprime arrays can estimate large number of sources greater than the number of their antenna elements. Basically, the number of unique lags and the number of



consecutive lags in the difference coarray give an upper bound on the achievable DOFs [33]. The difference coarray can be obtained by taking all pairwise differences of the array physical element locations [34]. Since DOA estimation depends on the correlation of the received signal, the virtual element locations which appear in the difference coarray can be exploited instead of just the original element locations [52]. Figure 4-1 (a) shows an example of coprime array with  $M_1 = 2$  and  $M_2 = 3$ . The array has a hole-free difference coarray as Figure 4-1 (b) illustrates. As a result, the virtual array is equivalent to a ULA that extends from  $[-4d: 4d]$ . More details about the difference coarray are presented in Section 5.3.

#### *B. Moving Coprime Array*

A moving coprime array is used to reduce the number of antennas and receivers. This can be achieved using a single antenna that moves and stops along the array axis to take the measurement at  $\mathbb{P}$  positions. Therefore, only one antenna element is active at one of the  $N$  positions. The accuracy of the antenna position is moved in a precise manner using a high resolution stepped motor and microcontroller. The microcontroller receives the instructions from a PC where a code is used to define  $\mathbb{P}$  according to the values of  $M_1$  and  $M_2$ . More details are presented in Section 4.1.4. Once the moving antenna covers all locations, the data collected is organized in a column vector or a matrix in case of single or multiple snapshot(s), respectively.

(a) Coprime array with  $M_1 = 2$  and  $M_2 = 3$ 

(b) Corresponding difference coarray

**Figure 4-1:** Coprime array structure and the corresponding difference coarray

### C. Far-Field Based DOA Estimation for a Single Frequency via Sparse Representation

The sources maybe located in the far-field, near-field or a mix of both fields. In the far-field, all antenna elements have the same DOA for each source. Sources at distance greater than  $\frac{2D^2}{\lambda}$  where  $\lambda$  is the signal wavelength are considered to be in the far-field [28]. For the

near-filed case, the range and angle variations across the array elements are very evident.

In this work, the sources are assumed to be located in the far-field.

Assume that  $K$  uncorrelated narrowband signals located in the far-field impinging on a coprime array from angles  $\boldsymbol{\theta} = [\theta_1, \theta_2, \dots, \theta_K]^T$  as Figure 4-2 depicts. The received signal at the output of the array over  $T$  samples can be expressed as:

$$\mathbf{y}(t) = \mathbf{A}(\boldsymbol{\theta})\mathbf{s}(t) + \mathbf{n}(t), t \in \{t_1, t_2, \dots, t_T\} \quad (4-2)$$

where  $\mathbf{s}(t)$  is the transmitted signal of the  $K$  sources,  $\mathbf{A}(\boldsymbol{\theta})$  is the steering matrix of size  $N \times K$  and  $\mathbf{n}(t)$  is the white Gaussian complex noise with zero-mean. The received discretized signal is  $\mathbf{y}(t) = [y_1(t_1), y_2(t_2), \dots, y_N(t_T)]^T$ . Let  $\mathbf{p} = [p_1d, p_2d, \dots, p_Nd]^T$  denote the positions of the sensors, where  $p_id \in \mathbb{P}$ , for  $i = 1, \dots, N$ . For the given model, the steering vectors can be expressed as:

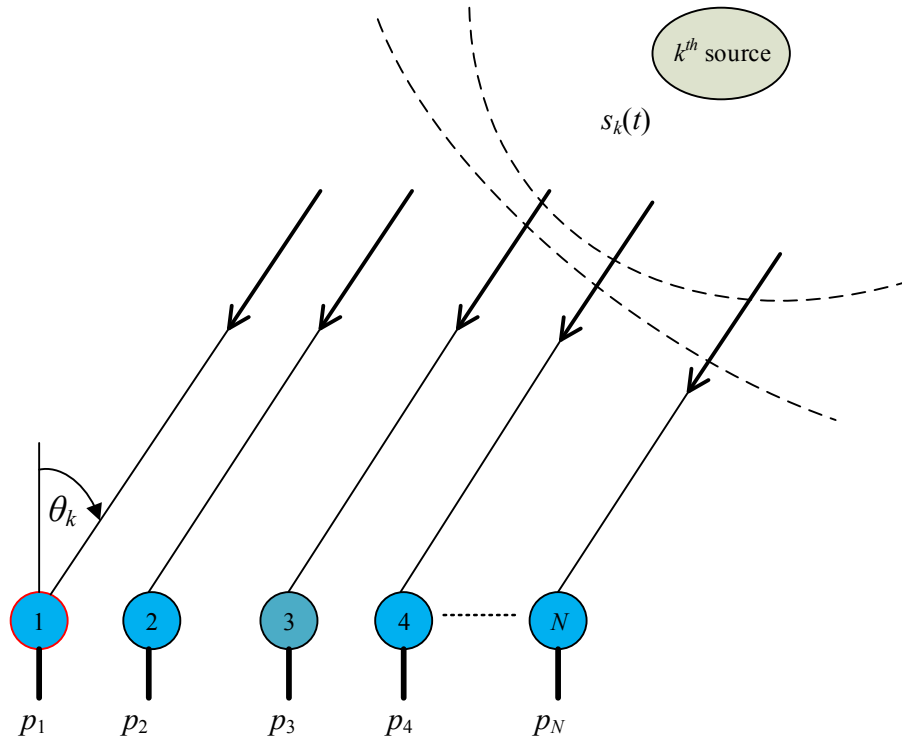


Figure 4-2: System model for DOA estimation

$$\mathbf{a}(\theta_i) = \left[ \exp\left(\frac{j2\pi p_1 d \sin(\theta_i)}{\lambda}\right), \dots, \exp\left(\frac{j2\pi p_N d \sin(\theta_i)}{\lambda}\right) \right]^T \quad (4-3)$$

The received signal can be written in a matrix format as:

$$\mathbf{Y} = \mathbf{A}(\boldsymbol{\theta})\mathbf{S} + \mathbf{N} \quad (4-4)$$

where  $\mathbf{Y} = [\mathbf{y}(t_1), \dots, \mathbf{y}(t_T)]$ ,  $\mathbf{N} = [\mathbf{n}(t_1), \dots, \mathbf{n}(t_T)]$  are matrices of size  $N \times T$  and  $\mathbf{S} = [\mathbf{s}_1(t), \mathbf{s}_2(t), \dots, \mathbf{s}_K(t)]^T$  is a matrix of size  $K \times T$ . The covariance matrix of the received signal is given by:

$$\mathbf{R}_{\mathbf{Y}\mathbf{Y}} = E[\mathbf{Y}\mathbf{Y}^H] = \mathbf{A}\mathbf{R}_{\mathbf{S}\mathbf{S}}\mathbf{A}^H + \sigma_n^2 \mathbf{I}_N \quad (4-5)$$

where  $\mathbf{R}_{\mathbf{S}\mathbf{S}} = E[\mathbf{S}\mathbf{S}^H] = \text{diag}([\sigma_1^2, \sigma_2^2, \dots, \sigma_K^2])$  represents the covariance matrix of the transmitted signal and  $\sigma_k^2$  is the signal power of the  $k^{th}$  source,  $k = 1, 2, \dots, K$ .

Assume that the first element in  $\mathbf{p}$  is used as a reference, hence  $p_1 d = 0$ . The  $(i, j)^{th}$  entry in the covariance matrix of the received signal  $\mathbf{R}_{\mathbf{Y}\mathbf{Y}}$  with lag  $p_i d - p_j d$  produces virtual sensors of a difference coarray,  $\mathbb{C}_P$ , resulting from  $0 \leq (i, j) \leq N = M_1 + M_2 - 1$ , as in [33], [63]:

$$\mathbb{C}_P = \{\mathbf{z} | \mathbf{z} = \mathbf{u} - \mathbf{v}, \mathbf{u} \text{ and } \mathbf{v} \in \mathbb{P}\} \quad (4-6)$$

Coprime arrays can estimate large number of sources greater than the number of antenna elements used. The achieved DOFs of the array is determined by the number of unique lags and the number of consecutive lags generated from the difference coarray [33]. Coprime arrays can generate  $M_1 M_2$  unique or distinct lags [33], [52], [63], [64].

### D. DOA Estimation Algorithms

There are different DOA estimation algorithms. For example, MUSIC algorithm excels in performance if the sources to be estimated are uncorrelated. Prior processing, like spatial smoothing [34], can be applied to reduce the correlation. Sparse reconstruction via CS algorithm can be also applied for DOA estimation since the problem in hand is sparse in the spatial domain. The two algorithms realize different DOFs because sparse reconstruction's algorithms exploit all unique lags whereas MUSIC algorithm exploit half of the number of consecutive lags in the difference coarray [33]. In the following, two DOA estimation approaches namely CS and MUSIC algorithms are adjusted in the context of MLPA.

To perform DOA estimation, we rely on the difference coarray in order to increase the number of estimated sources as virtual antenna locations are used instead of the physical locations.

#### 1. Sparse reconstruction via CS

Based on the presented DOA model, vectorizing the covariance matrix of the received signal yields a vector  $\mathbf{z}$  that amounts to the received data coming from an extended coarray aperture as [33], [63], [64]:

$$\mathbf{z} = \text{vec}(\mathbf{R}_{\mathbf{Y}\mathbf{Y}}) = \tilde{\mathbf{A}}\mathbf{b} + \sigma_n^2 \tilde{\mathbf{I}}_{N^2} = \mathbf{B}\mathbf{r} \quad (4-7)$$

where  $\tilde{\mathbf{A}} = [\tilde{\mathbf{a}}(\theta_1), \tilde{\mathbf{a}}(\theta_2), \dots, \tilde{\mathbf{a}}(\theta_K)]$ , of size  $(N^2 \times K)$ ,  $\tilde{\mathbf{a}}(\theta_K) = \mathbf{a}^*(\theta_K) \otimes \mathbf{a}(\theta_K)$  with  $\otimes$  denotes the Kronecker product,  $\mathbf{b} = [\sigma_1^2, \sigma_2^2, \dots, \sigma_K^2]^T$ ,  $\tilde{\mathbf{I}} = \text{vec}(\mathbf{I}_N)$ ,  $\mathbf{B} = [\tilde{\mathbf{A}}, \tilde{\mathbf{I}}]$  and  $\mathbf{r} = [\mathbf{b}^T, \sigma_n^2]^T$ . The operator  $(*)$  denotes the complex conjugate without transpose. Since the virtual source signal model is a single snapshot of  $\mathbf{b}$ , the rank of the noise free covariance

function  $\mathbf{R}_{zz}$  is one. In this case, the sources become fully correlated. Consequently, subspace-based DOA estimation such as MUSIC algorithm cannot be used directly when more than one source are present in the scene [52].

The formula above is equivalent to (4-2) but with larger measurement matrix,  $\tilde{\mathbf{A}}$ . This is why coprime arrays can estimate  $\mathcal{O}(M_1 M_2)$  sources using  $N$  elements. The previous formula can be solved as an optimization problem

$$\hat{\mathbf{r}} = \min_{\mathbf{r}} \|\mathbf{r}\|_0 \text{ subject to } \|\mathbf{z} - \mathbf{B}\mathbf{r}\|_2 < \epsilon \quad (4-8)$$

where  $\epsilon$  is a user specified bound [33], [63], [64]. Sparse signal recovery using Lasso can be used to solve such problems based on the  $l_1$ -norm. Let  $\mathbf{B}^g$  be constructed using steering vectors of all possible angles with grid search taken as:  $\theta_1^g, \theta_2^g, \dots, \theta_{N_\theta}^g$ , where  $N_\theta \gg K$  represents the total number of grid search angles. The Lasso objective function can be expressed as [63]:

$$\hat{\mathbf{r}}^g = \min_{\mathbf{r}^g} \left[ \frac{1}{2} \|\mathbf{z} - \mathbf{B}^g \mathbf{r}^g\|_2 + \lambda_t \|\mathbf{r}^g\|_1 \right] \quad (4-9)$$

where  $\lambda_t$  is a regularization parameter. For complex data, the previous equation can be rewritten as [63]:

$$\hat{\mathbf{r}}^g = \min_{\mathbf{r}^g} \left[ \frac{1}{2} \|\tilde{\mathbf{z}} - \tilde{\mathbf{B}}^g \mathbf{r}^g\|_2 + \lambda_t \|\mathbf{r}^g\|_1 \right] \quad (4-10)$$

where  $\tilde{\mathbf{B}}^g = [\text{real}(\mathbf{B}^g)^T, \text{imag}(\mathbf{B}^g)^T]^T$  and  $\tilde{\mathbf{z}} = [\text{real}(\mathbf{z})^T, \text{imag}(\mathbf{z})^T]^T$ . The locations of the nonzero indices within the sparse estimated vector,  $\hat{\mathbf{r}}^g$ , denote the estimated DOAs and their values give the corresponding signal power. In addition, the last entry represents the estimated noise variance.

### 2. MUSIC algorithm with spatial smoothing

To apply spatial smoothing, the measurements that are based on the consecutive lags are extracted from  $\mathbf{z}$  and arranged in a new vector  $\mathbf{z}_1$  where the redundant lags within the consecutive lags are averaged [33]. Since the coprime array has a symmetric difference coarray around the origin, the number of consecutive lags,  $l_{cg}$ , is odd. The set of consecutive lags in the difference coarray is  $[-l_x, l_x]$  where  $l_x = (l_{cg} - 1)/2$ . We can rewrite [34]:

$$\mathbf{z}_1 = \tilde{\mathbf{A}}_1 \mathbf{b} + \sigma_n^2 \tilde{\mathbf{I}}_1 \quad (4-11)$$

where  $\tilde{\mathbf{A}}_1$  is a steering matrix of size  $l_{cg} \times K$  like that of a ULA with  $l_{cg}$  antenna elements located at  $\{-l_x d: l_x d\}$  and  $\tilde{\mathbf{I}}_1$  is a vector of length  $l_{cg} \times 1$  with “1” at the  $(l_x + 1)^{th}$  location and the remaining entries are zeros. This new virtual array is then divided into  $l_x + 1$  subarrays,  $\mathbf{z}_{1i}$ ,  $i = 1, 2, \dots, l_x + 1$ . The subarrays overlap and have elements at positions  $(-i + 1 + k)d$  for  $k = 0, 1, \dots, l_x$ . Each subarray,  $\mathbf{z}_{1i}$ , has covariance matrix  $\mathbf{R}_{\mathbf{z}_{1i}\mathbf{z}_{1i}} = \mathbf{z}_{1i} \mathbf{z}_{1i}^H$ . By considering all subarrays, the averaged covariance matrix which has a full-rank is given as [34]:

$$\mathbf{R}_{\mathbf{zz}}^{ss} = \frac{1}{l_x + 1} \sum_{i=1}^{l_x+1} \mathbf{R}_{\mathbf{z}_{1i}\mathbf{z}_{1i}} \quad (4-12)$$

Therefore, MUSIC algorithm can be implemented directly on the spatially smoothed matrix  $\mathbf{R}_{\mathbf{zz}}^{ss}$  and  $l_x$  DOFs can be realized. After performing eigenvalue decomposition, the eigenvectors that span the space of  $\mathbf{R}_{\mathbf{zz}}^{ss}$  can be divided into signal subspace,  $\mathbf{U}_s$ , and noise subspace,  $\mathbf{V}_n$ , which are orthogonal. The signal subspace is spanned by eigenvectors that corresponds to the  $K$  largest eigenvalues, while the noise subspace is spanned by the

eigenvectors that corresponds to the  $l_{cg} - K$  smallest eigenvalues of  $\mathbf{R}_{zz}^{ss}$ . We can perform eigenvalue decomposition on  $\mathbf{R}_{zz}^{ss}$  as [28]:

$$\mathbf{R}_{xx}^{ss} = [\mathbf{U}_s \quad \mathbf{V}_n] \mathbf{\Sigma} \begin{bmatrix} \mathbf{V}_n^H \\ \mathbf{U}_s^H \end{bmatrix} \quad (4-13)$$

where  $\mathbf{\Sigma}$  is a diagonal matrix that contains the eigenvalues in descending order. Since the steering vectors of the sources span the signal subspace, this makes them orthogonal to the noise subspace as well, i.e.  $\mathbf{a}^H(\theta)\mathbf{V}_n\mathbf{V}_n^H\mathbf{a}(\theta) = \mathbf{0}$ . Therefore, the estimated spectrum of MUSIC algorithm can be expressed as [28] :

$$P_{\text{MUSIC}}(\theta) = \frac{1}{\mathbf{a}^H(\theta)\mathbf{V}_n\mathbf{V}_n^H\mathbf{a}(\theta)} \quad (4-14)$$

where  $\theta$  is an arbitrary scanning angle. The  $K$  largest peaks of  $P_{\text{MUSIC}}(\theta)$  correspond to estimated DOAs of the unknown sources.

#### 4.1.3 Latency (Waiting Time)

In a moving coprime array, offline processing is performed after collecting the data at all locations. Let  $t_c$  be the waiting time required to collect the data at each location. For a given aperture size,  $D$ , the latency can be defined as the time required to move the antenna along the required aperture and collect the data at  $N$  positions and is given as:

$$t_D = \frac{D}{v_s} + Nt_c \quad (4-15)$$

where  $v_s$  is the speed of the moving antenna. We can rewrite the previous formula as:

$$t_D = \frac{(M_2 - 1)M_1d}{v_s} + (M_1 + M_2 - 1)t_c \quad (4-16)$$



In our experiments, we use  $t_c = 8$  to  $10$  sec and  $v_s$  can be calculated from the data sheet of the stepper motor and other related factors. For simplicity, we assume  $v_s = 1$  m/s,  $t_c = 10$  sec, and we use  $f = 10$  GHz which makes the unit inter-element spacing be  $d = \lambda/2 = 0.015$  m. The latency is plotted versus the total number of antenna elements in Figure 4-3 for different coprime pair. We can conclude that the latency increases with  $N$  and  $D$  according to (4-15).

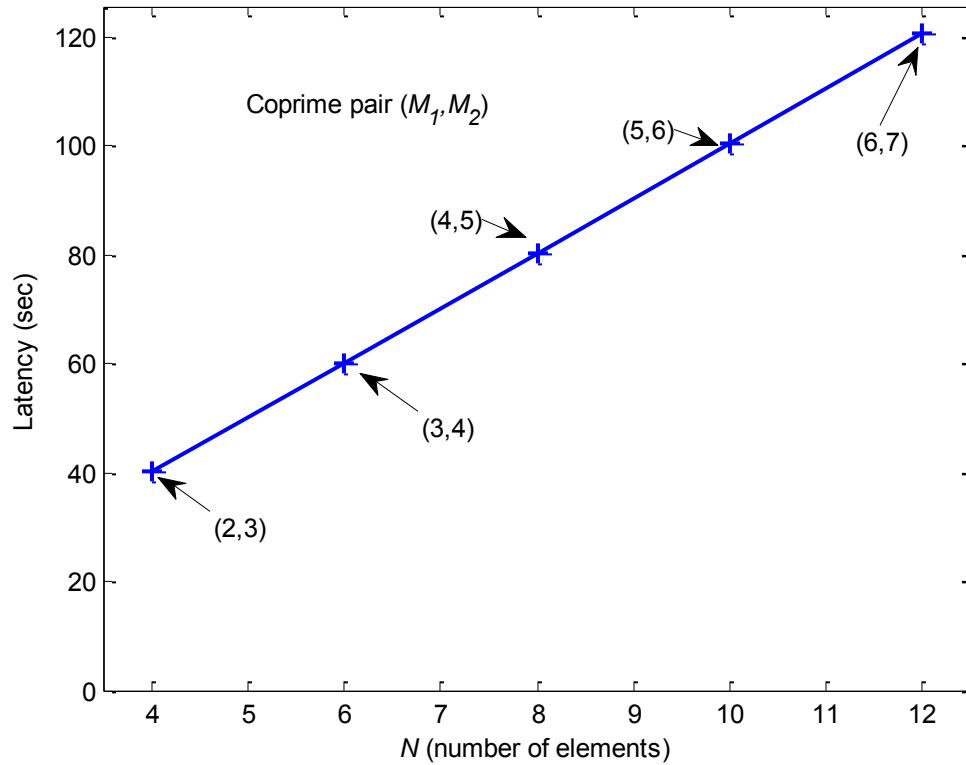


**Figure 4-3:** Latency versus the total number of antenna elements

#### 4.1.4 Experimental Setup and Discussion of Results

Experiments were carried out in the Telecommunication Research Lab (TRL) at King Fahd University of Petroleum and Minerals (KFUPM). The setup, shown in Figure 4-4, consists of a calibrated vector network analyzer (VNA) Agilent N9918A, PC, microcontroller and two broadband horn antennas (Type JXTXLB-10180) in addition to some tools for distance and angle adjustments. One fixed horn antenna represents the active source to be localized and the other moving antenna is the receiving element in the coprime array. The high gain and directivity of the horn antennas are useful for reducing the multipath effect. A microcontroller is used to move the antenna along the array axis such that it covers the required positions specified by  $\mathbb{P}$  in (4-1). The source is located 5 m away from the array but at different angles and both antennas were at a height of 120 cm. The source is located in the far-field. One source is considered at a time and can be in one of three different locations (Tx1, Tx2 and Tx3). The horizontal distance shown in Figure 4-4 are  $x_1 = 65$  cm,  $x_2 = 32.5$  cm, and  $x_3 = 195$  cm. While the vertical distance between the array axis and the transmitter's axis is  $y_1 = 5$  m. The actual angles of Tx1, Tx2 and Tx3 are approximately  $\theta = [-7.4, 3.7, 24.4]$  degrees respectively where antenna one is used as a reference, see Figure 4-4. Those angles demonstrate the dependence of the source location and the capability of the array to estimate the DOA. At each location, the  $S_{21}$  parameters are recorded using the VNA. SFCW signal over ultra-wideband (UWB) from 30 kHz to 10 GHz with a total of 1000 equally spaced frequencies. Lower frequency range than the supported by the horn antenna are used to check the accuracy if we operate the antenna out of band.



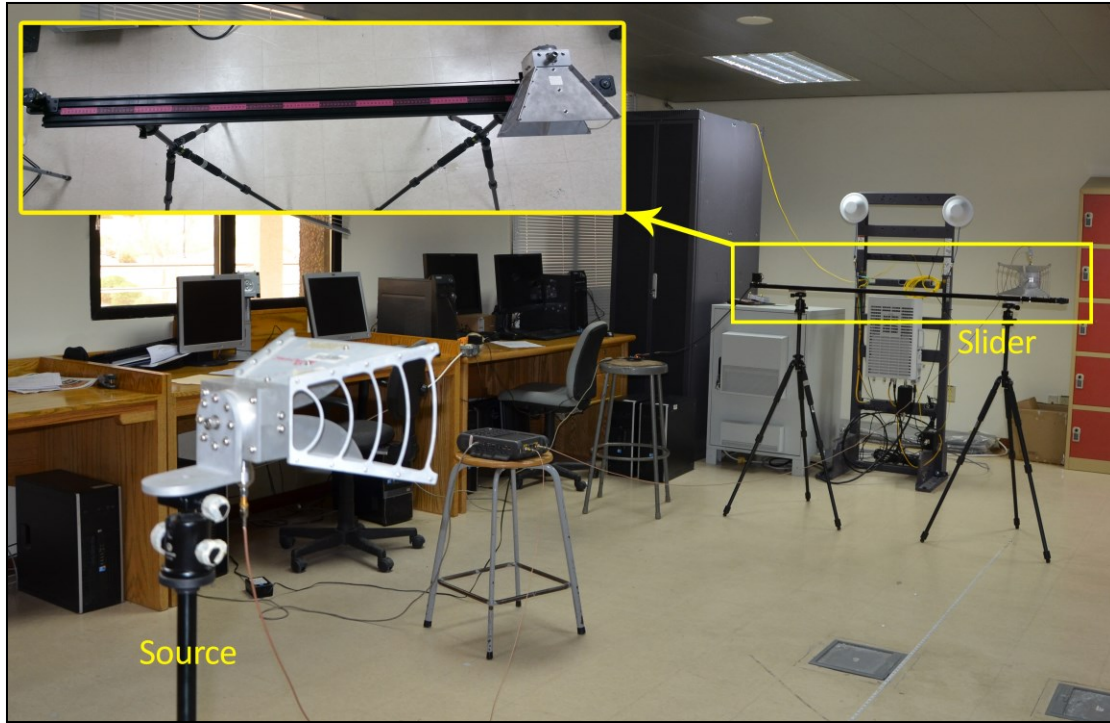


Figure 4-5: Measurements setup

The normalized spectrum is plotted versus both the estimated angles and the operating frequency as shown in Figure 4-6 and Figure 4-7 for moving coprime array and ULA, respectively. The figures in the first, second, and third rows represent DOA estimation for Tx1, Tx2 and Tx3, respectively. Moving coprime arrays are used in Figure 4-6 (a) and (b) with  $N = 4$  and  $N = 8$  elements, respectively. Whereas, a ULA is use in Figure 4-7 (a) and (b) with  $N = 4$  and  $N = 8$  elements, respectively. MUSIC algorithm is used for DOA estimation for the ULA whereas Lasso is used when the moving coprime array is utilized. MUSIC algorithm can be also used for moving coprime arrays but a prior processing is needed [33].

Figure 4-6 (a) illustrates the performance of a moving coprime array using  $N = 4$  elements with  $M_1 = 2$  and  $M_2 = 3$ . Below 1 GHz and around 10 GHz, there are ambiguities because

the antenna/system bandwidth does not support these frequencies. Another interesting observation is the presence of some interfering sources at frequency around 2 GHz.

The estimation performance in case of the ULA is worse compared with moving coprime array because of the large DOFs provided by the coprime array. It is evident from the third rows of the plots that the width of the estimated spectra around the true angle is large. Large degradation appears in the performance of Tx3 because of the high directionality of the utilized horn antennas hence some position within the array cannot see Tx3.

The impact of increasing the number of antenna elements to  $N = 8$  where  $M_1 = 4$  and  $M_2 = 5$  is shown in Figure 4-6 (b). In this scenario, the estimation is more robust as the normalized spectrum width around the true angles is very narrow and sharp. Furthermore, better estimation is realized for Tx3 because more locations were considered. In this case, adding more positions allows the array to receive some power from Tx3 and thus makes up for the high directionality of the antennas.

The performance using moving coprime array with  $N = 4$  elements is better than that using a ULA with  $N = 8$  elements as Figure 4-6 (a) and Figure 4-7 (b) illustrate. This is due to the fact that the moving coprime array realizes a total of nine virtual lags as explained in Section 4.1.2-A.

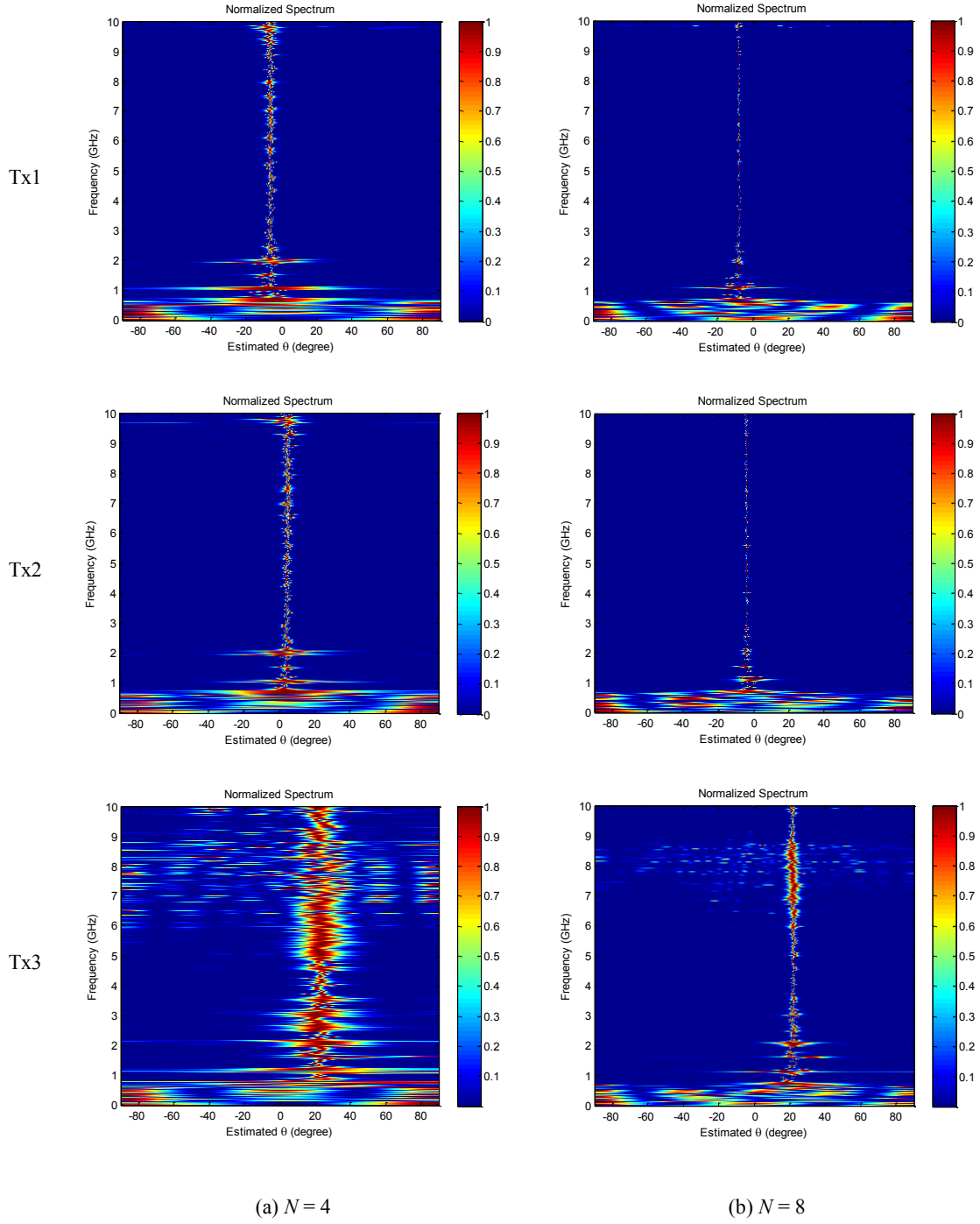


**Figure 4-6:** Normalized spectrum versus frequency and estimated DOA using Lasso algorithm for moving coprime array

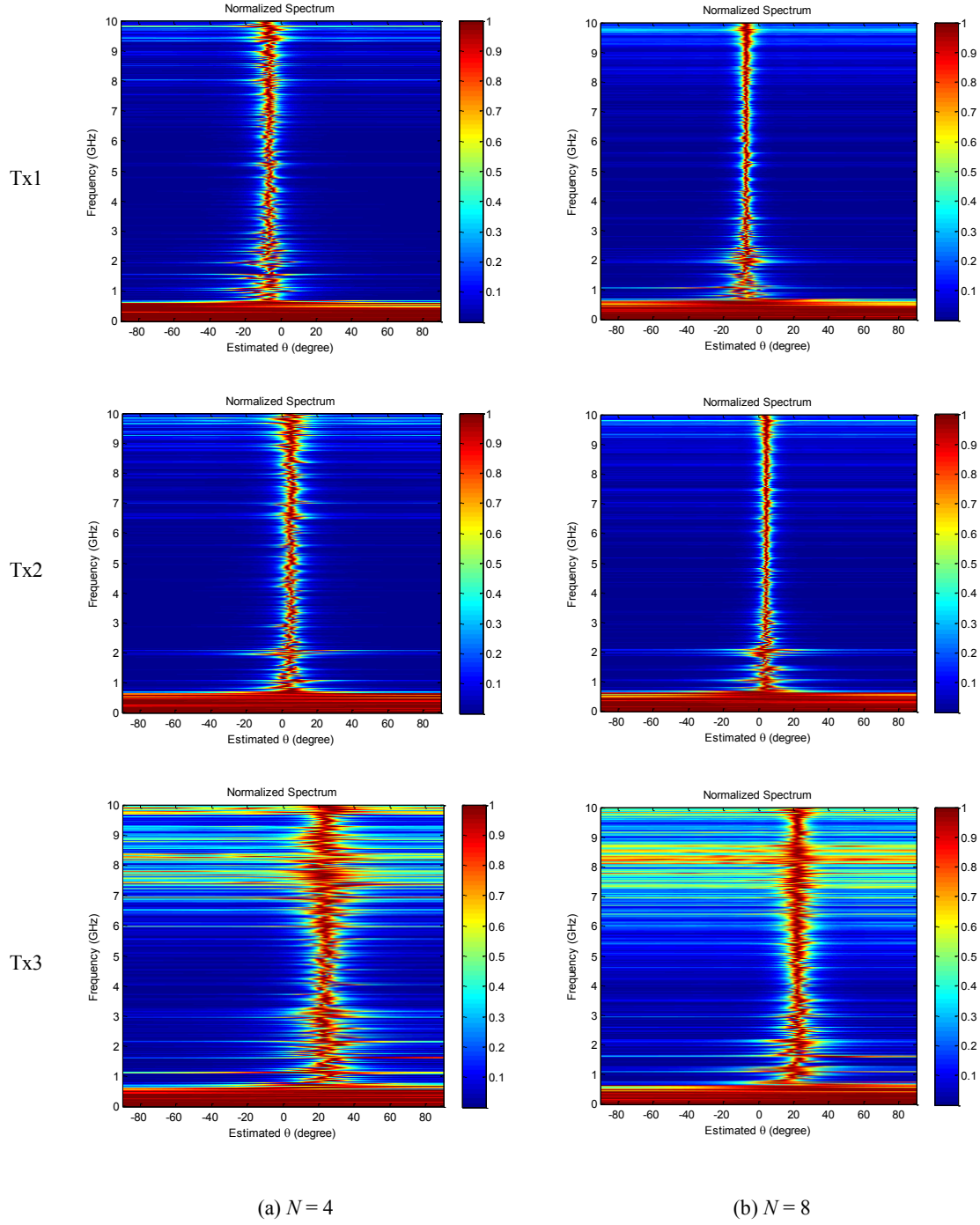


**Figure 4-7:** Normalized spectrum versus frequency and estimated DOA using MUSIC algorithm for a ULA

#### 4.1.5 Concluding Remarks

In this section, a moving coprime array under sparse reconstruction has been constructed for DOA estimation. Based on the proposed configuration both complexity and mutual

coupling effect can be reduced. In addition, experimental results based on single snapshot were conducted to evaluate the advantage proposed array configuration over the ULA configuration. It is shown that the beamwidth is narrower for the case of coprime sampling. The impact of antenna directivity was observed which is an important topic for further future research.

Due to the scanning delay and the off line data processing of the moving coprime array, more flexible system is suggested and tested in the next section

## **4.2 Sparse DOA Estimation Based on Software-Defined Radio**

### **Platform**

In this section, sparse DOA estimation system is implemented on an SDR platform for a linear array. Three different DOA estimation algorithms are implemented. The performance of the implemented system is experimentally evaluated using two different array configurations.

#### **4.2.1 Introduction**

Using multiple antennas, the best DOA estimate can be found by comparing the signals from these antennas and their phase shifts. Optimizing the arrangements of these antennas can greatly increase the accuracy of the system and decrease the cost of a radio DF system. In this section, SDR platform is implemented for sparse DOA estimation based on sparse array configurations. The results show that it is practically possible to estimate the location of more sources without increasing the number of antennas using sparse arrays.



DOA estimation requires expensive hardware as well as capable processing units that can estimate the angle within the desired time. The use of SDR allows researchers to implement DOA estimation systems with relative ease. This is because such devices can be controlled using computers and the received signals can be easily analyzed. One type of these devices is the universal software radio peripheral designed by National Instruments (NI-USRP). This specific type of SDR can be controlled using laboratory virtual instrument engineering workbench (LabVIEW).

The number of antenna elements in the array affects the resolution and accuracy of the estimation [65]. Furthermore, the shape and size of the antenna also affect the range of frequencies for proper DOA estimation [65]. The elements of the array can be placed linearly, rectangularly, or even in a circle [66]. Another factor needs to be taken into consideration is the inter-element spacing between elements, which can be uniform as in the ULA, or nonuniform as in the interesting sparse systems.

Most of the researchers have used ULA based on SDR platform [1], [2] [67]. For instance, the authors in [2] used a ULA in which they placed four NI-USRPs to estimate the angle in order to locate illegal repeaters. It is also possible to implement an array with limited number of antennas. Such a system was presented in [1] and [67] where two NI-USRPs were utilized for estimating a single source where an error of around  $3^\circ$  was obtained. The purpose of using fewer antennas is reducing the cost of the system. In [67], three different environments were tested and the system was only capable of properly estimating angles greater than  $30^\circ$ . In addition, the system estimated the real angle and its reflection. Such a system can estimate the location of one target at most. This is because a ULA of  $N$  elements can only estimate  $N - 1$  sources.

Instead of using a ULA, some researchers used a sparse antenna array. In sparse arrays, the inter-element spacing is not uniform, and it can be represented as an arrangement of ULAs but with missing elements. One of these arrangements is shown in [53], where two ULAs were interleaved and used with the number of antennas in the two arrays being coprime integers. The system was able to estimate the correlations, signal spectra, and DOA at a significantly higher resolution compared with ULA. Another example is presented in [68], where a sparse array was used to construct a virtual ULA from the data collected but with fewer antennas. The number of estimated sources was more than the number of the array elements, which is a very important advantage of sparse arrays over ULAs. Despite the possibility of many array configurations [69], [70], most of the research in this area is done using a ULA with different number of antennas as can be seen in [71]–[78].

One of the most commonly used algorithms in literature is MUSIC, which is an Eigen-structure which assumes orthogonality between the noise and the signal subspaces [67]. The authors in [66] showed that the simulation done using MUSIC delivered improved performance because the noise was reduced significantly. While in [67], they showed that using MUSIC algorithm results in an efficient estimation. Because of all these advantages, MUSIC algorithm is widely used [1], [73], [74], [79]. Capon algorithm was compared with MUSIC algorithm in [67]. It has a good estimation capability though the estimated sources should be uncorrelated. Both Capon and MUSIC algorithms realized narrower beamwidth at the estimated angle compared with that using Bartlett algorithm.

Some studies in literature relied on software simulations, some relied on hardware implementation, and other combined the two approaches. The authors in [66] used only simulations using MATLAB® and LabVIEW. On the other hand, the authors in [73] first

simulated the system and then implemented it on a Peripheral Component Interconnect (PCI) eXtensions for Instrumentation (PXI) platform designed by NI. The advantage of building the system after simulation is to make sure it can operate in imperfect situations where the presence of noise and multipath might affect the results.

From the discussion above, it is clear that there is a need for a simple, practical, and experimentally-tested system. This part uses SDR to implement a DOA-estimation system and test its performance. In our research, we use several SDRs (NI-USRP-2950R), and a PXI platform to implement the system based on coprime array structure. The advantage of such array is that we can achieve results similar to those obtained from a ULA with more elements, which reduces the cost of the system. We use LabVIEW to control the USRPs, process the received signals, and perform DOA estimation via sparse reconstruction, MUSIC, and Capon algorithms. Finally, we compare the results we obtained with others based on ULAs.

This section is organized as follows. Section 4.2.2 presents the considered model in which we discuss the main features of the SDR and LabVIEW software. Section 4.2.3 shows the experimental setup, while Section 4.2.4 discusses the results. Conclusion remarks for the second section are presented in Section 4.2.5.

#### 4.2.2 System Model

We implement a general DOA estimation system based on SDR platform for a linear array. The system is validated using a ULA and sparse array (coprime array). Similar model to the one shown in Figure 4-1 (a) is considered. All receive antenna elements are active at the same time. Coprime array presented in Section 4.1.2-A is used in this part.

*A. Software-Defined Radio*

A software-defined radio (SDR) is a system for radio communication in which components like mixers, amplifiers, and filters are implemented using software instead of hardware. There are different USRP modules of different specifications. The USRP-2950R delivers a unified hardware and software solution for fast prototyping high-performance wireless communication systems. With the flexible hardware architecture and the LabVIEW integrated design flow, researchers can prototype faster and significantly shorten time to results. You can model a wide range of advanced research applications that comprise MIMO, RF, compressive sampling, spectrum sensing, beamforming, and DF.

The USRP-2950R has a frequency range of 50 MHz to 2.2 GHz with a maximum bandwidth up to 40 MHz and I/Q sampling rate up to 200 MS/sec as shown in Table 4-1. The table contains information about the bandwidth, frequency range along with the number of available input/output channels. The USRP has two transmit ports and two receive ports as Figure 4-8 depicts. Therefore, we can have a 2x2 MIMO system within the USRP. The USRP-2950R has a GPS-disciplined oscillator (GPSDO), which permits us to lock the internal clocks to a GPS reference signal, synchronize using GPS timing information, and query GPS position information if needed.

**Table 4-1:** NI-USRP 2950R specifications

<b>Bandwidth</b>	<b>Frequency Range</b>	<b>Maximum I/Q Rate</b>	<b>Input/output Channels</b>
40 MHz or 120 MHz	50 MHz to 2.2 GHz	200 MS/sec	Two



**Figure 4-8:** NI-USRP 2950R module

### *B. LabVIEW Software*

A LabVIEW is a system design platform developed by NI. It comprises of a user interface part and a programming part. The user interface part works with a drag and drop palette of visualization blocks, such as buttons, input fields, knobs, graphs, numerical displays etc. The programming part is done graphically, similar to flowchart programming or block-based programming, where individual functions is divided into blocks with dedicated input and outputs. LabVIEW has a big amount of signal generation, data acquisition, and analysis function libraries. It also has a text-based component for programming called MathScript which uses a syntax compatible with MATLAB®. If you run a LabVIEW application, the host PC will run the application in real-time, taking in and processing any requested measurements from external interfaces such as the USRP module.

### 4.2.3 Experimental Setup

We examined two array configurations. The first system uses a ULA with four antennas while the second system uses a sparse array. In the former, two SDRs (NI-USRP-2950R) are used to estimate the DOA. Two antennas are connected to each of these USRPs using their RX ports. A synchronization device, called the NI-OctoClock-G CDA-2990, is

connected to the USRPs, see Figure 4-9. To ensure synchronization of the frequencies of both USRPs, we connected their REF IN ports to the OctoClock. This is important to ensure that the differences in the phases of the received signals are caused only by the difference in their positions. The transmitted antenna is connected to another USRP using the Tx port, and is also connected to the Octoclock. The carrier frequency of the signal is set to  $1.2\text{ GHz}$ . We placed the receiving antennas with inter-element spacing equal to half the wavelength of the signal, which makes the space between two antennas  $12.5\text{ cm}$ , to avoid spatial aliasing. The transmitter was at least  $1.5\text{ m}$  away from the array in all different tested angles, to make sure that the signal is received as a plane wave, see Figure 4-10. The number of samples is  $T = 16384$  samples. Both the array and the transmitter were  $1\text{ m}$  above the ground. The experiments were conducted in the TRL at KFUPM.

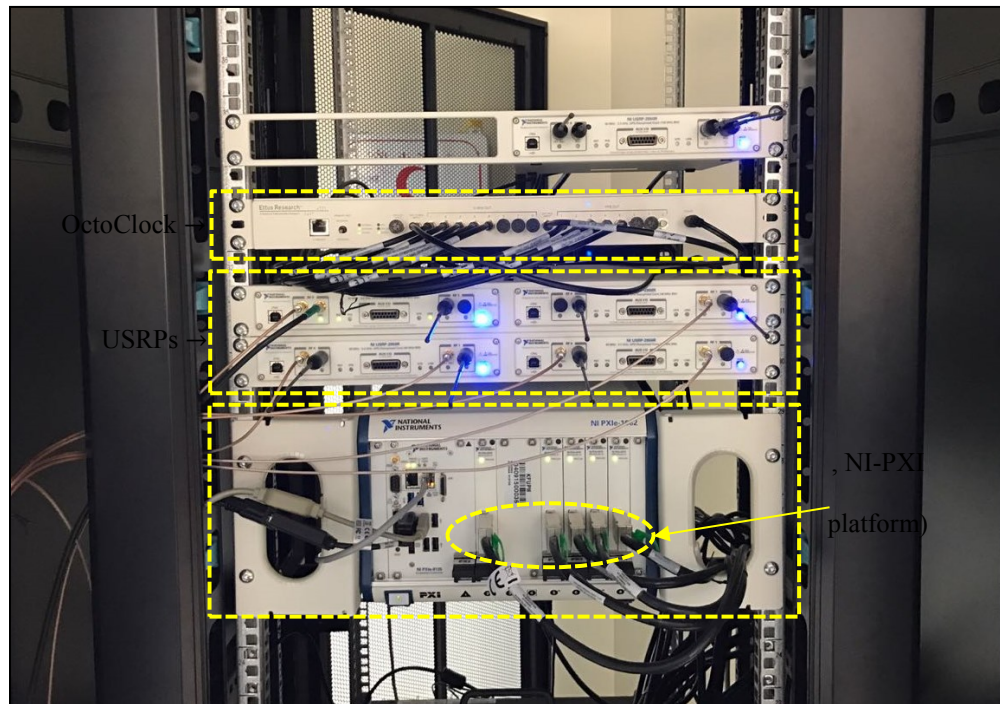
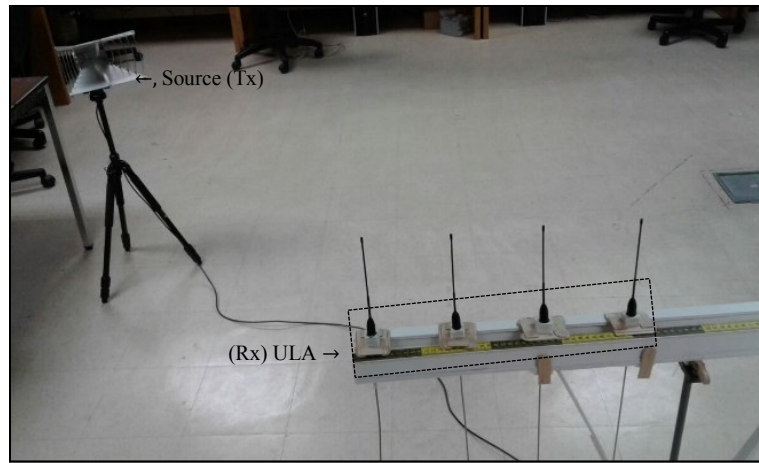
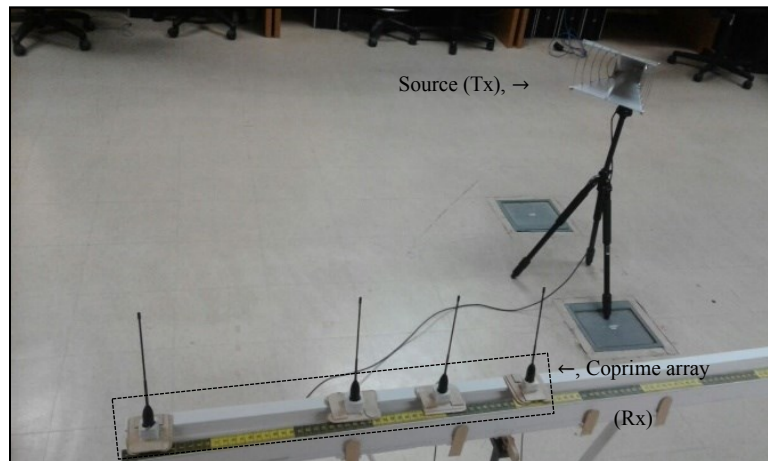


**Figure 4-9:** The whole system installed on a rack

As shown in Figure 4-10, the array uses monopole antennas (Vert 400: 144 MHz, 400 MHz, 1200 MHz tri band vertical antenna). The transmitter, on the other hand, is a broadband horn antenna (Type JXTXLB-10180 and bandwidth of 1 – 18 GHz), which helps to direct the signal toward the receiving antennas and reduce the multipath effects.



(a) ULA

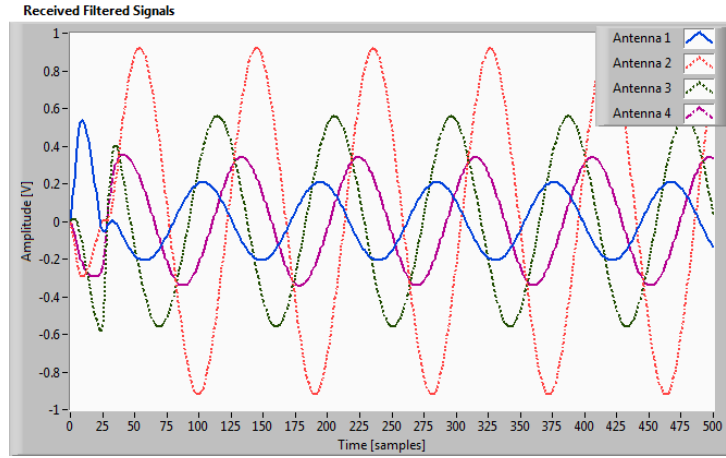


(b) Coprime array

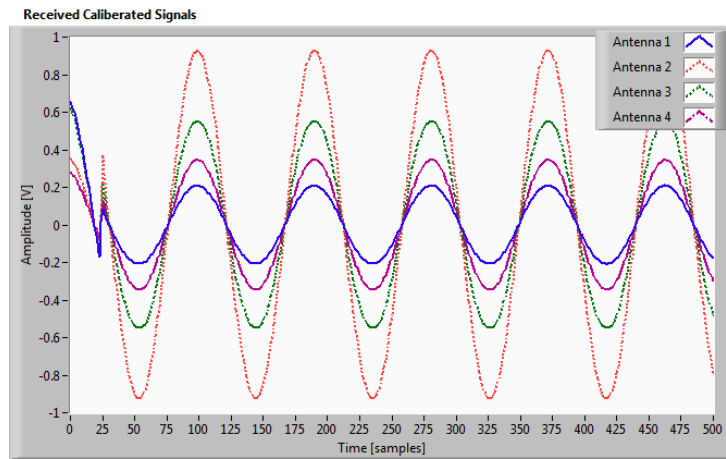
**Figure 4-10:** DOA estimation setup

The described system, including the receivers (Rx) and the transmitter (Tx), is controlled through a developed LabVIEW code. The first part of the code defines the transmitter. A single-tone signal can be used as the unmodulated message with  $10\text{ kHz}$ . The second part is for the receiving USRPs. Before running the code, we place the transmitter at a reference angle  $0^\circ$  and perform phase calibration. The corresponding received signals before and after phase calibration are shown in Figure 4-11. This is achieved by comparing the phases of the received signal by all antennas, and eliminating the differences in the phases. The first antenna, the one on the left, is considered as a reference as shown in Figure 4-1. The received phases before and after calibration are shown in Figure 4-12. After phase calibration, the signals are passed through a filter and then they are fed into DOA estimation algorithms. To get smooth results, we plot the average of the last 20 estimated angles. The second experiment is performed using coprime array which has two subarrays with  $M_1 = 2$  and  $M_2 = 3$  as Figure 4-1 (a) depicts.



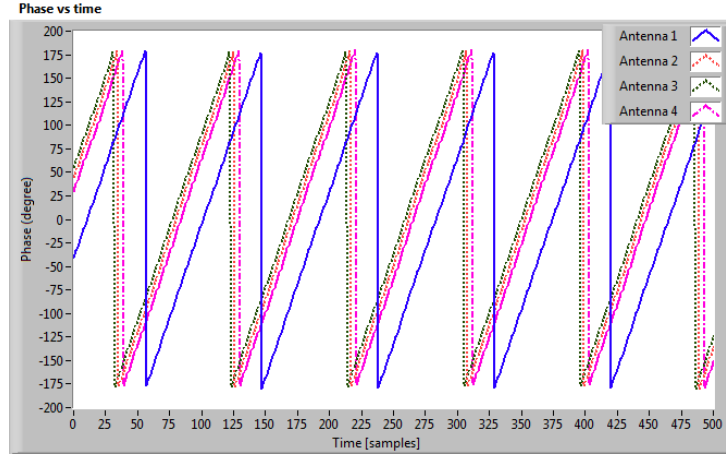


(a) Before phase calibration

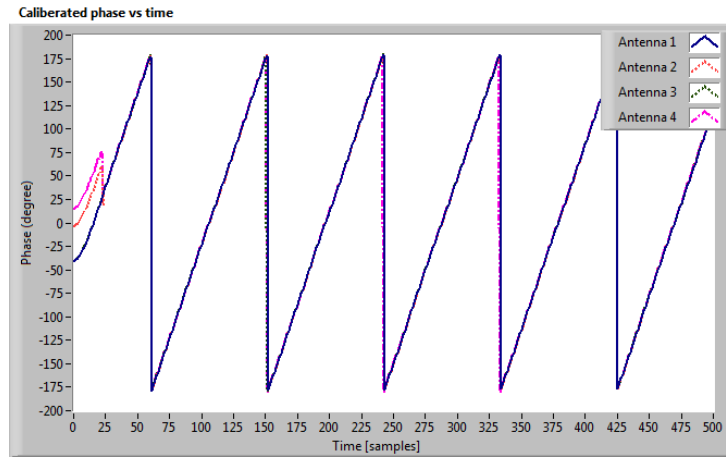


(b) After phase calibration

**Figure 4-11:** The received signals before and after phase calibration



(a) Received phase



(b) Calibrated phase

**Figure 4-12:** The phase of the received signals when the transmitter at zero degree

#### 4.2.4 Results and Discussion

First, we have tested the system capability to estimate different angles at different directions for both configurations. A single transmitter with a single tone at approximately  $-34^\circ$  is assumed in the first scenario and the signal is received with a ULA of four elements. Figure 4-13 (a) and (b) show the normalized spectra of Capon and MUSIC algorithms, respectively.

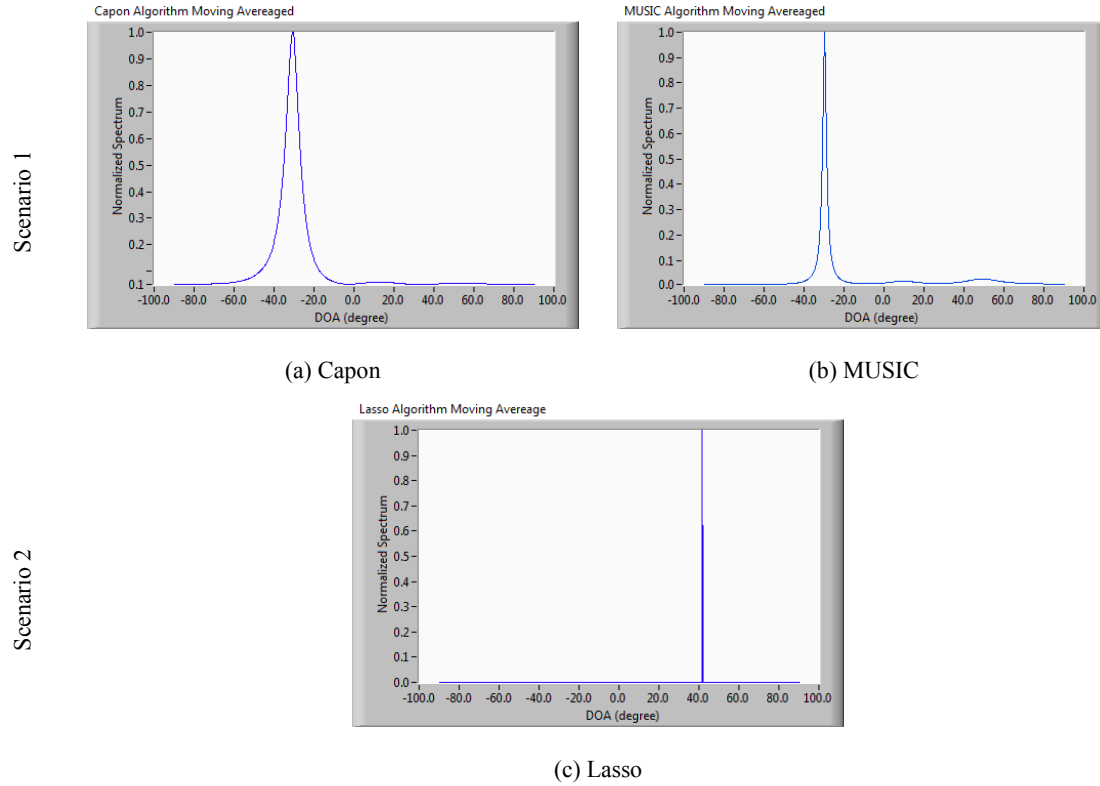


**Figure 4-13:** The normalized spectrum using different algorithms

The same transmitter is located then at approximately  $45^\circ$  from a coprime array in the second scenario where the normalized spectrum of Lasso algorithm is demonstrated in Figure 4-13 (c). The beamwidth at the estimated angle using Lasso algorithm is significantly sharper than those produced by MUSIC and Capon. However, all algorithm realize the same error. Although, Capon and MUSIC have similar estimated angles, MUSIC algorithm has better resolution, i.e. smaller beamwidth at the estimated angle.

Second, we have tested more angles at diverse directions from the arrays. The results obtained from the ULA and the coprime array are presented in Figure 4-14 where we plot the estimated angles versus the actual angles for a single transmitter using MUSIC and Lasso algorithms. The error in the estimated angles becomes negligible as we get closer to  $0^\circ$ . Angles near  $+90^\circ$  are not estimated accurately due to a strong multipath component,

though this is not the case at  $-90^\circ$ . Since the error is not oscillating, it can be calibrated easily as we have done at  $0^\circ$ . The main cause of error is most probably related to the dense surrounding environment and the monopole antenna elements receive the received signal and the reflected ones from all directions. Strong multipath components were received in some cases due to the structure of the room, steel ceil, and other reflectors affected the system. The error is also due to the noise where the selected Tx's position (far-field) is SNR dependent. The error at angles less than  $-50^\circ$  (negative angles) is a bit large where the source is close to the reference antenna. In this case, the estimated angle is affected because the received signals at the output of the remaining three elements become very weak compared with that of the reference antenna, especially for the coprime array. In addition, the source at these angles is close to the wall of the lab, which also affects the performance.

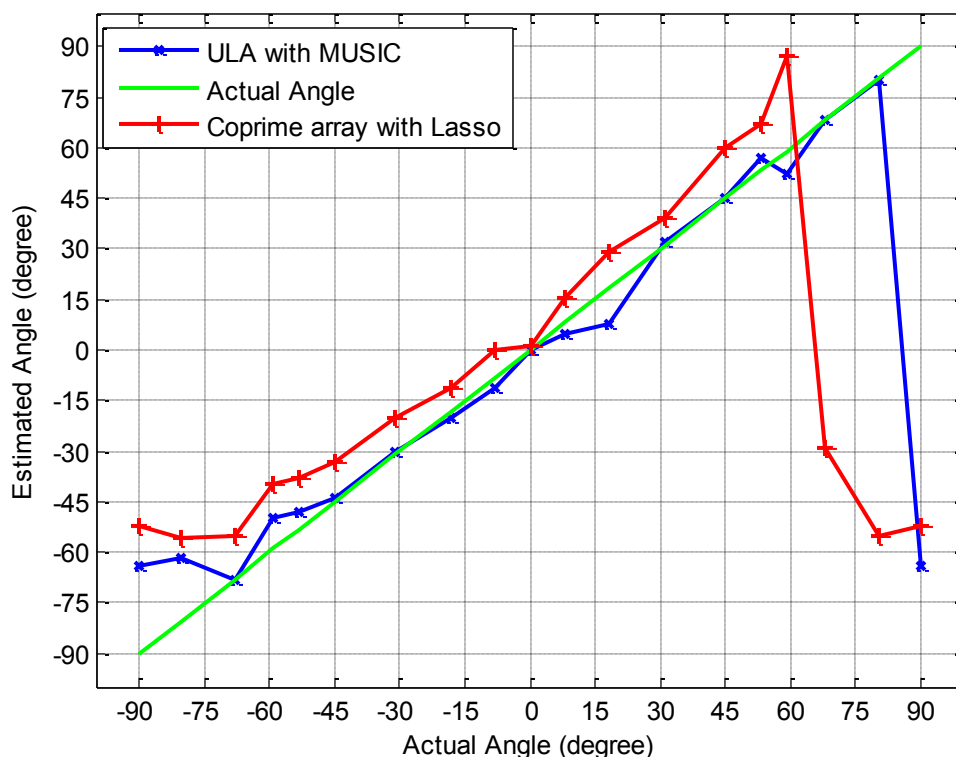


Figure 4-14: Estimated angles versus actual angles based on ULA and coprime array for a single transmitter

#### 4.2.5 Concluding Remarks

In this section, we have implemented DOA estimation system based on SDR (NI-USRP-2950R) platform for a linear array. The system was validated using a ULA and coprime array. The advantage of the system based on coprime array is the flexibility and the ability to locate more sources than possible using ULAs, and reducing mutual coupling of the receiving antennas. We took into account the issues of synchronizing the USRPs and calibrating the phases of the received signals. The implemented system was tested in a laboratory with dense multipath environment and the results with both configurations were compared. MUSIC, Capon, and Lasso algorithms have been successfully implemented for DOA estimation. The results show that CS produces sharper beams in the normalized spectrum than those produced by the other algorithms.

### 4.3 Prototyping Coprime Arrays with Directive Radiation Pattern

This section proposes a sparse DOA estimation method for directive coprime arrays. The complex radiation patterns are extracted using an electromagnetic simulator and then incorporated in the DOA estimation. Three designed antenna arrays with monopole and patch elements are experimentally evaluated with the help of our SDR system implemented in Section 4.2. Three DOA algorithms are compared including Capon, MUSIC, and Lasso based on CS. It is shown that when the DOA increases in the elevation plane, the performance degrades faster when using real antenna elements with directive patterns.

#### 4.3.1 Introduction

Recently, increasing the number of estimated sources in terms of DOA have received more attention. Sparse arrays can efficiently handle such situation including but not limited to nested arrays [34] and coprime arrays [52]. Coprime arrays for DOA estimation was proposed mainly for omnidirectional antenna. The array has antennas with a unit gain and fixed phase in all directions. In practical, antennas usually have different gain and different phase which is a function of the DOA.

The effect of the antenna radiation pattern has been studied in [80]. The authors used different radiation pattern within a ULA in MIMO systems to alleviate the DOA uncertainty. Opposite radiation patterns were used namely broadside and monopole-like pattern. The performance was evaluated in terms of the spectral efficiency. The DOA was assumed to be the angle between the transmitter and the receiver and no DOA estimation algorithms was utilized.

Antenna arrays with different polarization were proposed in [81], [82]. In [81], diverse polarization was considered in which maximum likelihood, adapted angular response, and MUSIC algorithms were adjusted to include the polarization effect. The steering vectors were adjusted to include the effect of the diverse polarization [82]. UCAs with ten [81] and eight [82] antenna elements were exploited to estimate up to two sources. The authors in [82] used linear frequency modulation signals with 50 MHz bandwidth at  $f_c = 10\text{ GHz}$ , and SNR = 20 dB. Whereas, the array in [81] has a diameter of  $6.67\lambda$  with  $\lambda$  being the wavelength of the signal.

Mutual coupling compensation based on experimental results [83], [84] and simulated data [85] applied for DOA estimation was also proposed. The authors in [83] used 7-elements UCAs of radius 9 cm and the operation frequency was 1.88 GHz. While in [84], the authors used a 4-element ULA with monopole antennas spaced by  $\lambda/4$  and operated at 2.4 GHz. A horn antenna that can work on range of 1.5 – 18 GHz was employed as a transmitter and the error in estimating the azimuth angle was  $0.8^\circ$  and  $0.72^\circ$  for the elevation angle. DOA estimation was achieved using MUSIC [83], [84], [85] and Bartlett algorithms [83].

Antenna radiation pattern was exploited for DOA estimation by considering directive [86], [87], [88] and sectorized [89] antennas. Both simulated [86], [88] and experimental data [88], [87], [89] were evaluated. A 4-element UCA with a rectangular microstrip patch antenna at 1.0 GHz was designed and simulated using electromagnetics simulator [88]. A reconfigurable leaky-wave antennas [89] at 2.4 GHz ISM band were exploited [87], [89]. A ULA with 8-elements spaced by  $0.2\lambda$  was utilized in the presence of three sources [86]. The estimated angles were attained through MUSIC algorithm [86] and the three-stage simplified least squares [89]. A RMSE of around  $2^\circ$  was realized at 10 dB SNR [89]. It has

been shown that perfect DOA estimation is realized using directional antennas only if the direction of received signal is within the radiation pattern of main beam [86].

Experimental results for sparse DOA estimation with coprime arrays were developed in [59], [90]. The effect of radiation pattern is implicitly involved through the experiments. A total of eight receive antenna elements were employed in [59]. In addition, ten uncorrelated acoustic sources at 5 *kHz* to 10 *kHz* and  $\lambda_{min} = 3.4\text{ cm}$  at speed of 340 *m/s* were evaluated. Moving coprime array was proposed in [90]. In that approach, a single horn antenna was used as a transmitter. One horn antenna working as a receiver was moved to cover and implement coprime arrays of four and eight antennas. Moreover, a ULA with four elements was also implemented and examined. Thus, the mutual coupling effect and complexity were reduced. However, the signal processing unit (DOA estimation) has to wait for a certain delay which is proportional the number of antenna elements in coprime array.

In this section, sparse DOA estimation with directive coprime arrays is proposed. Coprime array for DOA estimation was mainly proposed for omnidirectional antenna. This part extends the model for directive antennas. The radiation pattern for a coprime array is extracted using high frequency structure simulator (HFSS). Then, a coprime array with four number of antenna elements is exploited for DOA estimation under sparse reconstruction framework. In addition, printed array configurations with monopole and patch elements are evaluated and experimentally tested based on an SDR platform. The results show that the performance is affected by the radiation pattern even in noise free environment. In noisy environment, better performance is realized based on coprime array



compared with a ULA with eight antenna elements. The estimation of the latter is performed using Capon and MUSIC algorithms.

The rest of the section is organized as follows. The system model is presented in Section 4.3.2 in which we incorporate the effect of the antenna radiation pattern. Section 4.3.3 presents the evaluated coprime array. In Section 4.3.4, the gain and phase response of the array in Section 4.3.4 are demonstrated. Section 4.3.5 presents simulation and results based on the simulated arrays with HFSS simulator and 4.3.6 presents experimental results based on the fabricated configurations. Finally, Section 4.3.7 concludes the section.

#### 4.3.2 DOA Signal Model with Directive Antennas

The model of DOA estimation using isotropic antenna elements is the same as the one presented in Section 4.1.2. In this section, antenna elements are not isotropic anymore.

The gain of a directed antenna is a function of the angle of arrival. Let the possible angle of arrival be in the following range  $[\theta_{min}: \theta_l^g: \theta_{max}]$  where  $\theta_l^g$  represents the step in degree.

Thus, the gain of an array with  $N$  antennas can be formulated as:

$$\mathbf{G}(\boldsymbol{\theta}) = \begin{bmatrix} \mathbf{g}_1(\boldsymbol{\theta}) \\ \mathbf{g}_2(\boldsymbol{\theta}) \\ \vdots \\ \mathbf{g}_N(\boldsymbol{\theta}) \end{bmatrix} \quad (4-17)$$

where  $\mathbf{g}_i(\boldsymbol{\theta})$  is a row vector which denotes the complex gain of the  $i$ th antenna and can be written as:

$$\mathbf{g}_i(\boldsymbol{\theta}) = [g_{\theta_{min}}(\theta_{\theta_{min}}), \dots, g_0(\theta_0), \dots, g_{\theta_{max}}(\theta_{\theta_{max}})] \quad (4-18)$$

To include the radiation pattern, the columns of the steering matrix should be modified as:

$$\mathbf{A}_d(\boldsymbol{\theta}) = \begin{bmatrix} g_1(\theta_1)e^{\frac{j2\pi p_1 d \sin(\theta_1)}{\lambda}} & \cdots & g_1(\theta_K)e^{\frac{j2\pi p_1 d \sin(\theta_K)}{\lambda}} \\ \vdots & \ddots & \vdots \\ g_N(\theta_1)e^{\frac{j2\pi p_N d \sin(\theta_1)}{\lambda}} & \cdots & g_N(\theta_K)e^{\frac{j2\pi p_N d \sin(\theta_K)}{\lambda}} \end{bmatrix} \quad (4-19)$$

The received signal in (4-4) is modified according to the new steering matrix,  $\mathbf{A}_d(\boldsymbol{\theta})$ , and finally DOA estimation is performed based on that.

#### 4.3.3 Array Configuration

Structured sparse arrays such as coprime arrays were proposed as an alternative configuration for those implemented through computer search. Coprime arrays have a closed form expression for the array structure and the maximum number of sources that can be estimated. Those arrays are also attractive to reduce the mutual coupling effect since the antennas have large inter-element spacing in between. Working with antennas of large size greater than half-wavelength creates a difficulty in implementing a ULA.

The prototype coprime array [52] constructed as in Section 4.1.2-A and shown in Figure 4-1 is considered. A total of  $N = 4$  elements is used where  $M_1 = 2, M_2 = 3$ , and an aperture size of  $(M_2 - 1)M_1 d$ . The unit inter-element spacing is  $d = \lambda/2$ . The array has a hole-free difference coarray,  $[-4d: 4d]$ .

For comparison purpose, coprime array with four elements is compared with a ULA with equal number of elements (four). In addition, a ULA with five antenna elements is considered to compare against equal aperture size.

#### 4.3.4 Gain and Phase Responses

The gain of an isotropic antenna is distributed equally and uniformly in all directions (angles). Such antenna has also constant phase response. Directed antennas radiate their power in a certain direction and have small power or nulls in some cases in other directions.

##### *A. Simulated Arrays*

In this part, a coprime with four patch elements as shown in Figure 4-1 (a) is designed that is operating at  $f_c = 5.7 \text{ GHz}$  at the Antennas and Microwave Structure Design Laboratory (AMSDL)<sup>1</sup> at KFUPM. Then the radiation patterns were extracted using HFSS simulator. Almost all antennas have similar gain response which is approximately constant between  $-10^\circ$  to  $10^\circ$  as shown in Figure 4-15 (a).

The gain is reduced as we go toward  $-90^\circ$  or  $90^\circ$ . On the other hand, the antennas exhibit constant phase response over a wider range around  $-50^\circ$  to  $50^\circ$  as Figure 4-15 (b) demonstrates. We can also observe similar phase response for the two antennas located at the edges. Due to such responses, performance degradation is expected for different DOAs.

---

<sup>1</sup> The design was done by Mr. Ahmed Oweis and supervised by Dr. Mohammad Sharawi

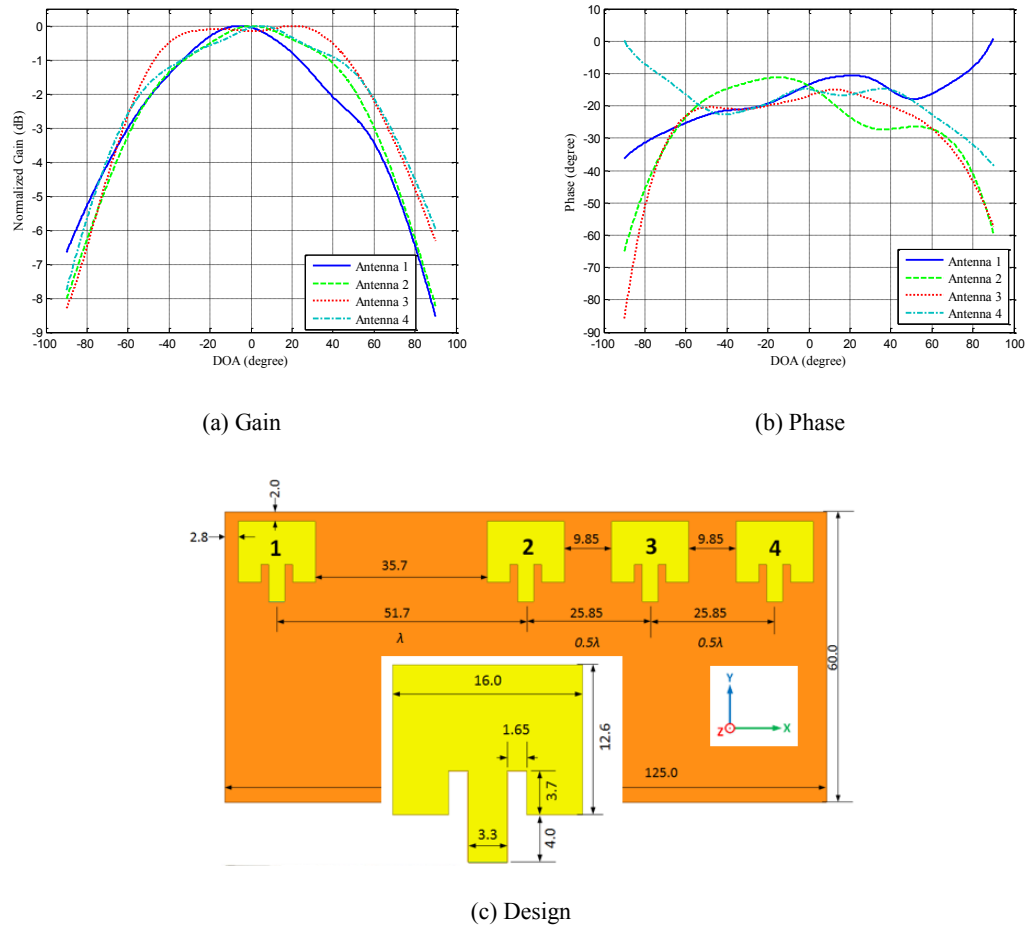


**Figure 4-15:** Characteristics and layout of coprime array of patch elements

### B. Fabricated Arrays

The array designed in Section 4.3.4-A cannot be experimentally tested with our system implemented in Section 4.2 because it requires a frequency larger than the capability of the NI-USRP-2950R. That USRP can handle up to  $2.2\text{ GHz}$ . For this reason, we reduced the frequency to  $f_c = 2.1\text{ GHz}$ . Again with the help of our colleges at AMSDL, three different configurations were designed that were a coprime array, a 4-element ULA, and a 5-element ULA. Monopole and Patch antenna elements were used to implement each array configuration. Therefore, we have a total of six different configurations. The radiation

pattern of all configurations were extracted using HFSS. All configurations were fabricated at Pioneer Company in Jeddah, Saudi Arabia.

The two fabricated coprime arrays are illustrated in Figure 4-16 together with the corresponding gain and phase responses. The fabricated 4-element and 5-element ULAs with monopole and patch elements are shown in Figure 4-17 and Figure 4-18, respectively.

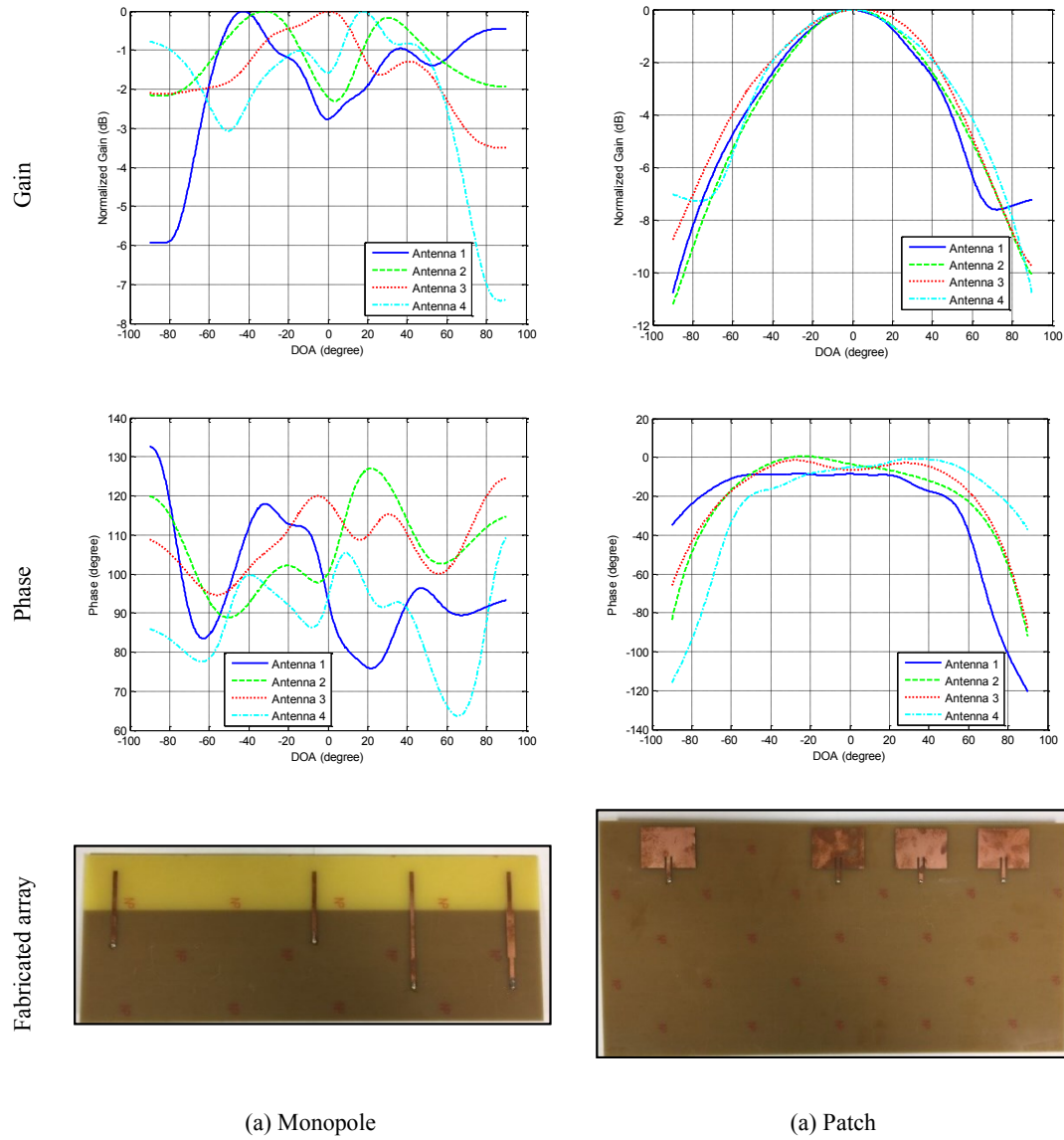
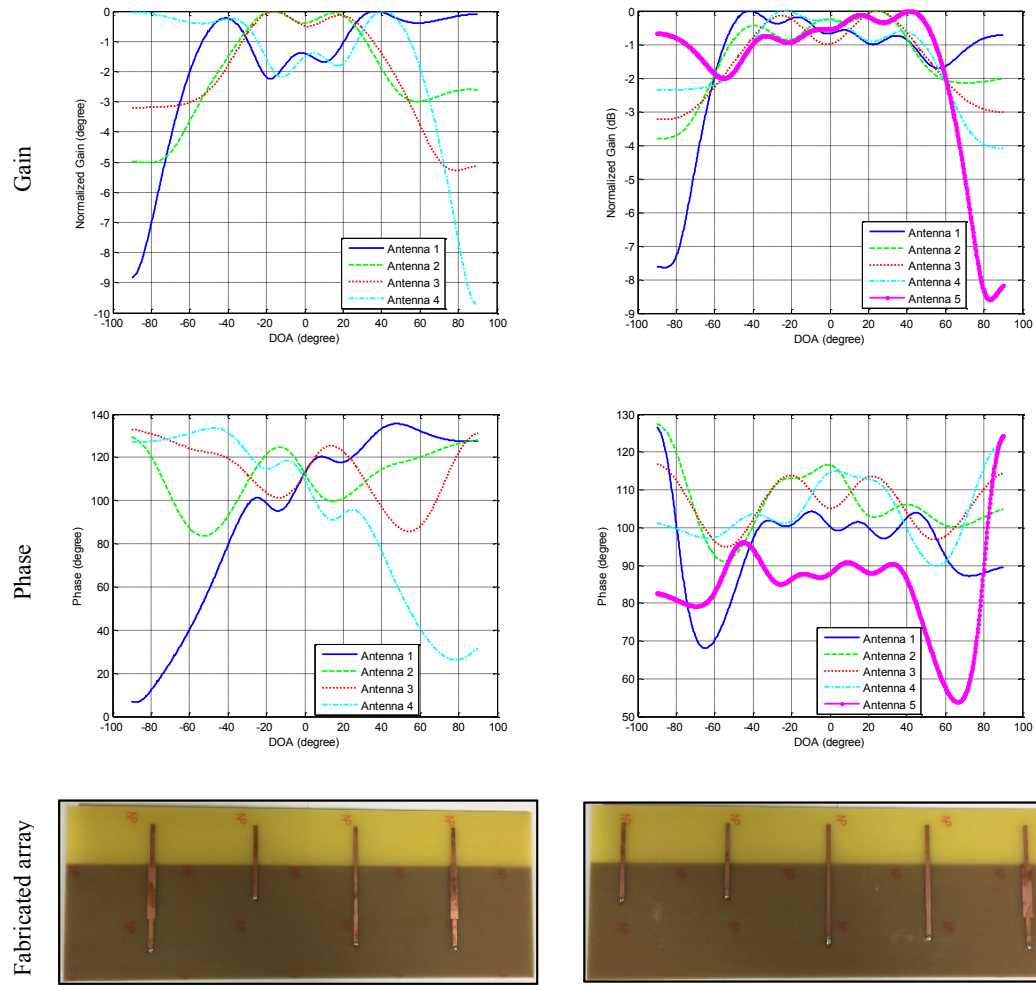


**Figure 4-16:** Gain and phase responses for a printed coprime array with monopole and patch elements

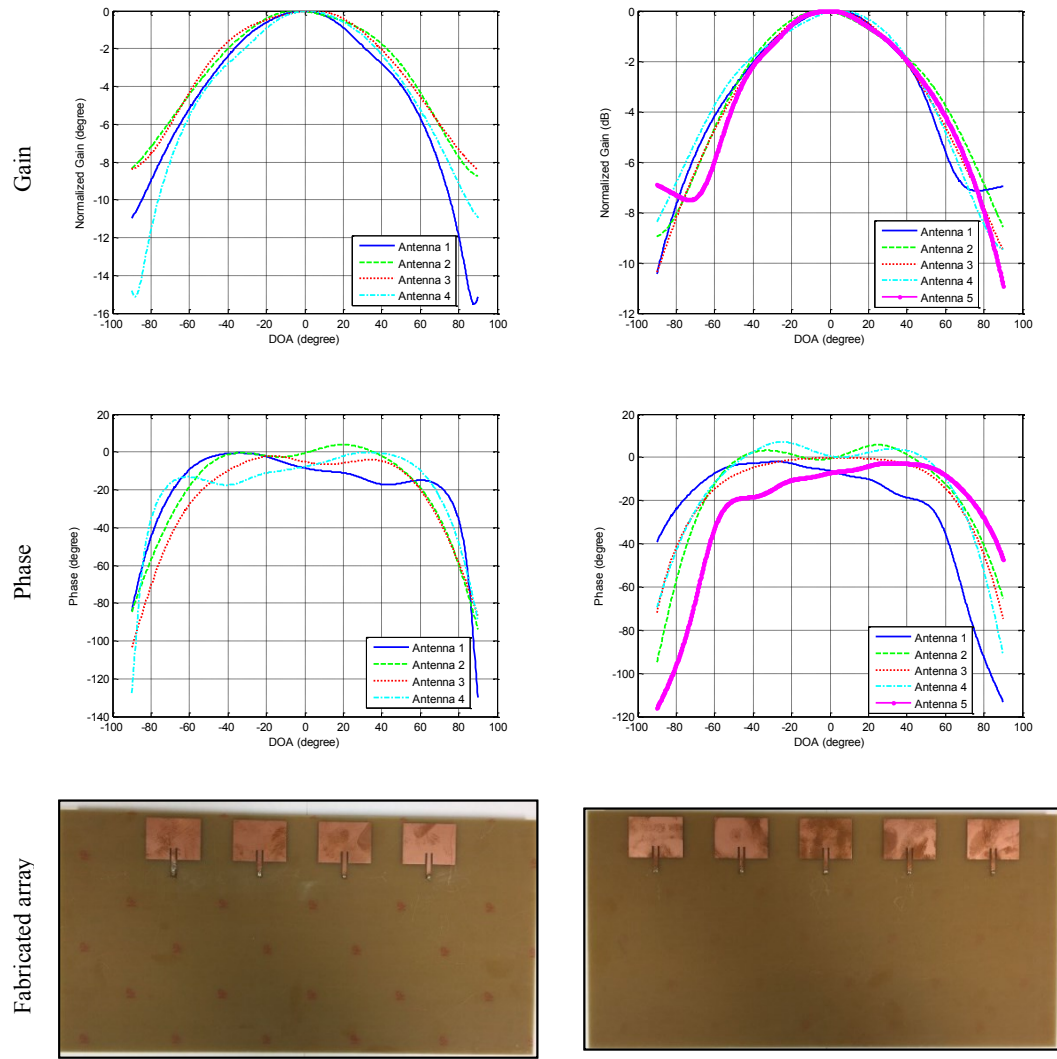


(a) 4-Element ULA

(a) 5-Element ULA

**Figure 4-17:** Gain and phase responses for printed ULAs of monopole elements

High directional gains are realized using patch elements where almost all elements have similar response. In addition, the phase is almost constant within  $[-50^\circ, 50^\circ]$ . On the other hand, the antenna elements have wider and oscillating gain responses using monopole elements for all configurations and the phase response is changing across the whole range.



(a) 4-Element ULA

(a) 5-Element ULA

**Figure 4-18:** Gain and phase responses for printed ULAs of patch elements

#### 4.3.5 Simulation and Results Based on Simulated Arrays

To evaluate the sparse DOA estimation with directive coprime arrays, the following parameters are considered. The configuration presented in Section 4.3.4-A is considered. Lasso algorithm is used to estimate the DOAs as in [33]. Four narrowband and uncorrelated sources,  $K = 4$ , located in the far-field are assumed to impinge on a coprime array with four antenna elements where  $M_1 = 3$  and  $M_2 = 2$ . A total of  $T = 1000$  samples are

collected and a total of  $I_{iter} = 1000$  independent trials are used. The unit inter-element spacing is adjusted as  $d = \lambda/2$  and the regularized parameter is  $\lambda_t = 0.85$  as in [33]. The grid search is uniformly distributed from  $[-90: \theta_i^g: 90]$  with grid search angle of  $\theta_i^g = 0.25^\circ$ . All these parameters are fixed unless stated otherwise. We start by presenting examples to show the estimation capability of the utilized algorithms under different DOA range of arrivals. Then Monte Carlo simulations are illustrated.

If we have a prior knowledge about the number of sources, the  $K$  largest values in the estimated spectrum represent the estimated DOAs. A threshold can be applied to find the largest  $K$  values and then the corresponding DOAs. However, large and very close values at a candidate DOA can cancel some desired angles that have small values. This happens when the algorithm has low resolution which results in a wide beamwidth at the estimated DOAs. As a result, the accuracy of the estimation is degraded if we rely on the threshold. For this reason, a grid refinement can be utilized to overcome this problem [25].

In the normalized estimated spectrum, a window of an odd number of grid points,  $\delta$ , is used to refine the grid around each candidate DOA which correspond to  $(\delta - 1) \times \theta_i^g$  degree. First, we pick the largest value in the estimated spectrum and then force  $(\delta - 1)$  grid points around it to zero and form a new estimated spectrum. So only one estimated angle within a total of  $\delta$  grid points centered at the largest value is assumed. The process is repeated until we cover all  $K$  largest values. The grid refinement makes the estimated spectrum less noisy and sparser.



#### A. Radiation Pattern in Noise Free Environment

Noise free scenario is used to show the effect of including the radiation pattern of the antennas on the performance. Three different ranges of arrivals are considered including:  $\theta \sim U[-40^\circ, 40^\circ] = -40^\circ, -13^\circ, 13^\circ, 40^\circ$ ,  $\theta \sim U[-50^\circ, 50^\circ] = -50^\circ, -17^\circ, 17^\circ, 50^\circ$ , and  $\theta \sim U[-60^\circ, 60^\circ] = -60^\circ, -20^\circ, 20^\circ, 60^\circ$ . The normalized spectra versus the DOA is plotted in Figure 4-19 using Lasso algorithm [33]. The figures on the left represents the spectra of the isotropic antennas. While those on the right represents the spectra of the directed antennas. It is evident that perfect estimation is realized with isotropic antennas for all cases. On the other hand, not all sources have been resolved correctly with directed antennas due to the radiation pattern. The maximum errors in estimating a source among the assumed four sources with isotopic and directive antennas are  $0.5^\circ$  and  $2.5^\circ$ , respectively.

#### B. Grid Refinement

The size of the window has an effect on the performance which we investigate in Figure 4-20 for  $\theta \sim U[-40^\circ, 40^\circ]$ . The evaluated window sizes are: 3, 5, 7, 9, and 11 grid points which correspond to  $0.5^\circ, 1^\circ, 1.5^\circ, 2^\circ$ , and  $2.5^\circ$  respectively around the peak. The angles are estimated using Lasso algorithm [33]. The RMSE is reduced as we increase  $\delta$  at low SNR. This effect disappears at high SNR. For equal window size, the RMSE using the directed antennas is greater than that of the isotropic antennas as shown in lower and the upper subplots respectively.

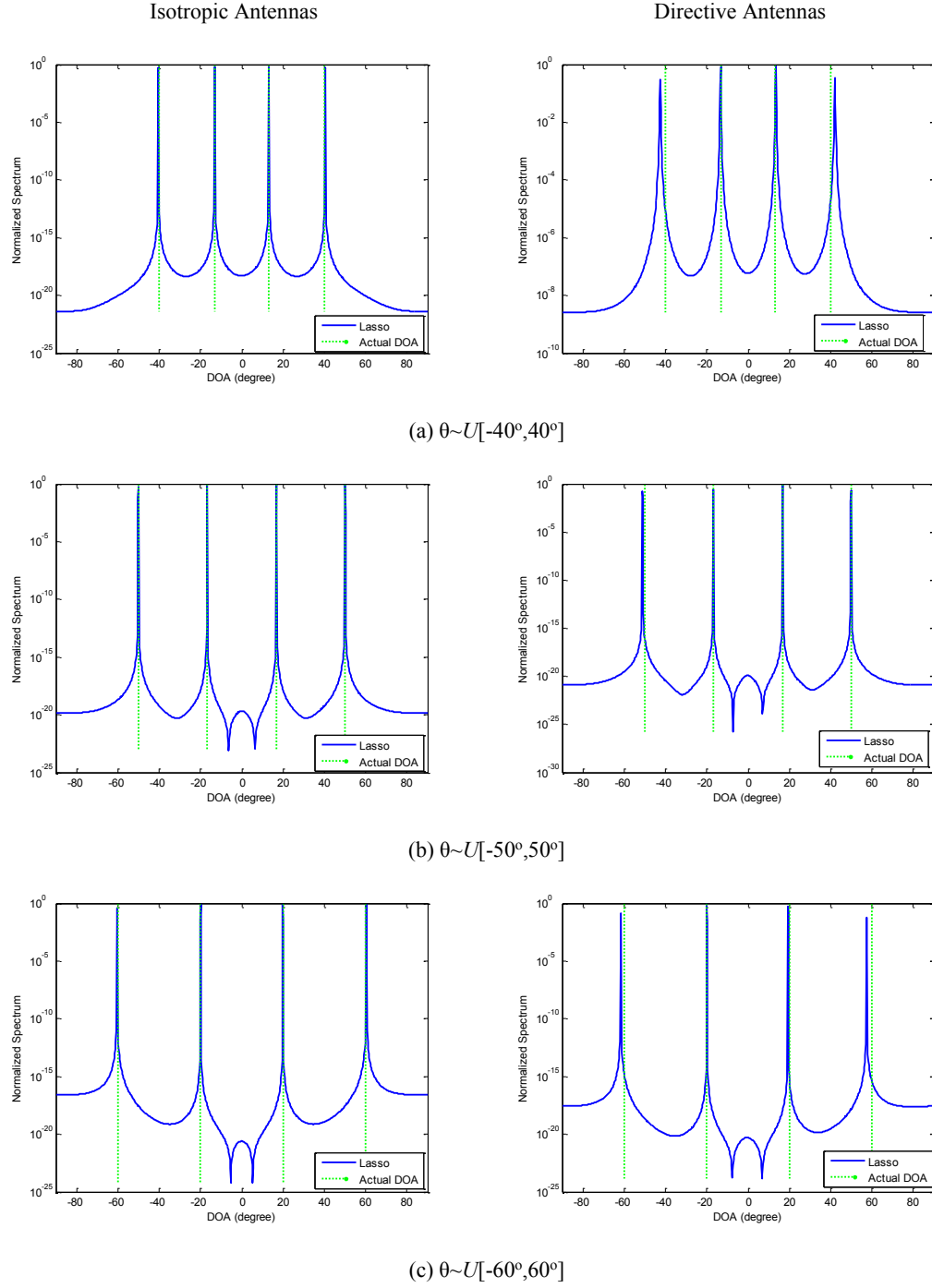


**Figure 4-19:** Normalized spectra using Lasso versus DOA in noise free environment for coprime array with isotropic and directive antennas

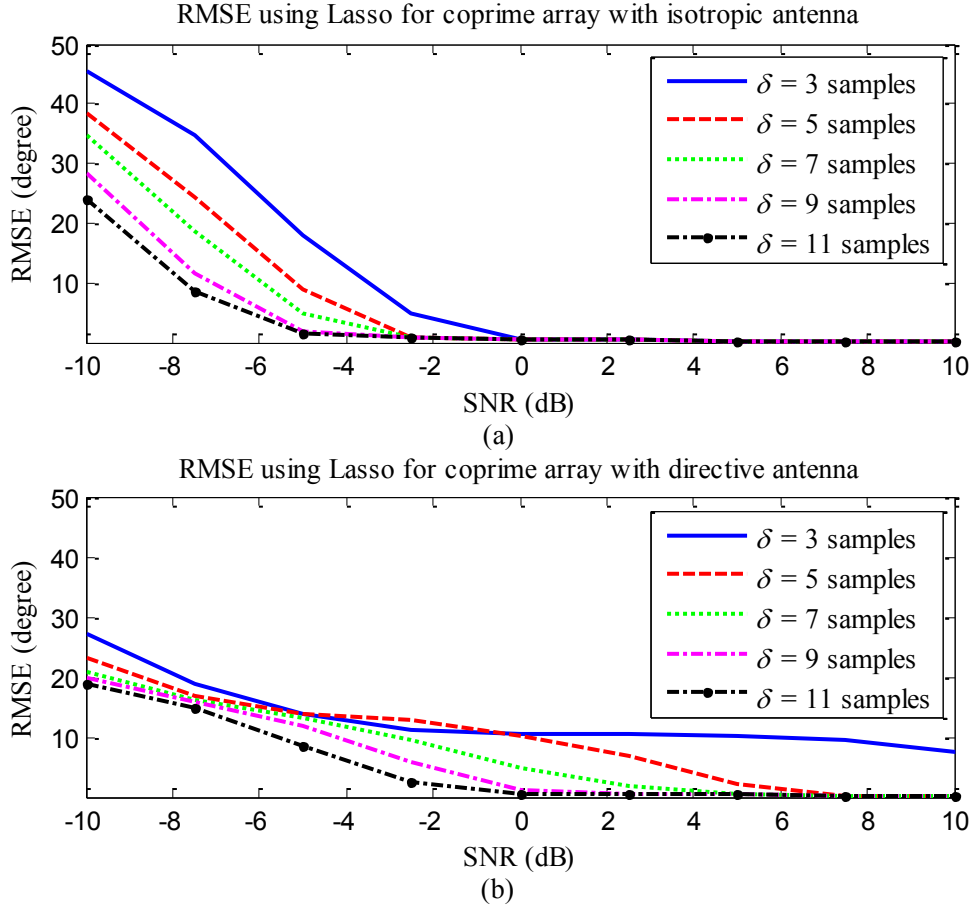


**Figure 4-20:** RMSE versus SNR when  $\theta \sim [-40^\circ, 40^\circ]$  using Lasso algorithm for (a) isotropic and (b) directed antenna

### C. Signal to Noise Ratio and DOA Algorithms

The RMSE versus SNR is plotted in Figure 4-21 for different algorithms when  $\delta = 11$  grid points. The sources are assumed to be uniformly distributed as  $\theta \sim U[-40^\circ, 40^\circ]$  (solid lines),  $\theta \sim U[-50^\circ, 50^\circ]$  (dashed lines), and  $\theta \sim U[-60^\circ, 60^\circ]$  (dotted lines). The results using the isotropic and the directed antennas are generated using Lasso algorithm for coprime array. A ULA with eight antennas is also included for comparison purpose in which MUSIC and Capon algorithms [28] are used in the estimation.

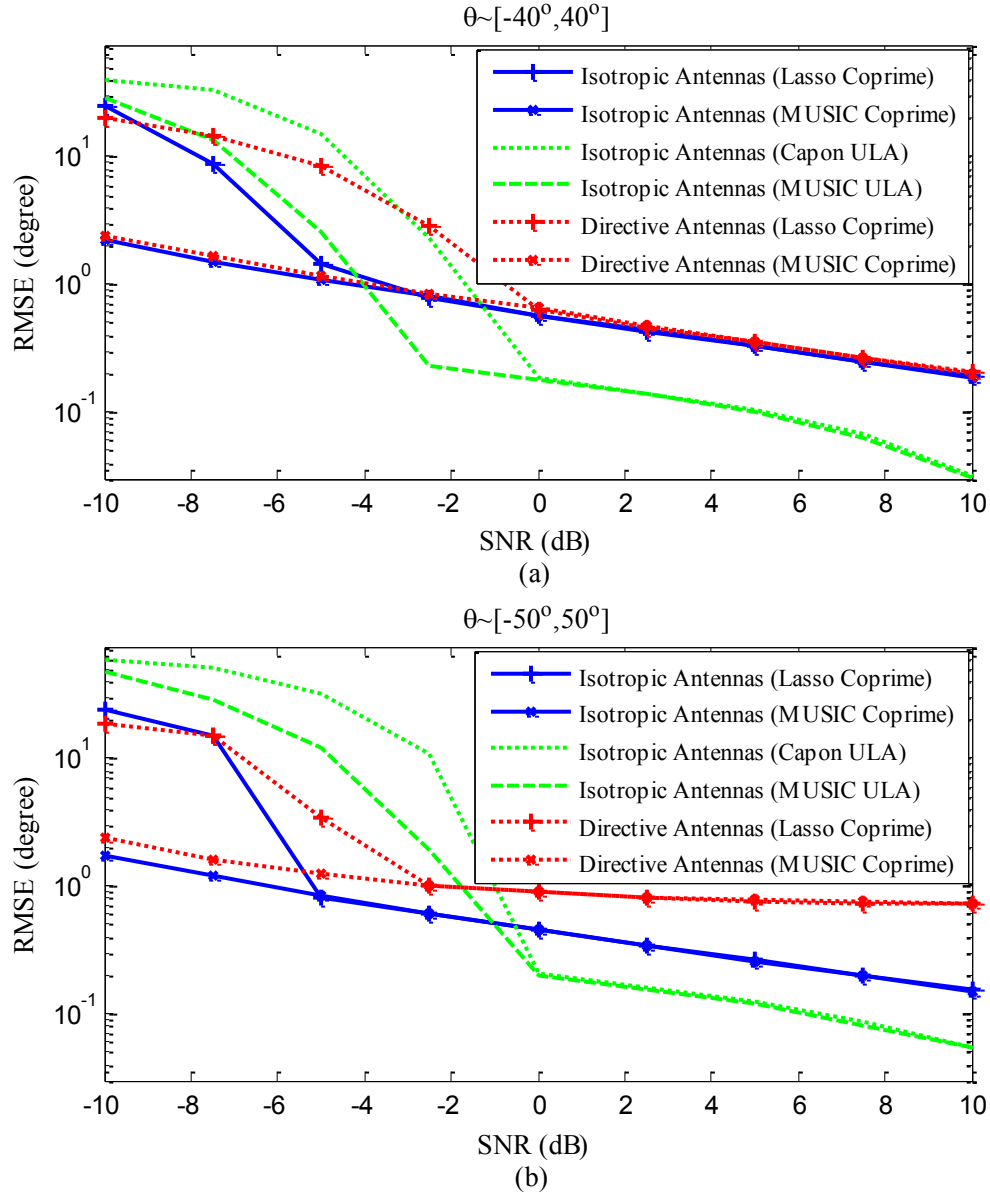


**Figure 4-21:** RMSE versus SNR for different source distributions (a)  $\theta \sim [-40^\circ, 40^\circ]$  and (b)  $\theta \sim [-50^\circ, 50^\circ]$  based on different algorithms with  $\delta = 11$

As the separation between the four sources increases, the RMSE increases due to the effect of the radiation pattern and vice versa. The RMSE based on the isotropic antennas for a certain source distribution is smaller than that of the directed antennas for coprime arrays because of the radiation pattern. Coprime array performs better than the ULA at low SNR

The ULAs with the isotropic antennas have similar behavior using both MUSIC and Capon algorithms.

#### *D. Number of Samples*

The RMSE versus the number of samples is plotted in Figure 4-22. The four sources in Figure 4-22 (a) and (b) are equally spaced between  $[-40^\circ, 40^\circ]$  and  $[-50^\circ, 50^\circ]$ , respectively. In each subplot, we are comparing the isotropic antennas versus the directive antennas with Lasso and MUSIC algorithm with  $\text{SNR} = 0$  dB. It is evident that the RMSE decreases as the number of samples increases. The RMSE using Lasso is smaller than that with MUSIC algorithm because CS algorithm can exploit all unique lags in the difference coarray whereas MUSIC can use half of the number of consecutive lags. Due to the large variations in the gain and phase responses of the considered antennas, see Figure 4-15, the effect of the radiation pattern on the performance is more significant when the sources are between  $[-50^\circ, 50^\circ]$  as illustrated in Figure 4-22 (b).

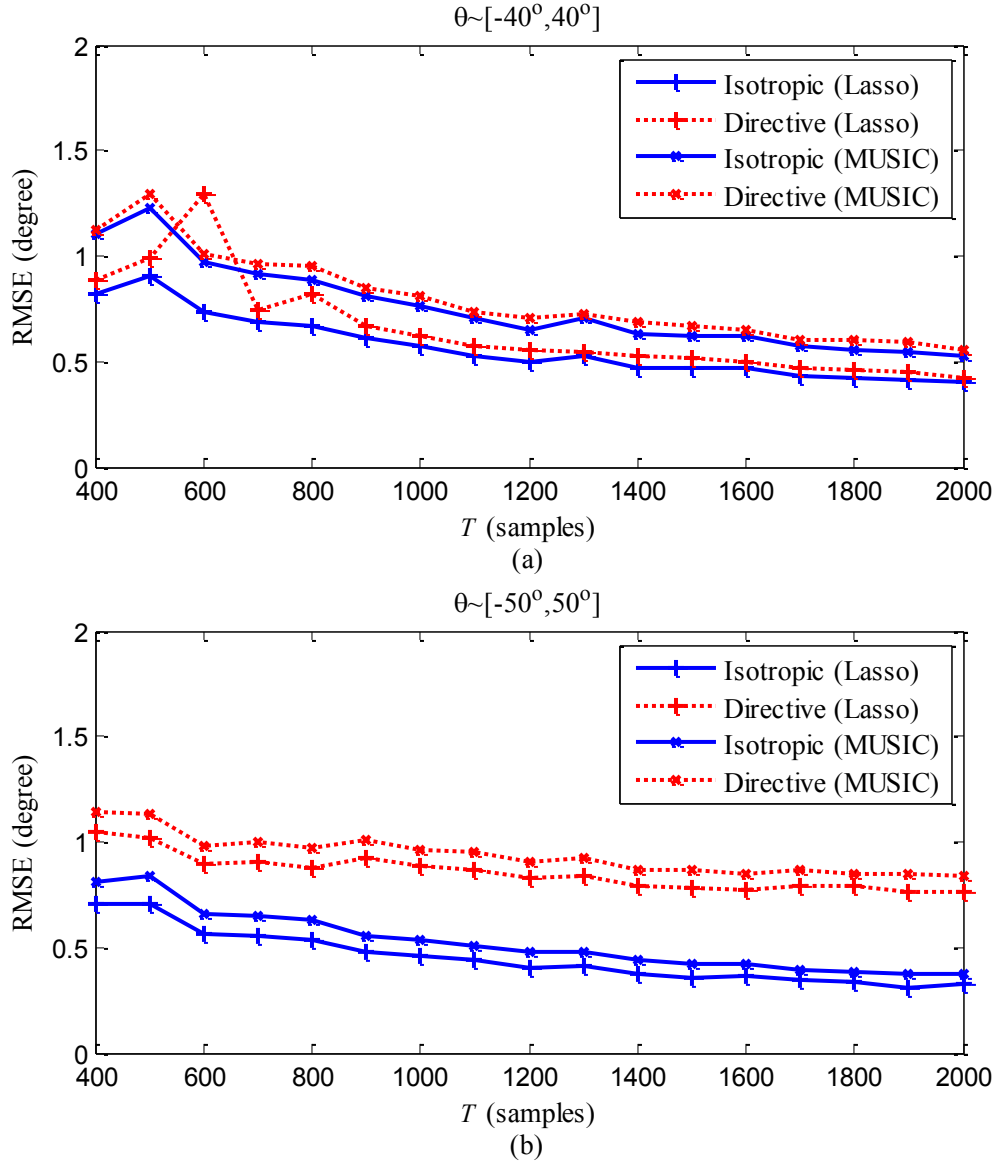


**Figure 4-22:** RMSE versus number of samples for different source arrivals based on different algorithms with  $\delta = 11$

#### E. Unit Inter-Element Spacing

In this part, we examine the effect of the unit inter-element spacing,  $d$ . The one suggested with the conventional coprime array,  $d = \lambda/2$ , is compared with  $d = 2\lambda/5$ . The performance in Figure 4-23 (a) and (b) is achieved using MUSIC and Lasso algorithms, respectively. Reducing the unit inter-element spacing affects the radiation pattern of the

elements. This leads to higher mutual coupling and consequently the RMSE is increased as Figure 4-23 demonstrates.

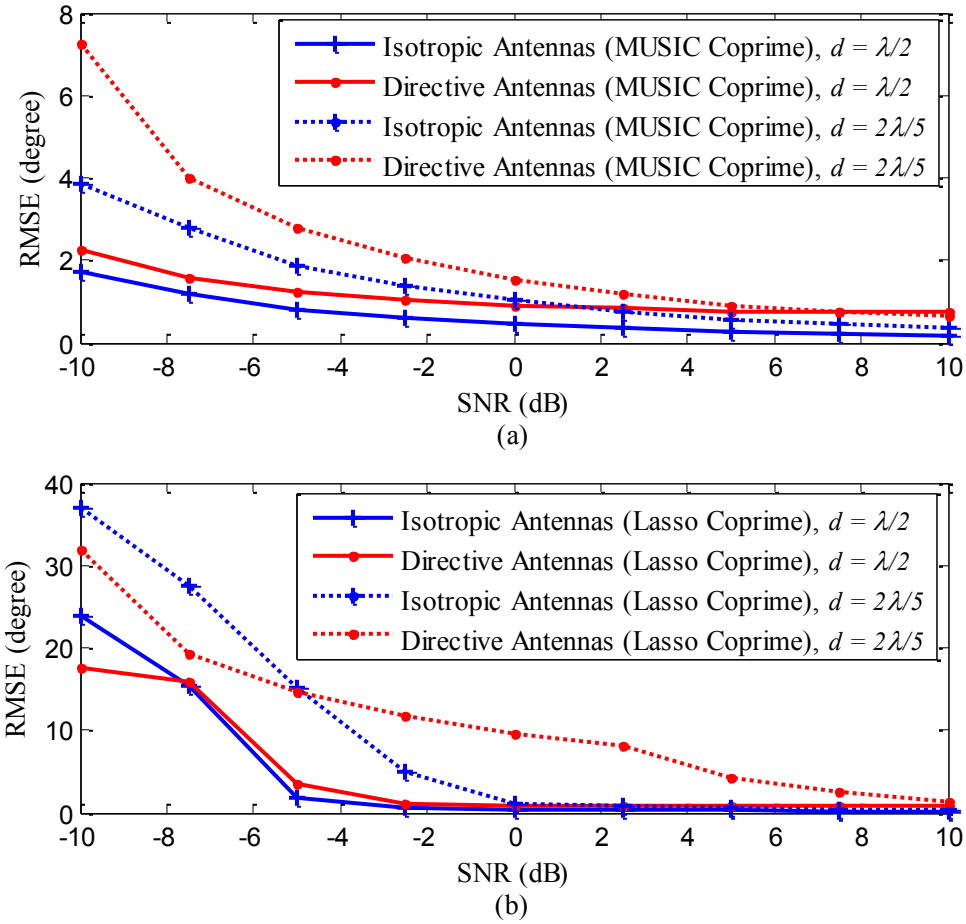


**Figure 4-23:** RMSE versus SNR when  $\theta \sim [-50^\circ, 50^\circ]$  using (a) MUSIC and (b) Lasso algorithms with isotropic and directive antennas for different unit inter-element spacing,  $K = 4$  sources, and  $\delta = 11$

#### 4.3.6 Simulation and Results Based on Fabricated Arrays

The configurations presented in Section 4.3.4-B are considered next. Simulation results for the fabricated arrays are presented taken into account the complex radiation pattern and then some experimental results are conducted to verify the effect of antenna directionality.

##### *A. Monopole versus Patch Elements Based on Simulated Data*

The main parameters are adjusted as in Section 4.3.5. The radiation pattern of all designs are extracted using HFSS. Then we incorporate their effect on the DOA estimation. In Figure 4-24, the RMSE versus the SNR based on the coprime array of isotropic, monopole, and patch elements are compared using Lasso and MUSIC algorithm. Within each subplot, the DOA is different that is the four sources are equally spaced within  $\theta \sim U[-40^\circ, 40^\circ]$ ,  $\theta \sim U[-50^\circ, 50^\circ]$ , and  $\theta \sim U[-60^\circ, 60^\circ]$ . The RMSE is improved as SNR increases and the performance using isotropic elements is better compared with directive elements due to the radiation pattern as Figure 4-24 (a)-(c) and (b)-(d) confirm. The RMSE with patch elements is smaller than that with monopole elements due to the directivity, see Figure 4-24 (c) and (d). Since the phase response of the patch elements is almost constant from  $-50^\circ$  to  $50^\circ$ , the accuracy degrades as the sources are located at angles beyond this range. Although, the sources are located within the range of the constant phase when  $\theta \sim U[-40^\circ, 40^\circ]$ , the algorithm gives larger RMSE because of the smaller separation in between. This is not the case of the monopole elements where the phase response is changing across the whole range. Therefore, larger RMSE is achieved when the separation between the sources increases due to the larger range of phase fluctuation.



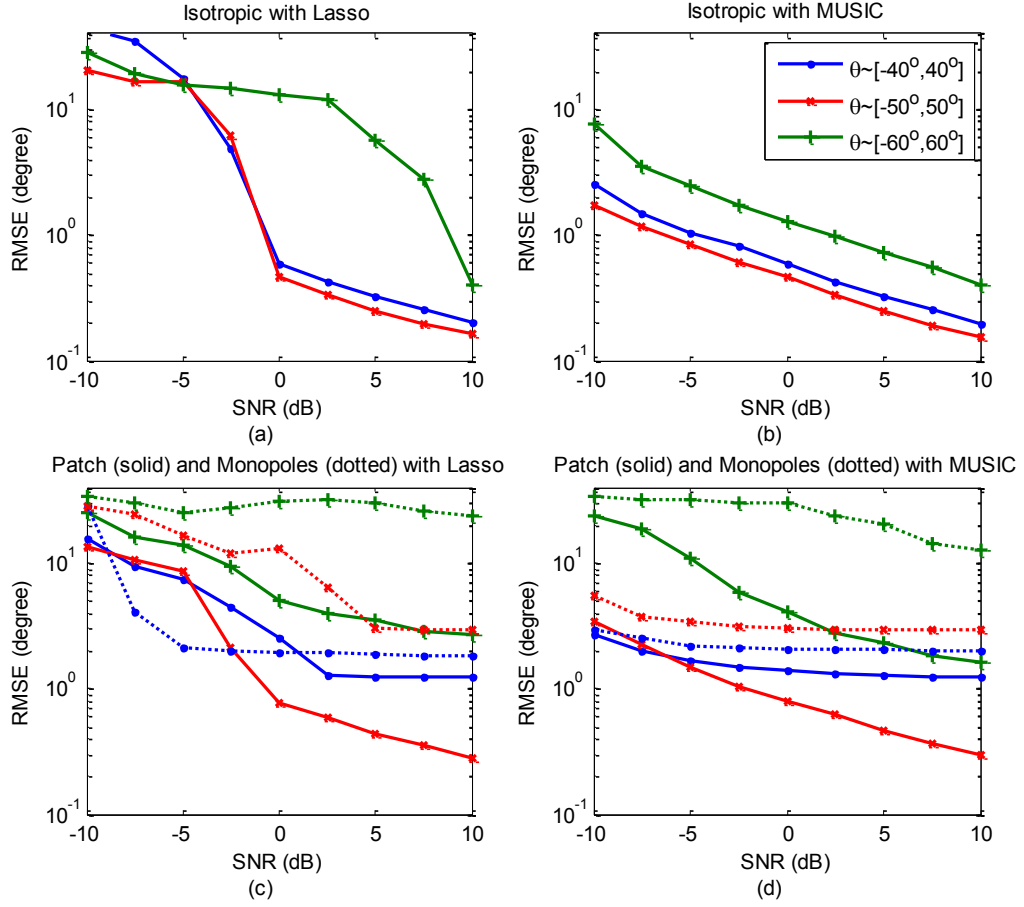


**Figure 4-24:** RMSE versus SNR of coprime array of monopole and patch elements for different source distributions using Lasso and MUSIC algorithms with  $\delta = 11$

#### B. Monopole versus Patch Elements Based on Experimental Data

We also conduct some experiments to assess the estimation accuracy of the printed arrays presented in Section 4.3.4-B. The system implemented in Section 4.2.3 is used but at  $f_c = 2.1 \text{ GHz}$ . The experiments to located a single source are repeated three times for all configurations and the remaining parameters are as in Section 4.2.3. We also do phase calibration every time we restart the system. All configurations are tested in the TRL at KFUPM. Figure 4-25 depicts the setup for 5-element ULA of patch antenna elements.



**Figure 4-25:** Experimental setup with 5-element ULA using patch antenna elements

In Figure 4-26, we plot the estimated angle versus the actual angle in degree for all fabricated arrays using Lasso algorithm. The coprime array with patch elements realizes the best performance. The 4-element ULA with monopole elements has got the largest error since it has the smallest number of virtual lags that is  $[-3d: 3d]$ . The maximum error is around  $15^\circ$  at the left edge. In addition, the monopole elements receive the signal from all directions which is not the case with patch elements. Coprime array and 5-element ULA on the other hand have virtual lags  $[-4d: 4d]$  and both require equal aperture size. However, coprime array uses only four elements. There are many scatters in the Lab which are the main cause of error since they introduce strong multipath components. The error in the negative range is due to multipath and the received signal strength at a specific angle, which SNR is dependent. Moreover, the transmitter in this range is closer to the reference element and far from the remaining three elements. Consequently, the received signals at the output of the three elements are weaker which degrade the accuracy. In other words, the far-field assumption is not fulfilled.

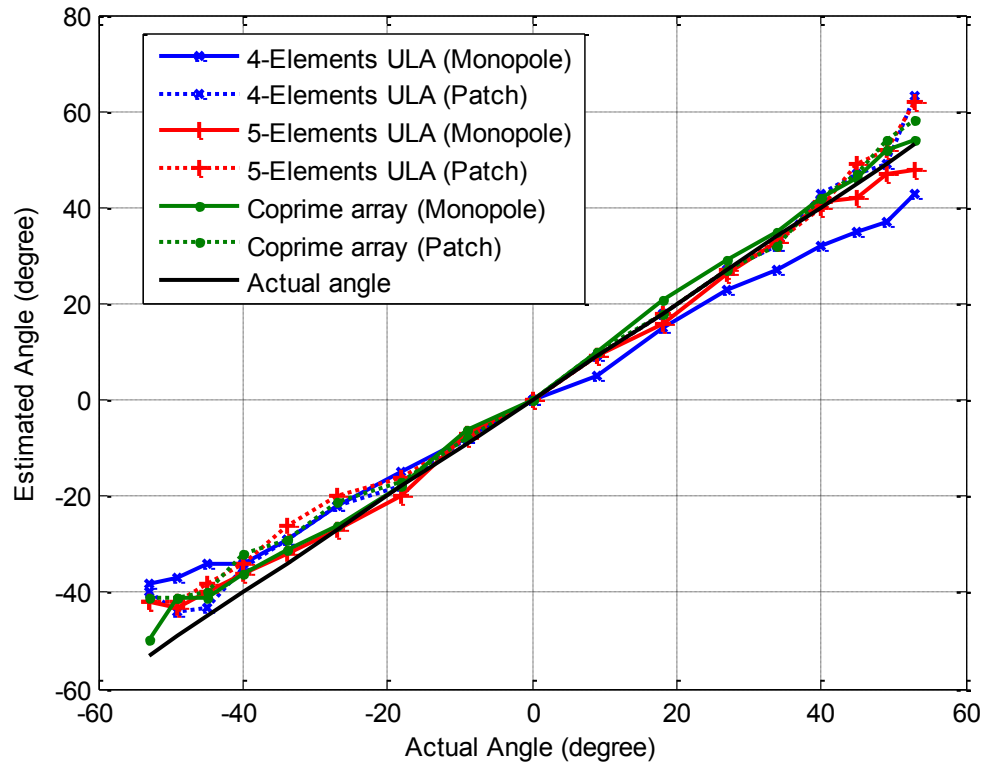


**Figure 4-26:** Estimated DOA versus the actual angle using six different printed arrays with monopole and patch antenna elements

#### 4.3.7 Concluding Remarks

In this section, sparse DOA estimation with directive coprime arrays is proposed. Six different designs were evaluated and experimentally tested. We have found that the radiation pattern has a direct impact on the estimation accuracy. For example, when the separation between the sources increases, the RMSE increases due to the effect of the radiation pattern and vice versa. Due to the radiation pattern, it is difficult to estimate any source of an angle outside the main beam of the directional antenna even in noise free circumstances. Since we have information about the radiation patterns of the antennas, can we do pattern compensation?. We shall answer this interesting question in our future research.

Based on our discussion in this chapter, the designers always have some limitations. Therefore, an array configuration that requires a small aperture size and at the same time it has an efficient DOA estimation capability is desired. In the next chapter, a novel array configuration that fulfills the aforementioned characteristics is proposed.

## CHAPTER 5 GENERALIZED MULTI-LEVEL PRIME

### ARRAYS FOR SPARSE SAMPLING

Sensor array configurations such as coprime and nested arrays have attracted many researchers because they increase the DOFs. For example, in DOA estimation, the number of sources that can be estimated is greater than the total number of sensors. This chapter proposes a multi-level prime array (MLPA) configuration for sparse sampling that can further increase the DOFs. The proposed array uses multiple uniform linear subarrays where the number of sensors in the subarrays are pairwise coprime integers. The inter-element spacing between the sensors is formulated as a scaled multiple of half-wavelength where the subarrays share only their first element. For a fixed number of sensors, multiple MLPA configurations can be constructed by controlling the number of sensors in the subarrays or by adjusting the inter-element spacing. For a given number of sensors, the proposed array has smaller aperture and achieves more unique and consecutive lags compared with coprime arrays. The proposed configuration has limited holes in the difference coarray. The analytical expressions of both the difference coarray and the aperture size are derived. Simulation results confirm the advantage of the proposed configurations compared to the two level coprime arrays.

#### 5.1 Introduction

A sensor array consists of a set of sensors that are arranged in a certain geometry. Sensor arrays have been considered in spatial domain for range and angle estimation. Sensor arrays

have many civilian and military applications in radar and wireless communications such as beam steering, target tracking, interference suppression, and DOA estimation [28], [38], [39].

With  $N$  uniformly distributed sensors,  $N - 1$  sources can be estimated using subspace-based techniques such as MUSIC and ESPRIT [16]. The problem of estimating more sources than the number of sensors has attracted many researchers. This problem can be handled using configurations that exploit the difference coarray which is the set of pairwise differences of the array physical sensor locations. Basically, the achieved DOFs, which is a measure of the maximum number of sources that can be estimated, is determined by the number of unique lags and the number of consecutive lags of the difference coarray, and the aperture size of the array [33]. Array configurations such as the minimum redundancy arrays [91], minimum hole arrays [92], nested arrays [34], and coprime arrays [52] provide a solution to estimate more sources than the number of sensors.

Minimum redundancy arrays (MRAs) [91] form a class of non-uniform arrays which have the longest difference co-arrays. However, the sensor locations and DOFs of such arrays cannot be computed in a closed form for any arbitrary number of sensors and they are found through computer search. The authors in [93] combined several MRA subarrays in a structured form called nested MRA (NMRA). The new array achieves hole-free difference coarray where the sensor locations and the achievable DOFs can be found in a closed form provided that the parameters of those MRA subarrays are known. However, it requires large aperture size.

Nested array are usually constructed using two collinearly ULAs. The resultant array has a hole-free difference coarray. Those arrays achieve  $\mathcal{O}(N^2)$  DOFs using  $N$  sensors [34]. However, the inter-element spacing is very small and consequently the sensors suffer from mutual coupling effect [34]. Nested arrays were extended to multi-level nested arrays in [34]. Fourth-level nested array that has  $\mathcal{O}(N^4)$  DOFs using  $N$  sensors was proposed in [94]. The authors in [95], [96], [97] modified the structure of the nested array and proposed a super nested array. The array has the same features as the conventional nested array but with reduced mutual coupling.

On the other hand, coprime arrays are constructed using two ULAs having  $M_1$  sensors in the first subarray and  $M_2$  sensors in the second one where  $M_1$  and  $M_2$  are coprime integers [52], [98], [99]. The inter-element spacing of the first and second subarrays is  $M_2$ , and  $M_1$  units, respectively where the unit inter-element spacing is half-wavelength. This spacing reduces mutual coupling between the elements. Coprime arrays have a DOFs  $\mathcal{O}(M_1 M_2)$  using  $M_1 + M_2 - 1$  sensors [33]. The achieved DOFs can be increased by doubling the number of sensors in the subarray that has smaller number of elements [63], compressing the inter-element spacing of one subarray [33] and/or introducing a displacement between the two subarrays [64]. Other operations were also conducted on coprime arrays to increase the DOFs [100], [101]. In [102], both the difference and the sum coarray were exploited to increase the DOFs. While in [56], [57], a method to minimize and select the required number of sensors for coprime arrays was proposed. It has been shown that the optimal coprime pair is the one that has values of  $M_1$  and  $M_2$  as close to each other as possible. The DOFs can also be enhanced by interpolating the holes that appear in the difference coarray using a tractable convex framework [103].

A configuration based on three subarrays was presented in [104], [105], [106]. The authors in [104] proposed an array configuration that uses a ULA in addition to the conventional coprime array with no overlap in between. The array was optimized by adjusting the sensor locations of the additional ULA. The array achieved larger number of consecutive lags compared with two-level, four-level nested arrays and coprime arrays. However, the aperture size of the array is large [104]. Three subarrays with coprime inter-element spacing was used in [105], [106]. The used subarrays share more than one sensor and no structured way was presented to determine the sensor locations.

This chapter proposes a generalized multi-level prime array (MLPA) configuration that utilizes multiple uniform linear subarrays or levels where the number of sensors in the subarrays is pairwise coprime integers. The word “level” refers to “the number of subarrays” and we use both interchangeably. The inter-element spacing between the sensors in each subarray equals to the number of the sensors of another subarray scaled by half-wavelength such that the subarrays share only their first sensor. The inter-element spacing and sensor selection are very important and have a direct impact on the achievable DOFs since they determine the entries of the difference coarray. Based on the achievable DOFs, this chapter presents a procedure to select the configuration that maximizes the number of unique lags. For a given number of sensors, the proposed array requires a small aperture size and achieves more unique and consecutive lags compared with coprime arrays. This is attractive in antenna designs and array implementations where we have constraints in the physical size. In addition, the proposed configuration has limited holes in the difference coarray which is similar to the advantage provided by nested arrays. The analytical expression of the difference coarray and aperture size are derived. We also



consider some special configurations when the number of sensors in the subarrays satisfies certain relations. Coprime arrays represent a special case of the proposed array. It is worth to mention that recently, the authors in [107] extended the work in [33] for multi-level coprime arrays. The DOFs was enhanced by dividing the difference coarray into several multi-resolution coarrays that are uniformly spaced by a unit or multiple units of half-wavelength. Their proposed array requires very large aperture size. Moreover, the authors did not develop a structured way to divide the difference coarray. Our approach is very different in the sense that we generalized the prime array concept itself to multi-levels.

When deciding on the array configuration, there are different criteria to consider: the number of unique lags, number of consecutive lags, and aperture size. While providing the maximum number of unique lags and consecutive lags, nested arrays require larger aperture size and the minimal spacing between the sensors could result in mutual coupling. While coprime arrays are inferior when it comes to number of unique and consecutive lags, they minimize the mutual coupling effects. The proposed MLPA is a generalization to the concept which allows for more control on the design of the array and the expected performance characteristics. The proposed configurations archives large number of consecutive lags and unique lags close to the one provided by nested arrays while requiring a relatively small aperture size.

The rest of the chapter is organized as follows. The system model and the proposed configuration are presented in Section 5.2 where we derive the analytical expressions for the sensor locations and the aperture size. Section 5.3 presents the difference coarray prospective of the proposed array. MLPA design alternatives are discussed in Section 5.4. The optimum MLPA configurations are discussed in Section 5.5. An upper bound for the

achievable DOFs of certain MLPA level is derived in Section 5.6. Results and analysis are discussed in Section 5.7, and finally Section 5.8 concludes the chapter.

## 5.2 System Model

In this section, the generalized multi-level prime array is explained in first. Then some of the special cases are discussed.

### 5.2.1 Multi-Level Prime Array (MLPA)

The objective is to find a structured way to determine the sensors' locations such that the DOFs is increased. The sensors should be located within an array that is made of several ULAs and has smaller aperture size compared with coprime arrays. To achieve this, the proposed generalized multi-level prime array (MLPA) configuration utilizes multiple uniform linear subarrays or levels located along the same axis where the number of sensors in the subarrays is pairwise coprime integers. Those subarrays share only their first sensor. According to the number of subarrays, different array configurations can be constructed for the same number of sensors and coprime arrays are the two-level special case.

Let  $\mathbf{m} = [M_1, M_2, \dots, M_{N_p}]$  be a vector of  $N_p$  pairwise coprime integers with  $M_i$  represents the number of sensors in the  $i^{th}$  subarray,  $M_i > M_j, \forall i > j$ , and  $N_p$  representing the number of subarrays or the array level. The sensors of the proposed array, shown in Figure 5-1, are located at:

$$\mathbb{P} = \bigcup_{i=1}^{N_p} \{k_i \mathcal{S}_i d \mid 0 \leq k_i \leq M_i - 1, \mathcal{S}_i \neq M_i\} \quad (5-1)$$

where  $d = \lambda/2$  is the unit inter-element spacing and  $\mathcal{S}_i d$  denotes the inter-element spacing of the considered subarray. The ordered inter-element spacing for the subarrays,  $\mathcal{S}$ , is defined as:  $\mathcal{S} = \{\mathcal{S}d | \mathcal{S} \in \mathbf{m}\}$ . To keep the coprimality relation, the entries within the vector  $\mathcal{S}$  are ordered such that  $\mathcal{S}_i \neq M_i, \forall i = 1, 2, \dots, N_p$ . There are multiple options for the selection of  $\mathcal{S}_i$  for a given subarray as discussed in Section 5.4. As in conventional coprime arrays [52], the  $i^{th}$  subarray is not allowed to be spaced by  $\mathcal{S}_i d = M_i d$ . Moreover, to make sure that the subarrays share only the first sensor,  $k_i \mathcal{S}_i$  must equal to  $k_j \mathcal{S}_j$  only when  $k_i = k_j = 0, \forall i, j \in \{1, 2, \dots, N_p\}$  and  $i \neq j$ . Since there are  $N_p - 1$  shared sensors, the total number of physical sensors used in the MLPA is given as:

$$N = \sum_{i=1}^{N_p} M_i - (N_p - 1) \quad (5-2)$$

The number of possibilities for adjusting the inter-element spacing between the sensors is proportional to the total number of sensors and the number of subarrays (levels). In addition to the previous condition, the last two subarrays should be spaced by  $M_{N_p} d$  and/or  $M_{N_p-1} d$  respectively as discussed in details in Section 5.4.2. Consequently, the aperture size,  $D$ , of the resultant array configurations can be found by maximizing (5-1). For moderate number of levels, the maximum will be dominated by the maximum of either  $k_i$  or  $\mathcal{S}_i, \forall i \in \{N_p, N_p - 1\}$ . The aperture size can be expressed as:

$$D = \max\left(\mathcal{S}_{N_p-1} (M_{N_p-1} - 1) d, \mathcal{S}_{N_p} (M_{N_p} - 1) d\right) \quad (5-3)$$

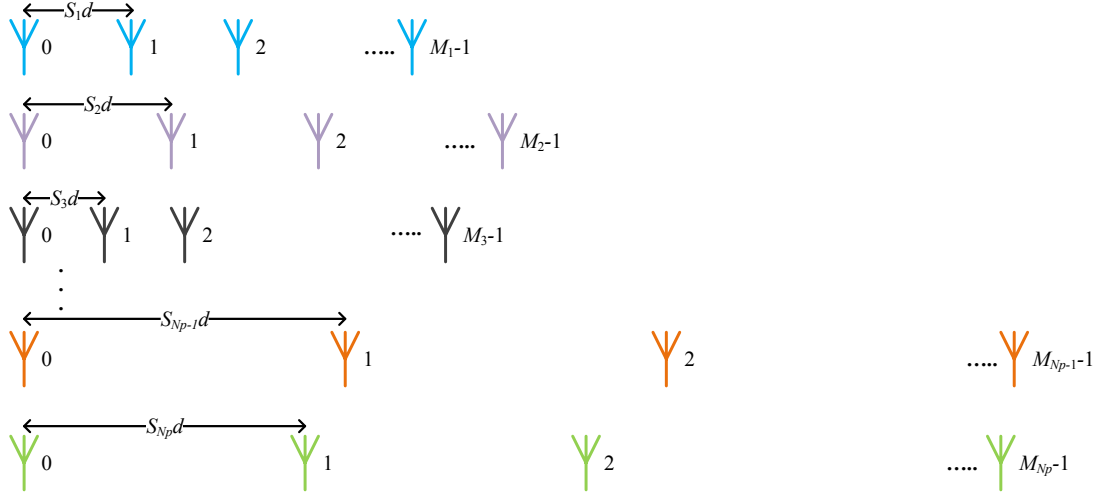


**Figure 5-1:** The MLPA configuration

### 5.2.2 Special Cases of MLPA Configurations

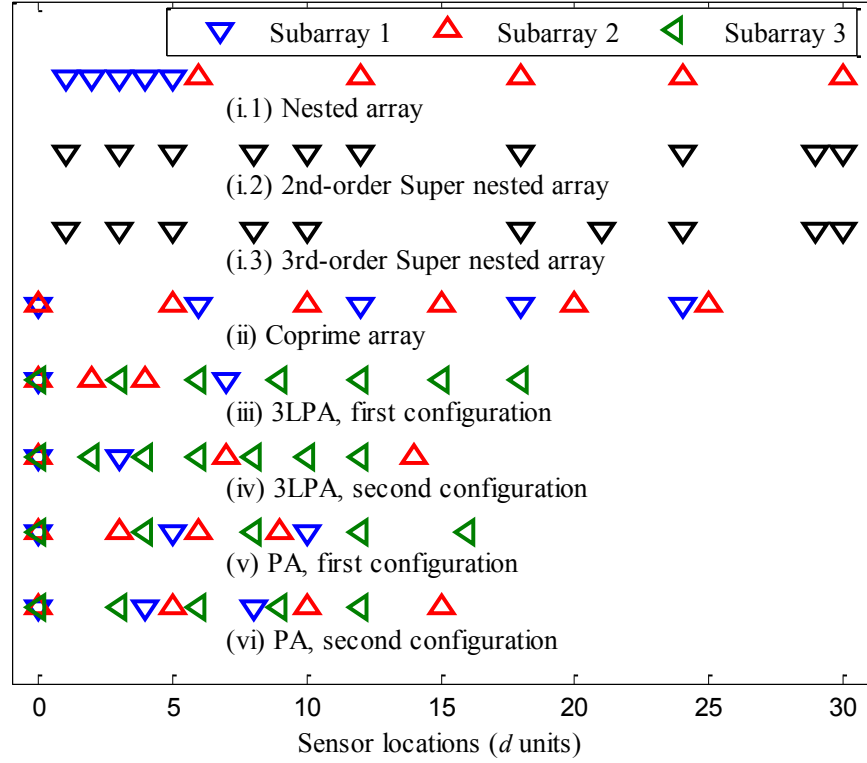
In the following subsections, we present the coprime arrays [52] and the three level prime arrays in [108] as special cases of the proposed MLPA configuration.

#### A. Coprime Arrays:

A coprime array represents a special case of the proposed MLPA with only two subarrays ( $N_p = 2$ ), thus there is a unique choice for adjusting the inter-element spacing. In this case, one subarray has  $M_1$  sensors spaced by  $M_2d$  and the other has  $M_2$  sensors spaced by  $M_1d$ . The locations of the sensors of this array given by (5-1) reduce to [52]:

$$\mathbb{P} = \{M_2k_1d | 0 \leq k_1 \leq M_1 - 1\} \cup \{M_1k_2d | 0 \leq k_2 \leq M_2 - 1\} \quad (5-4)$$

Figure 5-2 (ii) depicts an example of coprime array with  $\mathbf{m} = [5,6]$ . The two subarrays in this case share the first sensor, hence the total number of sensors is  $N = 10$  as predicted by (5-2). For the case of coprime, the aperture size in (5-3) reduces to  $M_1(M_2 - 1)d$ , which is  $25d$  for the given example.

Figure 5-2: MLPAs with  $N = 10$  sensors

### B. Three-Level Prime Array (3LPA) and Pythagorean Array:

When  $N_p = 3$ , the array utilizes three subarrays. The resultant array is referred to as a three-level prime array (3LPA) [108] and (5-1) for sensor locations results in:

$$\mathbb{P} = \{k_1 M_j d, j \neq 1\} \cup \{k_2 M_j d, j \neq 2\} \cup \{k_3 M_j d, j \neq 3\} \quad (5-5)$$

In 3LPA, the sensors within the first subarray can be spaced by either  $M_3 d$  or  $M_2 d$ . Based on this choice, the inter-element spacing of the remaining two subarrays is adjusted. Thus, there are two possibilities for the ordered inter-element spacing;  $\mathcal{S} = [M_3, M_1, M_2]d$  or  $\mathcal{S} = [M_2, M_3, M_1]d$ . Figure 5-2 (iii) and (iv) demonstrate an example of the 3LPA configurations with  $\mathbf{m} = [2, 3, 7]$ . Two different configurations are possible. The first configuration has ordered inter-element spacing  $\mathcal{S} = [7, 2, 3]d$ , see Figure 5-2 (iii). While,

the second configuration has ordered inter-element spacing  $\mathcal{S} = [3,7,2]d$  as illustrated in Figure 5-2 (iv). In this case, the 3LPA configurations have a total of  $N = \sum_i M_i - 2 = 10$  sensors [108]. The aperture size of the first and the second configurations is:  $D = M_2(M_3 - 1)d = 18d$  and  $D = M_3(M_2 - 1)d = 14d$ , respectively.

One way to reduce the aperture size of the 3LPA without dramatically sacrificing the number of lags is to select the three pairwise coprime numbers as a primitive Pythagorean triple (PPT). Pythagorean triple (PT) is any set of three numbers  $(a, b, c)$  that satisfies the Pythagorean theorem,  $c^2 = a^2 + b^2$ . A PPT set is a PT set in which the greatest common divisor (GCD) of  $a, b$  and  $c$  is one. When the number of sensors in the subarrays is a PPT, a special case of the 3LPA can be constructed which we refer to as Pythagorean array (PA) [108]. There are many techniques used to build PPT sets. One of these techniques is based on Barning-Hall tree in which a set of PPT can be generated through specific generator matrices [109].

Similar to the 3LPA configuration, PA uses three uniform linear subarrays. The inter-element spacing among the subarrays is adjusted as in the 3LPA configuration. PA configuration with the minimum number of sensors can be constructed with  $\mathbf{m} = [3,4,5]$  which yields  $N = 10$  sensors. The two possible ordered inter-element spacing are  $\mathcal{S} = [5,3,4]d$  and  $\mathcal{S} = [4,5,3]d$  as Figure 5-2 (v) and (vi) illustrate. The corresponding aperture sizes according to (5-3) are  $D = 16d$  and  $D = 15d$  which is smaller than that of the 3LPA. The achievable DOFs of the array is expected to decrease compared with the 3LPA configurations [108]. Other PA configurations require large number of sensors. For example, PA with  $N = 28$  and  $N = 38$  sensors can be constructed using  $\mathbf{m} = [5,12,13]$  and  $\mathbf{m} = [15,8,17]$  respectively.

### 5.3 The Difference Coarray Prospective in MLPA

In DOA applications, the number of sources that can be estimated is related to the DOFs which is proportional to the number of unique lags and number of consecutive lags in the difference coarray. We can estimate more than the total number of sensors if the difference coarray is exploited. In this section, we derive the analytical expression for the difference coarray (coarray equivalence) of the proposed configurations.

Recall that the sensors of the proposed array are located as in (5-1). The difference coarray is defined as the set of pairwise differences of the array physical sensor locations which produces virtual sensors [33], [101] located at:

$$\mathbb{C}_P = \{\mathbf{z} | \mathbf{z} = \mathbf{u} - \mathbf{v}, \mathbf{u} \text{ and } \mathbf{v} \in \mathbb{P}\} \quad (5-6)$$

Applications that depend on the correlation such as DOA estimation can make use of all possible DOFs in the difference coarray and therefore increase the number of estimated sources. The maximum achieved DOFs is determined by the number of unique lags (distinct entries in the set  $\mathbb{C}_P$ ) of the difference coarray that appear in the following set,  $\mathbb{L}_P$ , which is expressed as [33]:

$$\mathbb{L}_P = \{l_P | l_P d \in \mathbb{C}_P\} \quad (5-7)$$

The lags in the difference coarray consist of the self-differences,  $\mathbb{L}_S$ , and cross-differences,  $\mathbb{L}_C$ , and can be written as:

$$\mathbb{L}_P = \mathbb{L}_S \cup \mathbb{L}_C \quad (5-8)$$

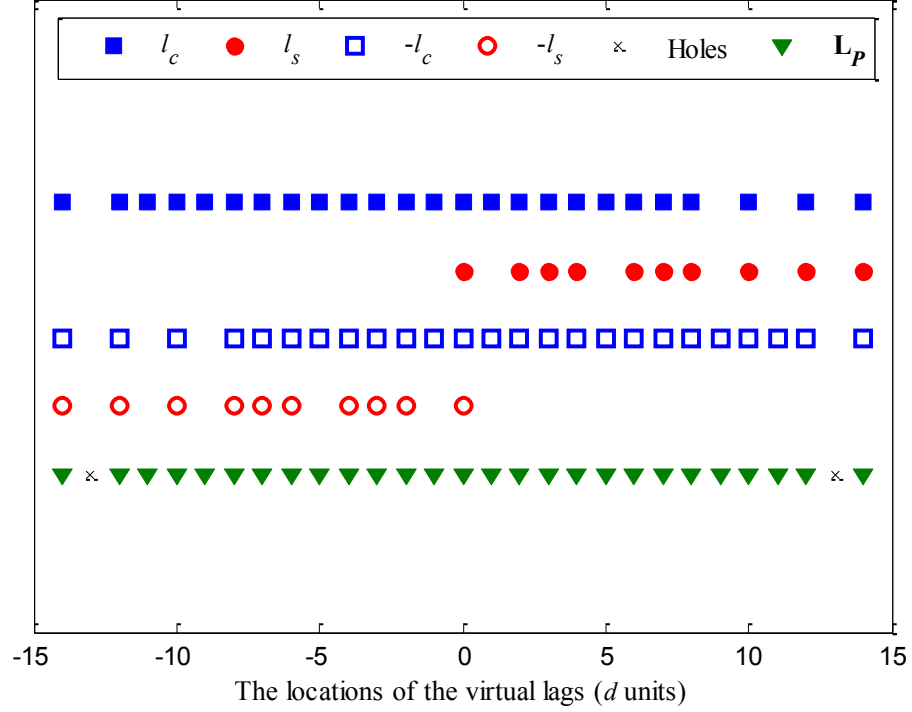


**Figure 5-3:** Difference coarray of the 3LPA configuration using  $\mathbf{m} = [2, 3, 7]$  and  $\mathcal{S} = [M_2, M_3, M_1]d$

The self-differences of the proposed array can be expressed as:

$$\mathbb{L}_s = \{\pm l_s | l_s d \in \mathbb{P}\} \quad (5-9)$$

Let's decompose  $\mathbb{P}$  into  $\{\mathbb{P}_1, \mathbb{P}_2, \dots, \mathbb{P}_{N_p}\} = \left(\bigcup_{i=1}^{N_p} \mathbb{P}_i\right)$ , where the  $\mathbb{P}_i^{th}$  subset denotes the sensor locations in the  $i^{th}$  subarray. The cross-differences can be obtained by considering two subarrays at a time, finding the element wise subtraction among the two subarrays, and taking the union of all. Thus, the cross-differences of the proposed array can now be expressed as:

$$\mathbb{L}_c = \bigcup_{i=1}^{N_p} \bigcup_{\substack{j=1 \\ i \neq j}}^{N_p} \{l_c | l_c d \in (\mathbb{P}_i(i_1) - \mathbb{P}_j(j_1))\}, \quad (5-10)$$



$$\forall 1 \leq i_1 \leq M_i, 1 \leq j_1 \leq M_j$$

where  $\mathbb{P}_i(i_1)$  denotes the  $i_1^{th}$  entry in the  $i^{th}$  subset. The mirrored positions of the self-differences and the mirrored positions of the cross-differences are already included in the previous formulas. Instead of compressing the spacing between the sensors in one subarray and/or introducing a displacement between the two subarrays [33], higher level ( $N_p > 2$ ) MLPA utilizes multiple subarrays in order to increase the DOFs. Thus, the number of unique lags and the number of consecutive lags are larger than that of coprime arrays.

Let's consider the 3LPA shown in Figure 5-2 (iv) for demonstrations. The corresponding self-differences and cross-differences of the array are plotted in Figure 5-3. The lags denoted by  $l_c$  are calculated based on (5-10)  $\forall j > i$ . Figure 5-3 illustrates that all self-differences are included in the cross-differences,  $\mathbb{L}_s \subseteq \mathbb{L}_c$ , which is equivalent to finding the cross-difference of each sensor location with the zero location. Moreover, there are some redundant lags because of the overlap between  $l_c$  and  $-l_c$  which reduces the DOFs of the array. There are two virtual lags missing 'holes' in the difference coarray which makes the number of consecutive lags less than the number of unique lags.

### 5.4 MLPA Design Alternatives

This section provides guidelines to construct the proposed MLPA. Specifying the number of sensors and the inter-element spacing determines the aperture size, the number of unique lags, and the number of consecutive lags. Sparse reconstruction algorithms can exploit all unique lags in the difference coarray whereas subspace-based algorithms such as MUSIC algorithm requires consecutive lags [33]. Thus, if the number of consecutive lags is smaller than the number of unique lags, sparse reconstruction algorithms will realize larger DOFs

compared with subspace-based algorithms. Two-stage constrained search is used to select the optimum array configuration among all possible MLPA configurations by evaluating their difference coarrays and selecting the one with maximum number of unique lags. For a fixed total number of sensors, we exhaust all possibilities to decide on the number of sensors and number of subarrays. A second constrained search is executed to optimize the inter-element spacing and select the best configuration.

#### 5.4.1 Selecting the Number of Sensors

For a specified  $N$  and  $N_p$ , there are usually several ways to select the number of sensors in each subarray and the inter-element spacing. Let  $\mathbf{M}$  be a matrix defined as:  $\mathbf{M} = [\mathbf{m}_1; \mathbf{m}_2; \dots; \mathbf{m}_{N_s}]$  that contains  $N_s$  rows of all possible pairwise coprime vectors. For a given row,  $\mathbf{m}_{n_s}$ , several MLPA configurations of different features can be constructed by adjusting the inter-element spacing. Figure 5-4 (a) depicts the number of pairwise coprime vectors,  $N_s$ , as a function of the total number of sensors,  $N$ , for different number of subarrays,  $N_p$ . A value of zero indicates that it is impossible to construct the array because there are no  $N_p$  pairwise coprime integers satisfy (5-2). In general, the value of  $N_s$  increases exponentially with  $N$  but with oscillation. Figure 5-4 (a) demonstrates that the minimum number of sensors for  $N_p = 2, 3, 4, 5$  and 6 is 4, 8, 14, 24 and 36 sensors respectively. The corresponding configurations are referred to as coprime array, 3LPA, 4LPA, 5LPA, and 6LPA.

To build an MLPA of  $N_p$  subarrays and  $N$  sensors, we have to find all possible pairwise coprime vectors needed to construct  $\mathbf{M}$ . Then, we build the array using  $\mathbf{m}_i, \forall i = 1, 2, \dots, N_s$  where all ordered inter-element spacing are examined according to Section 5.2.1. After

that, the difference coarrays of all MLPA configurations are generated. Finally, the configuration that maximizes the number of unique lags is selected.

Let  $l_{ug}$  and  $l_{cg}$  represent the number of unique lags and the number of consecutive lags, respectively. To maximize the number of unique lags for a fixed  $N$ , we do exhaustive search over  $N_p$  and  $\mathbf{M}$  as:

$$\max_{N_p, \mathbf{m}_{n_s}} l_{ug} \quad (5-11)$$

Subject to the following constraints:

- 1)  $N = \sum_{i=1}^{N_p} M_i - (N_p - 1), N_p \geq 2$
- 2)  $\min(\mathbf{m}_{n_s}) > 1$  and  $\mathbf{m}_{n_s} \in \mathbf{M}, n_s = 1, 2, \dots, N_s$

The first constraint implies that the subarrays share only the first sensor as in (5-2) and a minimum of two subarrays is required to exclude the ULA case. The second constraint requires at least two sensors within each subarray to exclude the nested array scenarios. If a subarray has only one sensor, then it will be the one shared with other subarrays and effectively we have  $N_p - 1$  subarrays. Furthermore, the proposed configuration becomes a ULA in case of two subarrays.

Table 5-1 summarizes how to build the matrix  $\mathbf{M}$ . A counter,  $n_s$ , is initialized to count all possible number of pairwise coprime vectors. Based on (5-2), a matrix  $\mathbf{A}_a$  is constructed in Step 1 from the range 2:  $(N - N_p + 1)$  where each row consists of  $N_p$  pairwise coprime integers. Step 3 checks if the sum of the  $i^{th}$  row in  $\mathbf{A}_a$  equals  $N + N_p - 1$ , then the  $i^{th}$  row contains one of the valid pairwise coprime vectors,  $\mathbf{m}_{n_s}$ . The procedure is then repeated for the  $(i + 1)^{th}$  row of  $\mathbf{A}_a$ .

Table 5-1: Main steps to select the number of sensors in each subarray

Step	Operation
<b>Input</b>	$N_p$ and $N$
<b>Initialization</b>	$n_s = 0$
<b>1</b>	<b>Construct</b> the matrix $\mathbf{A}_a$ with rows having $N_p$ pairwise coprime integers, i.e. the GCD of each row is one. All entries must be selected from the range 2: $(N - N_p + 1)$
<b>2</b>	$i = 1$
<b>3</b>	<b>If</b> $\sum \mathbf{A}_a(i, :) = N + N_p - 1$ $n_s = n_s + 1$ $\mathbf{M}(n_s, :) = \mathbf{A}_a(i, :)$ <b>End if</b>
<b>4</b>	$i = i + 1$ <b>If</b> $i \leq \# \text{ of rows}(\mathbf{A}_a)$ , Go to Step 3
<b>Output</b>	$\mathbf{M}, N_s = \# \text{ of rows}(\mathbf{M})$

#### 5.4.2 The Ordered Inter-Element Spacing

Following Section 5.2.1, a necessary condition to make sure that the subarrays only share the first sensor is to select the inter-element spacing for the last two subarrays as  $M_{N_p}d$  and/or  $M_{N_p-1}d$  respectively. Though, this condition is not sufficient since some of those cases result in  $k_i\mathcal{S}_i = k_j\mathcal{S}_j$  for a specified  $k_i \neq 0$  and  $k_j \neq 0$ . This condition directly fits in case of coprime arrays because there is only one option for the number of possible inter-element spacings,  $C_{co} = 1$ . The last two subarrays of coprime array, 3LPA, 4LPA, and 5LPA configurations result respectively in the following possible inter-element spacing:

$$C_{3\text{LPA}} = 1 \times \binom{|M_3d|}{1} \binom{|M_1d|}{1} + 1 \times \binom{|M_1d|}{1} \binom{|M_2d|}{1} \quad (5-12)$$

$$C_{4\text{LPA}} = 1 \times \binom{|M_4d|}{1} \binom{|\{M_1, M_2\}d|}{1} + 1 \times \binom{|\{M_1, M_2, M_4\}d|}{1} \binom{|M_3d|}{1} \quad (5-13)$$

$$C_{5\text{LPA}} = 3 \times \binom{|M_5 d|}{1} \binom{|\{M_1, M_2, M_3\} d|}{1} + 3 \times \binom{|\{M_1, M_2, M_3, M_5\} d|}{1} \binom{|M_4 d|}{1} \quad (5-14)$$

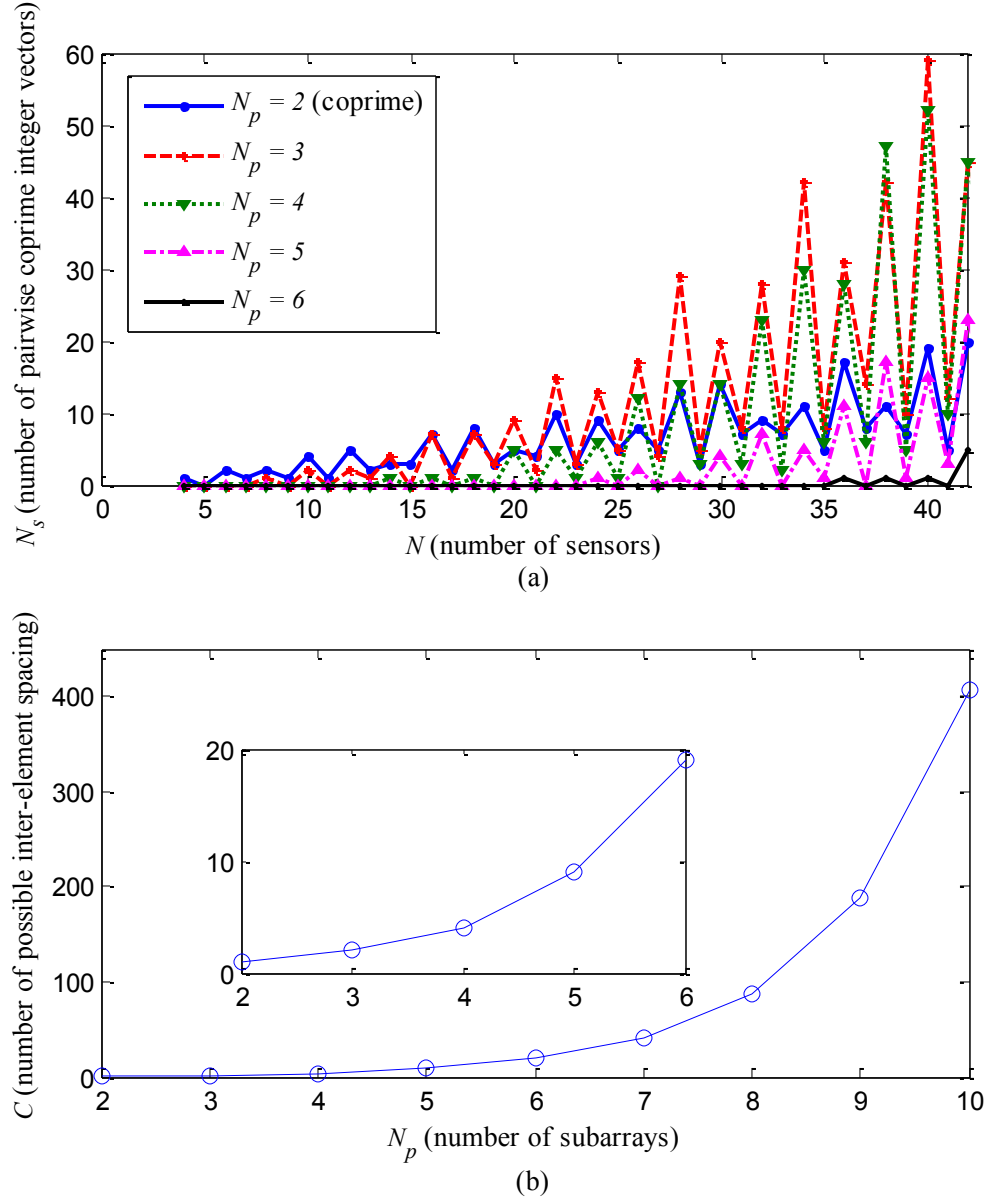
where the first and the second combinations in each term indicate the number of possible inter-element spacings for the  $(N_p - 1)^{th}$  and the  $N_p^{th}$  subarrays respectively and  $|\cdot|$  denotes the cardinality. The constant numbers represent the number of possible inter-element spacings of the remaining subarrays. Following (5-12), the inter-element spacing for the first subarray is one, so  $C_{3\text{LPA}} = 2$ . The first and the second subarrays in the 4LPA are left with only one possibility for the spacing based on (5-13). However, when the ordered inter-element spacing is  $\mathcal{S} = [M_2, M_3, M_4, M_1]d$ , the subarrays share more than one sensor. Therefore, the number of possible inter-element spacings reduces to  $C_{4\text{LPA}} = 4$ . In case of 5LPA, there are always three ways to select the inter-element spacing for the first three subarrays except two ways when the last two subarrays are spaced by  $M_5 d$  and  $M_4 d$  respectively. Thus, we end up with  $3 \times 1 \times 3 + (3 \times 4 \times 1 - 1) = 20$  possible inter-element spacing. However, 11 cases result in overlapped sensors which we should exclude and the number of possible inter-element spacings reduces to  $C_{5\text{LPA}} = 9$ . This includes three ordered inter-element spacing of the form  $\mathcal{S} = [X, X, X, M_1, M_4]d$ , two of the form  $\mathcal{S} = [X, X, X, M_2, M_4]d$ , three of the form  $\mathcal{S} = [X, X, X, M_5, M_1]d$ , and three of the form  $\mathcal{S} = [X, X, X, M_5, M_2]d$  where  $X$  denotes one of the possible  $M_i$ . As  $N_p$  increases, the number of possible inter-element spacings increases and any unwanted cases have to be excluded.

Table 5-2 illustrates the main steps used to construct the best MLPA for a specific  $N$  and  $N_p$ . One row,  $\mathbf{m}_{n_s}$ , is considered at a time from  $\mathbf{M}$  and initializes a counter  $c$  to count the number of possible inter-element spacings. In Step 1, a matrix  $\mathbf{A}_s$  is formed where the rows are made of all possible permutations of  $\mathbf{m}_{n_s}$  excluding any permutation with the  $i^{th}$  column equals  $M_i$  because the  $i^{th}$  subarray cannot be spaced by  $M_i$ . In addition, any permutation that do not contains  $M_{N_p}$  and/or  $M_{N_p-1}$  in the  $(N_p - 1)^{th}$  and  $N_p^{th}$  columns (last two columns) respectively are excluded. The rows of  $\mathbf{A}_s$  represent all candidate ordered inter-element spacing normalized by half-wavelength. In Step 4, the sensor locations in each subarray are calculated and combined by taking the union of all subarrays. In Step 5, if the subarrays share only their first sensor at the zero location, the inter-element spacing is valid so  $|\mathbb{P}| = N$  where  $|\mathbb{P}|$  is the cardinality of  $\mathbb{P}$ . Otherwise, (5-2) is not satisfied and therefore this inter-element spacing is not valid. For any valid configuration, the features of the resultant array are calculated. Once all rows of  $\mathbf{A}_s$  are considered, then we take the next  $\mathbf{m}_{n_s}$  and the process is repeated. The best MLPA configuration that maximizes the number of unique lags and its features as well as the number of possible inter-element spacings,  $C_{MLPA}$ , are obtained at the output.

The number of MLPA configurations for a specific  $N$  and  $N_p$  can be calculated as:  $N_c = N_s C_{MLPA}$  where  $N_s$  represents all possible vectors of pairwise coprime integers calculated in Table 5-1 and  $C_{MLPA}$  denotes all possible inter-element spacing calculated in Table 5-2. Among all valid configurations, the configuration that maximizes the number of unique lags is preferred. The value of  $N_s$  depends on both  $N$  and  $N_p$  whereas  $C_{MLPA}$  is only a function of  $N_p$  as Figure 5-4 (a) and (b) depict respectively.

Table 5-2: Main steps to decide on the inter-element spacing and select the best MLPA configuration

Step	Operation
<b>Input</b>	$N$ and $\mathbf{M} = [\mathbf{m}_1; \mathbf{m}_2; \dots; \mathbf{m}_{N_s}]$
1	$n_s = 1, c = 0$
2	<b>Construct</b> $\mathbf{A}_s$ with rows of all possible permutations of $\mathbf{m}_{n_s}$ excluding any permutation with the $i^{th}$ column entry equals $M_i$ and any permutation does not contains $M_{N_p}$ and/or $M_{N_p-1}$ in the last two columns
3	$t = 1$
4	$j = 1$ <b>While</b> $j \leq N_p$ $\mathbb{P}_j = \mathbf{A}_s(t, j) \times k_j d$ where $0 \leq k_j \leq M_j - 1$ $j = j + 1$ <b>End while</b> $\mathbb{P} = \bigcup_{k=1}^{N_p} \mathbb{P}_k$
5	<b>If</b> $ \mathbb{P}  = N$ $c = c + 1$ $\mathbb{L}_P = \mathbb{L}_s \cup \mathbb{L}_c;$ $\mathbf{L}_{ug}(c, n_s) =  \mathbb{L}_P $ $\mathbf{L}_{cg}(c, n_s) = l_{cg}$ (count the maximum number of consecutive lags in $\mathbb{L}_P$ ) $\mathbb{P}_{\text{total}}(c, n_s, :) = \mathbb{P}$ <b>End if</b>
6	$t = t + 1$ <b>If</b> $t \leq \text{rows}(\mathbf{A}_s)$ Go to Step 4
7	$n_s = n_s + 1$ <b>If</b> $n_s \leq N_s$ Go to Step 2
<b>Output</b>	$[c^o, n_s^o] = \underset{c, n_s}{\text{argmax}}(\mathbf{L}_{ug})$ $\mathbb{P} = \mathbb{P}_{\text{total}}(c^o, n_s^o, :)$ $l_{ug} = \mathbf{L}_{ug}(c^o, n_s^o)$ $C_{\text{MLPA}} = \# \text{ of rows}(\mathbf{L}_{ug})$



**Figure 5-4:** MLPA characteristics: (a) Number of pairwise coprime integer vectors versus  $N$ , (b) Number of inter-element spacing versus  $N_p$

The number of possible inter-element spacings,  $C_{\text{MLPA}}$ , is 1, 2, 4, 9, and 19 for coprime array, 3LPA ( $N_p = 3$ ), 4LPA ( $N_p = 4$ ), 5LPA ( $N_p = 5$ ), and 6LPA ( $N_p = 6$ ) respectively. Coprime arrays has  $C_{co} = 1$  because there are only two subarrays and only one choice for the inter-element spacing. Henceforth the number of configurations are



$N_c = N_s$ . As an example for  $N = 10$  or 12 sensors, the 3LPA has  $N_c = 2 \times 2 = 4$  configurations as in [108].

### 5.5 The Optimum MLPA Configurations

In the context of DOA estimation, large DOFs using MUSIC algorithm can be realized by maximizing the number of consecutive lags in the difference coarray. While, larger DOFs using CS techniques can be realized by exploiting all unique lags. There has been some work to find the optimal coprime array configuration [56], [57] which is a special case of the MLPA with just two subarrays. Our aim is to find the optimal configuration for the generalized MLPA.

Given an MLPA with  $N$  elements and  $N_p$  subarrays the optimum MLPA can be achieved by either maximizing the number of unique lags or maximizing the number of consecutive lags, which can be formulated as:

$$(\mathbf{m}, \mathcal{S}) \leftarrow \underset{M_i \in \mathbb{Z}^+}{\operatorname{argmax}} \{l_{ug}(\mathbf{m}, \mathcal{S})\} \quad (5-15)$$

$$(\mathbf{m}, \mathcal{S}) \leftarrow \underset{M_i \in \mathbb{Z}^+}{\operatorname{argmax}} \{l_{cg}(\mathbf{m}, \mathcal{S})\} \quad (5-16)$$

$$\text{subject to: } N = \sum_{i=1}^{N_p} M_i - (N_p - 1)$$

where  $\mathbb{Z}^+$  is the set of positive integers. It's worth to mention that, maximizing the number of consecutive lags is equivalent to minimizing the number of holes in the difference coarray.

When the solution of (5-15) and/or (5-16) is not unique, other factors like aperture size and reduced mutual coupling can be considered [96]. The mutual coupling is related to  $v_\Delta$  which is defined as the number of inter-element spacings, that equals to a unit spacing [110]. The array gets sparser as the value of  $v_\Delta$  decreases. If multiple solutions result in the same  $v_\Delta$ , then the configuration that minimizes aperture size,  $D$ , is recommended.

### 5.6 An Upper Bound of the Achievable DOFs of the 3LPA

This section derives an upper bound for the achievable DOFs realized by the 3LPA configurations [108]. The derived bounds are compared against the achieved DOFs and verified with simulation. Table 5-3 illustrates the 3LPA Config.A and 3LPA Config.B characteristics including: antenna locations, the ordered inter-element spacing, and aperture size. Since  $M_2 < M_3$ , the 3LPA Config.B always has larger aperture size, i.e.  $D_B > D_A$  for any  $\mathbf{m}$ .

Let's take each two subarrays alone and rewrite (5-10) as:

$$\begin{aligned} \mathbb{L}_{c_{ij}} &= \{l_c | l_c \in (p_m - p_n), p_m d \in \mathbb{P}_i, p_n d \in \mathbb{P}_j\}, \\ &\forall i, j \in \{1, 2, 3\}, i < j, 1 \leq m, n \leq N \end{aligned} \quad (5-17)$$

Thus the cross-differences can be expressed as a union of three subsets based on (5-17) as:

$$\mathbb{L}_c = \mathbb{L}_{c_{12}} \cup \mathbb{L}_{c_{13}} \cup \mathbb{L}_{c_{23}} \quad (5-18)$$

The mirrored positions can be calculated when  $i > j$ :

$$\mathbb{L}_c^- = \mathbb{L}_{c_{12}}^- \cup \mathbb{L}_{c_{13}}^- \cup \mathbb{L}_{c_{23}}^- \quad (5-19)$$

Table 5-3: 3LPA Config.A and Config.B characteristics

3LPA	Config.A	Config.B
$\mathbb{P}$	$k_1 M_2 \cup k_2 M_3 \cup k_3 M_1$	$k_1 M_3 \cup k_2 M_1 \cup k_3 M_2$
$\mathcal{S}$	$[M_2, M_3, M_1]d$	$[M_3, M_1, M_2]d$
$D$	$M_3(M_2 - 1)d$	$M_2(M_3 - 1)d$

where  $\mathbb{L}_{c_{ij}}^- = \mathbb{L}_{c_{ij}}, \forall i > j$ . Therefore, (5-8) can be re-written as:

$$\mathbb{L}_P = \mathbb{L}_c \cup \mathbb{L}_c^- \quad (5-20)$$

The achievable DOFs is determined by the total number of unique lags,  $\eta_P$ , in  $\mathbb{L}_P$  which equals to the number of unique integers in  $\mathbb{L}_c$  and number of unique integers in  $\mathbb{L}_c^-$  minus the overlapped or the common ones in between. Mathematically, we can write:

$$\begin{aligned} \text{DOFs} &= |\mathbb{L}_P| = |\mathbb{L}_c| + |\mathbb{L}_c^-| - |\mathbb{L}_c \cap \mathbb{L}_c^-| \\ &= 2|\mathbb{L}_{c_{12}}| + 2|\mathbb{L}_{c_{13}}| + 2|\mathbb{L}_{c_{23}}| - |\mathbb{L}_c \cap \mathbb{L}_c^-| \end{aligned} \quad (5-21)$$

where  $|\cdot|$  denotes the cardinality operation. The last term accounts for the repeated lags between  $\mathbb{L}_c$  and  $\mathbb{L}_c^-$ . This term can be separated into two parts. The first part includes the intersection between a subset and its mirrored position as:

$$\mathbb{L}_l = \begin{cases} \mathbb{L}_{c_{12}} \cap \mathbb{L}_{c_{12}}^-, & l = 1 \\ \mathbb{L}_{c_{13}} \cap \mathbb{L}_{c_{13}}^-, & l = 2 \\ \mathbb{L}_{c_{23}} \cap \mathbb{L}_{c_{23}}^-, & l = 3 \end{cases} \quad (5-22)$$

While the other includes the intersection between two different subsets as:

$$\mathbb{L}_l = \begin{cases} \mathbb{L}_{c_{12}} \cap \mathbb{L}_{c_{13}} = -(\mathbb{L}_{c_{12}}^- \cap \mathbb{L}_{c_{13}}^-), & l = 4 \\ \mathbb{L}_{c_{12}} \cap \mathbb{L}_{c_{23}} = -(\mathbb{L}_{c_{12}}^- \cap \mathbb{L}_{c_{23}}^-), & l = 5 \\ \mathbb{L}_{c_{13}} \cap \mathbb{L}_{c_{23}} = -(\mathbb{L}_{c_{13}}^- \cap \mathbb{L}_{c_{23}}^-), & l = 6 \\ \mathbb{L}_{c_{12}} \cap \mathbb{L}_{c_{13}}^- = -(\mathbb{L}_{c_{12}} \cap \mathbb{L}_{c_{13}}^-), & l = 7 \\ \mathbb{L}_{c_{12}} \cap \mathbb{L}_{c_{23}}^- = -(\mathbb{L}_{c_{12}} \cap \mathbb{L}_{c_{23}}^-), & l = 8 \\ \mathbb{L}_{c_{13}} \cap \mathbb{L}_{c_{23}}^- = -(\mathbb{L}_{c_{13}} \cap \mathbb{L}_{c_{23}}^-), & l = 9 \end{cases} \quad (5-23)$$

So, if we can find six of them, we just take their negatives to find all the twelve subsets.

Let  $\eta_c$  and  $\eta_c^-$  represent the number of unique lags in  $\mathbb{L}_c$  and  $\mathbb{L}_c^-$  respectively, we can rewrite (5-21) as:

$$\text{DOFs} = \eta_P = \eta_c + \eta_c^- - \sum_{l=1}^3 \eta_l - 2 \sum_{l=1}^6 \eta_l \quad (5-24)$$

where  $\eta_l$  represents the number of unique integers in  $\mathbb{L}_l$  subset,  $\eta_l = |\mathbb{L}_l|$  for  $l = 1, 2, \dots, 9$ .

Our objective is to find a closed form expression for each term in (5-24). The following lemma is used to find mathematical expressions for the first two terms.

**Lemma 1:** Let  $\eta_{12}, \eta_{13}$ , and  $\eta_{23}$  be the number of unique lags in  $\mathbb{L}_{c_{12}}, \mathbb{L}_{c_{13}}$ , and  $\mathbb{L}_{c_{23}}$  respectively. In addition, the number of unique lags in the corresponding mirrored positions  $\mathbb{L}_{c_{12}}^-, \mathbb{L}_{c_{13}}^-, \mathbb{L}_{c_{23}}^-$  are  $\eta_{12}^-, \eta_{13}^-,$  and  $\eta_{23}^-$  respectively. Both  $\mathbb{L}_{c_{ij}}$  and  $\mathbb{L}_{c_{ij}}^-$  have the same number of unique lags due to the coprimality between  $M_1, M_2$ , and  $M_3$ ,  $\forall i, j = 1, 2, 3$  and  $i < j$ . The number of unique integers in  $\mathbb{L}_{c_{12}}, \mathbb{L}_{c_{13}}$ , and  $\mathbb{L}_{c_{23}}$  are as follows, respectively:

$$\begin{aligned} \eta_{ij} &= \eta_{ij}^- = M_i M_j, \\ \forall i, j &\in \{1, 2, 3\}, i < j \end{aligned} \quad (5-25)$$

This lemma is used to express the first two terms in (5-24) in a closed form.

**Proof Lemma 1:** We prove the previous lemma by contradiction. We only show how we derive  $\eta_{12} = |\mathbb{L}_{c_{12}}|$  and the same steps can be followed for others. Both of the 3LPA configurations have the same results. The 3LPA Config.A is assumed and used in this proof. We start from (5-17) and based on Table 5-3, we have  $\mathbb{P}_1 = k_1 M_2$  and  $\mathbb{P}_2 = k_2 M_3$  where the indices  $0 \leq k_1 \leq M_1 - 1$  and  $0 \leq k_2 \leq M_2 - 1$ . Using contradiction, let  $l_{c_{12}}^m = k_1^m M_2 - k_2^m M_3$  and  $l_{c_{12}}^n = k_1^n M_2 - k_2^n M_3$  be two arbitrary lags in  $\mathbb{L}_{c_{12}}$ . The variables  $k_1^m, k_2^m, k_1^n$ , and  $k_2^n$  are integer indices defined as:  $0 \leq k_1^m, k_1^n \leq M_1 - 1$  and  $0 \leq k_2^m, k_2^n \leq M_2 - 1$ . Had  $l_{c_{12}}^m = l_{c_{12}}^n$ , we would have:

$$\frac{k_2^m - k_2^n}{k_1^m - k_1^n} = \frac{M_2}{M_3} \quad (5-26)$$

Since  $k_1^m - k_1^n < M_3$ , (5-26) cannot be hold due to the coprimality of  $M_2$  and  $M_3$ . Thus,  $l_{c_{12}}^m$  and  $l_{c_{12}}^n$  cannot be equal and consequently, there are  $|k_1||k_2| = M_1 M_2$  unique integers in  $\mathbb{L}_{c_{12}}$ .

Therefore, the number of unique integers in  $\mathbb{L}_c$  and  $\mathbb{L}_c^-$  are given respectively as:

$$\begin{aligned} \eta_c &= \eta_{12} + \eta_{13} + \eta_{23} = M_1 M_2 + M_1 M_3 + M_2 M_3 \\ \eta_c^- &= \eta_{12}^- + \eta_{13}^- + \eta_{23}^- = M_1 M_2 + M_1 M_3 + M_2 M_3 \end{aligned} \quad (5-27)$$

The third term in (5-24) can be obtained by finding the subsets  $\mathbb{L}_i$  for  $i = 1, 2, 3$  and then find their cardinalities. The 3LPA configurations will have different sets since it's a function of the differences between element locations within two subarrays.

The objective of the next two subsections is to find the third term in (5-24) based on the 3LPA Config.A and 3LPA Config.B. Specifically, we derive an upper bound of the DOFs for each configuration.

## 5.6.1 An Upper Bound of DOFs for the 3LPA Config.A

The 3LPA Config.A can be constructed with  $\mathcal{S}_A = [M_2, M_3, M_1]d$ , and the elements within the array are located at:

$$\mathbb{P}_A = \{\mathbb{P}_1 \cup \mathbb{P}_2 \cup \mathbb{P}_3\}d \quad (5-28)$$

where  $\mathbb{P}_1 = k_1 M_2$ ,  $\mathbb{P}_2 = k_2 M_3$ , and  $\mathbb{P}_3 = k_3 M_1$ . The overlapped integers between the subset  $\mathbb{L}_{c_{ij}}$  and corresponding mirrored positions  $\mathbb{L}_{c_{ij}}^-$  can be calculated from the cardinality of their intersection.

The following lemma is used to find a mathematical expression for the third term in (5-24) for the 3LPA Config.A.

**Lemma 2:** The following facts hold for the 3LPA Config.A based on (5-22) regarding  $\mathbb{L}_l$ :

1. There are  $2(M_1 M_2 + M_1 M_3 + M_2 M_3)$  unique lags in  $\mathbb{L}_{c_{12}}, \mathbb{L}_{c_{12}}^-, \mathbb{L}_{c_{13}}, \mathbb{L}_{c_{13}}^-, \mathbb{L}_{c_{23}},$  and  $\mathbb{L}_{c_{23}}^-$  including the overlapped lags
2. The subset  $\mathbb{L}_{c_{12}}$  overlaps with  $\mathbb{L}_{c_{12}}^-$  only at the zero position, i.e.  $\eta_1 = 1$
3. The number of overlapped lags between  $\mathbb{L}_{c_{13}}$  and  $\mathbb{L}_{c_{13}}^-$  is  $\eta_2 = (M_1 - 1)(M_2 + 1) + 1$
4. The number of overlapped lags between  $\mathbb{L}_{c_{23}}$  and  $\mathbb{L}_{c_{23}}^-$  is  $\eta_3 = (M_1 + 1)(M_3 - 1) + 1$

**Proof Lemma 2:** The above relations can be verified as follows. We start by finding the

set  $\mathbb{L}_1$  and then its cardinality  $\eta_1$ . Given two arbitrary lags  $l_{c_{12}}^m = k_1^m M_2 - k_2^m M_3$  and

$l_{c_{12}}^n = k_2^n M_3 - k_1^n M_2$  in the subsets  $\mathbb{L}_{c_{12}}$  and  $\mathbb{L}_{c_{12}}^-$  respectively where  $0 \leq k_1^m, k_1^n \leq M_1 -$

1 and  $0 \leq k_2^m, k_2^n \leq M_2 - 1$ . Had  $l_{c_{12}}^m = l_{c_{12}}^n$  been held, we would have  $(k_1^m + k_1^n)M_2 =$

$(k_2^m + k_2^n)M_3$ . It is evident that they overlap at 0 position when  $k_1^m = k_1^n = k_2^m = k_2^n =$

0. To find the overlapped lags when  $k_2^m + k_2^n \neq 0$ , we have to find the solution for the following:

$$\frac{k_1^m + k_1^n}{k_2^m + k_2^n} = \frac{M_3}{M_2} \quad (5-29)$$

Since we have pairwise coprime integers, the above formula is valid if and only if:

$$\begin{aligned} k_1^m + k_1^n &= M_3, \\ k_2^m + k_2^n &= M_2 \end{aligned} \quad (5-30)$$

As  $0 \leq k_1^n \leq M_1 - 1$  and  $0 \leq k_2^n \leq M_2 - 1$ , the requirement is equivalent to:

$$\begin{aligned} M_3 - (M_1 - 1) &\leq k_1^m \leq M_3, \\ 1 &\leq k_2^m \leq M_2, \end{aligned} \quad (5-31)$$

Since  $0 \leq k_1^m \leq M_1 - 1$  and  $0 \leq k_2^m \leq M_2 - 1$ , we end up with:

$$\begin{aligned} \max(M_3 - (M_1 - 1), 0) &\leq k_1^m \leq \min(M_3, M_1 - 1), \\ \max(1, 0) &\leq k_2^m \leq \min(M_2, M_2 - 1), \end{aligned} \quad (5-32)$$

As  $M_3 > M_2 > M_1$ , the terms  $M_3 - (M_1 - 1)$  is always greater than zero, so we can rewrite:

$$\begin{aligned} M_3 - (M_1 - 1) &\leq k_1^m \leq M_1 - 1, \\ 1 &\leq k_2^m \leq M_2 - 1 \end{aligned} \quad (5-33)$$

Again  $M_3 - (M_1 - 1)$  is always greater than  $M_1 - 1$ . Therefore,  $\mathbb{L}_{c_{12}}$  and  $\mathbb{L}_{c_{12}}^-$  overlap only at zero position, so  $\eta_1 = 1$ .

The same procedures can be followed to find the set  $\mathbb{L}_2$  and its cardinality  $\eta_2$ . Given two arbitrary lags  $l_{c_{13}}^m = k_1^m M_2 - k_3^m M_1$  and  $l_{c_{13}}^n = k_3^n M_1 - k_1^n M_2$  in the subsets  $\mathbb{L}_{c_{13}}$  and  $\mathbb{L}_{c_{13}}^-$  respectively where  $0 \leq k_1^m, k_1^n \leq M_1 - 1$  and  $0 \leq k_3^m, k_3^n \leq M_3 - 1$ . Had  $l_{c_{13}}^m = l_{c_{13}}^n$  been held, we would have  $(k_1^m + k_1^n)M_2 = (k_3^m + k_3^n)M_1$ . It is clear that they overlap at 0

position when  $k_1^m = k_1^n = k_3^m = k_3^n = 0$ . To find the overlapped lags when  $k_3^m + k_3^n \neq 0$ , we have to find the solution for the following:

$$\frac{k_1^m + k_1^n}{k_3^m + k_3^n} = \frac{M_1}{M_2} \quad (5-34)$$

Since we have pairwise coprime integers, the above formula is valid if and only if:

$$\begin{aligned} k_1^m + k_1^n &= M_1, \\ k_3^m + k_3^n &= M_2 \end{aligned} \quad (5-35)$$

Since  $0 \leq k_1^n \leq M_1 - 1$  and  $0 \leq k_3^n \leq M_3 - 1$ , the requirement is equivalent to:

$$\begin{aligned} 1 &\leq k_1^m \leq M_1, \\ M_2 - (M_3 - 1) &\leq k_3^m \leq M_2 \end{aligned} \quad (5-36)$$

Since  $0 \leq k_1^m \leq M_1 - 1$  and  $0 \leq k_3^m \leq M_3 - 1$ , we end up with:

$$\begin{aligned} 1 &\leq k_1^m \leq \min(M_1, M_1 - 1), \\ \max(M_2 - (M_3 - 1), 0) &\leq k_3^m \leq \min(M_2, M_3 - 1), \end{aligned} \quad (5-37)$$

Based on our assumption,  $M_2 - (M_3 - 1) \leq 0$  and  $M_2 \leq M_3 - 1$ , so we can rewrite:

$$\begin{aligned} 1 &\leq k_1^m \leq M_1 - 1, \\ 0 &\leq k_3^m \leq M_2 \end{aligned} \quad (5-38)$$

Therefore, in addition to the overlap at the zero position, there are  $M_1 - 1$  and  $M_2 + 1$  integers in the range of  $k_1^m$  and  $k_3^m$ , respectively. Consequently,  $\eta_2 = (M_1 - 1)(M_2 + 1) + 1$ .

To find  $\eta_3 = |\mathbb{L}_3|$ , let's assume  $l_{c_{23}}^m = k_2^m M_3 - k_3^m M_1$  and  $l_{c_{23}}^n = k_3^n M_1 - k_2^n M_3$  be two arbitrary lags in the subsets  $\mathbb{L}_{c_{23}}$  and  $\mathbb{L}_{c_{23}}^-$  respectively where  $0 \leq k_2^m, k_2^n \leq M_2 - 1$  and  $0 \leq k_3^m, k_3^n \leq M_3 - 1$ . Had  $l_{c_{23}}^m = l_{c_{23}}^n$  been held, we would have  $(k_2^m + k_2^n)M_3 =$



$(k_3^m + k_3^n)M_1$ . It is obvious that they overlap at 0 position when  $k_2^m = k_2^n = k_3^m = k_3^n = 0$ . To find the overlapped lags when  $k_3^m + k_3^n \neq 0$ , we have to find the solution for the following:

$$\frac{k_2^m + k_2^n}{k_3^m + k_3^n} = \frac{M_1}{M_3} \quad (5-39)$$

Since we have pairwise coprime integers, the above relation is valid if and only if:

$$\begin{aligned} k_2^m + k_2^n &= M_1, \\ k_3^m + k_3^n &= M_3 \end{aligned} \quad (5-40)$$

Since  $0 \leq k_2^n \leq M_2 - 1$  and  $0 \leq k_3^n \leq M_3 - 1$ , the requirement is equivalent to:

$$\begin{aligned} M_1 - (M_2 - 1) &\leq k_2^m \leq M_1, \\ 1 &\leq k_3^m \leq M_3 \end{aligned} \quad (5-41)$$

Meanwhile  $0 \leq k_2^m \leq M_2 - 1$  and  $0 \leq k_3^m \leq M_3 - 1$ , we end up with:

$$\begin{aligned} 0 &\leq k_2^m \leq M_1, \\ 1 &\leq k_3^m \leq M_3 - 1 \end{aligned} \quad (5-42)$$

As a result, in addition to the overlap at the zero position, there are  $M_1 + 1$  and  $M_3 - 1$  integers in the range of  $k_2^m$  and  $k_3^m$ , respectively. Thus,  $\eta_3 = (M_1 + 1)(M_3 - 1) + 1$ .

We have not derived yet the last term of (5-24). It is complicated to find all subsets in (5-23) since there are three indices,  $k_1$ ,  $k_2$ , and  $k_3$ . There are six subsets in (5-23) and the mirrored position which we ignore since our objective is to derive an upper bound of the achieved DOFs. Therefore, the upper bound of the achievable DOFs for the 3LPA Config.A can be expressed as:

$$\text{DOFs} < 2\eta_c - \sum_{l=1}^3 \eta_l \quad (5-43)$$

$$= M_1 M_2 + M_1 M_3 + 2M_2 M_3 - M_3 + M_2 - 1$$

where  $\eta_1 = 1$ ,  $\eta_2 = (M_1 - 1)(M_2 + 1) + 1$ , and  $\eta_3 = (M_1 + 1)(M_3 - 1) + 1$ .

### 5.6.2 An Upper Bound of DOFs for the 3LPA Config.B

The 3LPA Config.B uses an ordered inter-element spacing vector of  $\mathcal{S}_B = [M_3, M_1, M_2]d$ .

This array has elements located at:

$$\mathbb{P}_B = \{k_1 M_3 \cup k_2 M_1 \cup k_3 M_2\}d \quad (5-44)$$

We can proceed as we did in Section 5.6.1 but with  $\mathbb{P}_1 = k_1 M_3$ ,  $\mathbb{P}_2 = k_2 M_1$ , and  $\mathbb{P}_3 = k_3 M_2$ .

**Lemma 3:** The following facts hold for the 3LPA Config.B based on (5-22) regarding  $\mathbb{L}_l$ :

1. There are  $2(M_1 M_2 + M_1 M_3 + M_2 M_3)$  unique lags in  $\mathbb{L}_{c_{12}}, \mathbb{L}_{c_{12}}^-, \mathbb{L}_{c_{13}}, \mathbb{L}_{c_{13}}^-, \mathbb{L}_{c_{23}}$ , and  $\mathbb{L}_{c_{23}}^-$  including the overlapped lags
2. The subset  $\mathbb{L}_{c_{12}}$  overlaps with  $\mathbb{L}_{c_{12}}^-$  at  $\eta_1 = \max(2M_2 - M_3 - 1, 0)(M_1 - 1) + 1$  position
3. The number of overlapped lags between  $\mathbb{L}_{c_{13}}$  and  $\mathbb{L}_{c_{13}}^-$  is  $\eta_2 = \max(2M_1 - M_2 - 1, 0)(M_3 - 1) + 1$
4. The number of overlapped lags between  $\mathbb{L}_{c_{23}}$  and  $\mathbb{L}_{c_{23}}^-$  is  $\eta_3 = (M_2 - 1)(M_1 + 1) + 1$

The aforementioned relations can be proved by following the same steps as in Section 5.6.1.

Therefore, the upper bound of the achievable DOFs for the 3LPA Config.B can be expressed as:

$$\begin{aligned} \text{DOFs} &< 2\eta_c - \sum_{l=1}^3 \eta_l \\ &= 2\{M_1M_3 + M_2M_3\} + M_1M_2 - M_2 + M_1 - a(M_1 - 1) - b(M_3 - 1) - 2 \end{aligned} \quad (5-45)$$

where  $a = \max(2M_2 - M_3 - 1, 0)$  and  $b = \max(2M_1 - M_2 - 1, 0)$ .

## 5.7 Results and Analysis

This section presents some results to verify the correctness of the derived expressions and effectiveness of the proposed configurations. First, we investigate the proposed configurations using the minimum possible number of sensors. Then array configurations with three and four subarrays are presented and compared based on the difference coarray. The number of lags and the required aperture size as a function of the total number of sensors are evaluated for different MLPA levels. The number of unit inter-element spacings are then evaluated as a function of the total number of sensors. Finally, the upper bounds of the achievable DOFs of the 3LPA configurations derived in Section 5.6 are compared against the maximum DOFs.

### 5.7.1 MLPAs with Minimum Number of Sensors

This subsection investigates the effectiveness of the proposed configurations using the minimum number of sensors (the extreme cases). The purpose of this investigation is to explore how the proposed configurations perform at such extremes.

Table 5-4 illustrates the minimum number of sensors needed to construct the proposed MLPA configuration with 2, 3, 4, 5, and 6 levels. Based on Figure 5-4 (a), the minimum

number of sensors for  $N_p = 2, 3, 4, 5$  and 6 is 4 (coprime array), 8 (3LPA), 14 (4LPA), 24 (5LPA), and 36 (6LPA) sensors respectively. For each case the minimum, the maximum, the mean, and the variance of the number of unique lags, the number of consecutive lags, and the aperture size are calculated. Moreover, each MLPA configuration is compared with coprime array for a fixed  $N$ .

The results in the table are generated by considering all possible  $N_c$  configurations. For the considered configurations, the proposed arrays always achieve larger number of consecutive lags,  $l_{cg}$ , compared with coprime arrays whereas the number of unique lags,  $l_{ug}$ , is less. Therefore, only very few holes appear in the difference coarray of the proposed configurations which is not the case in coprime arrays. Additionally, the proposed configurations always require smaller aperture size,  $D$ , compared with coprime arrays. Coprime arrays always achieve a fixed number of consecutive lags [52] for a fixed  $N$ , this is why the variance of  $l_{cg}$  is zero. The numbers in the table were calculated based on the derived equations and were verified by actual simulation of the listed scenarios.

### 5.7.2 Array Configurations

In this subsection, we present some examples for MLPA with three and four subarrays and compare them with coprime array in [52], nested array in [34], and super nested arrays in [97]. For a given  $N$ , coprime arrays are constructed such that they achieve the largest  $l_{ug}$  where the two entries of  $\mathbf{m}$  should be as close as possible [56], [57]. In addition, nested arrays and super nested arrays are constructed as in [34], [97] such that they can achieve the maximum DOFs where difference coarray has no holes,  $l_{ug} = l_{cg}$ .

**Table 5-4:** MLPA configurations using the minimum possible number of sensors

	Minimum	Maximum	Mean	Variance	$N$
<b>Parameters</b>		Coprime array configuration			
$l_{ug}$	9	9	9	0	4
$l_{cg}$	9	9	9	0	
$D$ ( $d$ units)	4	4	4	0	
<b>Parameters</b>		3LPA configuration			
$l_{ug}$	19	23	21	8	8
$l_{cg}$	17	21	19	8	
$D$ ( $d$ units)	10	12	11	2	
<b>Parameters</b>		Coprime array configuration			
$l_{ug}$	21	27	24	18	8
$l_{cg}$	17	17	17	0	
$D$ ( $d$ units)	12	16	14	8	
<b>Parameters</b>		4LPA configuration			
$l_{ug}$	53	59	57.5	9	14
$l_{cg}$	39	57	52.5	81	
$D$ ( $d$ units)	28	30	29.5	1	
<b>Parameters</b>		Coprime array configuration			
$l_{ug}$	39	69	55	228	14
$l_{cg}$	29	29	29	0	
$D$ ( $d$ units)	24	49	37.667	160.33	
<b>Parameters</b>		5LPA configuration			
$l_{ug}$	121	139	133.44	41.778	24
$l_{cg}$	97	137	121	206	
$D$ ( $d$ units)	66	70	68.667	4	
<b>Parameters</b>		Coprime array configuration			
$l_{ug}$	69	179	137	1590	24
$l_{cg}$	49	49	49	0	
$D$ ( $d$ units)	44	144	107.11	1333.6	
<b>Parameters</b>		6LPA configuration			
$l_{ug}$	245	263	254.16	31.251	36
$l_{cg}$	169	261	204.47	989.26	
$D$ ( $d$ units)	130	132	131.37	0.91228	
<b>Parameters</b>		Coprime array configuration			
$l_{ug}$	105	377	281	7854	36
$l_{cg}$	73	73	73	0	
$D$ ( $d$ units)	68	324	236	7012.5	

The considered, nested array, 2nd, and 3rd order super nested arrays can have equal aperture size if  $N_1 = N/2$  is an odd number [97]. Apart from the 2nd order, when  $N_1$  is an even number, the 3rd order super nested array cannot be constructed with  $N_1 = N_2$  [97]. As a result, the two numbers have to be different and we end up with an array of a quite smaller aperture size and smaller number of lags compared with nested arrays. In some

cases, holes might appear in the corresponding difference coarray [97]. In this chapter, the 2nd and 3rd order super nested arrays are constructed such that they realize equal aperture size.

*A. MLPA with Three Subarrays:*

The 3LPA and PA configurations with  $\mathbf{m}_1 = [2,3,7]$ ,  $\mathbf{m}_2 = [3,4,5]$  respectively are compared versus coprime arrays [52] using  $\mathbf{m} = [5,6]$  and nested arrays [34] for  $N = 10$  sensors. The array structures for those configurations are as shown in Figure 5-2 and the corresponding difference coarrays are plotted in Figure 5-5. The proposed configurations are compared in terms of the aperture size, number of unique lags, and number of consecutive lags as Table 5-5 summarizes.

The physical aperture is a function of the inter-element spacing and can be either  $18d$  or  $14d$  in 3LPA whereas PA has aperture size equals  $16d$  or  $15d$ , see Figure 5-2. On the other hand, coprime array has larger aperture sizes by at least  $7d$  and consequently the number of unique lags is larger and equals 39 lags. In addition, 21 lags out of them are consecutive so there are 18 holes. However, the number of consecutive lags of the proposed configurations are larger with only 2 and 4 holes in each configuration for any inter-element spacing as Figure 5-5 illustrates.

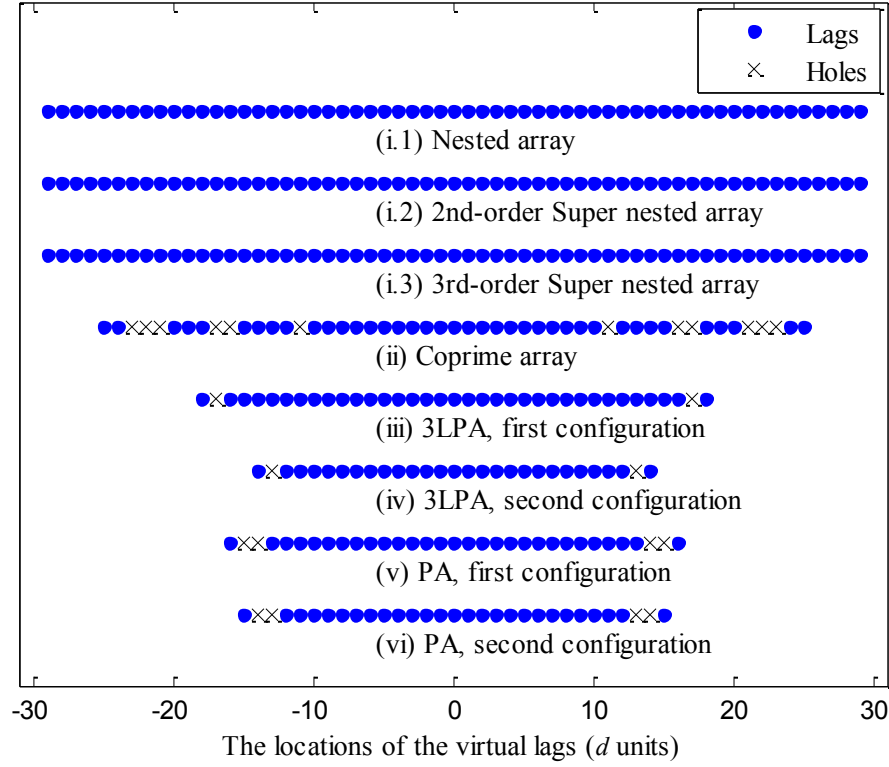


Figure 5-5: The difference coarray of 3LPA configurations and PA configurations

Table 5-5: Comparison between array's characteristics for  $N = 10$

Configuration	$\mathbf{m}$	$\mathcal{S}$	$D$	$l_{ug}$	$l_{cg}$
Nested array	$N_1=N_2=5$	as in Ref. [34]			
2 <sup>nd</sup> order Super nested		as in Ref. [97]	$29d$	59	-29:29=59
3 <sup>rd</sup> order Super nested					
Coprime array	$\mathbf{m}=[5,6]$	$[6,5]d$	$25d$	39	-10:10=21
3LPA	$\mathbf{m}_1=[2,3,7]$	$[7,2,3]d$	$18d$	35	-16:16=33
		$[3,7,2]d$	$14d$	27	-12:12=25
PA	$\mathbf{m}_2=[3,4,5]$	$[5,3,4]d$	$16d$	29	-13:13=27
		$[4,5,3]d$	$15d$	27	-12:12=25

For larger number of sensors  $N = 12$ , four 3LPA configurations can be constructed using  $\mathbf{m}_1 = [3,4,7]$  and  $\mathbf{m}_2 = [2,5,7]$ . Figure 5-6 (a) demonstrates those configurations compared with coprime array using  $\mathbf{m} = [6,7]$  where the corresponding difference coarrays are as depicted in Figure 5-6 (b). Different aperture sizes are required, which controlled by the ordered inter-element spacing,  $\mathcal{S}$ . The 3LPA configurations using the

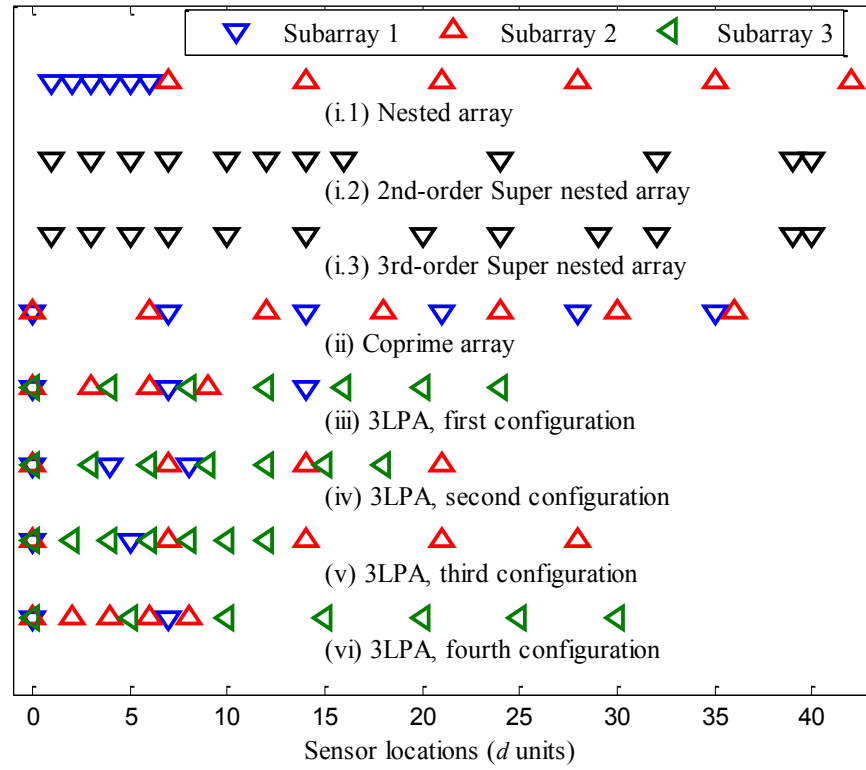
second vector realize larger aperture size. Therefore, the number of unique lags and the number of consecutive lags in Figure 5-6 (b) is larger and reaches up to 57 and 53 lags respectively as Table 5-6 summarizes. Additionally, we can achieve the same number of unique lags as in coprime array even with smaller aperture size and the number of consecutive lags is almost doubled. The 3LPA can even achieve more lags by changing the ordered inter-element spacing to  $\mathcal{S} = [7,2,5]d$  and even with smaller aperture size of  $6d$ .

In Table 5-5 and Table 5-6, nested arrays and super nested arrays require the largest aperture size among all considered configurations, and achieve hole-free difference coarrays as demonstrated in Figure 5-5 and Figure 5-6 (b). Large number of elements in nested arrays are spaced by a unit inter-element spacing which increases the mutual coupling effect. This is not the case in super nested arrays [97]. In addition, higher order super nested arrays can overcome this problem more but may have smaller aperture size and consequently fewer lags [97]. Increasing the number of sensors to  $N = 12$  makes  $N_1 = N/2$  to be an even number. Therefore, the 3rd order super nested array cannot be constructed with  $N_1 = N_2 = 6$  in order to get equal aperture size,  $41d$  as shown in Table 5-6.

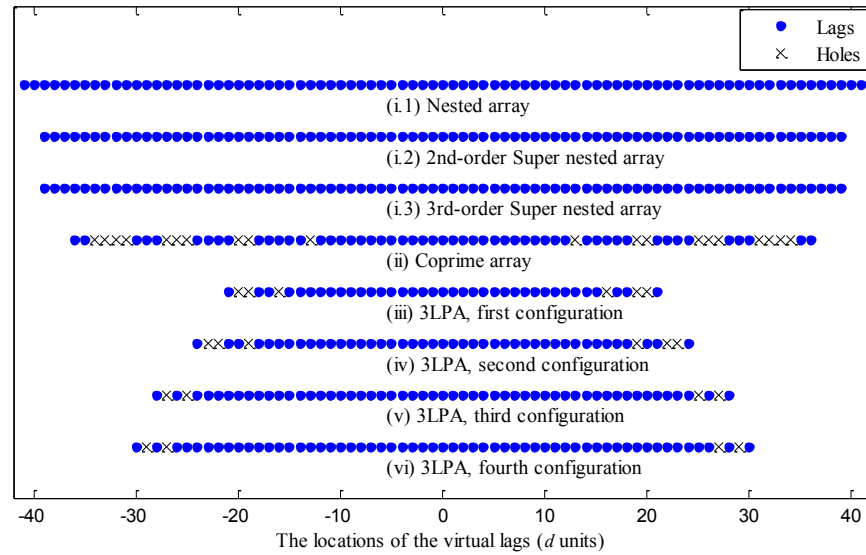
**Table 5-6:** 3LPA characteristics for  $N = 12$

Configuration	$\mathbf{m}$	$\mathcal{S}$	$D$	$l_{ug}$	$l_{cg}$
Nested array	$N_1=N_2=6$	as in Ref. [34]	$41d$	83	$-41:41=83$
2 <sup>nd</sup> order Super nested	$N_1=7, N_2=5$	as in Ref. [97]	$39d$	79	$-39:39=79$
3 <sup>rd</sup> order Super nested					
Coprime array	$\mathbf{m}=[6,7]$	$[7,6]d$	$36d$	53	$-12:12=25$
3LPA	$\mathbf{m}_1=[3,4,7]$	$[7,3,4]d$	$24d$	43	$-18:18=37$
		$[4,7,3]d$	$21d$	37	$-15:15=31$
	$\mathbf{m}_2=[2,5,7]$	$[5,7,2]d$	$28d$	53	$-24:24=49$
		$[7,2,5]d$	$30d$	57	$-26:26=53$





(a) 3LPA configurations



(b) Corresponding difference coarray

**Figure 5-6:** 3LPAs with  $N = 12$  sensors (ii)-(iii) using  $\mathbf{m}_1 = [3, 4, 7]$  and (iv)-(v) using  $\mathbf{m}_2 = [2, 5, 7]$

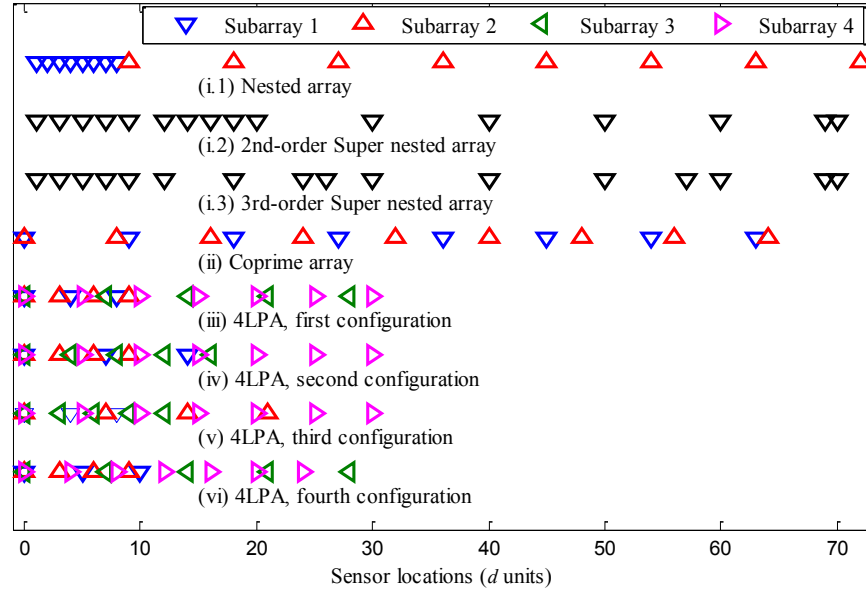
*B. MLPA with Four Subarrays:*

A 4LPA with a total of  $N = 16$  sensors is considered using  $\mathbf{m} = [3,4,5,7]$  and compared with coprime array using  $\mathbf{m} = [8,9]$ . Four 4LPA configurations can be constructed by selecting the ordered inter-element spacing among the subarrays. Figure 5-7 shows the array structures and the corresponding difference coarrays respectively. Three configurations have different ordered inter-element spacing and sensor locations. The three configurations result in equal aperture size but may have different difference coarray. The number of unique lags and number of consecutive lags are summarized in Table 5-7. The difference coarray of the first configuration has only two holes. While the fourth 4LPA configuration with smaller aperture results in less number of unique lags and consecutive lags, see Figure 5-7 (b). Compared with coprime array in [52], the best scenario has got 28 less unique lags, 24 more consecutive lags, and needed a smaller aperture size by  $34d$ .

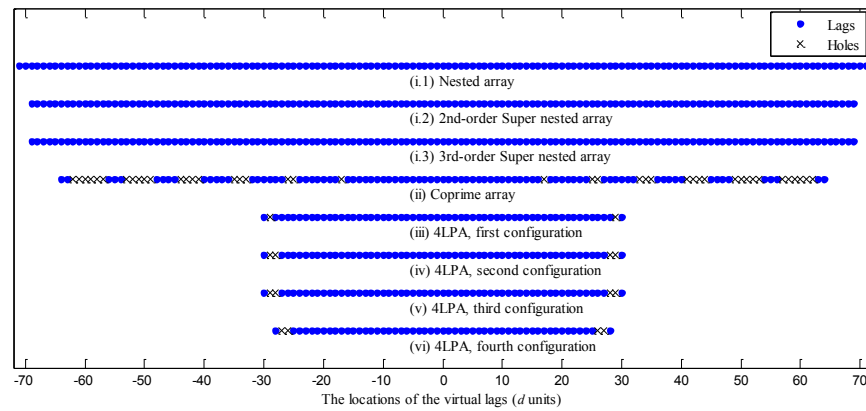
The considered and studied case implies that the difference between the number of unique lags and the number of consecutive lags is quite small compared with the 3LPA configurations. However, the array becomes less sparse where the sensors become close to each other. Consequently, the mutual coupling effect increases. The number of antenna elements spaced by a unit inter-element spacing in the considered case is comparable with that of nested array as shown in Figure 5-7 (a). This number can be further reduced using the 2nd and 3rd order super nested arrays. Those configurations also have hole-free difference coarrays as Figure 5-7 (b) depicts. The aperture size of higher order super nested arrays is smaller than that of nested arrays.

Table 5-7: 4LPA characteristics for  $N = 16$ 

Configuration	$\mathbf{m}$	$\mathcal{S}$	$D$	$l_{ug}$	$l_{cg}$
Nested array	$N_1=N_2=8$	as in Ref. [34]	$71d$	143	$-71:71=143$
2 <sup>nd</sup> order Super nested	$N_1=9, N_2=7$	as in Ref. [97]	$69d$	139	$-69:69=139$
3 <sup>rd</sup> order Super nested					
Coprime array	$\mathbf{m}=[8,9]$	$[9,8]d$	$64d$	87	$-16:16=33$
4LPA	$\mathbf{m}=[3,4,5,7]$	$[4,3,7,5]d$		59	$-28:28=57$
		$[7,3,4,5]d$	$30d$	57	$-27:27=55$
		$[4,7,3,5]d$			
		$[5,3,7,4]d$	$28d$	53	$-25:25=51$



(a) 4LPA configurations



(b) Corresponding difference coarray

Figure 5-7: 4LPAs with  $N = 16$  sensors using  $\mathbf{m} = [3,4,5,7]$

*C. The Optimal Number of Sensors within the Subarrays and the Optimal Ordered Inter-element Spacing:*

As in coprime arrays and nested arrays, in this part we want to find a relation between the entries of  $\mathbf{m}$  that leads to a better MLPA configuration and find the optimal ordered inter-element spacing. To achieve this purpose, 3LPA and 4LPA are considered with large number of sensors such that  $\mathbf{M}$  has multiple rows. Table 5-8 shows a comparison between different 3LPA and 4LPA configurations with  $N = 20$  sensors where we only consider the configuration with the largest  $l_{ug}$ . The 3LPA and 4LPA configurations with  $\mathbf{m}_1$  achieves the largest  $l_{ug}$  and  $l_{cg}$  among the same level and need aperture size of  $90d$  and  $70d$  respectively. Generally speaking, the 3LPA needs larger aperture size compared with the 4LPA. It can be concluded from this example that going to higher level at equal aperture size leads to higher DOFs. It can be concluded that, as the entries in of  $\mathbf{m}$  get closer, the aperture size becomes smaller and consequently the values of  $l_{ug}$  and  $l_{cg}$  are decreased and vice-versa. The best ordered inter-element spacing is the one that leads to the least number of overlapped lags between the cross-differences and the mirrored positions and produces the largest aperture size. Based on (5-3), the aperture size can take only one of two values. Since the number of ordered inter-element spacing for the 3LPA is  $C_{3LPA} = 2$ , the optimal inter-element spacing is the one that maximizes the aperture size which is  $\mathcal{S} = [M_3, M_1, M_2]d$  where Table 5-8 confirms this. An extensive simulations have been conducted and verified that a 4LPA achieves its maximum number of unique lags when the ordered inter-element spacing is either  $\mathcal{S} = [M_2, M_4, M_1, M_3]d$  or  $\mathcal{S} = [M_2, M_1, M_4, M_3]d$ . However, other ordered inter-element spacing gives also the same DOFs as Table 5-8 depicts.

Table 5-8: 3LPA versus 4LPA characteristics for  $N = 20$ 

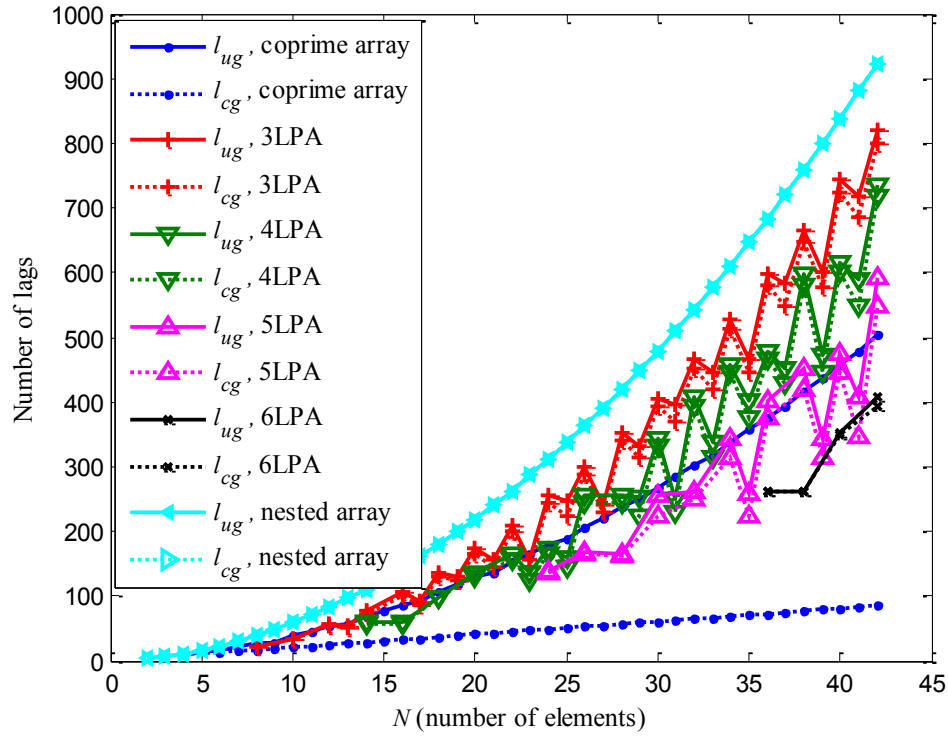
Configuration	$\mathbf{m}$	$\mathcal{S}$	$\mathcal{S}$	$D$	$l_{ug}$	$l_{cg}$
3LPA	$\mathbf{m}_1 = [2, 9, 11]$	$[M_3, M_1, M_2]d$	$[11, 2, 9]d$	$90d$	173	165
	$\mathbf{m}_2 = [2, 7, 13]$		$[13, 2, 7]d$	$84d$	163	147
	$\mathbf{m}_3 = [3, 8, 11]$		$[11, 3, 8]d$	$80d$	147	133
	$\mathbf{m}_4 = [3, 5, 14]$		$[14, 3, 5]d$	$65d$	123	115
	$\mathbf{m}_5 = [4, 7, 11]$		$[11, 4, 7]d$	$70d$	123	105
	$\mathbf{m}_6 = [4, 5, 13]$		$[13, 4, 5]d$	$60d$	109	97
	$\mathbf{m}_7 = [5, 8, 9]$		$[9, 5, 8]d$	$64d$	107	83
	$\mathbf{m}_8 = [5, 6, 11]$		$[11, 5, 6]d$	$60d$	101	81
	$\mathbf{m}_9 = [2, 3, 17]$		$[17, 2, 3]d$	$48d$	95	93
4LPA	$\mathbf{m}_1 = [2, 3, 7, 11]$	$[M_2, M_4, M_1, M_3]d$	$[3, 11, 2, 7]d$	$70d$	137	129
	$\mathbf{m}_2 = [2, 3, 5, 13]$	$[M_2, M_4, M_1, M_3]d$	$[3, 13, 2, 5]d$	$60d$	119	117
		$[M_4, M_1, M_2, M_3]d$	$[13, 2, 3, 5]d$			
	$\mathbf{m}_3 = [2, 5, 7, 9]$	$[M_4, M_1, M_2, M_3]d$	$[9, 2, 5, 7]d$	$56d$	109	105
		$[M_2, M_4, M_1, M_3]d$	$[5, 9, 2, 7]d$			
		$[M_2, M_1, M_4, M_3]d$	$[5, 2, 9, 7]d$			
	$\mathbf{m}_4 = [3, 5, 7, 8]$	$[M_2, M_1, M_4, M_3]d$	$[5, 3, 8, 7]d$	$49d$	97	93
	$\mathbf{m}_5 = [3, 4, 5, 11]$	$[M_4, M_1, M_2, M_3]d$	$[11, 3, 4, 5]$	$50d$	95	85
		$[M_2, M_4, M_1, M_3]d$	$[4, 11, 3, 5]d$			
		$[M_2, M_1, M_4, M_3]d$	$[4, 3, 11, 5]d$			

### 5.7.3 The Number of Lags versus the Number of Sensors

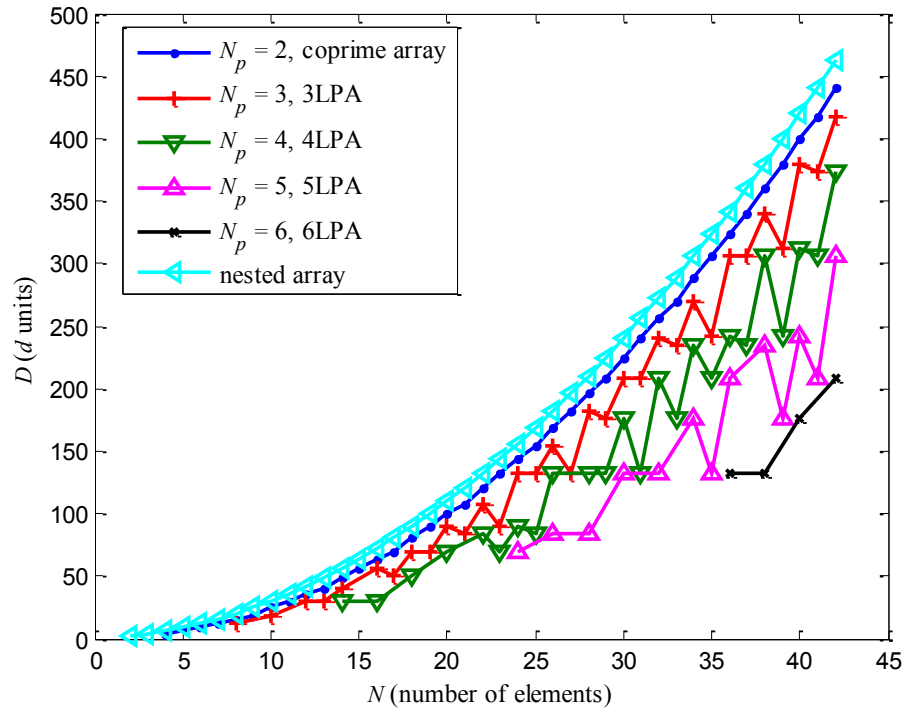
In Figure 5-8 (a) and (b) we generalize the result and plot the maximum number of unique lags, the maximum number of consecutive lags, and the maximum aperture size respectively as a function of  $N$  for coprime array, 3LPA, 4LPA, 5LPA, and 6LPA. For a certain  $N$ , it is sometimes impossible to build an MLPA because there are no pairwise coprime integers that satisfies (5-2). Similar curves in Figure 5-8 (a) indicate that only few holes appear in the difference coarray. The number of consecutive lags converges to the number of unique lags for the proposed MLPAs which is not the case for coprime array. The proposed array configurations always achieve more unique lags and consecutive lags as the number of subarrays decreases from  $N_p = 6$  to  $N_p = 3$  and vice-versa. The 3LPA and 4LPA almost realize more  $l_{ug}$  compared with coprime array for all  $N$ . The 3LPA attains the maximum possible  $l_{ug}$  and 6LPA achieves the minimum possible  $l_{ug}$  compared with others.

Figure 5-8 (b) demonstrates that as the array level decreases, the aperture size increases and vice-versa. The proposed configurations always have large number of consecutive lags compared with coprime arrays, see Figure 5-8 (a). The worst case (6LPA) achieves large  $l_{cg}$  which is more than four and half times of that realized by coprime array and even with smaller aperture. For comparison purpose, nested arrays are also included which have a hole-free difference coarray, i.e.  $l_{ug} = l_{cg}$  as Figure 5-8 (a) depicts. Nested arrays followed by coprime arrays need the largest aperture size among all configurations when  $N$  is fixed as Figure 5-8 (b) reveals. Nested array achieves 104 unique lags and 122 consecutive lags more compared with 3LPA configuration for  $N = 42$  sensors.

For equal aperture size, we can use Figure 5-8 (b) to determine the number of sensors and then use Figure 5-8 (a) to find the associated number of unique lags and number of consecutive lags. For example, when  $D = 132d$ , an MLPA with 3 levels requires 24 sensors to achieve 255 unique lags and 245 consecutive lags. On the other hand and for the same  $D$ , coprime arrays with 23 sensors realize 165 unique lags and only 47 consecutive lags. While nested arrays require 22 sensors and generate 263 unique and 263 consecutive lags. MLPA attains comparable DOFs of that of nested arrays with similar equal aperture size while reducing the mutual coupling effect.



(a) Maximum number of unique lags and maximum number of consecutive lags



(b) Maximum aperture size

**Figure 5-8:** MLPA features including 3LPA, 4LPA, 5LPA, and 6LPA versus the number of sensors

#### 5.7.4 Optimum Arrays

The optimum MLPA configurations are constructed for  $N_p = 3, 4, 5$ , and 6. The required inter-element spacing of the subarrays is plotted versus the total number of elements,  $N$ , in Figure 5-9, Figure 5-10, Figure 5-11, and Figure 5-12. There are a total of  $2N_p$  traces in each figure. Half of the traces maximizes the number of unique lags and the other half maximizes the number of consecutive lags. There are cases where (5-2) cannot be satisfied, like the cases of  $N = 11$  for 3LPA and  $N = 15$  for 4LPA. This explains the missing values in Figure 5-9 and Figure 5-10. For the same reason, there is a minimum number of elements after which MLPA configuration can be constructed namely  $N = 8$ , and 14 elements for 3LPA and 4LPA, respectively.

As demonstrated in Figure 5-9, except for the case with  $N = 23$  elements, a unique configuration jointly realizes the maximum  $l_{ug}$  and  $l_{cg}$ . This demonstrated by overlapping markers. The second subarray is always spaced by  $2d$  or  $3d$ . As a result, the first subarray consists of two or three elements ( $M_1 = 2$  or  $3$ ). The first subarray always has the maximum inter-element spacing of  $M_3d$ . Consequently, the best ordered inter-element spacing is  $\mathcal{S}_{3\text{LPA}} = [M_3, M_1, M_2]d$ . For the special case of  $N = 23$ ,  $\mathcal{S} = [11, 5, 9]d$  maximizes the unique lags, while the number of consecutive lags is maximized when  $\mathcal{S} = [17, 3, 5]d$ .

In most of the 4LPA, the joint optimization of unique and consecutive lags results in a unique design as depicted by the overlapping markers in Figure 5-10. There are four cases with multiple solutions highlighted in the figure with arrows. Table 5-9 summarizes the design alternatives for 4LPA. The case of  $N = 14$  or 18 elements has three design alternatives which jointly optimize the number of unique and consecutive lags as Table 5-9



illustrates. For  $N = 23$  elements, there are three design options to maximize the number of consecutive lags. The best option is when  $\mathcal{S} = [5, 3, 11, 7]d$  which also maximizes  $l_{ug}$ . Joint optimization cannot be achieved for  $N = 31$  elements. As the optimal ordered inter-element spacing for  $l_{cg}$  is  $\mathcal{S} = [5, 19, 3, 7]d$  which is not the same as the two design alternatives illustrated in Table 5-9 that maximizes  $l_{ug}$ .

In general, the second and the third subarrays have the maximum and the minimum inter-element spacing respectively in most of the considered scenarios. Therefore, the best ordered inter-element spacing is  $\mathcal{S}_{4\text{LPA}} = [M_2, M_4, M_1, M_3]d$ .

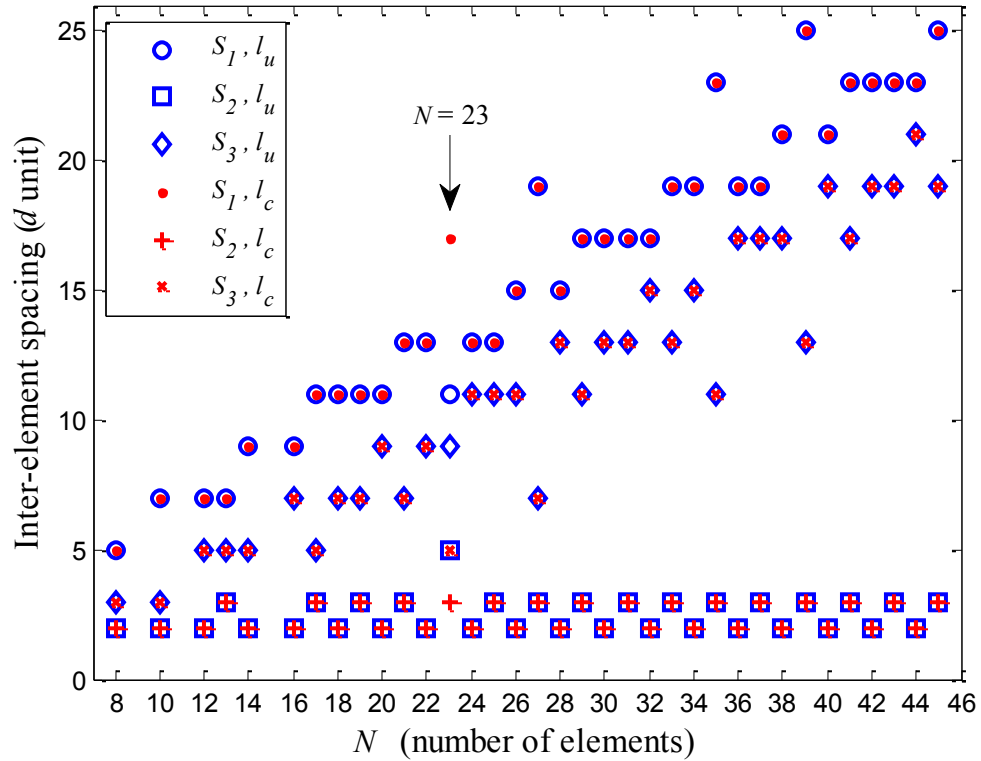


**Figure 5-9:** The optimal inter-element spacing versus  $N$  for 3LPA

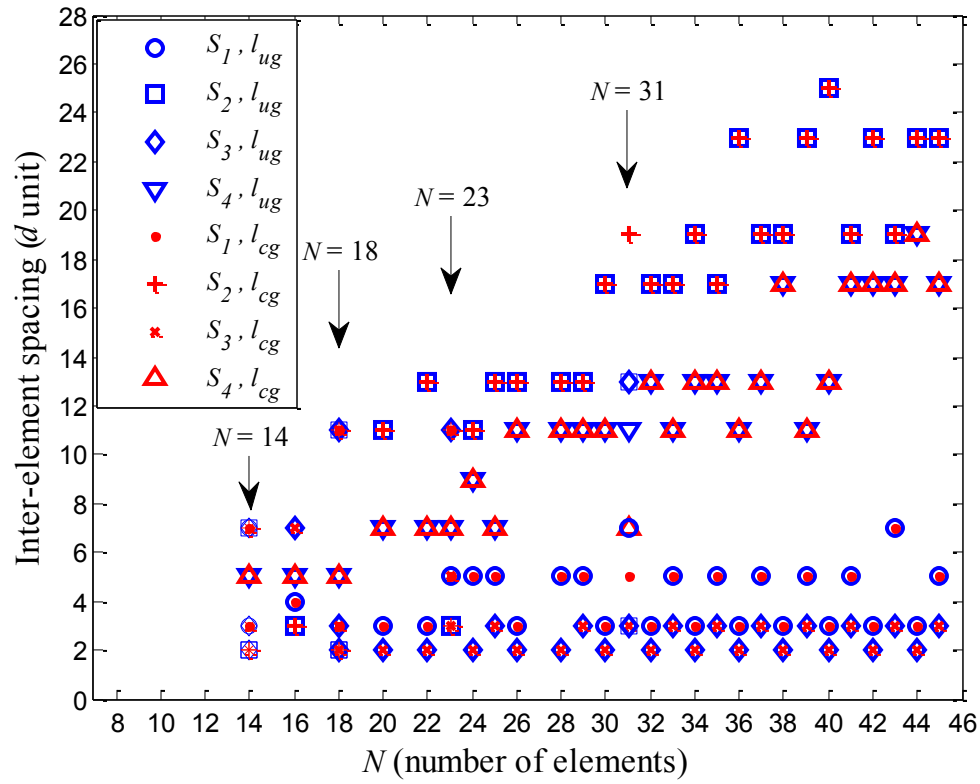
Figure 5-10: The optimal inter-element spacing versus  $N$  for 4LPA

Table 5-9: Design alternatives for 4LPA

$\mathcal{S}$ $N$	$\mathcal{S}_1$	$\mathcal{S}_2$	$\mathcal{S}_3$	$\mathcal{S}_4$	Lags
14	7	2	3	5	$l_{ug}, l_{cg}$
	3	7	2	5	
	3	2	7	5	
18	11	2	3	5	$l_{cg}$
	3	11	2	5	
	3	2	11	5	
23	11	3	5	7	$l_{ug}$
	5	11	3	7	
	<b>5</b>	<b>3</b>	<b>11</b>	<b>7</b>	
31	7	13	3	11	$l_{ug}$
	7	3	13	11	

In 5LPA, the number of design alternatives increases compared with 4LPA. Figure 5-11 specifies that  $\mathcal{S} = [5, 2, 17, 3, 13]d$  maximizes  $l_u$ , while the number of consecutive lags is maximized when  $\mathcal{S} = [5, 2, 19, 3, 11]d$  when  $N = 36$  elements. In Table 5-10, we present

only the design alternatives that maximize either  $l_{ug}$  or  $l_{cg}$ . For  $N = 30$  and 44 elements, one of those alternatives also jointly maximizes the number of consecutive lags as Figure 5-11 and Table 5-10 confirm. Joint optimization cannot be achieved for  $N = 32$  and 41 elements.

Others jointly maximize both lags are not included in the table because of the space. For example, the case of  $N = 28$  elements has six design alternatives which jointly maximize both lags. In addition, two design alternatives at  $N = 26, 35$  elements and three design alternatives when  $N = 24$  elements are jointly improve both lags. In Figure 5-11 and Table 5-10, most of the investigated scenarios have ordered inter-element spacing of  $\mathcal{S}_{5LPA} = [M_3, M_1, M_5, M_2, M_4]d$  or  $\mathcal{S}_{5LPA} = [M_3, M_1, M_2, M_5, M_4]d$ .

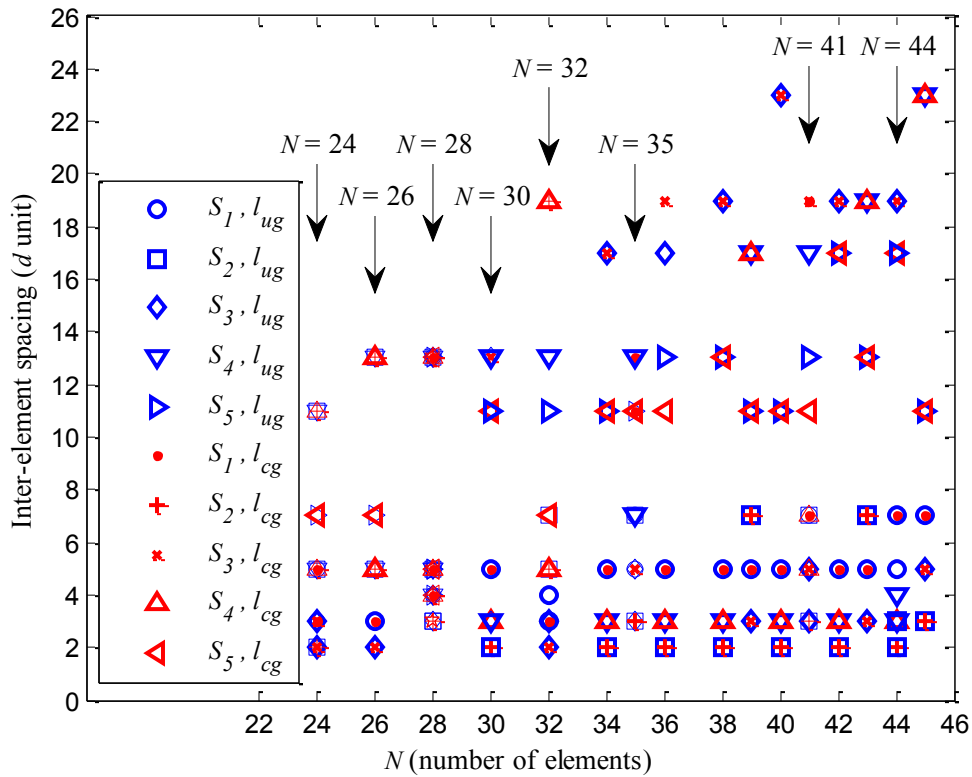


Figure 5-11: The optimal inter-element spacing versus  $N$  for 5LPA

Table 5-10: Design alternatives for 5LPA

$\begin{smallmatrix} \mathcal{S} \\ N \end{smallmatrix}$	$\mathcal{S}_1$	$\mathcal{S}_2$	$\mathcal{S}_3$	$\mathcal{S}_4$	$\mathcal{S}_5$	Lags
24	5	2	3	11	7	$l_{ug}, l_{cg}$
	3	5	2	11	7	
	3	11	2	5	7	
26	3	5	2	13	7	
	3	13	2	5	7	
28	13	3	4	5	7	
	5	3	13	4	7	
	5	3	4	13	7	
	4	5	3	13	7	
	4	13	3	5	7	
	4	3	13	5	7	
30	5	2	13	3	11	
	5	2	3	13	11	$l_{ug}$
32	3	7	2	13	11	$l_{ug}$
	4	5	3	13	11	$l_{ug}$
	3	5	2	19	7	$l_c$
	3	19	2	5	7	
35	7	3	5	13	11	$l_{ug}, l_{cg}$
	5	7	3	13	11	
41	7	3	5	17	13	$l_{ug}$
	5	7	3	17	13	
	19	3	5	7	11	$l_{cg}$
	7	3	19	5	11	
	5	19	3	7	11	
44	7	2	19	3	17	$l_{ug}$
	5	3	19	4	17	

Larger MLPA levels require large number of elements, 36 in case of 6LPA. The 6LPA with  $N = 42$  elements attains its maximum  $l_{ug}$  with  $\mathcal{S} = [7, 2, 3, 5, 17, 13]d$ , see Figure 5-12. On the other hand, it has got two ordered inter-element spacings that maximize  $l_{cg}$  as Table 5-11 depicts namely:  $\mathcal{S}_1 = [7, 2, 3, 5, 19, 11]d$  and  $\mathcal{S}_2 = [5, 2, 7, 3, 19, 11]d$  based on different  $\mathbf{m}$ .

Table 5-11: Design alternatives for 6LPA

$\begin{smallmatrix} \mathcal{S} \\ N \end{smallmatrix}$	$\mathcal{S}_1$	$\mathcal{S}_2$	$\mathcal{S}_3$	$\mathcal{S}_4$	$\mathcal{S}_5$	$\mathcal{S}_6$	Lags
36	7	2	3	5	13	11	$l_{ug}, l_{cg}$
	3	7	2	5	13	11	
38	7	3	4	5	13	11	$l_{ug}, l_{cg}$
	5	3	7	4	13	11	
	4	7	3	5	13	11	
	4	3	7	5	13	11	
42	7	2	3	5	19	11	$l_{cg}$
	5	2	7	3	19	11	

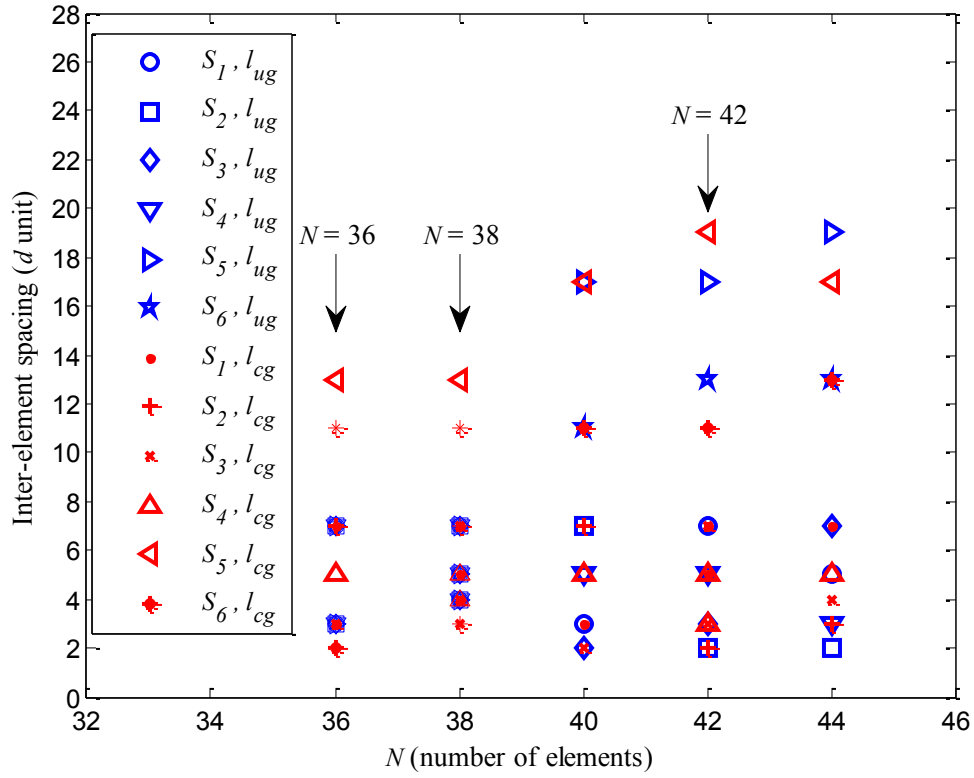


**Figure 5-12:** The optimal inter-element spacing versus  $N$  for 6LPA

### 5.7.5 Number of Unit Spacings

In Figure 5-13, the number of unit spacings,  $v_{\Delta}$ , for the 3LPA and 4LPA configurations is plotted as a function of the total number of elements. Nested arrays, super nested arrays, and coprime arrays are included for comparison. The value of  $v_{\Delta}$  is either 3 or 4 for the 3LPA regardless of the total number of elements. For the special case of  $N = 23$  elements, the configurations that maximizes the number of unique lags has  $v_{\Delta} = 4$ , while the other that maximizes the number of consecutive lags has  $v_{\Delta} = 3$ . In 4LPA,  $v_{\Delta}$  is oscillating between 5 and 9. There are some design alternatives that result in equal  $v_{\Delta}$  when  $N = 18$  and 23 elements. While, others generate different  $v_{\Delta}$  values as in  $N = 14$  and 31 elements.

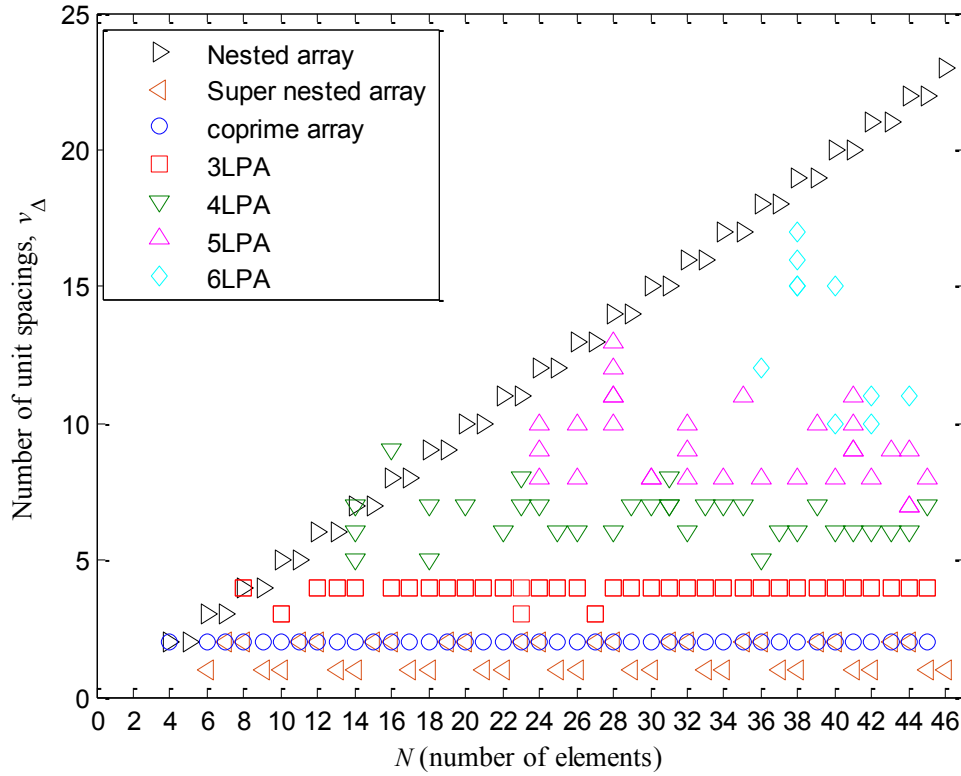


**Figure 5-13:** Number of unit spacings versus the total number of elements

In comparison, coprime arrays have two pairs of elements spaced by half wavelength, so  $v_{\Delta} = 2$ . The value of  $v_{\Delta}$  increases with the number of elements  $N$  in nested arrays [96], [97]. On the other hand, there is a maximum of two unit spacings for super nested arrays. The later was mainly proposed to mitigate the mutual coupling effect in nested arrays. The value of  $v_{\Delta}$  in 3LPA is not very far from that of coprime array. In addition, the 3LPA has fewer holes and it requires smaller aperture size [111].

#### 5.7.6 Upper Bound of the DOFs of 3LPA

The derived bounds according to Section 5.6 are plotted in Figure 5-14 versus the total number of antenna elements,  $N$ . To evaluate the derived upper bounds, the maximum number of unique lags (DOFs) achieved by each configuration is also included. In each

point of our simulation, we first find all possible  $\mathbf{m}$  vectors and then we adjust the ordered inter-element spacing either  $\mathcal{S}_A$  or  $\mathcal{S}_B$ . Based on  $\mathbf{m}$  and each inter-element spacing vector, we might end up with several configurations where we finally pick the one that maximizes the number of unique lags. The corresponding  $\mathbf{m}$  vector is used to find the upper bound in (5-43) and (5-45).

When  $N = 10$  as an example, we can construct the arrays with  $\mathbf{m}_1 = [2, 3, 7]$  or  $\mathbf{m}_2 = [3, 4, 5]$ . Based on  $\mathcal{S}_A = [M_2, M_3, M_1]d$  with  $\mathbf{m}_1$ , and with  $\mathbf{m}_2$ , we can have up to 27 unique lags. Thus, the one that maximizes the bound is selected. For the 3LPA Config.A and based on  $\mathbf{m}_1$ , we have  $\eta_1 = 1$ ,  $\eta_2 = 5$ ,  $\eta_3 = 19$ , and DOFs  $< 57$ . Whereas with  $\mathbf{m}_2$ ,  $\eta_1 = 1$ ,  $\eta_2 = 11$ ,  $\eta_3 = 17$ , and DOFs  $< 65$ . Consequently, the second vector is selected to find the upper bound.

While  $\mathcal{S}_B = [M_3, M_1, M_2]d$  with  $\mathbf{m}_1$  and with  $\mathbf{m}_2$  produce 35 and 29 unique lags, respectively. Thus, we pick  $\mathbf{m}_1$  and apply (5-45) to find the upper bound of the 3LPA Config.B which makes  $\eta_1 = 1$ ,  $\eta_2 = 1$ ,  $\eta_3 = 7$ , and DOFs  $< 73$ . Similar strategies are used and followed for any value of  $N$ .

Figure 5-14 confirms that the DOFs realized with  $\mathcal{S}_B$  is larger than that of  $\mathcal{S}_A$  because the former has larger aperture size. The derived bounds for both configurations are valid. Moreover, the bound of the 3LPA Config.B is a little bit tighter than that of the 3LPA Config.A for the same reason.

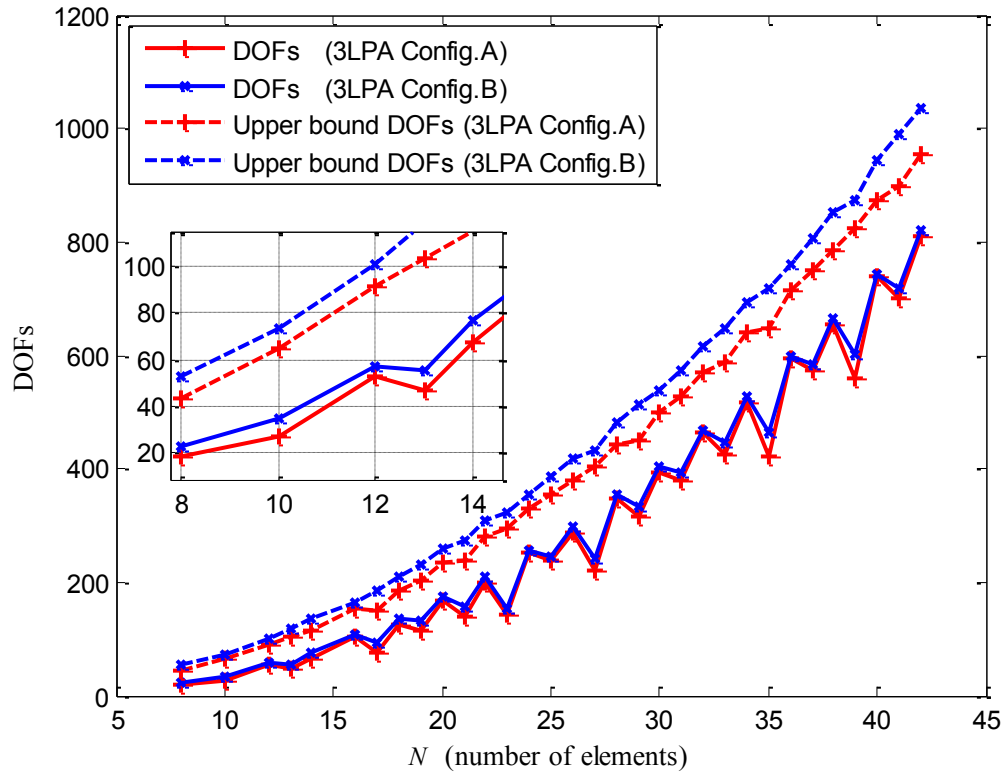


Figure 5-14: The upper bounds of the achievable DOFs for 3LPA Config.A and Config.B

## 5.8 Chapter Summary

In this chapter, new array configurations that can be used for sparse DOA estimation are proposed. The proposed MLPA uses multiple uniform linear subarrays where the number of sensors is pairwise coprime integers. The inter-element spacing between the sensors in each subarray equals to the number of the sensors of another subarray scaled by half-wavelength such that the subarrays share only their first sensor. It has been shown that there are more than one way to select the number of sensors in the subarrays and the ordered inter-element spacing, which result in different configurations of different features. The inter-element spacing and sensor selection are very important and have a direct impact on the achievable DOFs since they determine the entries of the difference coarray. Procedures



used for selecting the number of sensors and determining the number of ordered inter-element spacing as well as finding the best MLPA configuration are presented. The difference coarray of the proposed MLPA and its aperture have been derived. The performance of the proposed configurations was evaluated based on their difference coarray, DOFs, aperture size, number of unique lags, and number of consecutive lags. We have found that the proposed arrays need small aperture size and can achieve large DOFs. This is attractive in antenna designs and array implementations. The proposed configuration also has limited holes in the difference coarray which is similar to the advantage provided by nested arrays. The proposed array configurations tend to have more unique lags and more consecutive lags as the number of subarrays decreases and vice-versa. We have found that MLPAs can achieve higher DOFs compared with coprime arrays provided  $N$  is large enough through all  $N_p$  levels. Under equal aperture size and comparable DOFs with that of nested arrays, the proposed MLPA results in less mutual coupling effects when considered.

We have also found that there is a unique solution which jointly maximizes the number of unique lags and the number of consecutive lags which makes the optimum MLPA configuration unique. The number of design alternatives increases as the level of the array increases. In this case, multiple solutions realize the maximum number of lags and other factors like reduced mutual coupling can be used to make the final selection. In addition, we have derived an upper bound of the DOFs achieved by the 3LPA configurations. Simulation results are conducted to verify the derived bounds. Those bounds are also compared with the maximum achievable DOFs by each configuration.

## CHAPTER 6 SPARSE DOA ESTIMATION BASED ON MULTI-LEVEL PRIME ARRAY WITH COMPRESSION

Multi-level prime array (MLPA) uses multiple uniform linear subarrays where the number of elements in the subarrays are pairwise coprime integers. The MLPA requires smaller aperture size which is important in mobile applications. Different MLPA configurations can be constructed for a given number of antennas and the one that maximizes the DOFs is exploited. These configurations have a difference coarray with large number of consecutive lags and few holes. The number of consecutive lags can be increased by properly compressing the inter-element spacing of one subarray under a fixed number of antennas and without changing the aperture size. This chapter proposes a new compressed MLPA configuration and demonstrates its superior performance in sparse DOA estimation. The resultant array, MLPA with compressed subarray (MLPAC), can have a hole-free difference coarray as in nested array case. Sparse reconstruction algorithm is utilized based on the difference coarray. MLPAC can estimate larger number of sources using both MUSIC and sparse reconstruction algorithms. Simulation results confirm the achievable DOFs and the advantage of the proposed configuration in DOA estimation.

### 6.1 Introduction

Antenna arrays have many applications including improved signal reception, interference mitigation, and direction-of-arrival (DOA) estimation [28], [38], [39]. The accuracy of

DOA estimation depends on the signal characteristics at the array outputs, the array geometry, and the characteristics of the propagation medium<sup>2</sup>.

Recent works have been directed towards increasing the number of estimated sources or the DOFs to be greater than the number of elements. Array configurations that rely on the difference coarray including minimum redundancy arrays [91], minimum hole arrays [92], coprime arrays [52], and nested arrays [34] can achieve that. The achievable DOFs is determined by the properties of the difference coarray [33].

Minimum redundancy arrays (MRAs) [91] and minimum hole arrays [92] are nonuniform linear arrays generated respectively by maximizing the number of consecutive lags and minimizing the number of holes in the resulting difference coarray for a given number of antennas.

Coprime arrays has the ability to resolve  $\mathcal{O}(M_1 M_2)$  sources using  $M_1 + M_2 - 1$  elements [52], [53], [54], [55]. The optimal coprime pair is the one that has values of  $M_1$  and  $M_2$  as close as possible [56], [57]. To enhance the DOFs, doubling the number of elements of one subarray was suggested in [63]. A coprime array with compressed inter-element spacing and with displaced subarrays was proposed in [33]. With compression, the inter-element spacing for one subarray is reduced while with displacement, a proper shift is introduced between the two subarrays. Though, the mutual coupling effect and the aperture size are increased because of the compression and the displacement, respectively. Instead of processing the entire coprime array, the complexity of the estimation process can be

---

<sup>2</sup> There is an overlap in the review of this chapter and that of chapter 5. Readers who are familiar with that can skip to Section 6.2.

reduced by processing each subarray alone and then combine the results to reduce the ambiguities [112], [113], [114].

Nested arrays are constructed using collinearly dense and sparse uniform linear subarrays having  $M_1$  and  $M_2$  antenna elements respectively [34]. The antennas in the dense array are spaced by a unit inter-element spacing. The antennas in the sparse subarray are spaced by  $(M_1 + 1)$  units and the unit inter-element spacing is half-wavelength. Nested arrays always have a hole-free difference coarray. Although the array suffers from the mutual coupling effect, nested arrays can resolve  $\mathcal{O}(N^2)$  sources using  $N = M_1 + M_2$  antennas [34], [115], [116], [54], [117], [118]. The DOFs can be enhanced by increasing the separation between the dense and the sparse subarrays [119]. Nested arrays have larger DOFs compared with coprime arrays because the difference coarray for coprime arrays has some redundant lags [52]. The redundant entries can be exploited to reduce complexity of the estimation problem [120].

Array configurations using three linear subarrays were considered to improve the DOFs [104], [105], [106], [108], [121]. A Coprime array collinear with a ULA was suggested in [104]. The number of consecutive lags can be increased by properly selecting the location of the appended ULA, though large aperture size is required. In [105] and [106], three overlapped ULAs with coprime inter-element spacing was proposed. Compressed nested array was proposed in [121] by appending another similar sparse subarray to the other side of the dense subarray. This array improves the DOFs but at the expense of increased number of antennas and aperture size.

Generalizing the above to multi-level configurations which have more than three subarrays has received more attention recently. The coprime array in [33] was extended to multi-level coprime array [107]. Nested arrays was extended to multi-level in [34]. Fourth-level nested array, which can resolve  $\mathcal{O}(N^4)$  sources [94], was developed for narrowband [122] and wideband [123] DOA estimation. Super nested array [96], [95] which is a recent developed configuration of nested arrays was extended to multi-level in [97], [124]. To gain more from such generalization, the fourth order difference coarray statistics was exploited to increase the DOFs based on coprime arrays [104], [125] and nested arrays [121], [94], [126].

In addition to the spatial domain, the concept of sparsity was also implemented in the frequency domain for DOA estimation in radar applications [115], [127], [29], [101], [128], [129], [130]. Array configuration with two coprime frequencies was exploited in [127], [29]. The two subarrays used equal number of antennas,  $N$ , and the spacing was adjusted as an integer multiple of half-wavelength at both frequencies. The scheme in [127], [29] was extended to multiple coprime frequencies [101] where  $Q \geq 2$  signals are transmitted. The achievable DOFs was derived for two frequencies case [127], [101] and improved by properly selecting the coprime pairs and the number of antennas. The achievable DOFs was upper bounded and proportional to  $\mathcal{O}(N^2 Q^2)$  in case of multiple coprime frequencies [101]. Multi-frequency operation was also utilized to fill the missing lags in the difference coarray and consequently the DOFs was enhanced [131]. Though, this approach needs the sources to have large bandwidth to cover the exploited frequencies. The DOFs was enhanced by interpolating the holes that appear in the difference coarray [103], [132], [133], [134] and by exploiting the difference coarray and the sum coarray [102], [115].

Based on the above literature review, there is room to improve the performance of DOA estimation without increasing the aperture size which is very important in hand-held and mobile devices. In this chapter, sparse DOA estimation based on MLPAs is demonstrated. MLPA uses multiple uniform subarrays “or levels” where the number of antenna elements of the subarrays are pairwise coprime integers [111]. By selecting the number of antennas of the subarrays and controlling the inter-element spacing, various MLPAs of different features can be constructed. The configuration that realizes the maximum number of unique lags is recommended because the DOFs is upper bounded by the number of lags [33]. For DOA estimation, sparse reconstruction algorithms exploit all unique lags in the difference coarray whereas subspace-based algorithms such as MUSIC algorithm requires consecutive lags [33]. The MLPA configuration [111] is further optimized in order to increase the DOFs by compressing the inter-element spacing of one subarray but without changing the number of antennas nor the aperture size. A proper selected compression factor and a specific subarray can maximize the number of lags and results in a hole-free difference coarray. We demonstrate that large number of sources can be detected based on MLPA configurations using sparse reconstruction and MUSIC algorithms. The newly proposed compressed MLPA configuration can resolve larger number of sources compared with MLPA due to the increased number of lags.

The rest of the chapter is organized as follows. The system model is presented in Section 6.2 in which MLPA configuration is introduced followed by the model for DOA estimation. In Section 6.3, the compressed version of MLPA configuration is proposed. Simulation and results are presented in Section 6.4, and Section 6.5 concludes the chapter.

## 6.2 System Model

In this section, the generalized MLPA [111] that includes coprime [53] and Pythagorean [108] arrays as special cases is introduced briefly. Then the model for DOA estimation is presented.

### 6.2.1 Multi-Level Prime Array (MLPA)

An array configuration that combines multiple uniform linear subarrays located along the  $x$ -axis is referred to as “MLPA” [111]. An MLPA with  $N_p$  subarrays or a level has  $M_i$  antenna elements within the  $i^{th}$  subarray where the number of elements in the subarrays are pairwise coprime integers. The elements of the  $i^{th}$  subarray are located at:  $\mathbb{P}_i = k_i \mathcal{S}_i d$  where  $0 \leq k_i \leq M_i - 1$  and  $\mathcal{S}_i d$  is the inter-element spacing which equals to multiple units of half-wavelength. The inter-element spacing of all  $N_p$  subarrays can be ordered and combined in a vector of unique entries,  $\mathcal{S} = [\mathcal{S}_1, \mathcal{S}_2, \dots, \mathcal{S}_{N_p}] d$ . More details are presented in Section 5.2.1.

When the number of subarrays is  $N_p = 2, 3$ , or  $4$ , we refer to the array as coprime array, 3LPA, or 4LPA respectively. For a given number of antenna elements,  $N$ , and MLPA level,  $N_p$ , there could be multiple  $\mathbf{m}$  vectors that satisfy (5-2) and multiple ordered inter-element spacing for each  $\mathbf{m}$ . Thus, several MLPA configurations can be constructed. The generalized MLPA covers special cases like the Pythagorean array (PA) [108] which is a special case of the 3LPA when the entries of  $\mathbf{m}$  are also primitive Pythagorean triple,  $M_1^2 + M_2^2 = M_3^2$ . In case of two subarrays ( $N_p = 2$ ), it becomes a coprime array [52].

Table 6-1: The ordered inter-element spacing for different MLPA levels

Configurations	Coprime Array	3LPA	4LPA	5LPA
Levels ( $N_p$ )	2	3	4	5
$\mathbf{m}$	$[M_1, M_2]$	$[M_1, M_2, M_3]$	$[M_1, M_2, M_3, M_4]$	$[M_1, M_2, M_3, M_4, M_5]$
Inter-Element Spacing	$\mathcal{S}_1$	$[M_2, M_1]d$	$[M_2, M_3, M_1]d$	$[M_4, M_1, M_2, M_3]d$
	$\mathcal{S}_2$	$[M_3, M_1, M_2]d$	$[M_2, M_4, M_1, M_3]d$	$[M_5, M_1, M_2, M_3, M_4]d$
	$\mathcal{S}_3$		$[M_3, M_1, M_4, M_3]d$	$[M_4, M_1, M_2, M_5, M_3]d$
	$\mathcal{S}_4$		$[M_2, M_1, M_4, M_3]d$	$[M_3, M_1, M_5, M_2, M_4]d$
	$\mathcal{S}_5$		$[M_3, M_1, M_4, M_3]d$	$[M_3, M_1, M_2, M_5, M_4]d$
	$\mathcal{S}_6$			$[M_2, M_4, M_1, M_5, M_3]d$
	$\mathcal{S}_7$			$[M_2, M_3, M_1, M_5, M_4]d$
	$\mathcal{S}_8$			$[M_2, M_5, M_1, M_3, M_4]d$
	$\mathcal{S}_9$			$[M_2, M_1, M_5, M_3, M_4]d$
				$[M_2, M_1, M_4, M_5, M_3]d$

Table 6-1 lists the ordered inter-element spacing for different MLPA levels. Higher MLPA levels can be also constructed for large  $N$ . For a given  $\mathbf{m}$ , there exists one coprime array, two 3LPAs, four 4LPAs, and nine 5LPAs. For example, a 3LPA with  $N = 12$  can be constructed using either  $\mathbf{m}_1 = [3, 4, 7]$  or  $\mathbf{m}_2 = [2, 5, 7]$ . Based on each vector, two different 3LPAs can be constructed by setting the ordered inter-element spacing as  $\mathcal{S}_1 = [M_2, M_3, M_1]d$  or  $\mathcal{S}_2 = [M_3, M_1, M_2]d$ , see Table 6-1.

### 6.2.2 DOA Signal Model

Assume that there are  $K$  uncorrelated narrowband signals impinging on an array with  $N$  elements from DOAs  $\boldsymbol{\theta} = [\theta_1, \theta_2, \dots, \theta_K]^T$ , see Figure 4-2. The received signal,  $\mathbf{y}(t) = [y_1(t), y_2(t), \dots, y_N(t)]^T$ , at the array output over  $T$  samples can be expressed as:

$$\mathbf{y}(t) = \mathbf{A}(\boldsymbol{\theta})\mathbf{s}(t) + \mathbf{n}(t) \quad (6-1)$$



$$t \in \{t_1, t_2, \dots, t_T\}$$

where  $\mathbf{s}(t) = [s_1(t), s_2(t), \dots, s_K(t)]^T$  is the transmitted signal vector of size  $K \times 1$ ,  $\mathbf{A}(\boldsymbol{\theta}) = [\mathbf{a}(\theta_1) \quad \mathbf{a}(\theta_2) \quad \dots \quad \mathbf{a}(\theta_K)]$  is the steering matrix of size  $N \times K$ , and  $\mathbf{n}(t)$  is the white Gaussian complex noise vector of size  $N \times 1$  whose elements are assumed to be independent and identically distributed (i.i.d.) with zero-mean and variance  $\sigma_n^2$ . Let  $p_i d \in \mathbb{P}$  represents the position of the  $i^{th}$  antenna element along the array axis with  $p_1 = 0$  as a reference. When all sources are located in the far-field, the steering vector can be expressed as [33]:

$$\mathbf{a}(\theta_i) = [1, \exp(j2\pi p_2 d \sin(\theta_i) / \lambda), \dots, \exp(j2\pi p_N d \sin(\theta_i) / \lambda)]^T \quad (6-2)$$

The received signal can be written in a matrix format as:

$$\mathbf{Y} = \mathbf{A}(\boldsymbol{\theta})\mathbf{S} + \mathbf{N} \quad (6-3)$$

where  $\mathbf{Y} = [\mathbf{y}(t_1), \dots, \mathbf{y}(t_T)]$ ,  $\mathbf{N} = [\mathbf{n}(t_1), \dots, \mathbf{n}(t_T)]$  are matrices of size  $N \times T$  and  $\mathbf{S} = [\mathbf{s}(t_1), \mathbf{s}(t_2), \dots, \mathbf{s}(t_T)]^T$  is a matrix of size  $K \times T$ . When the noise is assumed to be uncorrelated with all sources the covariance matrix of the received signal is given by:

$$\mathbf{R}_{\mathbf{Y}\mathbf{Y}} = \mathbb{E}[\mathbf{Y}\mathbf{Y}^H] = \mathbf{A}\mathbf{R}_{\mathbf{S}\mathbf{S}}\mathbf{A}^H + \sigma_n^2 \mathbf{I}_N \quad (6-4)$$

where  $\mathbf{R}_{\mathbf{S}\mathbf{S}} = \mathbb{E}[\mathbf{S}\mathbf{S}^H] = \text{diag}([\sigma_1^2, \sigma_2^2, \dots, \sigma_K^2])$  represents the covariance matrix of the transmitted signal where  $(\cdot)^H$  is the conjugate transpose and  $\sigma_i^2$  is the signal power of the  $i^{th}$  source,  $i = 1, 2, \dots, K$ . Given the received data  $\mathbf{Y}$  and the array geometry, our objective is to estimate the DOAs,  $\hat{\boldsymbol{\theta}}$ . The matrix  $\mathbf{R}_{\mathbf{Y}\mathbf{Y}}$  can be estimated as:

$$\hat{\mathbf{R}}_{\mathbf{Y}\mathbf{Y}} = \frac{1}{T} \sum_{i=1}^T \mathbf{y}(t_i) \mathbf{y}^H(t_i) = \frac{1}{T} \mathbf{Y} \mathbf{Y}^H \quad (6-5)$$

### 6.3 Multi-Level Prime Array With Compressed Subarray (MLPAC)

The advantage of MLPA configuration can be demonstrated through its difference coarray. Consider an MLPA configuration with  $N$  antenna elements. The pairwise differences of the array can be expressed as:

$$\mathbb{D} = \{p_i - p_j | p_i d, p_j d \in \mathbb{P}\} \quad (6-6)$$

The difference coarray,  $\mathbb{D}_u$ , is defined as the set of distinct or unique integers in the set  $\mathbb{D}$ . Applications that rely on the correlation depend on all distinct virtual lags given by the difference coarray. The achievable DOFs which is a measure of the maximum number of sources that can be estimated in DOA applications is related to the number of unique lags in  $\mathbb{D}_u$ . The weight function,  $w(l_D)$ , where  $l_D \in \mathbb{D}$ , is defined as the number of occurrences of every lag in  $\mathbb{D}$ .

The array structure and the corresponding weight function for the 3LPA with  $N = 16$ ,  $\mathbf{m} = [4, 5, 9]$ , and  $\mathcal{S}_2 = [9, 4, 5]d$  are plotted in Figure 6-1 (a). The symmetric difference coarray has 69 unique lags,  $l_{ug}$ , and 57 consecutive lags,  $l_{cg}$ . There are few missing lags (holes) in addition to some redundant lags as demonstrated by the weight function. There is room to improve the weight distribution to realize larger DOFs which motivates us to modify the MLPA.

The DOFs of the MLPA can be enhanced by compressing the inter-element spacing while maintaining the number of antennas and aperture size fixed. Therefore, the subarray that affects the number of antennas or the aperture size as in (5-3) should not be compressed. If the  $i^{th}$  entry in  $\mathbf{m}$  can be factored into two integers  $c$  and  $\tilde{M}_i$ , that is  $M_i = c\tilde{M}_i$ , then the inter-element spacing of the subarray spaced by  $M_i d$  can be compressed by a factor,  $c$ . When  $M_i$  is a prime number, the only nontrivial compression factor is  $c = M_i$ . Since  $\mathbf{m}$  contains pairwise coprime integers,  $\tilde{M}_i$  is also coprime with all remaining entries.

For a given MLPA, our objective is to find the proper subarray to be compressed and the value of the compression factor that increases the number of consecutive lags which is a function of  $\mathbf{m}$  and  $\mathcal{S}$ . The optimization operation can be expressed as:

$$(M_i, c) = \underset{M_i, c \in \mathbb{Z}^+}{\operatorname{argmax}} \{l_{cg}(\mathbf{m}, \mathcal{S})\} \quad (6-7)$$

subject to:

$$M_i \neq \begin{cases} M_{N_p}, & \mathcal{S}_{N_p-1}(M_{N_p-1} - 1) < \mathcal{S}_{N_p}(M_{N_p} - 1), \forall i \in \{1, 2, \dots, N_p\} \\ M_{N_p-1}, & \text{otherwise} \end{cases}$$

$$N = \sum_{i=1}^{N_p} M_i - (N_p - 1)$$

where  $\mathbb{Z}^+$  is the set of positive integers. The first constraint avoids compressing the subarray that determines the aperture size. The second constraint ensures that the number of elements are the same for both MLPA and its compressed version. The optimized compressed subarray results in larger number of consecutive and unique lags. It may also result in hole-free difference coarray.

The resultant array is referred to as MLPA with compressed subarray (MLPAC). The ordered inter-element spacing of the proposed MLPAC is the same as the corresponding MLPA except that the inter-element spacing of the compressed subarray becomes  $\mathcal{S}_i d/c$ . Therefore, the location of the antenna elements of the  $i$ th compressed subarray,  $\mathbb{P}_i$ , is given by:

$$\mathbb{P}_i = \bigcup_{k=0}^{M_i-1} \{k\mathcal{S}_i/c \mid \mathcal{S}_i \neq M_i\} \quad (6-8)$$

For notation purposes, we start with the number of levels,  $N_p$ , then “LPA” and in case of compression, we append the letter “C” indicating compression and two additional digits indicating the compressed subarray number and the compression factor “ $N_p$ LPAC $i$  $c$ ”. As an example, consider the 3LPA configuration with  $\mathbf{m} = [4,5,9]$  and ordered inter-element spacing  $\mathcal{S}_2 = [9,4,5]d$  shown in Figure 6-1: (a). According to (5-3), the required aperture size is determined by the third subarray,  $D = \max(4(5-1)d, 5(9-1)d) = 40d$ . Therefore, the third subarray cannot be compressed while maintaining equal aperture size. There is a possibility to compress the first or the second subarrays. If the first subarray is compressed, the ordered inter-element spacing becomes  $\mathcal{S}_2 = [9/c, 4, 5]d$  with  $c = 3$  or  $c = 9$ . The corresponding arrays are referred to as 3LPAC13 and 3LPAC19, respectively. The arrays structure and the corresponding weight functions are illustrated in Figure 6-1 (b) and (c). In the second alternative compression, the ordered inter-element spacing can be  $\mathcal{S}_2 = [9, 4/c, 5]d$  with  $c = 2$  or  $c = 4$  which corresponds to 3LPAC22 and 3LPAC24, respectively.

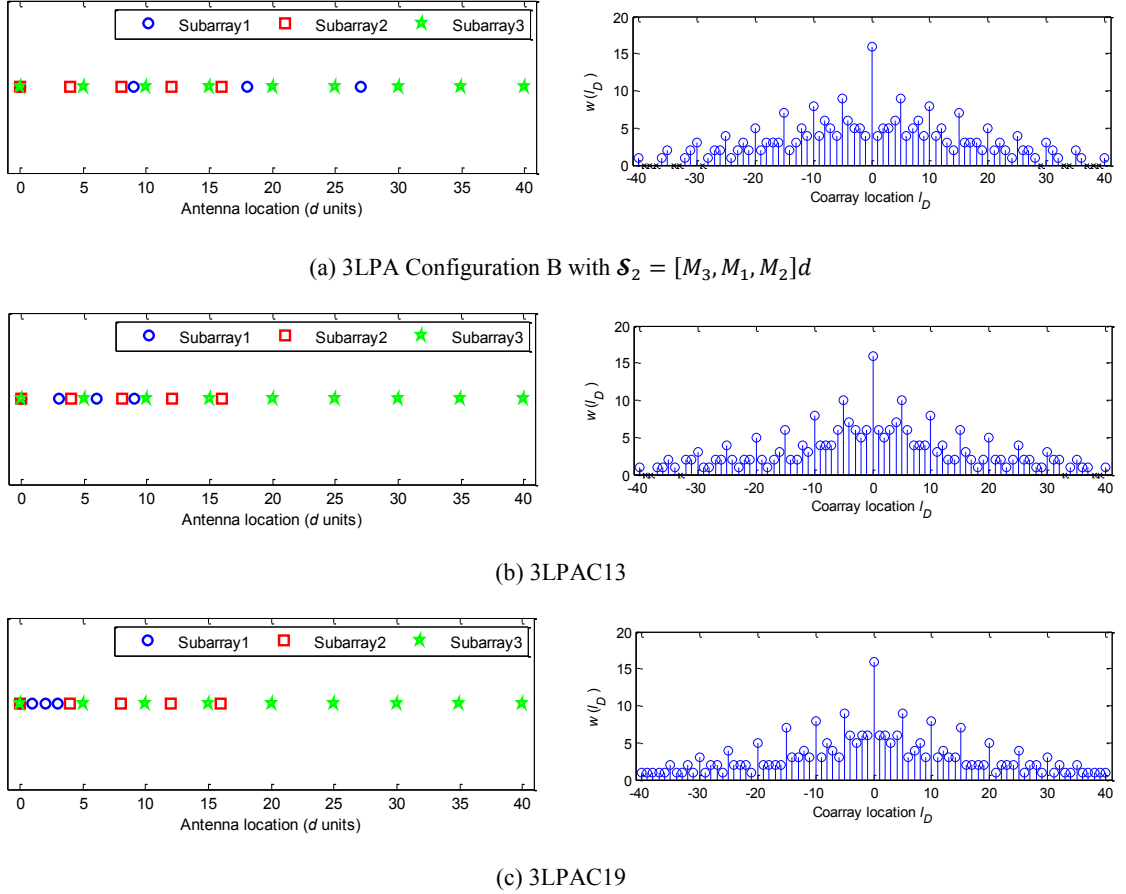


**Figure 6-1:** The 3LPA and 3LPAC configurations and the corresponding weight

Although 3LPA has large number of consecutive lags, twelve missing lags appear in the corresponding weight function, see Figure 6-1 (a). Through compression, the weight function has been redistributed and some of the redundant lags were moved to the missing lags as shown in Figure 6-1 (b) and (c). The 3LPAC19 and 3LPAC24 achieve hole-free difference coarrays where all lags are unique and consecutive. The price paid for this improvement is the reduction in the inter-element spacing of the compressed subarray.

In Table 6-2, Table 6-3, and Table 6-4 the 3LPA, 3LPAC, 4LPA, and 4LPAC configurations are compared in terms of the aperture size, number of unique lags, and number of consecutive lags. The conventional coprime arrays [33], [56], [57] and nested arrays [34] that achieve the maximum DOFs are also included. A total of  $N = 10$  antenna

elements are used to construct 3LPA and PA configurations. All 3LPA and PA configurations in Table 6-2 have larger number of consecutive lags and requires smaller aperture size compared with coprime array and nested array at the expense of reduced number of unique lags.

In Table 6-3, we increase the number of antennas to  $N = 12$  elements. As the aperture size of the 3LPA increases, the number of unique lags and the number of consecutive lags increase. We can achieve larger number of unique lags with smaller aperture size compared with that of coprime array and the number of consecutive lags is almost doubled. There are some 3LPAC and PA with compressed subarray (PAC) configurations which achieve hole-free difference coarrays.

With  $N = 14$ , four 4LPA configurations can be constructed by selecting the ordered inter-element spacing as shown in Table 6-4. Although three 4LPA configurations have different inter-element spacing and antenna locations, they result in equivalent difference coarrays where  $D = 30d$ ,  $l_{ug} = 59$ , and  $l_{cg} = 57$ . Few holes appear in the difference coarray which can be removed through compression. The number of consecutive lags can be improved using different compression factors. As a result, 4LPAC configurations with hole free difference coarrays are realized. Note that, the number of unique lags in all considered cases of Table 6-2, Table 6-3, and Table 6-4 are increased as well.

Table 6-2: Comparison between array's characteristics for  $N = 10$

Configuration	$\mathbf{m}$	Compressed Subarray	$c$	$\mathcal{S}$	$D$	$l_{ug}$	$l_{cg}$
Nested array	as in Ref. [34]	NA		as in Ref. [34]	$29d$	59	59
Coprime array	$\mathbf{m} = [5,6]$	NA		$[6,5]d$	$25d$	39	21
3LPA	$\mathbf{m}_1 = [2,3,7]$	NA		$[7,2,3]d$		35	33
3LPAC17		1	7	$[1,2,3]d$	$18d$	37	37
3LPAC22		2	2	$[7,1,3]d$			
3LPA	Config.B	NA		$[3,7,2]d$	$14d$	27	25
3LPAC		1	3	$[1,7,2]d$		29	29
PA	$\mathbf{m}_2 = [3,4,5]$	NA		$[5,3,4]d$		29	27
PAC15		1	5	$[1,3,4]d$	$16d$	33	33
PAC23		2	3	$[5,1,4]d$			
PA		NA		$[4,5,3]d$		27	25
PAC12		1	2	$[2,5,3]d$	$15d$	29	27
PAC14	Config.B	1	4	$[1,5,3]d$		31	31

Table 6-3: 3LPA and 3LPAC characteristics for  $N = 12$

Configuration	$\mathbf{m}$	Compressed Subarray	$c$	$\mathcal{S}$	$D$	$l_{ug}$	$l_{cg}$
Nested array	as in Ref. [34]	NA		as in Ref. [34]	$41d$	83	83
Coprime array	$\mathbf{m} = [6,7]$	NA		$[7,6]d$	$36d$	53	25
3LPA	$\mathbf{m}_1 = [3,4,7]$	NA		$[7,3,4]d$		43	37
3LPAC17		1	7	$[1,3,4]d$	$24d$	49	49
3LPAC23		2	3	$[7,1,4]d$			
3LPA	Config.B	NA		$[4,7,3]d$		37	31
3LPAC12		1	2	$[2,7,3]d$	$21d$	41	39
3LPAC14		1	4	$[1,7,3]d$		43	43
3LPA	Config.C	NA		$[7,2,5]d$		57	53
3LPAC17		1	7	$[1,2,5]d$	$30d$	59	53
3LPAC22		2	2	$[7,1,5]d$		61	61
3LPA	Config.D	NA		$[5,7,2]d$	$28d$	53	49

Table 6-4: 4LPA and 4LPAC characteristics for  $N = 14$

Configuration	$\mathbf{m}$	Compressed Subarray	$c$	$\mathcal{S}$	$D$	$l_u$	$l_c$
Nested array	as in Ref. [34]	NA		as in Ref. [34]	$71d$	143	143
Coprime array	$\mathbf{m} = [7,8]$	NA		$[8,7]d$	$49d$	69	29
4LPA	$\mathbf{m} = [2,3,5,7]$	NA		$[7,2,3,5]d$		59	57
4LPAC17		1	7	$[1,2,3,5]d$		61	61
4LPA		NA		$[3,7,2,5]d$	$30d$	59	57
4LPA	Config.C	NA		$[3,2,7,5]d$		59	57
4LPAC22		2	2	$[3,1,7,5]d$		61	61
4LPA	Config.D	NA		$[5,2,7,3]d$		53	39
4LPAC15		1	5	$[1,2,7,3]d$	$28d$	55	45
4LPAC22		2	2	$[5,1,7,3]d$		55	47

## 6.4 Simulation and Results

This section verifies the effectiveness of the proposed configuration in DOA estimation. Narrowband and uncorrelated sources located in the far-field are assumed. The sources are uniformly distributed between  $-60^\circ$  and  $60^\circ$  and their number is greater than the number of antenna elements,  $K > N$ . Isotropic antenna elements are assumed in all simulations. For comparison with Ref. [33], the grid search is uniform with a step size of  $0.25^\circ$  within  $[-90^\circ, 90^\circ]$ , number of samples is  $T = 1000$ , and the unit inter-element spacing is set to  $d = \lambda/2$ . All these parameters are fixed unless stated otherwise. Both MUSIC [33], [34] and CS algorithms are used for DOA estimation. CS based on Yall1 [135] is used due to its fast computation compared with Lasso which implemented on CVX toolbox. The maximum number of correctly estimated sources using the generalized MLPA and MLPAC is evaluated with numerical examples. The performance of the proposed configurations is further evaluated based on Monte Carol simulations.

### 6.4.1 Impact of Compression on the DOFs

In this subsection, the results are examined in terms of the maximum number of sources that can be estimated using MLPA and MLPAC configurations. A total of  $T = 1000$  noise free samples are used.

Figure 6-2 shows the spatial spectra estimated using MUSIC (upper subplots) and CS (lower subplots) algorithms for the PA (column 1), PAC15 (column 2), and PAC23 (column 3) Config.A with  $N = 10$  elements when  $K = 16$  sources. In all figures, the estimated spatial spectra are plotted versus the DOA in degrees where the actual DOAs are indicated by dotted vertical lines.



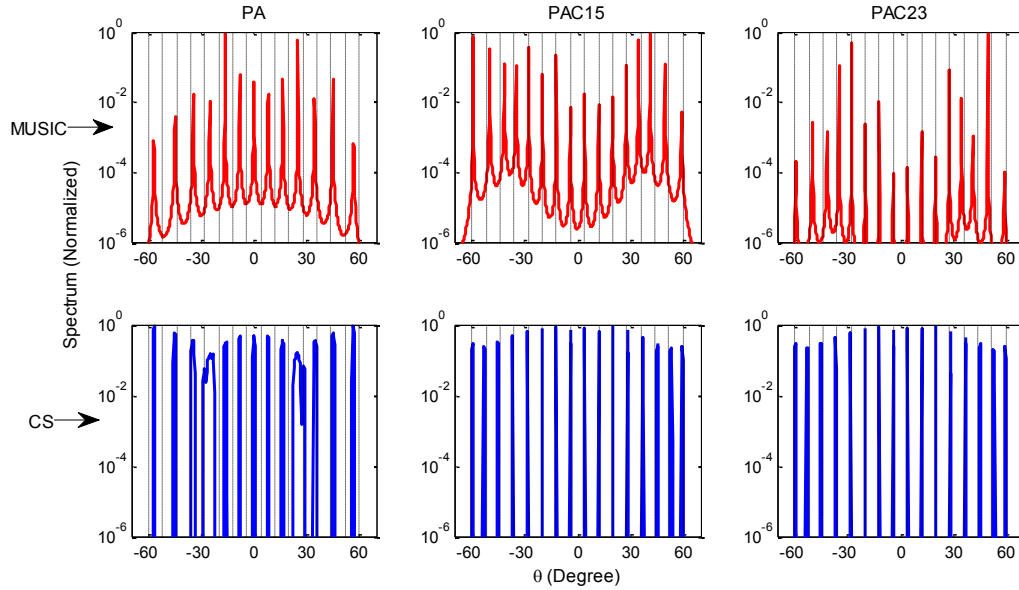


**Figure 6-2:** Spatial spectra estimated using MUSIC (upper subplots) and CS (lower subplots) algorithms for PA (column 1), PAC15 (column 2), and PAC23 (column 3) Config.A using  $N = 10$  and with  $K = 16$

Based on Table 6-2, configurations with DOFs larger than 16 can estimate all sources. For MUSIC algorithm, only half the number of consecutive lags can be exploited. In case of CS algorithm, higher number of sources can be estimated because all unique lags are utilized. Therefore, for the same configuration, the performance using CS algorithm is better than that with MUSIC algorithm (row 1 and row 2). On the other hand, the performance is improved after compression (column 2 and 3) compared with that of PA (column 1). Consequently, PAC configurations can resolve all the 16 sources correctly, while PA cannot due to its small DOFs as shown in Figure 6-2.

#### 6.4.2 Statistical Error Analysis

The effectiveness of the proposed configurations is further verified through Monte Carlo simulations. A grid refinement is applied to find the RMSE as defined in Section 4.3.5. According to our assumption that the sources are uniformly distributed between  $-60^\circ$  and  $60^\circ$ , any two adjacent sources are separated by:

$$\Delta_{\theta} = \frac{120}{K-1} \quad (6-9)$$

This makes any two adjacent sources spaced by  $\lfloor \Delta_{\theta} / \theta_i^g \rfloor$  grid points where  $\lfloor . \rfloor$  denotes the floor operation. In our simulation, we use  $I_{iter} = 5000$  independent trials. The RMSE is evaluated as a function of the SNR, number of samples,  $T$ , and grid refinement,  $\delta$ .

#### A. RMSE versus SNR

Array configurations are compared with respect to the SNR using MUSIC and CS algorithms with a grid refinement of  $\delta = 3$  grid points. The results are presented in Figure 6-3 where we divide the figure into four subplots (a)-(d). The performance of the selected MLPA configuration and its compressed versions are plotted in the same subplot. The performance of each array configuration and its compressed versions is plotted in the same subplot using MUSIC and CS algorithms, respectively. In addition, coprime array and nested array are included and plotted for comparison purposes in subplot (b) and (d), respectively. In the following figures, similar colors and similar markers within a subplot or a figure denote the same array configuration where the dotted and solid lines represent the performance using MUSIC and CS algorithms, respectively.

The RMSE of the configurations presented in Table 6-2 is plotted versus the SNR in Figure 6-3 using MUSIC and CS algorithms for  $K = 12$  sources. In this case, all sources are located on the grid search. Based on Figure 6-3, it is evident that the performance improves as the SNR increases for all cases using both algorithms. Smaller RMSE was realized using CS algorithm (solid lines) as Figure 6-3 shows compared with that using MUSIC algorithm (dotted lines) based all configurations. Since MUSIC algorithm utilizes only half the number of consecutive lags and CS algorithm uses all unique lags. The

performance of the 3LPA in Figure 6-3 (a) is better than that of PA configurations presented in Figure 6-3 (c) and (d) since it has got more unique lags. Nested array achieves the best performance because it achieves the largest number of lags. Coprime array has the worst RMSE using MUSIC algorithm due to the low number of consecutive lags, see Figure 6-3 (b). Though, nested and coprime arrays require larger aperture size as demonstrated in Table 6-2 and Table 6-3.

With compression, the RMSE for all corresponding configurations have been improved as demonstrated in Figure 6-3. The difference between the RMSE of a 3LPA and that of its compressed versions is a function of the difference in the number of lags. For example, this difference is only two lags for the 3LPA Config.A and its compressed versions, see Table 6-2. Although the performance has enhanced, the RMSE of all configurations are comparable as shown in Figure 6-3 (a). While, it is four lags for the PA Config.A and its compressed versions which leads to evident improvement in the performance. After applying compression for the PA Config.A, the RMSE was reduce by around  $3.63^\circ$  and  $3.92^\circ$  using CS at SNR = -3 dB based on the PAC15 and PAC23, respectively. On the other hand, the RMSE was decreased by around  $9^\circ$  at SNR = 6 dB using MUSIC algorithm based on both the PAC15 and PAC23. Both 3LPAC17 and 3LPAC22 Config.A realize similar RMSE which is the minimum RMSE among all proposed configurations as shown in Figure 6-3 (a) since they have got the largest number lags. To realize a RMSE of  $1^\circ$  with CS algorithm, MUSIC algorithm requires more than 6 dB SNR based on the compressed versions of the 3LPA Config.A. due to the lack of lags. The large errors floor in Figure 6-3 (b) and (d) are due to the lack of lags in the corresponding configurations. At 0 dB SNR, the RMSE based on the 3LPAC17 and 3LPAC22 Config.A is larger than that based on

nested array by around  $0.05^\circ$  using CS algorithm. On the other hand, it is around  $2^\circ$  and  $2.6^\circ$  larger based on the 3LPAC22 and 3LPAC17 Config.A respectively using MUSIC algorithm. Though, the proposed configurations require smaller aperture size by  $11d$ .

Similarly, the RMSE of the 3LPA configurations presented in Table 6-3 is plotted versus the SNR in Figure 6-4 for  $K = 15$  sources using MUSIC and CS algorithms. In this case, we have off-grid sources. The compressed versions in Figure 6-4 (a) have equal number of lags and attain similar RMSE at around SNR = 2 dB. Although, comprssing the inter-element spacing led to higher number of consecutive lags, the improvement in the RMSE is not significant of the 3LPA Config.C and its comprssed versions due to the small difference in the number of consecutive lags. This is not the case with the remaing configurations. Generally speacking, the results match what we have summarized in Table 6-3. Using CS algorithm, the improvement in the RMSE of the compressed versions of the 3LPA Config.A is very clear as Figure 6-4 (a) demonstrates. Those configurations have got six unique lags more compared with the corresponding 3LPA configuration. The performances of the compressed versions in Figure 6-4 (c) are affected differently. A reduction in the RMSE can be related to the enhancement in the number of unique lags, while degradation in the RMSE is as a result of wrong estimation for some lags and the corresponding measurement. The large error floor in Figure 6-4 (b) is due to the lack of lags in the corresponding configurations.

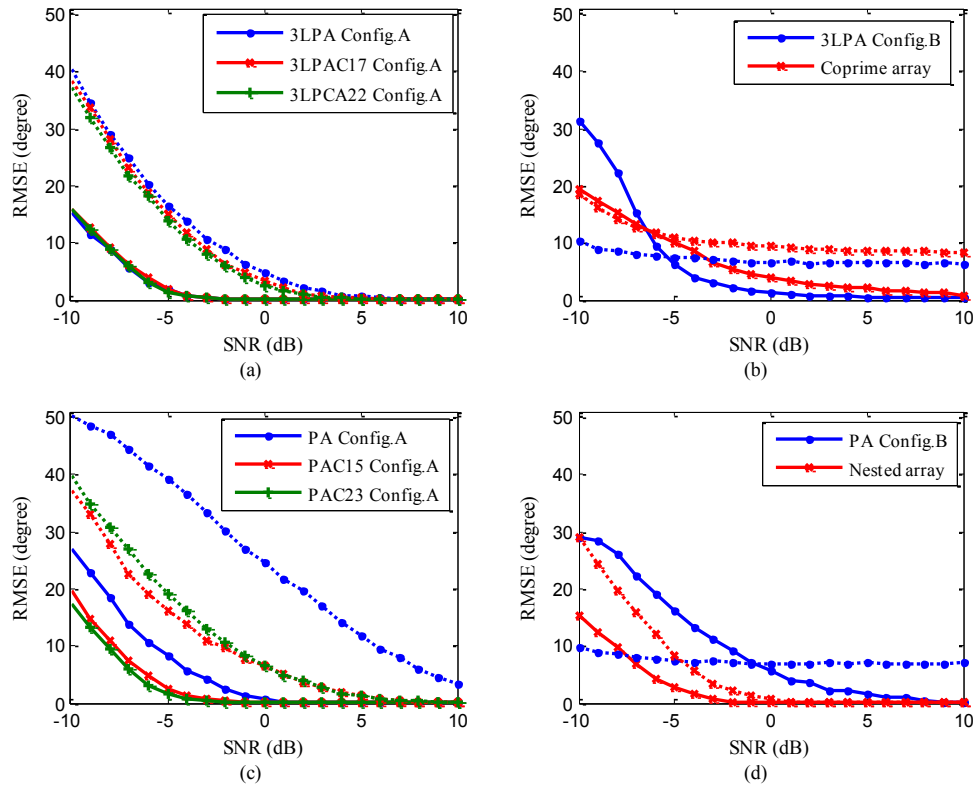


**Figure 6-3:** RMSE versus SNR for (a)-(b) 3LPA and 3LPAC (c)-(d) PA and PAC with  $K = 12$  sources, and  $N = 10$ . MUSIC (dotted lines) and CS (solid lines)

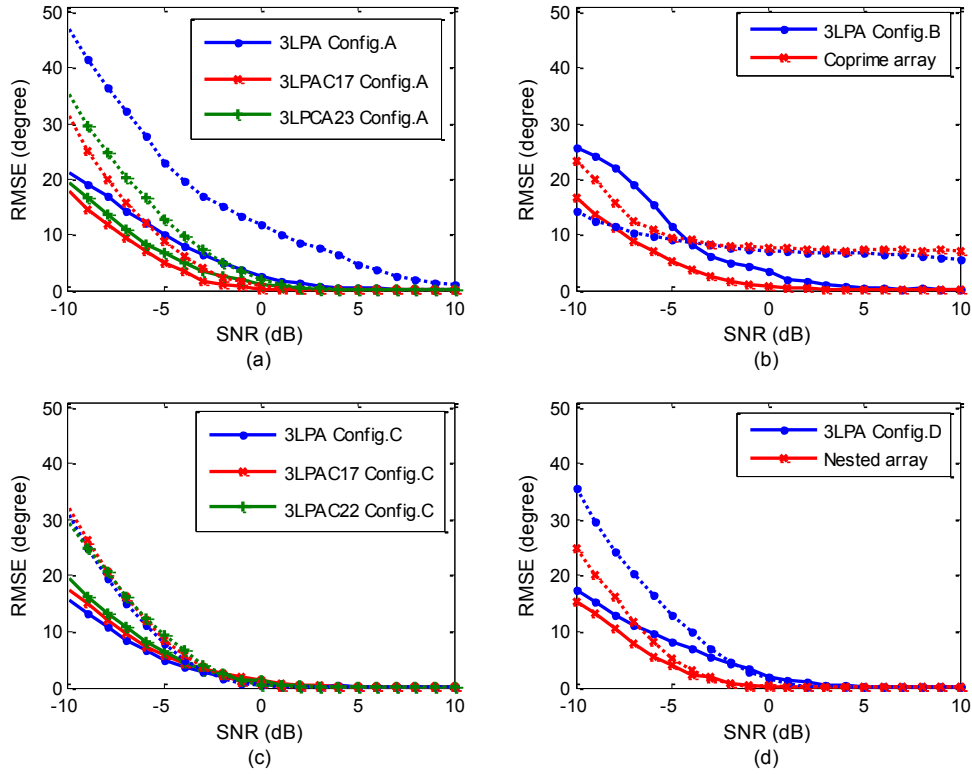


**Figure 6-4:** RMSE as a function of the SNR for 3LPA and 3LPAC with  $K = 15$  sources and  $N = 12$  elements. MUSIC (dotted lines) and CS (solid lines)

### B. RMSE versus Number of Samples

The RMSE versus number of samples of the 3LPA Config.A and its compressed versions presented in Table 6-2 is plotted in Figure 6-5 using MUSIC and CS algorithms. The same number of sources is assumed,  $K = 12$ , with  $\delta = 3$  grid points, and  $\text{SNR} = 0$  dB. It is apparent the performance is enhanced with increase of the number of samples. As the number of samples increases, better estimation for the covariance matrix of the received signal is achieved and consequently, the RMSE is reduced. The performance using CS algorithm is better than that with MUSIC algorithm since all unique lags can be exploited.

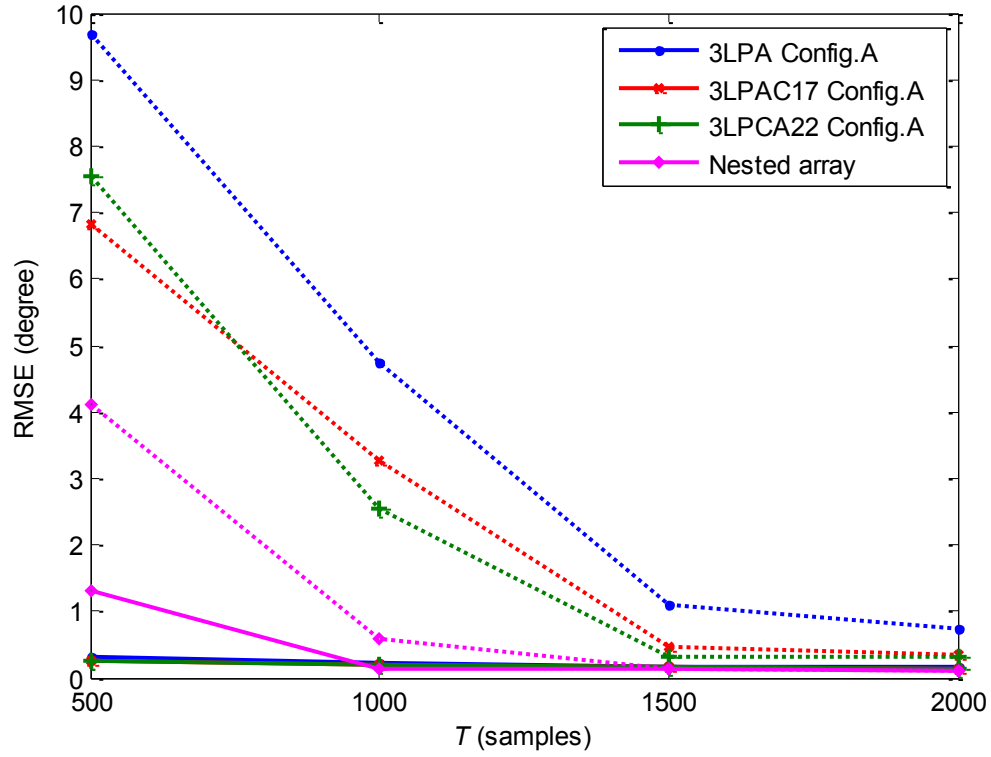


**Figure 6-5:** RMSE versus number of samples for the 3LPA Config.A and its compressed versions with  $K = 12$  sources, SNR = 0 dB, and  $N = 10$  elements. MUSIC (dotted lines) and CS (solid lines)

### C. RMSE versus Number of Grid Points

Finally, the RMSE using MUSIC and CS algorithms is plotted in Figure 6-6 as a function of  $\delta$ . A total of  $K = 12$  sources is assumed with  $T = 1000$  samples, and SNR = 0 dB. The 3LPA Config.A and its compressed versions arrays with  $N = 10$  elements are constructed as in Table 6-2. Six values of the window size are assumed that is  $\delta = 0, 3, 5, 7, 9$ , and 11 grid points where the first value indicates no grid refinement. Those are equivalent to 0, 0.5, 1, 1.5, 2, and 2.5 degree, respectively. Large RMSE is achieved without using grid refinement. Refine the grid search improves the RMSE for all configurations. Increasing  $\delta$  above certain value does not enhance the performance (array dependent) which means that the estimation is perfect and consequently error floor appears.

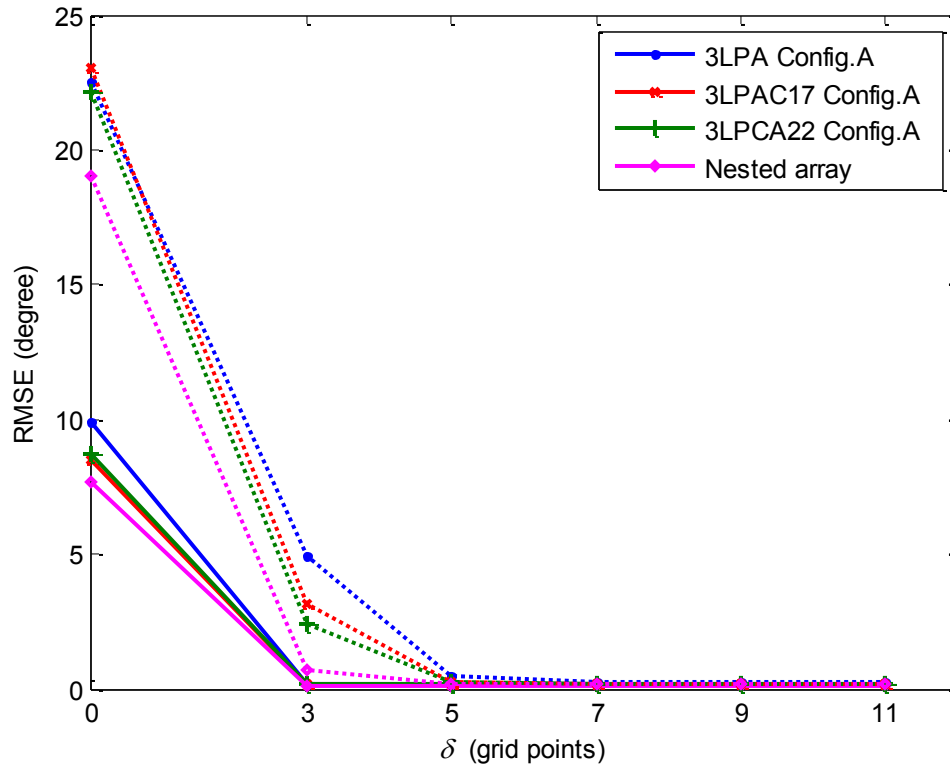


**Figure 6-6:** RMSE versus different window size for the 3LPA Config.A and its compressed versions with  $K = 12$  sources,  $\text{SNR} = 0$  dB, and  $N = 10$  elements. MUSIC (dotted lines) and CS (solid lines)

## 6.5 Chapter Summary

In this chapter, MLPA is proposed for sparse DOA estimation. The MLPA configuration uses multiple uniform linear subarrays where the number of elements is pairwise coprime integers. The array has closed form expressions for the antenna locations and the corresponding aperture size. There are more than one way to select the number of elements in the subarrays and to select the spacing in between which result in different configurations of different features. Although few missing lags or holes appear in the difference coarray, large DOFs can be achieved. Motivated by this, this chapter proposed a compressed version of the MLPA by compressing the inter-element spacing of one subarray under fixed number of antenna elements and fixed aperture size. The resultant



MLPAC can realize a hole-free difference coarray by properly selecting the compression factor and the intended subarray. MLPA and MLPAC configurations require smaller aperture size compared with nested and coprime arrays. MLPAC can estimate larger number of sources compared with MLPA using both MUSIC and sparse reconstruction algorithms. The effectiveness of the proposed configuration has been investigated through simulation for DOA estimation. We have shown that the RMSE of the PA Config.A can be reduced by around  $3.63^\circ$  and  $3.92^\circ$  using CS at SNR = -3 dB based on the PAC15 and PAC23, respectively. Additionally, the RMSE was decreased by around  $9^\circ$  at SNR = 6 dB using MUSIC algorithm based on the PAC15 and PAC23.

## CHAPTER 7 DOA ESTIMATION WITH TWO DIMENSIONAL MLPA ARRAY CONFIGURATION

A multi-level prime array (MLPA) uses multiple uniform linear subarrays along one axis where the number of elements within the subarrays are pairwise coprime integers. This chapter proposes two-dimensional direction of arrival (2D-DOA) estimation using parallel MLPAs. In this approach, we use two MLPA configurations located on the  $x$ - $y$  plane with half-wavelength spacing in between. The array has a closed form expression for the antenna locations. The corresponding difference coarray has large number of consecutive lags and few holes. A hole-free difference coarray can be realized if compressed MLPAs (MLPAC) are used. Simulation results verify the effectiveness of the proposed array with examples for 2D-DOA estimation.

### 7.1 Introduction

Recently, the problem of the two-dimensional direction-of-arrival (2D-DOA) estimation has attracted many researchers. Increasing the degrees-of-freedom (DOFs) was one of the main objectives. Researchers have developed different configurations and diverse algorithms to solve the estimation problem. This includes two parallel subarrays [136]–[139], L-shape [140], [141], cross-shape coprime arrays [142], coprime planar arrays [143]–[146] L-shape nested arrays [147], [148], planar nested arrays [149]–[152], two parallel subarrays based nested structure [153], hourglass configurations and others [154].

Sparse reconstruction [136]–[139], [141], [143], [153], [155], [156], and 2D MUSIC algorithm [140], [144], [146], [149], [152] were among the most widely used algorithms.

Two parallel uniform linear subarrays were used to implement a 2D-coprime array [136]–[139]. The two subarrays are spaced by half-wavelength and the number of elements in the second subarray was doubled [138], [139]. The elevation angle was estimated using Lasso [139], SPGL1 [136], and complex multitask Bayesian compressive sensing [138] and then the result was combined through a least square process to estimate the azimuth angle [138], [139]. At SNR = 0 dB, the RMSEs of the elevation and azimuth angles of two sources were around  $0.07^\circ$  and  $1^\circ$ , respectively [139].

Coprime arrays implemented in multiple axes were proposed [140]–[142]. Two coprime arrays were combined to perform an L-shape array [140], [141]. A 2D-DOA with MUSIC algorithm was exploited with phase ambiguity elimination in [140]. On the other hand, 1D search grid based on a sparse reconstruction was performed in [141]. A cross shape array that includes two symmetric coprime arrays in each axis was proposed in [142]. Based on the fourth-order-cumulant, the improved subspace algorithm was used where there is no issue of angle ambiguity but the complexity increases. The RMSEs at 0 dB SNR of two sources [140], [142] and three sources [141] were around  $0.08^\circ$ ,  $1.5^\circ$ , and  $0.3^\circ$  using nineteen [140], seventeen [141], and thirty [142] antenna elements, respectively.

Planar coprime arrays was proposed in [143]–[146] for 2D-DOA estimation. In [143], aperture extension was realized by relying on the sum-difference coarray. Moreover, sparse representation was used based on multiple 1D search grids. A 2D MUSIC algorithm was utilized in [144] where the complexity was reduced through 1D partial search grid. The

authors in [145] generalized the work in [146] which is based on 2D MUSIC algorithm and phase ambiguity elimination. At SNR = 0 dB, the RMSEs of two sources were around  $0.3^\circ$  and  $0.03^\circ$  using twenty four [143] and seventy three [146] antenna elements, respectively. Moreover, the RMSEs for the elevation and the azimuth angles of two sources were around  $0.05^\circ$  and  $0.09^\circ$  respectively at 0 dB SNR and using forty antenna elements [144]. On the other hand, a RMSE of around  $0.03^\circ$  and  $0.04^\circ$  was obtained for estimating the elevation and the azimuth angles respectively of two sources at SNR = 0 dB and using eighty eight antenna elements [145].

A 2D-DOA estimation was performed using L-shape nested arrays [147], [148] and planar nested arrays [149]–[152]. The angles were estimated and paired automatically by signal subspace joint diagonalization algorithm [147], a 2D MUSIC algorithm with spatial smoothing [152], and with augmented matrix approach [149]. The authors in [148] proposed an algorithm based on the minimum-norm and the least square techniques which does not require either the number of sources or pair matching, no need to find the corresponding azimuth angle for each elevation angle. The authors in [152] constructed a covariance-like matrix of much larger size based on the virtual difference coarray. So, large number of sources can be estimated greater than the number of antenna elements. Two parallel subarrays, coprime array with compressed inter-element spacing (CACIS)-like nested array, were used with the weighted  $l_1$ -norm algorithm [153]. At SNR = 0 dB, the RMSE of both angles of three source was around  $3^\circ$  using seven antenna elements [147]. The RMSEs of the azimuth and elevation angles of two sources were around  $0.1^\circ$  and  $2^\circ$  respectively using nine antenna elements [153]. Whereas in [148], both angles realize almost equal RMSEs that is  $0.05^\circ$  using eleven antenna elements. The authors in [152]

were able to estimate thirty six sources using twenty two elements with RMSEs of around  $0.7^\circ$  and  $0.6^\circ$  for the azimuth and elevation angles, respectively.

A hole-free difference coarray was realized with nested planar arrays and few holes appear in coprime planar arrays [149]. Large number of elements with nested planar array are spaced by half-wavelength which leads to significant mutual coupling. The authors in [157] proposed several generalized planar arrays. Those arrays have closed form expressions for antenna locations and have hole-free difference coarrays. Moreover, the mutual coupling effect was reduced in [154] and further mitigated in [157]. A 2D unitary ESPRIT algorithm was exploited for 2D-DOA estimation [157].

An MLPA uses multiple uniform linear subarrays [111]. The number of elements in the subarrays are pairwise coprime integers and the subarrays share the first element. The array was proposed as an extension of coprime array in 1D-plane. In this chapter, we combine two parallel MLPAs to perform a 2D-MLPA as a generalization of multiple subarrays along two parallel axes. This configuration can estimate the elevation and the azimuth angles in the  $x$ - $y$  plane. The difference coarray of the proposed 2D-MLPA is investigated. Few holes appear in the difference coarray, which motivates us to further enhance the 2D-MLPA. A 2D-MLPA with compressed subarray (2D-MLPAC) is also proposed by compressing the inter-element spacing of a specific subarray without changing the number of elements and the aperture size. The 2D-MLPAC realizes a hole-free difference coarray. Sparse 2D-DOA estimation is used to find the angles, which paired automatically. Simulation results are presented to further verify the proposed 2D configuration. We have shown that the array can estimate two angles of sources larger than the number of its

antenna elements. The advantage of the proposed configuration is that it includes coprime arrays as special case.

The rest of the chapter is organized as follows. The system model is presented in Section 7.2 where the proposed array is presented. In Section 7.3, we present a sparse signal recovery for 2D-DOA estimation. Simulation and results are discussed in Section 7.4, and finally Section 7.5 concludes the chapter.

## 7.2 System Model

In this section, the proposed array is introduced. Then the considered model for 2D-DOA estimation is presented.

### 7.2.1 Proposed Array

In this subsection, the MLPA proposed in 0 is extended into 2D in the  $x$ - $y$  plane. Consider two vectors  $\mathbf{m}^{(l)} = [M_1^{(l)}, M_2^{(l)}, \dots, M_{N_p^{(l)}}^{(l)}]$  of length  $N_p^{(l)}$  where  $M_i^{(l)} < M_j^{(l)}, \forall j > i$  and  $l = 1, 2$ . The entries within each vector are selected to be pairwise coprime integers. As a special case, the value of  $l = 0$  represents the 1D MLPA presented in 0. Let us assume that we have two parallel MLPAs separated by a distance  $d$  as Figure 7-1 depicts. The elements of the first MLPA are located along the  $y$ -axis. While the elements of the second MLPA are located along  $x = d$  where  $d = \lambda/2$  with  $\lambda$  being the signal wavelength. The first and the second MLPAs have  $N_p^{(l)}$  uniform linear subarrays “levels”, for  $l = 1, 2$ , respectively. The subscript “ $\cdot^{(l)}$ ” is used to distinguish between the two parallel MLPAs where  $l = 1$  refers to the MLPA along the  $y$ -axis and  $l = 2$  is for that along  $x = d$ .

The  $i^{th}$  subarray has  $M_i^{(l)}$  elements spaced by multiple units of half-wavelength,  $\mathcal{S}_i^{(l)}d$ , where  $\mathcal{S}_i^{(l)} \in \mathbf{m}^{(l)}$ , for  $i = 1, 2, \dots, N_p^{(l)}$ . Consequently, the elements of the  $i^{th}$  subarray are located at:  $\mathbb{P}_i^{(l)} = k_i \mathcal{S}_i^{(l)}d$  where  $0 \leq k_i \leq M_i^{(l)} - 1$ . The inter-element spacing of all  $N_p^{(l)}$  subarrays can be ordered and combined in a vector of unique entries,  $\mathcal{S}^{(l)} = [\mathcal{S}_1^{(l)}, \mathcal{S}_2^{(l)}, \dots, \mathcal{S}_{N_p^{(l)}}^{(l)}]d$ . The vector  $\mathcal{S}^{(l)}$  comprises all entries in  $\mathbf{m}^{(l)}$  scaled by  $d$  but with different order such that  $\mathcal{S}_i^{(l)} \neq M_i^{(l)}$  for  $l = 1, 2$ , respectively.

The two MLPAs can have similar structure or might be different. Taking all subarrays into consideration, the first and second MLPA have elements located respectively at [111]:

$$\mathbb{P}^{(l)} = \bigcup_{i=1}^{N_p^{(l)}} \{k_i \mathcal{S}_i^{(l)}d \mid 0 \leq k_i \leq M_i^{(l)} - 1, \mathcal{S}_i^{(l)} \neq M_i^{(l)}\} \quad (7-1)$$

The first and the second MLPA has a total of [111]:

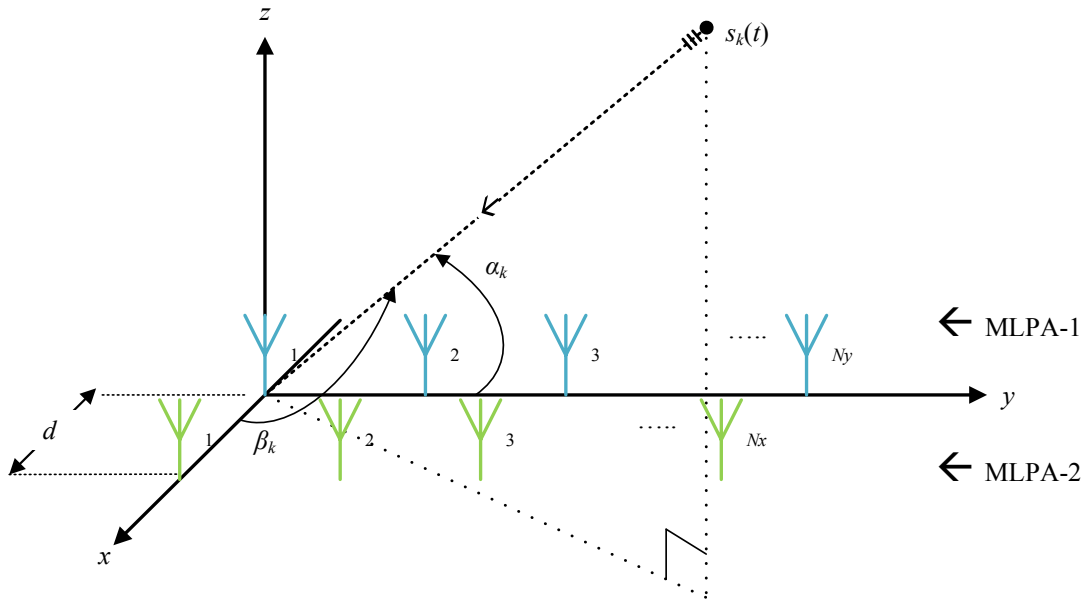


**Figure 7-1:** Parallel MLPA configurations for 2D-DOA estimation

$$N^{(l)} = \sum_{i=1}^{N_p^{(l)}} M_i^{(l)} - (N_p^{(l)} - 1) \quad (7-2)$$

antenna elements for  $l = 1$  and  $l = 2$ , respectively. The required aperture sizes by the two MLPAs are given as [111]:

$$D^{(l)} = \max \left( \mathcal{S}_{N_p^{(l)}-1}^{(l)} (M_{N_p-1}^{(l)} - 1), \mathcal{S}_{N_p}^{(l)} (M_{N_p}^{(l)} - 1) \right) \quad (7-3)$$

Combining these two MLPAs yields a two dimensional MLPA (2D-MLPA) where the locations of its elements are given by taking the union of (7-1) for  $l = 1$  and  $l = 2$  as:

$$\mathbb{P}_{2D} = \mathbb{P}^{(1)} \cup \mathbb{P}^{(2)} \quad (7-4)$$

There are no shared antenna element between the two MLPAs. Consequently, the number of antenna elements of the 2D-MLPA is:

$$N = N^{(1)} + N^{(2)} = N_y + N_x \quad (7-5)$$

where  $N^{(1)} = N_y$  and  $N^{(2)} = N_x$ .

### 7.2.2 2D-DOA Estimation

Consider  $K$  uncorrelated narrowband sources located in the far-field impinging on the 2D-MLPA from directions  $(\alpha_k, \beta_k)$ ,  $k = 1, 2, \dots, K$  where  $\alpha_k$  is the angle between the line that connects the  $k^{th}$  source to the origin and the  $y$ -axis, while  $\beta_k$  is the angle between the line that connects the  $k^{th}$  source to the origin and the  $x$ -axis as shown in Figure 7-1.

Let  $\mathbf{p}_y = [p_1^{(1)}d, p_2^{(1)}d, \dots, p_{N_y}^{(1)}d]^T$  and  $\mathbf{p}_x = [p_1^{(2)}d, p_2^{(2)}d, \dots, p_{N_x}^{(2)}d]^T$  be two vectors that

represent the antenna locations of the two MLPAs where  $p_i^{(l)}d \in \mathbb{P}^{(l)}$  for  $l = 1, 2$ .



The steering vectors of the MLPA located on the  $y$ -axis ( $l = 1$ ) and  $x = d$  axis ( $l = 2$ ) can be expressed as [137], [138], [158]:

$$\mathbf{a}^{(l)}(\alpha_i) = \begin{cases} \tilde{\mathbf{a}}^{(l)}(\alpha_i) e^{j\pi \cos(\beta_i)}, & l = 1 \\ \tilde{\mathbf{a}}^{(l)}(\alpha_i), & l = 2 \end{cases} \quad (7-6)$$

$$\tilde{\mathbf{a}}^{(l)}(\alpha_i) = \left[ \exp(j\pi p_2^{(l)} \cos(\alpha_i)), \dots, \exp(j\pi p_{N^{(l)}}^{(l)} \cos(\alpha_i)) \right]^T \quad (7-7)$$

The received signal vector at time instant  $t$  along each axis can be written as [137], [138], [158]:

$$\mathbf{y}^{(1)}(t) = \tilde{\mathbf{A}}^{(1)} \mathbf{A}_\beta \mathbf{s}(t) + \mathbf{n}^{(1)}(t) \quad (7-8)$$

$$\mathbf{y}^{(2)}(t) = \tilde{\mathbf{A}}^{(2)} \mathbf{s}(t) + \mathbf{n}^{(2)}(t) \quad (7-9)$$

where  $\mathbf{n}^{(1)}(t)$  and  $\mathbf{n}^{(2)}(t)$  are zero mean white complex Gaussian noise vectors that are independent from each other and independent from the signal. The two modified steering matrices are given as:  $\tilde{\mathbf{A}}^{(l)} = [\tilde{\mathbf{a}}^{(l)}(\alpha_1) \quad \tilde{\mathbf{a}}^{(l)}(\alpha_2) \quad \dots \quad \tilde{\mathbf{a}}^{(l)}(\alpha_K)]$  for  $l = 1, 2$  and the matrix  $\mathbf{A}_\beta$  is given as [137], [138], [158]:

$$\mathbf{A}_\beta = \text{diag}([e^{j\pi \cos(\beta_1)}, \dots, e^{j\pi \cos(\beta_K)}]) \quad (7-10)$$

which is a diagonal matrix of size  $K \times K$ . In matrix format, the received signal over  $T$  samples can be rewritten as:

$$\mathbf{Y}^{(1)} = \tilde{\mathbf{A}}^{(1)} \mathbf{A}_\beta \mathbf{S} + \mathbf{N}^{(1)} \quad (7-11)$$

$$\mathbf{Y}^{(2)} = \tilde{\mathbf{A}}^{(2)} \mathbf{S} + \mathbf{N}^{(2)} \quad (7-12)$$

where  $\mathbf{Y}^{(1)} = [\mathbf{y}^{(1)}(t_1), \dots, \mathbf{y}^{(1)}(t_T)]$ ,  $\mathbf{N}^{(1)} = [\mathbf{n}^{(1)}(t_1), \dots, \mathbf{n}^{(1)}(t_T)]$  are matrices of size  $N_y \times T$ ,  $\mathbf{Y}^{(2)} = [\mathbf{y}^{(2)}(t_1), \dots, \mathbf{y}^{(2)}(t_T)]$ ,  $\mathbf{N}^{(2)} = [\mathbf{n}^{(2)}(t_1), \dots, \mathbf{n}^{(2)}(t_T)]$  are matrices of size  $N_x \times T$ , and  $\mathbf{S} = [\mathbf{s}(t_1), \mathbf{s}(t_2), \dots, \mathbf{s}(t_T)]^T$  is a matrix of size  $K \times T$ . When the noise along the two axes are independent and uncorrelated with the signals, the cross correlation matrix of the received signals is given by [137], [138], [158]:

$$\mathbf{R}_{\mathbf{Y}^{(2)}\mathbf{Y}^{(1)}} = \mathbb{E}[\mathbf{Y}^{(2)}\mathbf{Y}^{(1)H}] = \tilde{\mathbf{A}}^{(2)}\mathbf{R}_{\mathbf{SS}}\mathbf{A}_\beta^H\tilde{\mathbf{A}}^{(1)H} \quad (7-13)$$

where  $\mathbf{R}_{\mathbf{SS}} = \mathbb{E}[\mathbf{SS}^H] = \text{diag}([\sigma_1^2, \sigma_2^2, \dots, \sigma_K^2])$  represents the covariance matrix of the transmitted signal and  $\sigma_i^2$  is the signal power of the  $i^{th}$  source,  $i = 1, 2, \dots, K$ . Given the received data  $\mathbf{Y}^{(1)}, \mathbf{Y}^{(2)}$ , and the array geometry, our objective is to come up with  $\hat{\boldsymbol{\alpha}}$  and  $\hat{\boldsymbol{\beta}}$  estimate. In practice, the statistics are not available and we rely on the sample average of the covariance matrix as:

$$\hat{\mathbf{R}}_{\mathbf{Y}^{(2)}\mathbf{Y}^{(1)}} = \frac{1}{T} \sum_{i=1}^T \mathbf{y}^{(2)}(t_i)\mathbf{y}^{(1)H}(t_i) = \frac{1}{T} \mathbf{Y}^{(2)}\mathbf{Y}^{(1)H} \quad (7-14)$$

### 7.3 2D-DOA Estimation via Sparse Representation

For a 2D array specified by  $\mathbb{P}_{2D}$ , its difference coarray,  $\mathbb{D}_{2D}$ , is defined as the differences between all sensor locations:

$$\mathbb{D}_{2D} = \{\mathbf{p}_m - \mathbf{p}_n | m, n = 1, 2, \dots, N\} \quad (7-15)$$

where  $\mathbf{p}_m$  and  $\mathbf{p}_n$  are vectors and  $\mathbf{p}_m d, \mathbf{p}_n d \in \mathbb{P}_{2D}$ . It is always desired to maximize the number of lags and minimize the holes in the difference coarray. The proposed configuration is compared with others in Section 7.4 based on their difference coarrays.

Column-wise vectorization of the cross correlation matrix produces a vector  $\mathbf{z}$  of length  $N_x N_y \times 1$  as follows:

$$\mathbf{z} = \text{vec}(\mathbf{R}_{\mathbf{Y}(2)\mathbf{Y}(1)}) = \tilde{\mathbf{A}}\mathbf{b} \quad (7-16)$$

where  $\tilde{\mathbf{A}} = [\tilde{\mathbf{a}}(\alpha_1), \tilde{\mathbf{a}}(\alpha_2), \dots, \tilde{\mathbf{a}}(\alpha_K)]$  is an extended steering matrix of size  $N_x N_y \times K$ ,  $\tilde{\mathbf{a}}(\alpha_k) = \tilde{\mathbf{a}}^{(2)}(\alpha_k) \otimes \tilde{\mathbf{a}}^{(1)*}(\alpha_k)$  with  $\otimes$  denotes the Kronecker product,  $\mathbf{b} = [\sigma_1^2 e^{-j\pi \cos(\beta_1)}, \sigma_2^2 e^{-j\pi \cos(\beta_2)}, \dots, \sigma_K^2 e^{-j\pi \cos(\beta_K)}]^T$ , and the operator  $(*)$  denotes the complex conjugate. The signal model in (7-16) is a single snapshot of  $\mathbf{b}$  [34], so the rank of  $\mathbf{R}_{\mathbf{zz}}$  is one. Thus, the sources become fully correlated and consequently, subspace-based DOA estimation algorithm cannot be used directly [52]. To solve this, spatial smoothing can be performed before [34]. Spatial smoothing can be exploited if we have an array configuration that has consecutive lags [34]. Since the MLPA can achieve large number of consecutive lags, MUSIC algorithm can be applied for DOA estimation.

Sparse reconstruction algorithms can also be utilized for DOA estimation. The problem in (7-16) can be formulated to be a sparse one as:

$$\mathbf{z} = \text{vec}(\mathbf{R}_{\mathbf{Y}(2)\mathbf{Y}(1)}) = \tilde{\mathbf{A}}_z \mathbf{r} \quad (7-17)$$

where  $\tilde{\mathbf{A}}_z$  is a new steering matrix constructed using all possible angles of  $\alpha_1^g, \alpha_2^g, \dots, \alpha_{N_\alpha}^g$  where  $N_\alpha \gg K$ . The variable  $\mathbf{r}$  is a sparse vector with only  $K$  nonzero entries. Sparse signal recovery using Lasso can be used to solve such problem based on the  $l_1$ -norm as [33]:

$$\hat{\mathbf{r}}^g = \arg \min_{\mathbf{r}^g} \left[ \frac{1}{2} \|\mathbf{z} - \tilde{\mathbf{A}}_z \mathbf{r}^g\|_2 + \lambda_t \|\mathbf{r}^g\|_1 \right] \quad (7-18)$$

where  $\lambda_t$  is a regularization parameter. The positions of the nonzero entries of  $\hat{\mathbf{r}}^g$  represents  $\hat{\boldsymbol{\alpha}}$  and their values indicates the corresponding signals' power. Based on (7-16), the least square solution can be applied to estimate  $\mathbf{b}$  as [137], [138], [158]:

$$\hat{\mathbf{b}} = \left( \hat{\mathbf{A}}^H \hat{\mathbf{A}} \right)^{-1} \hat{\mathbf{A}}^H \mathbf{z} \quad (7-19)$$

where  $\hat{\mathbf{A}} = [\tilde{\mathbf{a}}(\hat{\alpha}_1), \tilde{\mathbf{a}}(\hat{\alpha}_2), \dots, \tilde{\mathbf{a}}(\hat{\alpha}_K)]$ . An estimate of  $\beta$  can be realized through [136], [137]:

$$-j\pi\cos(\hat{\beta}_k) = \arg(\hat{b}_k) \quad (7-20)$$

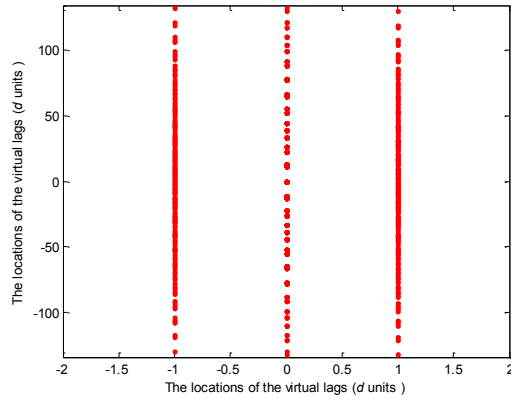
## 7.4 Simulation and Results

To validate the 2D-DOA estimation using parallel MLPAs, the following parameters are selected. Uncorrelated narrowband sources located in the far-field are assumed. The total number of samples is  $T = 1000$  samples. For comparison with [33], the grid search is uniform with a step size  $\alpha_i^g = 0.25^\circ$  within  $[0^\circ, 180^\circ]$  which is the range of both angles. Additionally, the regularization parameter is  $\lambda_t = 0.85$  and the minimum inter-element spacing is set to  $d = \lambda/2$ . All these parameters are fixed unless stated otherwise. CS based on Yall1 [135] algorithms is used for DOA estimation. The difference coarray is used to assess the performance. Then the maximum number of correctly estimated sources using the 2D-MLPA and MLPAC is evaluated with numerical examples. The performance of the proposed configuration is further evaluated based on Monte Carol simulations.

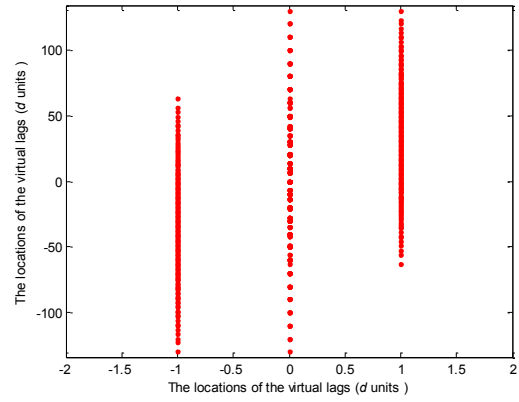
#### 7.4.1 Difference Coarray in 2D

A total of  $N = 24$  elements is assumed. The 2D-3LPA is constructed with  $\mathbf{m}^{(l)} = [2,5,7]$  and  $\mathcal{S}^{(l)} = [7,2,5]d$ . Whereas, the 2D-3LPAC22 is constructed with  $\mathbf{m}^{(l)} = [2,5,7]$  and  $\mathcal{S}^{(l)} = [7,1,5]d$ . The proposed configurations are compared with previous work which utilize two subarrays Ref. [136], [137], and those suggest to double the number of elements within one subarray Ref. [138], [139]. An array constructed according to Ref. [136], [137] with a coprime pair of [11,13] and with a coprime pair of [7,10] according to Ref. [138], [139] are considered. The corresponding difference coarrays are shown in Figure 7-2 (a) and (b), respectively.

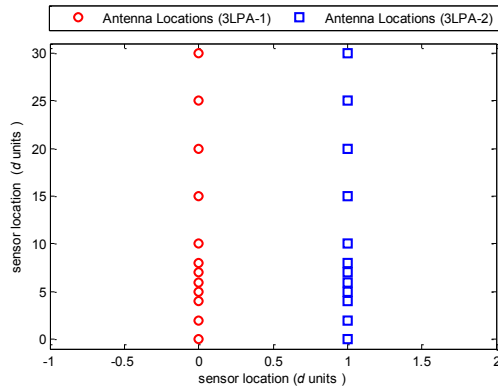
The 2D-3LPA and 2D-3LPAC22 require very small aperture size as illustrated in Figure 7-2 (c) and (e), respectively. The 2D-3LPAC22 realizes a hole-free difference coarray, while few holes appear using 2D-3LPA as shown in Figure 7-2 (f) and (d), respectively. On the other hand, all configurations based on Ref. [136], [137], and Ref. [138], [139] require much larger aperture size and there are a lot of holes in the corresponding difference coarray as shown in Figure 7-2 (b) and (d). The number of unique lags with Ref. [136], [137] and Ref. [138], [139], is 331 and 325, respectively. While, the 2D-3LPA attains 171 unique lags and the 2D-3LPAC22 manages 183 unique lags which are all consecutive. Thus, we reduce the required aperture which is the main scope of this dissertation at the expense of the number of lags.



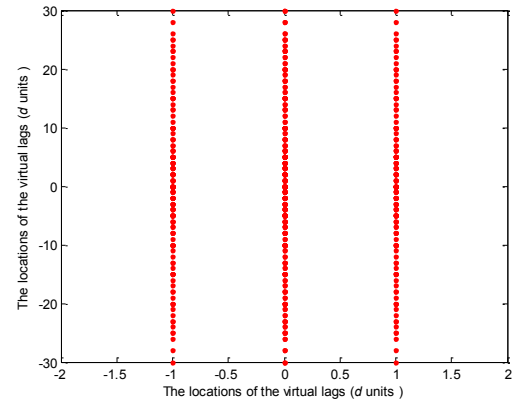
(a) The difference coarray of Ref. [136], [137]



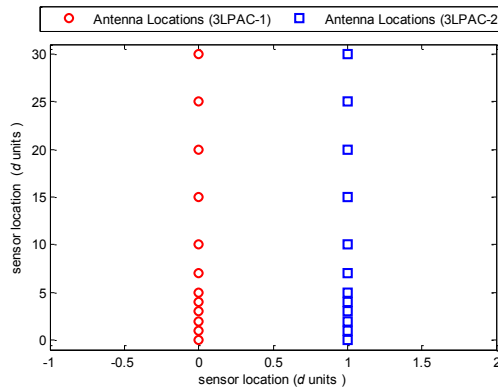
(b) The difference coarray of Ref. [138], [139]



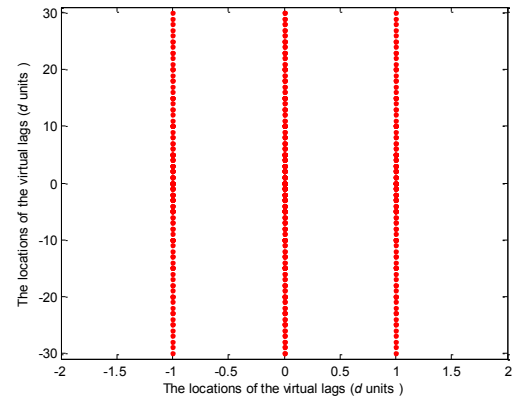
(c) 2D-3LPA



(d) corresponding difference coarray



(e) 2D-3LPAC22



(f) corresponding difference coarray

**Figure 7-2:** The difference coarray of (a) Ref. [138], [139], (b) Ref. [140], [141], (c)-(d) 2D-3LPA and its difference coarray (e)-(f) 2D-3LPAC22 and its difference coarray

### 7.4.2 Impact of Compression in 2D

A total of  $K = 26$  uniformly distributed sources between  $(\alpha, \beta) = (20^\circ, 20^\circ)$  and  $(160^\circ, 160^\circ)$  is assumed. The 2D-3LPA and 2D-3LPAC22 presented in Section 7.4.1 with  $N = 24$  elements,  $\text{SNR} = 0$  dB, and  $T = 1000$  samples are used. Figure 7-3 shows the 2D-DOA estimation using 2D-3LPA and 2D-3LPAC22. The latter configuration has larger number of lags, consequently most of the 26 sources are estimated correctly compared with those using 2D-3LPA. A 2D-coprime array is also simulated which realizes up to 159 unique lags. Consequently, its performance is the worst among the three configurations. There is a big error in detecting two and one sources with the 2D-coprime array and 2D-3LPA, respectively.

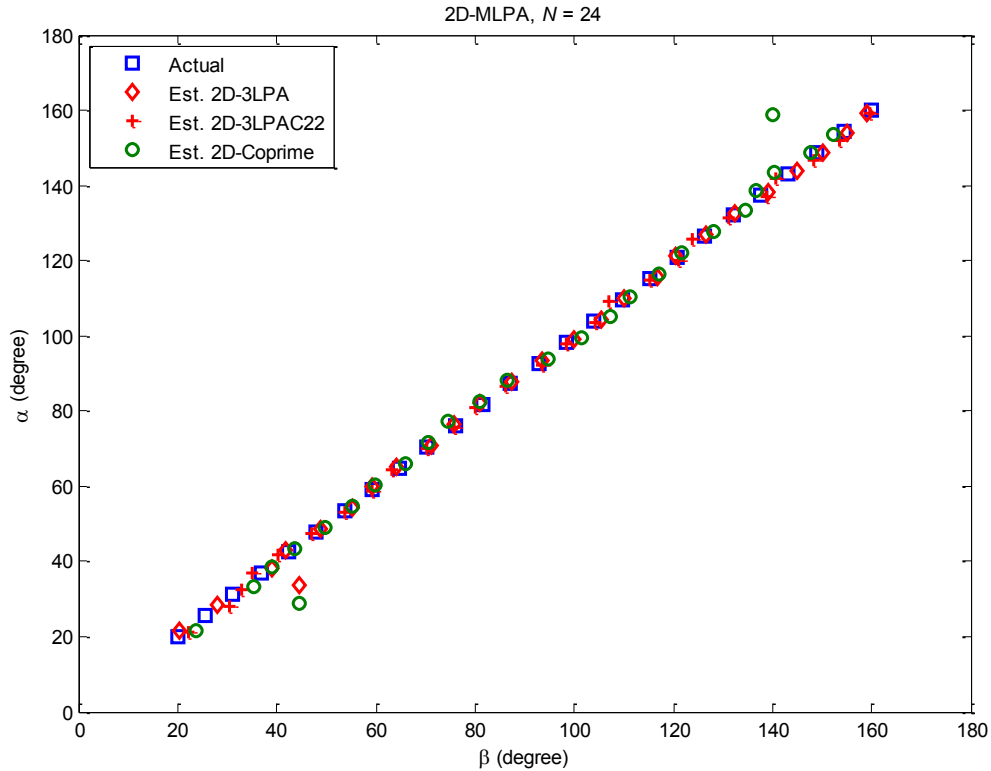


**Figure 7-3:** 2D-DOA estimation based on 2D-3LPA and 2D-3LPAC22 using CS with  $K = 26$  sources in noise free and  $N = 24$  elements

### 7.4.3 Statistical Error Analysis

The RMSE of the estimated DOA is defined as [143]:

$$\text{RMSE} = \sqrt{\frac{1}{I_{\text{iter}}K} \sum_{j=1}^{I_{\text{iter}}} \sum_{i=1}^K (\alpha_i - \hat{\alpha}_i(j))^2 + (\beta_i - \hat{\beta}_i(j))^2} \quad (7-21)$$

where  $\hat{\alpha}_i(j)$  and  $\hat{\beta}_i(j)$  are the estimates of  $\alpha_i$  and  $\beta_i$ , respectively, at the  $j^{\text{th}}$  Monte Carlo trial,  $j = 1, 2, \dots, I_{\text{iter}}$ . In our simulation, a total of  $I_{\text{iter}} = 5000$  independent trials are used. A total of  $K = 16$  uniformly distributed sources between  $(\alpha, \beta) = (20^\circ, 20^\circ)$  and  $(160^\circ, 160^\circ)$  with  $T = 1000$  samples and  $\delta = 3$  grid points are assumed.

The RMSE in degree versus the SNR using CS is plotted in Figure 7-4 for the 2D-3LPA and 2D-3LPAC22 presented in Section 7.4.1 with  $N = 24$  elements. It is evident that the RMSE is decreased with SNR for all configurations. The RMSE of the 2D-3LPAC22 is almost similar to that of the 2D-3LPA. A 2D-coprime array has the largest RMSE due to the lack of lags and it requires  $36d \times d$  aperture size. On the other hand, 2D-nested array has better performance since it has got around 249 lags. Though, most its elements are spaced by half-wavelength and it requires aperture size of  $41d \times d$ . This is not the case for the 2D-3LPA and its compressed version which need only  $30d \times d$ . are used. At SNR = 0 dB, around  $2^\circ$  RMSE is realized using the 2D-nested array. The 2D-3LPA and 2D-3LPAC22 both require a 1 dB SNR while the 2D-coprime array needs 8 dB SNR to achieve the same error.



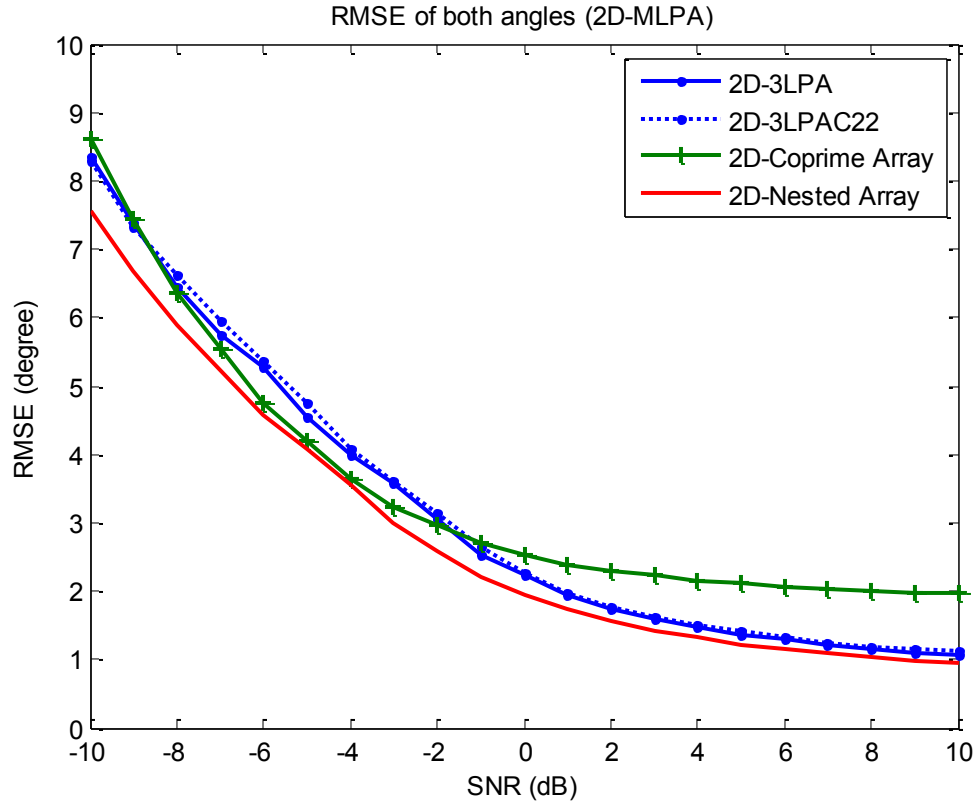


Figure 7-4: RMSE versus SNR based on 2D-3LPA and 2D-3LPAC22 using CS with  $K = 16$ ,  $\delta = 3$ , and  $N = 24$

## 7.5 Chapter Summary

In this chapter, two new array configurations were proposed by combining two parallel MLPAs or MLPACs. The 2D-MLPA and 2D-MLPAC can estimate two angles in the  $x$ - $y$  plane. The arrays have closed form expression for antenna locations and aperture size. The 2D-MLPA requires small aperture and has large number of lags with only few holes in the difference coarray. On the other hand, the 2D-MLPAC achieves a hole-free difference coarray. The effectiveness and validity of the proposed work was evaluated based on the difference coarray and further verified with numerical examples for 2D-DOA estimation. Simulations show that the proposed configuration can realize the same performance as the 2D-nested array by increasing the SNR by only 1 dB.

## CHAPTER 8 CONCLUSIONS AND FUTURE WORK

This dissertation focused on the problem of sparse DOA estimation with constrained antenna arrays. The main constraints are: limited number of receive antenna elements and limited inter-element spacing between these antennas which appear due to the available physical size in mobile handsets. For a given aperture size, fitting more elements can improve the DOA estimation, though mutual coupling effect will increase. On the other hand, large inter-element spacing degrades the accuracy due to the limited number of elements and may lead to grating lobe problem if the inter-element spacing goes beyond half-wavelength.

This dissertation comprises eight chapters where the main findings are summarized in the next section followed by recommendations and suggestions for future work.

### 8.1 Summary of Findings

CHAPTER 1 gave an introduction about the dissertation and summarized the main contributions. CHAPTER 2 provided the technical background and literature review.

In CHAPTER 3, we presented a comparative study on sparse DOA estimation with practical antenna arrays. The two elements arrays can support systems in a typical mobile phone or small wireless terminals. Other higher order arrays such as  $N = 4$ , or 8 elements can fit on larger devices (tablets, laptops, etc.) or access points. We have presented simulation results and compared the performance of beamforming, Capon, MUSIC, and  $l_1$ -SVD algorithms in terms of the RMSE, beamwidth, bias, PRR, and the sources resolvability in the presence of such constraints. The  $l_1$ -SVD algorithm realizes super-

resolution because the beamwidth at the DOA is very sharp. In addition, this algorithm exploits sparsity/SVD concepts and the processing time is reduced dramatically due to data reduction.

In CHAPTER 4, experimental setups for DOA estimation using sparse arrays in realistic channels were implemented and evaluated. Three main sections were included in this chapter. The first section suggested a moving coprime array under sparse reconstruction framework for DOA estimation. With this approach, both complexity and mutual coupling effect can be reduced. Experimental results using on single snapshot were conducted to evaluate the advantage of the moving coprime array. In the second section, an SDR (NI-USRP-2950R) platform system for a general 1D array configuration was implemented in order to provide more flexibility to the main parameters. We took into account the issues of synchronizing the USRPs and calibrating the phases of the received signals. The implemented setups in the first and second sections were tested in a laboratory with dense multipath environment. To the best of our knowledge, the performance of sparse arrays was not demonstrated experimentally in realistic environments. The third section incorporated the radiation pattern of the antennas in DOA estimation. Specifically, sparse DOA estimation with directive coprime arrays was proposed. We have quantified the impact of the radiation pattern on the DOA estimation accuracy. It is difficult to estimate any source of at angles outside the main beam of the directional antenna even in noise free circumstances.

0 proposed a new array configuration that can be used for sparse DOA estimation. The proposed MLPA uses multiple uniform linear subarrays where the number of sensors is pairwise coprime integers. There are more than one way to select the number of sensors in

the subarrays and the ordered inter-element spacing which have a direct impact on the achievable DOFs. Two different optimization criteria were used to design the optimum MLPA configuration. In most of the cases, there is a unique solution which jointly maximizes the number of unique lags and the number of consecutive lags which makes the optimum MLPA configuration unique. The number of design alternatives increases as the level of the array increases in this case, other factors like reduced mutual coupling can be used to make the final selection. We also derived an upper bound on the DOFs achieved by the 3LPA configurations and compared them with the maximum achievable DOFs.

A compressed version of the multi-level prime array (MLPAC) was proposed in CHAPTER 6. This configuration is constructed by compressing the inter-element spacing of one subarray under fixed number of antenna elements and fixed aperture size. MLPAC can realize a hole-free difference coarray by properly selecting the compression factor and the intended subarray. MLPA and MLPAC configurations require smaller aperture size compared with nested and coprime arrays. This is attractive in antenna design and array implementation. MLPAC can estimate larger number of sources compared with MLPA using both MUSIC and sparse reconstruction algorithms.

In CHAPTER 7, sparse 2D-DOA estimation based on two parallel MLPA configurations was proposed. The array has a closed form expression for the antenna locations and limited number of holes appears in the corresponding difference coarray. A hole-free difference coarray can be realized if the MLPAs are replaced by optimized MLPACs.

## 8.2 Suggestions for Future Work

The work in this dissertation considers sparse DOA estimation with constrained antenna arrays. There are still some open problems whose solutions could add advantages in the field of DOA estimation. We may summarize them in the following points:

- Evaluate the performance in the presence of antenna location perturbations
- Use practical antennas and practical radiation patterns to evaluate the performance of DOA estimation
- Develop an improved DOA estimation technique, which equalizes/compensates for the effect of the radiation pattern to improve the estimation accuracy. This requires knowledge about the complex radiation pattern of all antennas to account for the magnitude and phase variations at different angels.
- Derive a closed form expression for the achievable DOFs of the proposed MLPA and MLPAC for any number of subarrays
- Since the difference coarray of the MLPA is not a ULA (few holes), a great advantage will be achieved if higher order statistics are considered instead of the second order. In future, we shall consider MLPA and MLPAC with higher order statistics.
- Experimentally evaluate the performance for multiple sources, which we have already started. Since MLPAs, MLPACs, and other sparse arrays can estimate large number of sources greater than the number of elements, the advantage of these configurations will be more evident at their extremes. Thus, it will be interesting to

evaluate the performance and increase the capability of the SDR system in the presence of larger number of transmitters and/or receivers.

- Extend the work on 2D-DOA estimation for multiple scenarios and different constraints. There is room for experimental implementation and then validate the fabricated arrays with the developed SDR system.

## BIBLIOGRAPHY

- [1] H. B. Tuğrel, H. Alakoca, G. K. Kurt, and C. Ayyıldız, “Angle of Arrival (AoA) Estimation by using Software Defined Radios,” *24th Signal Process. Commun. Appl. Conf. Zo. Turkey*, pp. 1429–1432, May 2016.
- [2] W. Abdessamad, Y. Nasser, H. Artail, S. Chazbek, G. Fakher, and O. Bazzi, “An SDR Platform using Direction Finding and Statistical Analysis for the Detection of Interferers,” *8th Int. Congr. Ultra Mod. Telecommun. Control Syst. Work. (ICUMT), Lisbon, Port.*, pp. 43–48, Oct. 2016.
- [3] Y. Tang, X. Ma, W. Sheng, and Y. Han, “A New Transmit Beamforming Algorithm for Subarray MIMO RADAR,” *IEEE Int. Symp. Phased Array Syst. Technol. Waltham, MA, USA*, pp. 255–258, Oct. 2013.
- [4] M. B. Hawes and W. Liu, “Design of Low-Complexity Wideband Beamformers with Temporal Sparsity,” *9th Int. Symp. Commun. Syst. Networks Digit. Sign (CSNDSP), Manchester, UK*, pp. 580–584, Jul. 2014.
- [5] M. B. Hawes and W. Liu, “Sparse Array Design for Wideband Beamforming with Reduced Complexity in Tapped Delay-Lines,” *IEEE/ACM Trans. Audio, Speech, Language Process.*, vol. 22, no. 8, pp. 1236–1247, Aug. 2014.
- [6] F. Foroozan, A. Asif, and Y. Jin, “Direction Finding Algorithms for Time Reversal MIMO RADARs,” *IEEE Stat. Signal Process. Work. (SSP), Nice, Fr.*, pp. 433–436, Jun. 2011.
- [7] J. Capon, “High-Resolution Frequency-Wavenumber Spectrum Analysis,” *Proc. IEEE*, vol. 57, no. 8, pp. 1408–1418, 1969.
- [8] I. Pasya, N. Iwakiri, and T. Kobayashi, “Performance of Joint Direction-of-Departure and Direction-of-Arrival Estimation in an Ultra Wideband MIMO RADAR Depending on Bandwidths,” *IEEE Radar Conf. Cincinnati, OH, USA*, pp. 1353–1357, May 2014.
- [9] J. Yu, L. Zhang, and K. Liu, “Coherently Distributed Wideband LFM Source Localization,” *IEEE Signal Process. Lett.*, vol. 22, no. 4, pp. 504–508, 2015.
- [10] R. Schmidt and X. W. Af, “Multiple Emitter Location and Signal Parameter Estimation,” *IEEE Trans. Antennas Propag.*, no. 3, pp. 276–280, 1986.
- [11] J. Liang and D. Liu, “Passive Localization of Mixed Near-Field and Far-Field Sources Using Two-stage MUSIC Algorithm,” *IEEE Trans. Signal Process.*, vol. 58, no. 1, pp. 108–120, Jan. 2010.
- [12] J. He, M. N. S. Swamy, and M. O. Ahmad, “Efficient Application of MUSIC Algorithm Under the Coexistence of Far-Field and Near-Field Sources,” *IEEE*

- Trans. Signal Process.*, vol. 60, no. 4, pp. 2066–2070, 2012.
- [13] G. Hua and S. S. Abeysekera, “A comparison on DOA Parameter Identifiability for MIMO and Phased-Array Radar,” *9th Int. Conf. Information, Commun. Signal Process. Tainan, Taiwan*, pp. 1–5, Dec. 2013.
- [14] Guohong Liu and Xiaoying Sun, “Efficient Method of Passive Localization for Mixed Far-Field and Near-Field Sources,” *IEEE Antennas Wirel. Propag. Lett.*, vol. 12, pp. 902–905, 2013.
- [15] Z. Pan and Z. Liu, “Near-Field Source Localisation Using a Velocity Sensor Array,” *IET Radar, Sonar Navig.*, vol. 7, no. 7, pp. 727–735, Aug. 2013.
- [16] J. He, M. O. Ahmad, and M. N. S. Swamy, “Near-Field Localization of Partially Polarized Sources with a Cross-Dipole Array,” *IEEE Trans. Aerosp. Electron. Syst.*, vol. 49, no. 2, pp. 857–870, 2013.
- [17] C. Yu, X. Zhang, Y. Bai, and Z. Du, “DOD-DOA Estimation by Exploiting Signal Cyclostationarity for Bistatic MIMO RADAR,” *IEEE Int. Conf. Signal Process. Commun. Comput. (ICSPCC), KunMing, China*, pp. 1–4, Aug. 2013.
- [18] F. Liu and E. Optimization, “An Effective Virtual ESPRIT Algorithm for Multi-target Localization in Bistatic MIMO RADAR System,” *Int. Conf. Comput. Des. Applications (ICCD), Qinhuangdao, China*, pp. 412–415, Jun. 2010.
- [19] H. Jiang, D. Wang, and C. Liu, “Estimation of DOD and 2D-DOA and Polarizations for Bistatic MIMO RADAR,” *19th Annu. Wirel. Opt. Commun. Conf. (WOCC), Shanghai, China*, pp. 1–5, May 2010.
- [20] K. Han, Y. Wang, B. Kou, and W. Hong, “Parameters Estimation Using a Random linear Array and Compressed Sensing,” *3rd Int. Congr. Image Signal Process. Yantai, China*, pp. 3950–3954, Oct. 2010.
- [21] O. Balkan, K. Kreutz-delgado, and S. Makeig, “Localization of More Sources Than Sensors via Jointly-Sparse Bayesian Learning,” *IEEE Signal Process. Lett.*, vol. 21, no. 2, pp. 131–134, 2014.
- [22] C. Liu, Y. V. Zakharov, and T. Chen, “Broadband Underwater Localization of Multiple Sources Using Basis Pursuit De-Noising,” *IEEE Trans. Signal Process.*, vol. 60, no. 4, pp. 1708–1717, 2012.
- [23] W. Liu and M. B. Hawes, “Compressive Sensing-Based Approach to the Design of Linear Robust Sparse Antenna Arrays with Physical Size Constraint,” *IET Microwaves, Antennas Propag.*, vol. 8, no. 10, pp. 736–746, 2014.
- [24] A. Manikas, Y. I. Kamil, and Marc Willerton, “Source Localization Using Sparse Large Aperture Arrays,” *IEEE Trans. Signal Process.*, vol. 60, no. 12, pp. 6617–6629, 2012.
- [25] D. Malioutov, M. Çetin, and A. S. Willsky, “A Sparse Signal Reconstruction



- Perspective for Source Localization With Sensor Arrays,” *IEEE Trans. Signal Process.*, vol. 53, no. 8, pp. 3010–3022, 2005.
- [26] Z. Wang, C. Wang, H. Zhang, Y. Tang, and M. Liu, “SAR Tomography via Sparse Representation of Multiple Snapshots and Backscattering Signals — The L1-SVD Approach,” *IEEE Geosci. Remote Sens. Symp. Quebec City, QC, Canada*, pp. 1325–1328, Jul. 2014.
- [27] L. Guolong and H. Bo, “New Method of DOA Estimation in the Presence of Interference,” *IEEE 11th Int. Conf. Electron. Meas. Instruments, Harbin, China*, pp. 650–654, Aug. 2013.
- [28] Zhizhang Chen, G. Gokeda, and Y. Yu, *Introduction to Direction-of-Arrival Estimation*. Boston/ London: Artech House, 2010.
- [29] Y. D. Zhang, M. G. Amin, F. Ahmad, and B. Himed, “DOA Estimation Using A Sparse Uniform Linear Array With Two CW Signals of Co-Prime Frequencies,” *IEEE 5th Int. Work. Comput. Adv. Multi-Sensor Adapt. Process. (CAMSAP), St. Martin, Fr.*, pp. 404–407, Dec. 2013.
- [30] Z. Tan, P. Yang, and A. Nehorai, “Joint Sparse Recovery Method for Compressed Sensing With Structured Dictionary Mismatches,” *IEEE Trans. Signal Process.*, vol. 62, no. 19, pp. 4997–5008, Oct. 2014.
- [31] T.-J. Jung and K. Lee, “Closed-Form Algorithm for 3-D Single-Source Localization With Uniform Circular Array,” *IEEE Antennas Wirel. Propag. Lett.*, vol. 13, pp. 1096–1099, 2014.
- [32] A. Hassanien, M. W. Morency, A. Khabbazi, S. a. Vorobyov, J. Y. Park, and S. J. Kim, “Two-dimensional Transmit Beamforming for MIMO RADAR with Sparse Symmetric Arrays,” *IEEE Natl. Radar Conf. - Proceedings, Ottawa, ON, Canada*, pp. 1–6, Apr. 2013.
- [33] S. Qin, Y. D. Zhang, and M. G. Amin, “Generalized Coprime Array Configurations for Direction-of-Arrival Estimation,” *IEEE Trans. Signal Process.*, vol. 63, no. 6, pp. 1377–1390, 2015.
- [34] P. Pal and P. P. Vaidyanathan, “Nested Arrays: A novel Approach to Array Processing with Enhanced Degrees of Freedom,” *IEEE Trans. Signal Process.*, vol. 58, no. 8, pp. 4167–4181, 2010.
- [35] Z. Zhang and R. Xie, “Fast DOA Estimation for Monostatic MIMO RADAR with Arbitrary array Configurations,” *Proc. 2011 IEEE CIE Int. Conf. Radar, Chengdu, China*, pp. 959–962, Oct. 2011.
- [36] Mohammad Sharawi, *Printed MIMO Antenna Engineering*. Norwood, MA: Artech House, 2014.
- [37] T. Engin Tuncer and B. Friedlander, *Classical and Modern Direction-of-Arrival Estimation*. Boston/ London: Academic Press, 2009.

- [38] Sathish Chandran, *Advances in Direction-of-Arrival Estimation*. Boston/London: Artech House, Inc, 2006.
- [39] J. Foutz, A. Andreas Spanias, and M. K. Banavar, *Narrowband Direction of Arrival Estimation for Antenna Arrays*. CA, US: Morgan & Claypool Publishers series, 2008.
- [40] A. P. Petropulu, Y. Yu, and H. V. Poor, "Distributed MIMO RADAR Using Compressive Sampling," *42nd Asilomar Conf. Signals, Syst. Comput. Pacific Grove, CA, USA*, pp. 203–207, Oct. 2008.
- [41] Y. Yu, A. P. Petropulu, and H. V. Poor, "Compressive Sensing for MIMO RADAR," *IEEE Int. Conf. Acoust. Speech Signal Process. (ICASSP), Taipei, Taiwan*, pp. 3017–3020, Apr. 2009.
- [42] Y. Tian, X. Sun, and S. Zhao, "DOA and Power Estimation using a Sparse Representation of Second-order Statistics Vector and  $\ell_0$  -norm Approximation," *ELSERVIER, Signal Process.*, vol. 105, pp. 98–108, 2014.
- [43] A. Khabbazi-basmenj, S. A. Vorobyov, A. Hassanien, and M. W. Morency, "Transmit Beam-space Design for Direction Finding in Colocated MIMO RADAR with Arbitrary Receive Array and Even Number of Waveforms," *Conf. Rec. Forty Sixth Asilomar Conf. Signals, Syst. Comput. (ASILOMAR), Pacific Grove, CA, USA*, pp. 1307–1311, Nov. 2012.
- [44] F. a Bhatti, G. B. Rowe, K. W. Sowerby, and C. R. C. M. Silva, "Blind Signal Detection Using a Linear Antenna Array: An Experimental Approach," *IEEE Trans. Veh. Technol.*, vol. 63, no. 3, pp. 1135–1145, 2014.
- [45] S. Pazos, M. Hurtado, and C. H. Muravchik, "DOA Estimation Using Random Linear Arrays Via Compressive Sensing," *IEEE Bienn. Congr. Argentina*, pp. 219–222, Jun. 2014.
- [46] H. J. Chaloupka and X. Wang, "On the Properties of Small Arrays with Closely Spaced Antenna Elements," *IEEE Antennas Propag. Soc. Symp. Monterey, CA, USA*, pp. 2699–2702, Jun. 2004.
- [47] C. Lai and S. Chen, "Design Consideration of Closely Spaced Polarization- and Pattern-Diversity Antenna Pair," *IEEE Antennas Propag. Soc. Int. Symp. (APSURSI), Chicago, IL, USA*, pp. 1–2, 2012.
- [48] M. Martínez-Vázquez, "Considerations for the Design of Antennas Embedded in Mobile Communications Devices," *2010 Loughbrgh. Antennas Propag. Conf. Loughborough, UK*, pp. 36–40, Nov. 2010.
- [49] A. Gorcin and H. Arslan, "A Two-Antenna Single RF Front-End DOA Estimation System for Wireless Communications Signals," *IEEE Trans. Antennas Propag.*, vol. 62, no. 10, pp. 5321–5333, 2014.
- [50] J. Sheinvald and M. Wax, "Direction Finding with Fewer Receivers via Time-

- Varying Preprocessing,” *IEEE Trans. Signal Process.*, vol. 47, no. 1, pp. 2–9, 1999.
- [51] M. Grant and S. Boyd, “CVX: Matlab Software for Disciplined Convex Programming,” *version 2.0 beta*. [Online]. Available: <http://cvxr.com/cvx>.
- [52] P. P. Vaidyanathan and P. Pal, “Sparse Sensing with Co-prime Samplers and Arrays,” *IEEE Trans. Signal Process.*, vol. 59, no. 2, pp. 573–586, 2011.
- [53] P. Pal and P. P. Vaidyanathan, “Coprime Sampling and the MUSIC Algorithm,” *Digit. Signal Process. Signal Process. Educ. Meet. (DSP/SPE), Sedona, AZ, USA*, pp. 289–294, Jan. 2011.
- [54] C. Liu and P. P. Vaidyanathan, “One-Bit Sparse Array DOA Estimation,” *IEEE Int. Conf. Acoust. Speech Signal Process. (ICASSP), New Orleans, LA, USA*, pp. 3126–3130, Mar. 2017.
- [55] T. Jia, H. Wang, X. Shen, and X. Liu, “Direction of Arrival Estimation With Co-prime Arrays Via Compressed Sensing Methods,” *Ocean. 2016 - Shanghai*, pp. 1–5, Apr. 2016.
- [56] K. Adhikari, J. R. Buck, and K. E. Wage, “Beamforming with Extended Co-prime Sensor Arrays,” *IEEE Int. Conf. Acoust. Speech Signal Process. (ICASSP), Vancouver, BC, Canada*, pp. 4183–4186, May 2013.
- [57] K. Adhikari, J. R. Buck, and K. E. Wage, “Extending Coprime Sensor Arrays to Achieve the Peak Side Lobe Height of a Full Uniform Linear Array,” *EURASIP J. Adv. Signal Process.*, vol. 2014, no. 148, pp. 1–17, 2014.
- [58] J. R. Jr and J. Krolik, “Multiple Source Localization With Moving Co-Prime Arrays,” *IEEE Int. Conf. Acoust. Speech Signal Process. (ICASSP), Brisbane, QLD, Aust.*, pp. 2374–2378, Apr. 2015.
- [59] Q. Shen, W. Liu, W. Cui, S. Wu, Y. D. Zhang, and M. G. Amin, “Low-Complexity Direction-of-Arrival Estimation Based on Wideband Co-Prime Arrays,” *IEEE Trans. Audio, Speech Lang. Process.*, vol. 23, no. 9, pp. 1445–1456, 2015.
- [60] G. Di Martino, A. Iodice, and S. Medagli, “Orthogonal Coprime SAR,” *IEEE Int. Geosci. Remote Sens. Symp. (IGARSS), Milan, Italy*, pp. 3758–3761, Jul. 2015.
- [61] G. Di Martino and A. Iodice, “Coprime synthetic Aperture Radar (CopSAR): A New Acquisition Mode for maritime Surveillance,” *IEEE Trans. Geosci. Remote Sens.*, vol. 53, no. 6, pp. 3110–3123, 2015.
- [62] H. Shi and B. Jia, “SAR Imaging Method Based on Coprime Sampling and Nested Sparse Sampling,” *J. Syst. Eng. Electron.*, vol. 26, no. 6, pp. 1222–1228, 2015.
- [63] Y. D. Zhang, M. G. Amin, and B. Himed, “Sparsity-Based DOA Estimation Using Co-Prime Arrays,” *IEEE Int. Conf. Acoust. Speech Signal Process. (ICASSP), Vancouver, BC, Canada*, pp. 3967–3971, May 2013.

- [64] Y. D. Zhang, S. Qin, and M. G. Amin, "DOA Estimation Exploiting Coprime Arrays with Sparse Sensor Spacing," *IEEE Int. Conf. Acoust. Speech Signal Process. (ICASSP), Florence, Italy*, pp. 2267–2271, May 2014.
- [65] R. A. Scott, "An Electrically Small Multi-Port Loop Antenna for Direction of Arrival Estimation," *Master Thesis, Electr. Comput. Eng. Univ. Illinois, Urbana, Illinois*, 2014.
- [66] M. Shahedul Amin, M. Riyasat Azim, S. Prantik Rahman, M. Ferdous Habib, and M. Ashraful Hoque, "Estimation of Direction of Arrival (DOA) Using Real-Time Array Signal Processing and Performance Analysis," *IJCSNS Int. J. Comput. Sci. Netw. Secur.*, vol. 10, no. 7, pp. 43–57, 2010.
- [67] A. D. Redondo, T. Sanchez, C. Gomez, L. Betancur, and R. C. Hincapie, "MIMO SDR-based implementation of AoA algorithms for Radio Direction Finding in spectrum sensing activities," *IEEE Colomb. Conf. Commun. Comput. Popayan, Colomb.*, pp. 1–4, Jul. 2015.
- [68] S. Shakeri, D. D. Ariananda, and G. Leus, "Direction of Arrival Estimation Using sparse Ruler Array Design," *IEEE Int. Work. Signal Process. Adv. Wirel. Commun. Cesme, Turkey*, pp. 525–529, Jun. 2012.
- [69] A. A. Goncharova, R. J. Weber, and Y. Huang, "Sparse Array DOA Estimation in the Presence of Unknown Non-Uniform Noise," *IEEE Aerosp. Conf. Proceedings, Big Sky, MT, USA*, pp. 1–8, Mar. 2011.
- [70] D. Weibo, H. Bin, and W. Xiaochuan, "The Estimation for the Direction of Arrival Based on Sparse Array," *IET Int. Radar Conf. Hangzhou, China*, pp. 1–4, Oct. 2015.
- [71] M. C. Hua, C. H. Hsu, W. J. Liao, C. C. Yao, T. H. Yeh, and H. C. Liu, "Direction-of-Arrival Estimator Using Array Switching on Software Defined Radio Platform," *IEEE Int. Symp. Antennas Propag. (APSURSI), Spokane, W, USA*, pp. 2821–2824, Jul. 2011.
- [72] F. A. C. Garcia, R. Schena, F. M. Da Silva, M. Nogueira, E. Wolski, A. G. M. Lima, and L. R. A. X. De Menezes, "Estimation of DOA for a Smart Antenna using a front-end Based in FPGA Foreseeing a SDR Architecture," *First Eur. Conf. Antennas Propagation*, pp. 1–4, Nov. 2006.
- [73] N. Tayem, M. Omer, and A. A. Hussain, "DOA Estimation Method using R Matrix of the QR Factorized Data and its Prototype Implementation on NI-PXI Platform," *IEEE Mil. Commun. Conf. MILCOM, Balt. MD, USA*, pp. 333–337, Oct. 2014.
- [74] D. Kim, K. E. Lee, and J. Kang, "Performance Analysis of AOA-based Localization with Software Defined Radio," *Int. Glob. Navig. Satell. Syst. Soc. Gold Coast, Aust.*, Jul. 2015.
- [75] J. Mar, Y. Lin, G. Chen, C. H. Chou, and Y. Su, "Implementation of the SDR Beamformer System on a Digital Signal Processor," *IEEE 60th Veh. Technol. Conf.*

- Los Angeles, CA, USA*, pp. 3895–3899, Sep. 2004.
- [76] N. Tayem, M. Omer, M. El-Lakkis, S. A. Raza, and J. F. Nayfeh, “Hardware Implementation of a Proposed QR-TLS DOA Estimation Method and MUSIC, ESPRIT Algorithms on NI-PXI Platform,” *Prog. Electromagn. Res. C*, vol. 45, pp. 203–221, 2013.
- [77] N. Tayem, “Real Time Implementation for DOA Estimation Methods on NI-PXI Platform,” *Prog. Electromagn. Res. B*, vol. 59, pp. 103–121, 2014.
- [78] M. Păun, R. Tamas, and I. Marghescu, “A Software Defined Approach for Direction Finding,” *Univ. Politeh. Bucuresti Sci. Bull. Ser. C*, vol. 77, no. 4, 2015.
- [79] M. R. Naik, G. Suri, and P. Shetty, “Simulation of Direction of Arrival and Beamforming Algorithms Used in Smart Antenna System for Software-Defined Radio,” *18th Int. Conf. Microwaves, Radar Wirel. Commun. Vilnius, Lith.*, pp. 1–4, Jun. 2010.
- [80] O. Quevedo-Teruel, M. Sanchez-Fernandez, M. L. Pablo-Gonzalez, and E. Rajo-Iglesias, “Alternating Radiation Patterns to Overcome Angle-of-Arrival Uncertainty,” *IEEE Antennas Propag. Mag.*, vol. 52, no. 1, pp. 236–242, 2010.
- [81] E. R. Ferrara and T. M. Parks, “Direction Finding with an Array of Antennas Having Diverse Polarizations,” *IEEE Trans. Antennas Propag.*, vol. 31, no. 2, pp. 231–236, 1983.
- [82] Gao Ziyang and Xiao Yong, “Direction of arrival Estimation for Conformal Arrays with Diverse Polarizations,” *12th IEEE Int. Conf. Electron. Meas. Instruments (ICEMI), Qingdao, China*, no. 1, pp. 439–442, Jul. 2015.
- [83] K. R. Dandekar, H. Ling, and G. Xu, “Experimental Study of Mutual Coupling Compensation in Smart Antenna Applications,” *IEEE Trans. Wirel. Commun.*, vol. 1, no. 3, pp. 480–487, 2002.
- [84] H.-S. Lui, Y. Yu, H. T. Hui, and M. S. Leong, “Experimental Study of Mutual Coupling Compensation in Direction Finding Using a Compact Antenna Array,” *Asia-Pacific Int. Symp. Electromagn. Compat. Beijing, China*, no. 3, pp. 830–833, Apr. 2010.
- [85] Y. Shiji, S. Mingfeng, L. Chunmao, and S. Ying, “A New Method for Mutual Coupling Correction of Array Output Signal,” *Sixth Int. Conf. Instrum. Meas. Comput. Commun. Control (IMCCC), Harbin, China*, pp. 712–715, Jul. 2016.
- [86] R. Sanudin, N. H. Noordin, A. O. El-Rayis, N. Haridas, A. T. Erdogan, and T. Arslan, “Analysis of DOA Estimation for Directional and Isotropic Antenna Arrays,” *Loughbrgh. Antennas Propag. Conf. Loughborough, UK*, pp. 1–4, Nov. 2011.
- [87] N. Celik, M. F. Iskander, R. Emrick, and Z. Zhang, “Experimental evaluation of the hybrid smart antenna system with directional array elements,” *IEEE Antennas*

- Propag. Soc. Int. Symp. Charleston, SC, USA*, pp. 1–4, Jun. 2009.
- [88] B. R. Jackson, S. Rajan, B. J. Liao, and S. Wang, “Direction of Arrival Estimation Using Directive Antennas in Uniform Circular Arrays,” *IEEE Trans. Antennas Propag.*, vol. 63, no. 2, pp. 736–747, 2015.
- [89] J. Werner, J. Wang, A. Hakkarainen, N. Gulati, D. Patron, D. Pfeil, K. Dandekar, D. Cabric, and M. Valkama, “Sectorized antenna-based DoA estimation and localization: Advanced algorithms and measurements,” *IEEE J. Sel. Areas Commun.*, vol. 33, no. 11, pp. 2272–2286, 2015.
- [90] S. A. Alawsh, M. T. Alkhodary, A. H. Muqaibel, and M. S. Sharawi, “Experimental Evaluation of Coprime Sampler in Direction of Arrival Estimation,” *IEEE Middle East Conf. Antennas Propag. (MECAP), Beirut, Lebanon*, pp. 1–4, Sep. 2016.
- [91] A. T. Moffet, “Minimum-Redundancy Linear Arrays,” *IEEE Trans. Antennas Propag.*, vol. AP-16, no. 2, pp. 172–175, 1968.
- [92] G. S. Bloom and S. W. Golomb, “Applications of Numbered Undirected Graphs,” *Proc. IEEE*, vol. 65, no. 4, pp. 562–570, 1977.
- [93] M. Yang, A. M. Haimovich, B. Chen, and X. Yuan, “A New Array Geometry for DOA Estimation With Enhanced Degrees of Freedom,” *IEEE Int. Conf. Acoust. Speech Signal Process. (ICASSP), Shanghai, China*, pp. 3041–3045, Mar. 2016.
- [94] S. Li, W. He, X. Yang, M. Bao, and Y. Wang, “Direction-of-Arrival Estimation of Quasi-Stationary signals Using Two-Level Khatri-Rao Subspace and Four-Level Nested Array,” *J. Cent. South Univ.*, vol. 21, no. 7, pp. 2743–2750, 2014.
- [95] C. Liu and P. P. Vaidyanathan, “Super Nested Arrays : Sparse Arrays With Less Mutual Coupling Than Nested Arrays,” *IEEE Int. Conf. Acoust. Speech Signal Process. (ICASSP), Shanghai, China*, pp. 2976–2980, Mar. 2016.
- [96] C. L. Liu and P. P. Vaidyanathan, “Super Nested Arrays: Linear Sparse Arrays With Reduced Mutual Coupling-Part I: Fundamentals,” *IEEE Trans. Signal Process.*, vol. 64, no. 15, pp. 3997–4012, 2016.
- [97] C. L. Liu and P. P. Vaidyanathan, “Super Nested Arrays: Linear Sparse Arrays With Reduced Mutual Coupling—Part II: High-Order Extensions,” *IEEE Trans. Signal Process.*, vol. 64, no. 16, pp. 4203–4217, 2016.
- [98] E. Boudaher, F. Ahmad, and M. G. Amin, “Sparse Reconstruction for Direction-of-Arrival Estimation Using Multi-Frequency Co-Prime Arrays,” *EURASIP J. Adv. Signal Process.*, vol. 168, no. 1, pp. 1–11, 2014.
- [99] E. Boudaher, Y. Jia, F. Ahmad, and M. G. Amin, “Direction-of-Arrival Estimation Using Multi-Frequency Co-Prime Arrays,” *22nd Eur. Signal Process. Conf. (EUSIPCO), Lisbon, Port.*, pp. 1034–1038, Sep. 2014.
- [100] Y. Liu and J. R. Buck, “Detecting Gaussian Signals in the Presence of Interferers

- Using the Coprime Sensor Arrays with the Min Processor,” *49th Asilomar Conf. Signals, Syst. Comput. Pacific Grove, CA, USA*, pp. 370–374, Nov. 2015.
- [101] S. Qin, Y. D. Zhang, M. G. Amin, and B. Himed, “DOA Estimation Exploiting a Uniform Linear Array With Multiple Co-prime Frequencies,” *Signal Processing*, vol. 130, pp. 37–46, 2017.
- [102] X. Wang, X. Wang, and X. Lin, “Co-Prime Array Processing With Sum and Difference Co-array,” *49th Asilomar Conf. Signals, Syst. Comput. Pacific Grove, CA, USA*, pp. 380–384, Nov. 2015.
- [103] C. Liu, P. P. Vaidyanathan, and Piya Pal, “Coprime Coarray Interpolation for DOA Estimation via Nuclear Norm Minimization,” *IEEE Int. Symp. Circuits Syst. (ISCAS), Montr. QC, Canada*, pp. 2639–2642, May 2016.
- [104] Q. Shen, W. Liu, W. Cui, and S. Wu, “Extension of Co-Prime Arrays Based on the Fourth-Order Difference Co-Array Concept,” *IEEE Signal Process. Lett.*, vol. 23, no. 5, pp. 615–619, 2016.
- [105] Y. D. Zhang, S. Qin, and M. G. Amin, “Near-field Source Localization Based on Sparse Reconstruction of Sensor-Angle Distributions,” *IEEE Radar Conf. (RadarCon), Arlington, VA, USA*, pp. 0891–0895, May 2015.
- [106] S. Qin, Y. D. Zhang, Q. Wu, and M. G. Amin, “Structure-Aware Bayesian Compressive Sensing for Near-Field Source Localization Based on Sensor-Angle Distributions,” *Int. J. Antennas Propag.*, pp. 1–15, 2015.
- [107] J. Liu, Y. Zhang, Y. Lu, and W. Wang, “DOA Estimation based on Multi-Resolution Difference Co-array Perspective,” *Digit. Signal Process.*, vol. 62, pp. 187–196, 2017.
- [108] S. A. Alawsh and A. H. Muqaibel, “Three-Level Prime Arrays for Sparse Sampling in Direction of Arrival Estimation,” *IEEE Asia-Pacific Conf. Appl. Electromag (APACE), Langkawi, Malaysia*, pp. 277–281, Dec. 2016.
- [109] H. Saint-Geniès, D. Defour, and G. Revy, “Range Reduction Based on Pythagorean Triples for Trigonometric Function Evaluation,” *IEEE 26th Int. Conf. Appl. Syst. Archit. Process. (ASAP), Toronto, ON, Canada*, pp. 74–81, Jul. 2015.
- [110] R. Rajamaki and V. Koivunen, “Comparison of Sparse Sensor Array Configurations with Constrained Aperture for Passive Sensing,” *IEEE Radar Conf. (RadarConf), Seattle, WA, USA*, no. 1, pp. 0797–0802, May 2017.
- [111] Saleh A. Alawsh and Ali H. Muqaibel, “Multi-Level Prime Array for Sparse Sampling,” *IET Signal Process.*, vol. Online ISS, no. Available online: 12 February, p. DOI: 10.1049/iet-2017.0252, 2018.
- [112] F. Sun, B. Gao, and P. Lan, “Partial Spectral Search-based DOA Estimation method for Co-prime Linear Arrays,” *Electron. Lett.*, vol. 51, no. 24, pp. 2053–2055, 2015.

- [113] C. Zhou, Y. Gu, W. Song, Y. Xie, and Z. Shi, "Robust Adaptive Beamforming Based on DOA Support Using Decomposed Coprime Subarrays," *IEEE Int. Conf. Acoust. Speech Signal Process. (ICASSP)*, Shanghai, China, pp. 2986–2990, Mar. 2016.
- [114] C. Zhou, Z. Shi, Y. Gu, and X. (Sherman) Shen, "DECOM : DOA Estimation with Combined MUSIC for Coprime Array," *Int. Conf. Wirel. Commun. Signal Process. (WCSP)*, Hangzhou, China, pp. 1–5, Oct. 2013.
- [115] Y. Huang, G. Liao, J. Li, J. Li, and H. Wang, "Sum and Difference Coarray based MIMO Radar Array Optimization with its Application for DOA Estimation," *Multidimens. Syst. Signal Process.*, pp. 1–20, 2016.
- [116] W. Q. Wang and C. Ling, "Nested Array with Time-Delayers for Target Range and Angle Estimation," *3rd Int. Work. Compress. Sens. Theory its Appl. to Radar, Sonar Remote Sens. (CoSeRa)*, Pisa, Italy, pp. 249–252, Jun. 2015.
- [117] K. Han and A. Nehorai, "Wideband Direction of Arrival Estimation Using Nested Arrays," *5th IEEE Int. Work. Comput. Adv. Multi-Sensor Adapt. Process. (CAMSAP)*, St. Martin, Fr., no. 2, pp. 188–191, Dec. 2013.
- [118] H. Qiao and P. Pal, "On Maximum-Likelihood Methods for Localizing More Sources Than Sensors," *IEEE Signal Process. Lett.*, vol. 24, no. 5, pp. 703–706, 2017.
- [119] Y. Iizuka and K. Ichige, "Extension of Two-Level Nested Array with Larger Aperture and More Degrees of Freedom," *Int. Symp. Antennas Propag. (ISAP)*, Okinawa, Japan, pp. 442–443, Oct. 2016.
- [120] Q. Shen, W. Liu, W. Cui, and S. Wu, "Low-Complexity Compressive Sensing Based DOA Estimation for Co-Prime Arrays," *19th Int. Conf. Digit. Signal Process. Hong Kong, China*, pp. 754–758, Aug. 2014.
- [121] S. Li and D. Xie, "Compressed Symmetric Nested Arrays and Their Application for Direction-of-Arrival Estimation of Near-Field Sources," *Sensors*, vol. 16, no. 11, pp. 1–12, 2016.
- [122] P. Pal and P. P. Vaidyanathan, "Multiple Level Nested Array: An Efficient Geometry for 2qth Order Cumulant based Array Processing," *IEEE Trans. Signal Process.*, vol. 60, no. 3, pp. 1253–1269, 2012.
- [123] Q. Shen, W. Liu, W. Cui, S. Wu, Y. D. Zhang, and M. G. Amin, "Focused Compressive Sensing for Underdetermined Wideband DOA Estimation Exploiting High-Order Difference Coarrays," *IEEE Signal Process. Lett.*, vol. 24, no. 1, pp. 86–90, 2017.
- [124] C. Liu and P. P. Vaidyanathan, "High Order Super Nested Arrays," *IEEE Sens. Array Multichannel Signal Process. Work. (SAM)*, Rio Janerio, Brazil, pp. 1–5, Jul. 2016.



- [125] Y. Hu, Y. Liu, and X. Wang, "DOA Estimation of Coherent Signals on Coprime Arrays Exploiting Fourth-Order Cumulants," *Sensors*, pp. 1–19, 2017.
- [126] Q. Shen, W. Liu, W. Cui, and S. Wu, "Extension of Nested Arrays with the Fourth-order Difference Co-Array Enhancement," *IEEE Int. Conf. Acoust. Speech Signal Process. (ICASSP), Shanghai, China*, no. 3, pp. 2991–2995, Mar. 2016.
- [127] S. Qin, Y. D. Zhang, and M. G. Amin, "DOA Estimation Exploiting Coprime Frequencies," *n Proc. SPIE Wirel. Sensing, Localization, Proc. Conf., Balt. MD*, vol. 9103, p. 91030E1–91030E7, May 2014.
- [128] S. Qin, Y. D. Zhang, M. G. Amin, and F. Gini, "Frequency Diverse Coprime Arrays with Coprime Frequency Offsets for Multi-target Localization," *IEEE J. Sel. Top. Signal Process.*, vol. 11, no. 2, pp. 321–335, 2017.
- [129] S. Qin, Y. D. Zhang, and M. G. Amin, "Multi-target Localization Using Frequency Diverse Coprime Arrays with Coprime Frequency Offsets," *IEEE Radar Conf. (RadarConf), Philadelphia, PA, USA*, pp. 1–5, May 2016.
- [130] S. Qin, Y. D. Zhang, and M. G. Amin, "DOA Estimation of Mixed Coherent and Uncorrelated Targets Exploiting Coprime MIMO Radar," *Digit. Signal Process.*, vol. 61, pp. 26–34, 2017.
- [131] E. Boudaher, Y. Jia, F. Ahmad, and M. G. Amin, "Multi-Frequency Co-Prime Arrays for High-Resolution Direction-of-Arrival Estimation," *IEEE Trans. Signal Process.*, vol. 63, no. 14, pp. 3797–3808, 2015.
- [132] A. Liu, Q. Yang, X. Zhang, and W. Deng, "Direction-of-Arrival Estimation for Coprime Array Using Compressive Sensing Based Array Interpolation," *Int. J. Antennas Propag.*, vol. 2017, pp. 1–10, 2017.
- [133] E. Bou Daher, F. Ahmad, and M. G. Amin, "Performance Analysis of Sparsity-based Interpolation for DOA Estimation with Non-uniform Arrays," *Proc. SPIE Compressive Sens. VI Conf. Anaheim, CA*, p. 102110F–1–102110F–6, May 2017.
- [134] M. Guo, T. Chen, and B. Wang, "An Improved DOA Estimation Approach Using Coarray Interpolation and Matrix Denoising," *Sensors (Switzerland)*, vol. 17, no. 5, pp. 1–12, 2017.
- [135] Y. Zhang, "User's Guide for YALL1 : Your ALgorithms for L1 Optimization," *Tech. report, Rice Univ.*, pp. 1–9, 2009.
- [136] J. Li, D. Jiang, and X. Zhang, "Sparse Representation Based Two-Dimensional Direction of Arrival Estimation Using Co-prime Array," *Multidimens. Syst. Signal Process.*, pp. 1–13, 2016.
- [137] F. Sun, P. Lan, B. I. N. Gao, and G. Zhang, "An Efficient Dictionary Learning-Based 2-D DOA Estimation Without Pair Matching for Co-Prime Parallel Arrays," *IEEE Access*, vol. 6, pp. 8510–8518, 2018.

- [138] S. Qin, Y. D. Zhang, and M. G. Amin, "Two-Dimensional DOA Estimation Using Parallel Coprime Subarrays," *IEEE Sens. Array Multichannel Signal Process. Work. (SAM), Rio Janerio, Brazil*, pp. 1–4, Jul. 2016.
- [139] Z. Cheng, Y. Zhao, H. Li, and P. Shui, "Two-Dimensional DOA Estimation Algorithm with Co-prime Array via Sparse Representation," *Electron. Lett.*, vol. 51, no. 25, pp. 2084 – 2086, 2015.
- [140] D. Yang, W. Liu, Q. Cheng, Z. Xia, and X. Zhang, "2D-DOA Estimation for Coprime L-shaped Arrays with MUSIC Algorithm," *Int. Conf. Comput. Electron. Commun. Eng. (CECE), Sanya, China*, pp. 275–281, Jun. 2017.
- [141] Q. Liu, X. Yi, L. Jin, and W. Chen, "Two Dimensional Direction of Arrival Estimation for Co-prime L-shaped Array Using Sparse Reconstruction," *8th Int. Congr. Image Signal Process. (CISP), Shenyang, China*, pp. 1499–1503, Oct. 2015.
- [142] S. Liu, L. S. Yang, D. C. Wu, and J. H. Huang, "Two-Dimensional DOA Estimation Using a Co-Prime Symmetric Cross Array," *Prog. Electromagn. Res. C*, vol. 54, pp. 67–74, 2014.
- [143] J. Shi, G. Hu, X. Zhang, F. Sun, and H. Zhou, "Sparsity-Based Two-Dimensional DOA Estimation for Coprime Array: From Sum-Difference Coarray Viewpoint," *IEEE Trans. Signal Process.*, vol. 65, no. 21, pp. 5591–5604, 2017.
- [144] Z. Wang, Z. Xiaofei, and S. Zhan, "Two-Dimensional Direction of Arrival Estimation for Coprime Planar Arrays via a Computationally Efficient One-Dimensional Partial Spectral Search Approach," *IET Radar, Sonar Navig.*, vol. 11, no. 10, pp. 1581–1588, 2017.
- [145] W. Zheng, X. Zhang, and H. Zhai, "A Generalized Coprime Planar Array Geometry for Two-Dimensional DOA Estimation," *IEEE Commun. Lett.*, pp. 1–1, 2017.
- [146] Q. Wu, F. Sun, P. Lan, G. Ding, and X. Zhang, "Two-Dimensional Direction-of-Arrival Estimation for Co-Prime Planar Arrays: A Partial Spectral Search Approach," *IEEE Sens. J.*, vol. 16, no. 14, pp. 5660–5670, 2016.
- [147] Y.-Y. Dong, C.-X. Dong, Y.-T. Zhu, G.-Q. Zhao, and S.-Y. Liu, "Two-dimensional DOA Estimation for L-shaped Array with Nested Subarrays Without Pair Matching," *IET Signal Process.*, vol. 10, no. 9, pp. 1112–1117, 2016.
- [148] C. Niu, Y. Zhang, and J. Guo, "Interlaced Double-Precision 2-D Angle Estimation Algorithm using L-Shaped Nested Arrays," *IEEE Signal Process. Lett.*, vol. 23, no. 4, pp. 522–526, 2016.
- [149] N. Wu and Q. Liang, "Underwater DOA estimation based on Nested Array," *IEEE Mil. Commun. Conf. (MILCOM), Tampa, FL, USA*, pp. 216–221, Oct. 2015.
- [150] S. Yuan and Q. Liang, "To Achieve Massive MIMO with Much less Antennas by Nested Placement," *IEEE Conf. Comput. Commun. Work. (INFOCOM WKSHPS), San Fr. CA, USA*, pp. 668–673, Sep. 2016.

- [151] P. Pal and P. P. Vaidyanathan, "Nested Arrays in Two Dimensions, Part I: Geometrical Considerations," *IEEE Trans. Signal Process.*, vol. 60, no. 9, pp. 4694–4705, 2012.
- [152] P. Pal and P. P. Vaidyanathan, "Nested Arrays in Two Dimensions, Part II: Application in Two Dimensional Array Processing," *IEEE Trans. Signal Process.*, vol. 60, no. 9, pp. 4706–4718, 2012.
- [153] Y. Tian, Q. Lian, and K. Liu, "2-D Angles of Arrival Estimation Utilizing Two-Step Weighted  $\ell_1$  -Norm Penalty under Nested Coprime Array with Compressed Inter-Element Spacing," *IEICE TRANS. Fundam.*, vol. E100–A, no. 3, pp. 896–901, 2017.
- [154] C. L. Liu and P. P. Vaidyanathan, "Two-dimensional Sparse Arrays with Hole-free Coarray and Reduced Mutual Coupling," *50th Asilomar Conf. Signals, Syst. Comput. Pacific Grove, CA, USA*, pp. 1508–1512, Nov. 2017.
- [155] X. Luo, X. Fei, P. Wei, and L. Gan, "Sparse Representation-Based Method for Two-Dimensional Direction-of-Arrival Estimation with L-Shaped Array," *IEEE Int. Conf. Commun. Probl. (ICCP), Beijing, China*, pp. 277–280, Dec. 2014.
- [156] T. Basikolo, K. Ichige, and H. Arai, "Direction of Arrival Estimation for Quasi-Stationary Signals Using Nested Circular Array," *2016 4th Int. Work. Compress. Sens. Theory its Appl. to Radar, Sonar Remote Sens. (CoSeRa), Aachen, Ger.*, pp. 193–196, Sep. 2016.
- [157] C. L. Liu and P. P. Vaidyanathan, "Hourglass Arrays and Other Novel 2-D Sparse Arrays with Reduced Mutual Coupling," *IEEE Trans. Signal Process.*, vol. 65, no. 13, pp. 3369–3383, 2017.
- [158] X. Wu, W.-P. Zhu, and J. Yan, "Gridless Two-dimensional DOA Estimation With L-shaped Array Based on the Cross-covariance Matrix," *arXiv Prepr. arXiv*, no. 61372122, Dec. 2017.

## PUBLICATIONS FROM THE DISSERTATION

### Journal Publications

1. Muqaibel, Ali H., Abdi T. Abdalla, Alkhodary T. Mohammad, and **Alawsh A. Saleh**, "Through-the-wall Radar Imaging Exploiting Pythagorean Apertures with Sparse Reconstruction," *Digital Signal Processing* 61 (2017): 86-96.
2. **S. A. Alawsh** and Ali H. Muqaibel "Multi-Level Prime Array for Sparse Sampling," *IET Signal Processing*, Online ISSN 1751-9683 Available online: 12 February 2018  
DOI: 10.1049/iet-spr.2017.0252
3. **S. A. Alawsh** and Ali H. Muqaibel, "An Upper Bound of the Achievable Degrees-of-Freedom for a Three-Level Prime Arrays," *IEEE Access*. Under review.
4. **S. A. Alawsh** and Ali H. Muqaibel "Sparse DOA Estimation Based on Multi-Level Prime Array with Compression," To be submitted
5. **S. A. Alawsh** and Ali H. Muqaibel, "Optimum Multi-Level Prime Array Configurations," To be submitted
6. **S. A. Alawsh**, Ahmed Oweis, A. H. Muqaibel, and M. S. Sharawi, "DOA Estimation Based on Sparse Directional Antenna Arrays," To be submitted.

### Conference Publications

1. **S. A. Alawsh**, A. H. Muqaibel and M. S. Sharawi, "DOA estimation in MIMO systems with Compressive Sensing for future handsets," *2015 IEEE Jordan Conference on Applied Electrical Engineering and Computing Technologies (AEECT)*, Amman, Jordan, 2015, pp. 1-6.  
DOI: 10.1109/AEECT.2015.7360532
2. **S. A. Alawsh**, M. T. Alkhodary, A. H. Muqaibel and M. S. Sharawi, "Experimental evaluation of coprime sampler in direction of arrival estimation," *2016 IEEE Middle East Conference on Antennas and Propagation (MECAP)*, Beirut, Lebanon, 2016, pp. 1-4.  
DOI: 10.1109/MECAP.2016.7790089
3. S. M. Alamoudi, M. A. Aldhaheeri, **S. A. Alawsh**, and A. H. Muqaibel, "Sparse DOA estimation based on a shifted coprime array configuration," *2016 16th Mediterranean Microwave Symposium (MMS)*, Abu Dhabi, UAE, 2016, pp. 1-4.  
DOI: 10.1109/MMS.2016.7803789
4. **S. A. Alawsh** and A. H. Muqaibel, "Three-level prime arrays for sparse sampling in direction of arrival estimation," *2016 IEEE Asia-Pacific Conference on Applied Electromagnetics (APACE)*, Langkawi, Malaysia, 2016, pp. 277-281,  
DOI: 10.1109/APACE.2016.7916441
5. **S. A. Alawsh**, H. Muqaibel and M. S. Sharawi, "Sparse Direction-of-Arrival Estimation for Two Sources with Constrained Antenna Arrays," *2017 10th International Conference on Electrical and Electronics Engineering (ELECO)*, Bursa, Turkey, 2017, pp. 666-670.

6. **S. A. Alawsh**, O. A. A. Khazragi, A. H. Muqaibel and S. N. Al-Ghadhban, "Sparse Direction of Arrival Estimation Using Sparse Arrays Based on Software-Defined-Radio Platform," *2017 10th International Conference on Electrical and Electronics Engineering (ELECO)*, Bursa, Turkey, 2017, pp. 671-675.
7. **S. A. Alawsh**, Ahmed Oweis, A. H. Muqaibel, and M. S. Sharawi, "Sparse Direction-of-Arrival Estimation with Directive Coprime Arrays," *IEEE International Symposium on Antennas and Propagation (APS/URSI 2018)*, Boston, MA, USA, July 2018.
8. Ahmed Oweis, **S. A. Alawsh**, A. H. Muqaibel, and M. S. Sharawi, "A CoPrime Array of Patch Antennas for DOA Estimation in Mobile Handheld Devices," *IEEE International Symposium on Antennas and Propagation (APS/URSI 2018)*, Boston, MA, USA, July 2018.
9. **S. A. Alawsh** and Ali H. Muqaibel, "Multi-Level Prime Sampler in Time Domain for Sparse Sampling," To be submitted.

## Patents

1. **S. A. Alawsh** and Ali H. Muqaibel "Sparse DOA Estimation Based on a Multi-Level Prime Array with Compressed Subarray," Under review

## Vitae

Name : Saleh Ahmed Yaslam Alawsh

Nationality : Yemeni

Date of Birth : 1/4/1981

Email : alawsh21@gmail.com

Address : KFUPM main campus

Academic Background : Saleh A. Alawsh received his B.Sc. degree in Electronic and Communications from Hadhramout University, Mukalla, Yemen, in 2007, and M.Sc. degree in Telecommunication from King Fahd University of Petroleum and Minerals (KFUPM), Dhahran, Saudi Arabia, in 2013. He joined the electrical engineering department at KFUPM as a lecturer in 2013 where he got his PhD. degree in electrical engineering. His main area of interest includes ultra-wideband systems, narrow band interference mitigation, direction-of-arrival estimation, localization, and compressive sensing. He is also a graduate assistant at the Department of Electronics and Communication Engineering of Hadhramout University.

**Previous publications from MSc:**

1. **S. A. Alawsh** and A. H. Muqaibel, "Pilot symbols distribution for compressive sensing based NBI mitigation in UWB systems," *2013 IEEE International Conference on Ultra-Wideband (ICUWB)*, Sydney, NSW, 2013, pp. 148-153.
2. **S. A. Alawsh** and A. H. Muqaibel, "Compressive sensing for blind NBI mitigation in UWB systems," *2013 IEEE International Conference on Signal and Image Processing Applications*, Melaka, 2013, pp. 441-446.
3. **S. A. Alawsh** and A. H. Muqaibel, "Compressive sensing based NBI mitigation in UWB systems in the presence of multiuser interference," *2016 IEEE Wireless Communications and Networking Conference*, Doha, 2016, pp. 1-6.
4. Ali H. Muqaibel and **S. A. Alawsh**, "Training Sequence Design for NBI Mitigation in Compressive Sensing UWB Systems," *Wireless Personal Communication*, vol. 78, no. 2, pp. 1539–1554, 2014.
5. Ali H. Muqaibel, **S. A. Alawsh**, "Evaluation of compressed sensing in UWB systems with NBI", US Patent number: US 9154263, US 9455763, Oct. 6, 2015.



